

# Tau Accumulation in Degradative Organelles is Associated to Lysosomal Stress

A doctoral dissertation presented by  
Ester Piovesana

Under the supervision of  
Prof. Dr. Paolo Paganetti  
Dr. Stéphanie Papin

Submitted to the  
Faculty of Biomedical Sciences  
Università della Svizzera italiana

For the degree of  
Ph.D. in Biomedical Sciences

June, 2023

## SUMMARY

This thesis collects the main findings of my research projects conducted from September 2020 until June 2023 in the laboratory for Aging Disorders head by Prof. Dr. Paolo Paganetti of Ente Ospedaliero Cantonale (EOC) Switzerland. The research was performed under the supervision of Prof. Paganetti and Dr. Stéphanie Papin.

The thesis is organized as follow: **Chapter 1** presents a common introduction about neurodegeneration, tau protein, degradative systems in neurodegeneration and lysosomal storage disorders principally focusing on Gaucher disease and its link with tauopathies. **Chapter 2** contains the first findings of my research highlighting the involvement of degradative organelles in the encounter of endocytosed fibrillogenic tau transported by extracellular vesicles and the endogenous tau present in recipient cells. Additionally, in this work we tried to elucidate the implication of autophagy in tau prion-like transmission. The research is presented as a published article on September 2021, entitled *Tau Seeds in Extracellular Vesicles Induce Tau Accumulation in Degradative Organelles of Cells*. In this manuscript I contributed as co-author being highly involved in the revision process. **Chapter 3** describes the key findings of my main research project where we investigated the role of impaired degradative organelles, using an *in vitro* model mimicking Gaucher disease, in tau aggregation. We described the bidirectional effects on lysosomal homeostasis upon tau aggregation and how tau aggregation can further promote lysosomal dysfunctions. The study is presented as a submitted manuscript entitled *Tau Accumulation in Degradative Organelles is associated to Lysosomal Stress* in which I am first author. **Chapter 4** presents a common discussion of the previous sections with the main considerations, future perspectives and conclusions.

## TABLE OF CONTENTS

<b>INTRODUCTION .....</b>	<b>1</b>
<b>NEURODEGENERATIVE DISEASES AND PROTEIN AGGREGATION .....</b>	<b>1</b>
<b>PHYSIOLOGICAL AND PATHOLOGICAL TAU .....</b>	<b>3</b>
<b>TAU EXPRESSION AND DISTRIBUTION .....</b>	<b>3</b>
<b>TAU STRUCTURE AND MODIFICATIONS .....</b>	<b>5</b>
<b><i>TAU POST-TRANSLATIONAL MODIFICATIONS</i> .....</b>	<b>5</b>
<b>TAU PRION-LIKE TRANSMISSION .....</b>	<b>7</b>
<b>EXTRACELLULAR VESICLES (EVs) AND NEURODEGENERATION .....</b>	<b>9</b>
<b>CANONICAL AND NON CANONICAL TAU SEEDING LOCATIONS.....</b>	<b>9</b>
<b>DEGRADATIVE SYSTEMS IN NEURODEGENERATION .....</b>	<b>10</b>
<b>NEURODEGENERATION AND LYSOSOMAL STORAGE DISORDERS.....</b>	<b>13</b>
<b>GAUCHER DISEASE.....</b>	<b>13</b>
<b>GAUCHER DISEASE AND NEURODEGENERATION .....</b>	<b>14</b>
<b>RESULTS .....</b>	<b>16</b>
<b>HYPOTHESIS AND STUDY DESIGN: <i>TAU SEEDS IN EXTRACELLULAR VESICLES INDUCE TAU</i></b>	
<b><i>ACCUMULATION IN DEGRADATIVE ORGANELLES OF CELLS.....</i></b>	<b>16</b>
<b>HYPOTHESIS AND STUDY DESIGN: <i>TAU ACCUMULATION IN DEGRADATIVE ORGANELLES IS ASSOCIATED</i></b>	
<b><i>TO LYSOSOMAL STRESS</i> .....</b>	<b>51</b>
<b>DISCUSSION AND FUTURE PERSPECTIVES.....</b>	<b>82</b>
<b>CONCLUSIONS .....</b>	<b>86</b>
<b>BIBLIOGRAPHY .....</b>	<b>87</b>
<b>ABBREVIATIONS .....</b>	<b>96</b>
<b>ANNEXES.....</b>	<b>98</b>
<b>CURRICULUM VITAE .....</b>	<b>117</b>
<b>ACKNOWLEDGMENTS .....</b>	<b>120</b>

## ABSTRACT

Neurodegenerative diseases, characterized by brain deposition of insoluble amyloidogenic proteins such as  $\alpha$ -synuclein and tau, constitute a major health risk for the aging population. The autophagy lysosomal pathway (ALP) involved in the degradation of intracellular macromolecules and protein aggregates is often impaired during neurodegeneration. Misfolded proteins involved in neurodegenerative diseases spread from one original site to defined brain regions through transcellular prion-like mechanisms and one possible route of transport relies on extracellular vesicles (EVs). We first established an *in vitro* model using murine neuronal progenitor C17.2 cells to investigate EVs-contained protein delivery. EVs carrying a pro-aggregating tau domain were isolated from donor cells and incubated with recipient cells. EVs were mainly internalized by endocytosis and EVs content was released in defined subcellular localizations termed degradative organelles (DOs). Importantly, in recipient cells endogenous tau was targeted through autophagic stimulation in DOs encountering there the exogenous fibrillogenic tau. This encounter led to subsequent cellular consequences such as tau accumulation and pathological tau conversion, two typical early hallmarks of tauopathies. We highlighted a new role of DOs being not simple degradative organelles but structures involved in more complex cellular functions.

To better elucidate DOs functions in neurodegeneration we used a more relevant cellular system relying on human primary fibroblasts expressing fluorescent forms of tau in an inducible manner. When primary fibroblasts were incubated with pathological tau seeds extracted from Alzheimer's disease brain tissue, we observed tau accumulation in DOs and lysosomal stress. Reciprocally, tau accumulation is observed when lysosomal dysfunction is induced in presence of an inhibitor of GCase, , a lysosomal enzyme implicated in the lysosomal storage disorder Gaucher's disease. Mutations in GCase encoding gene are the most frequent genetic risk in Parkinson's disease. Our study supports a tight crosstalk between GCase activity, lysosomal dysfunction, and adverse tau accumulation, offering new clues for better understanding the pathogenesis of tauopathies such as Alzheimer's and Parkinson's disease.



## INTRODUCTION

### Neurodegenerative diseases and protein aggregation

Neurodegenerative diseases are characterized by the progressive deposition of insoluble protein aggregates in the central nervous system (CNS). The most common neurodegenerative disease is Alzheimer's disease (AD) accounting for 60-70% of all global dementia cases<sup>1</sup>. AD is due to the presence of amyloid plaques and neurofibrillary tangles, whose main components are amyloid-beta ( $A\beta$ ) and tau, respectively<sup>2</sup>. Neurofibrillary tangles, which consist in fibrillary aggregates of hyperphosphorylated forms of tau, are also present in frontotemporal dementia (FTD), the second most common form of dementia affecting patients younger than 65 years with 2.6% of incidence<sup>3</sup>. In FTD it is possible to observe additional inclusions of misfolded TAR DNA-binding protein 43 (TDP-43), aggregates also present in the motor neuron disease amyotrophic lateral sclerosis (ALS)<sup>4</sup>. In Parkinson's disease (PD) and in Lewy bodies dementia (DLB), aggregates are formed by  $\alpha$ -synuclein accumulation and other proteins such as ubiquitin, neurofilament protein,  $\alpha$  B crystallin and tau<sup>5</sup>. Other hereditary neurodegenerative diseases are due to mutant protein aggregates caused for instance by the polyglutamine (PolyQ) expansion in the huntingtin protein for Huntington's Disease (HD)<sup>6</sup>. PolyQ expansion can occur in other proteins such as in the androgen receptor for spino and bulbar amyotrophy (SBMA)<sup>7</sup>. Lastly, amyloid aggregates containing misfolded prion protein (PrP) cause the rare prion neurodegenerative diseases. Prion transmission relies on the transfer of the pathological misfolded PrP protein conformation onto physiological variant of the same protein<sup>8</sup> (**Table 1**).

Neurodegenerative Disease	Main Aggregating protein/s
Alzheimer's Disease (AD)	$A\beta$ , tau
Parkinson's Disease (PD)	$\alpha$ -synuclein, tau, ubiquitin, neurofilament protein, $\alpha$ B crystallin
Dementia with Lewy Bodies (DLB)	$\alpha$ -synuclein
Frontotemporal Dementia (FTD)	tau, TDP-43
Amyotrophic Lateral Sclerosis (ALS)	C9ORF72, TDP-43, SOD1
Huntington's Disease (HD)	huntingtin
Spino and Bulbar Amyotrophy (SBMA)	androgen receptor
Prion Diseases	Prp

**Table 1. Examples of neurodegenerative diseases and protein aggregates classification** Adapted from Monaco and Fraldi, 2020<sup>8</sup>.

The neurodegenerative diseases characterized by tau deposits in the brain are termed tauopathies. Currently more than 26 tauopathies have been described and they differ based on tau isoform aggregates, selective affected brain regions, cell type vulnerability and considering if tau is the major pathological component or not. In primary tauopathies like Pick's disease (PiD), progressive supranuclear palsy (PSP), corticobasal degeneration (CBD) and argyrophilic grain disease (AGD) tau is the main disease's driver. In secondary tauopathies, tau aggregation represents only a secondary effect due to other pathological proteins and events occurring before and during abnormal tau aggregation like  $A\beta$  aggregates formation in AD or repetitive brain injury in chronic traumatic encephalopathy (CTE)<sup>9</sup>.

### **Causes and clinical symptoms of tauopathies**

Clinically tauopathies present a wide range of phenotypes including cognitive, behavioral, motor and language impairments and nonspecific amnesic symptoms. In FTD, neurons and glial cells of the frontal and temporal cortices degenerate leading to dysfunctions of the executive functioning, emotional and behavioral changes, language and motor impairments<sup>10</sup>. FTD is a highly heritable disorder with around 30% of patients displaying a family history. The majority of the heritability are autosomal dominant mutations in three genes: *progranulin* (*GRN*), *microtubule associated protein tau* (*MAPT*) and *chromosome 9 open reading frame 72* (*c9orf72*). Currently, 114 *GRN* and 63 *MAPT* missense variants are identified<sup>11</sup>. PiD, a subtype of fronto temporal lobar dementia enriched in phospho tau (FTLD-tau) can be either inherited or highly sporadic, in fact only few cases are associated with *MAPT* mutations. PiD presents specific neuronal lesions termed ballooned neurons and Pick's bodies. Ballooned neurons are described as well in CBD and AGD<sup>12</sup>. PSP is mainly sporadic and only less than 5% of patients display familiar cases. It is characterized by oculomotor dysfunctions affecting eye movements and postural stability. Interestingly, in PSP phospho-tau aggregates are highly abundant in astrocytes and oligodendrocytes in addition to neurons<sup>13</sup>. CBD is mainly a sporadic tauopathy characterized by dysfunctions in executive system, language impairments and movements with parkinsonism. Ballooned neurons with aggregates of phospho tau and phosphorylated neuronal filaments protein are swollen mainly in the cerebral cortex and basal ganglia<sup>14</sup>. Patients suffering from AGD present spindle-shaped lesions in neuronal processes and oligodendrocytes of hippocampus, entorhinal cortex and limbic areas<sup>15</sup>. Clinically, AGD is associated with neuropsychiatric symptoms and memory impairments but not always with cognitive decline. Genetically AGD is characterized with a overrepresentation of *MAPT* H1 haplotype<sup>16</sup>. Importantly, the majority of tauopathies occur sporadically without any detectable causative mutations and only a small subset of the diseases is driven by genetic factors. Mutations in *MAPT* mainly affect the microtubule binding domain of the protein resulting into pathological tau filament deposition in neurons and glial cells<sup>17</sup>. Autosomal *MAPT* mutations are responsible for the frontotemporal dementia with parkinsonism linked to chromosome 17 (FTDP-17). Patients with FTDP-17 display variable cognitive impairments, behavioral and motor deficits and an early disease onset (49 years old)<sup>18</sup>. *MAPT* mutations can alter as well tau splicing like in the case of the missense mutations: N279K and  $\Delta$ 280K, respectively strengthening or weakening the enhancer of tau exon 10<sup>17</sup>. A higher degree of complexity is added in understating the origins of secondary tauopathies, being more complexes diseases and involving different players and different pathological mechanisms. For instance, AD is characterized by the presence of extracellular plaques made of amyloid-beta ( $A\beta$ ) and neurofibrillary tangles (NFTs) and neuropil threads (NT) composed by tau paired helical filaments (PHFs) or straights filaments (SFs).<sup>19</sup>. The  $A\beta$  plaques are caused by alterations in the metabolism of the membrane bound amyloid precursor protein (APP) leading to increased  $A\beta$  release and deposition in the cortex and the limbic system.  $A\beta$  plaques can accumulate in the walls of arteries and arterioles causing amyloid angiopathy (CCA)<sup>20</sup>. Alterations in *MAPT* are responsible for tau loss of function and tau fibrilization<sup>21</sup>. Clinically, AD starts with deficits in the recent memory, languages difficulties evolving in more severe cognitive impairments mainly due to reduced synaptic plasticity, synapses and neuronal loss<sup>22</sup>. The majority of AD cases are sporadic however there are some genetic risk factors that predispose to the disease. In fact, apolipoprotein E type 4 (APOE- $\epsilon$ 4) carriers have higher probability to develop AD and at lower age<sup>23</sup>. In addition, between 40 to 60% of patients with Down syndrome are more prone to develop AD, due to the triplication of chromosome 21

containing the *APP* gene<sup>24</sup>. It is well known that autosomal dominant mutations affecting either the membrane bound APP or the  $\gamma$ -secretase complex presenilin-1/2 (PS1/2), which metabolizes APP, are the main triggers for familial AD (FAD). FAD is a form of AD characterized by an early disease onset (before 65 years old) and more aggressive disease progression<sup>19</sup>. The production of more and longer amyloid peptides, A $\beta$ 1-42, was considered as the main AD initiator factor. These considerations led to the postulation of the amyloid cascade hypothesis in which amyloid deposition was considered the trigger event for neuronal dysfunction and cell death<sup>25</sup>. However, later it was demonstrated that the A $\beta$  accumulation and deposition was not correlating with cognitive decline and neuronal loss in patients and in transgenic APP or APP/PS1 mice modelling FAD<sup>26</sup>. On the other hand, it was shown that changes in tau NFTs and NTs brain distribution correlates with the disease severity and progression. In fact, NFTs follow a stereotypic distribution pattern, spreading from one area to the other through anatomically interconnected regions. Braak and Braak proposed 6 main stages correlating with the pathology progression where at the beginning NFTs develop on the transentorhinal region, then appear in limbic system including hippocampus and amygdala reaching isocortical regions such as primary cortices<sup>27</sup>. Based on these considerations, it was proposed that A $\beta$  aggregation leading to subsequential tau aggregation was provoking clinically relevant symptoms. However, as demonstrated in several studies, it seems that there is not a temporal or spatial correlation with A $\beta$  plaques and tau deposits, and tau pathology seems to progress independently from A $\beta$  deposition<sup>28, 29</sup>. Lastly, tau glial positive lesions were not observed in AD patients, however reactive astrocytes and activated microglial cells are frequently detected in impaired brain regions<sup>16</sup>. Overall, it is important to highlight that the clear understanding of the pathways and mechanisms underlying tauopathies is very challenging. Firstly, these diseases are highly heterogeneous in terms of players, aggregates composition, cells and brain areas affected and disease progression. Secondly, there are still major limitations in performing precise clinical diagnosis, especially ante mortem, therefore it is very complicated to discriminate one specific disease from the other and determine their cause.

## Physiological and pathological tau

Tau is a microtubule-associated protein essential for microtubules assembly and stabilization<sup>30</sup>. Tau is natively unfolded and normally it shows little tendency for aggregation, however in neurodegenerative diseases tau aggregates in paired helical filaments forming neurofibrillary tangles<sup>31</sup>. The mechanisms underlying tau aggregation and the exact pathways involved in neurodegenerative diseases are still not fully clarified.

### Tau expression and distribution

Human tau is encoded by the microtubule-associated tau gene, *MAPT*, located in chromosome 17q21 which comprises 16 exons<sup>32</sup>. Tau has two homologous proteins MAP2 and MAP4 which include 3 or 4 repeated microtubule binding domains (MTBDs) in the C-terminus<sup>33</sup>. The human primary tau transcript contains 13 exons as exon 4A, 6 and 8 are not transcribed<sup>31</sup>. Exon 1 (E1), E4, E5, E7, E9, E11, E12 and E13 are constitutive, and the other exons are subjected to alternative splicing. E0 and E1 encode for 5' end of the untranslated *MAPT* mRNA where E0 being part of the promoter is transcribed but not translated<sup>32</sup>; E14 is part of the 3' untranslated region<sup>32</sup>. Alternative splicing of exons 2, 3, and 10 generate 6 tau isoforms in the adult brain differing by the absence or the presence of one or two 29 amino acid inserts in the amino terminus encoded by E2 and E3, known as 0N, 1N or 2N. The function of the N-terminal inserts is still unknown, these

inserts may influence the spacing and insertion of microtubules affecting tau subcellular distribution<sup>32</sup>. In addition, tau can include three (R1, R3 and R4) or four repeated regions (R1-R4) in the carboxy-terminal part of the protein, with E10 encoding for R2.

The alternative splicing of E10 is highly associated with the manifestation of tauopathies, in fact aggregates enriched in 4R are typical for PSP, CBD and AGD, whereas 3R aggregates are present in PiD and 3R-4R tau aggregates are enriched in AD brains<sup>34</sup>. 4R tau shows higher affinity for microtubules than 3R resulting in more efficient microtubules assembly.

The shortest tau isoform, missing E2, E3 and E10, characterized by 352 amino acids and highly phosphorylated, is only present in the fetal brain (termed 0N3R)<sup>35</sup>. On the contrary the longest isoforms ranging from 352 to 441 amino acids are present only in the adult CNS<sup>32</sup> (**Figure 2**). In healthy adults the inclusion and exclusion of E10 is balanced in a ratio of 1:1 whereas a shift in this equilibrium is associated with neurodegenerative diseases<sup>31</sup>. Another less discussed tau isoform is Big tau, which is generated by the alternative splicing inclusion of E4A in the pre-mRNA leading to a protein characterized by a higher molecular weight of 110 kDa. Big tau contains few phosphorylation sites and shows a lower propensity to form pathological aggregates<sup>9</sup>.

Tau is widely distributed in the nervous system and its main localizations are peripheral nerves and brain. Besides neurons and glial cells, including both oligodendrocytes and astrocytes, tau is expressed in different non neuronal cells like in the liver, kidney, skeletal muscle, salivary glands, pancreas, breast, testes and heart suggesting additional tau functions which are not only limited to the CNS<sup>31, 36, 37</sup>. Tau subcellular distribution is tightly regulated during development becoming enriched in axons during neuronal maturation through different mechanisms involving isoforms specificity, local tau synthesis, preferential axonal microtubules binding and proteins axonal transport<sup>38</sup>. However tau is present in smaller amount as well in somatodendritic compartments including plasma membrane, endoplasmic reticulum, Golgi, nucleus and mitochondria<sup>37, 39</sup>.

Tau, therefore is an ubiquitous protein, highly dynamic with broad subcellular localizations and cellular functions. For instance, in the nucleus tau seems to be involved in DNA transcription, RNA synthesis, chromatin compaction and chromosomes stability<sup>40</sup>. Importantly tau can be secreted outside the cells through direct plasma membrane secretion or through extracellular vesicles (EVs) indicating a possible role of extracellular tau<sup>41</sup>. For instance, in tauopathies progression it is well known that extracellular tau contributes to the spatio-temporal spreading of altered tau forms across different brain areas<sup>42, 41</sup>.

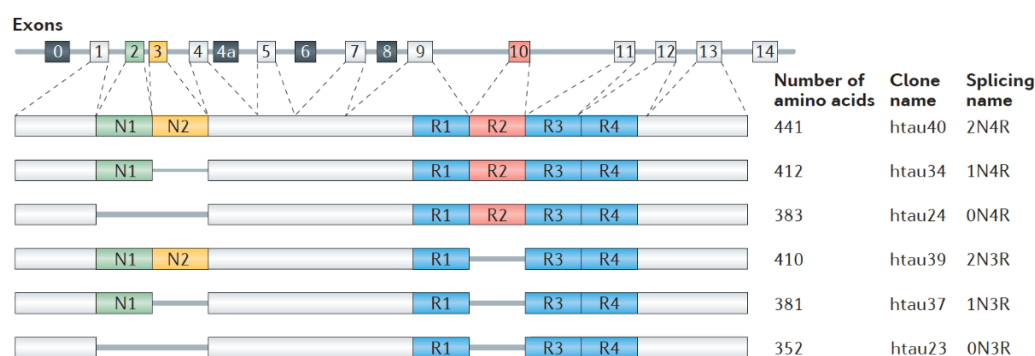


**Figure 2. Human tau splicing variants.** Modified from Wang and Madelkow, 2016<sup>32</sup>

### Tau structure and modifications

Tau functions are strictly dependent on the protein domains. Tau is highly hydrophilic and stable under acidic conditions and high temperatures<sup>43</sup>. Overall tau is a basic protein, nevertheless the N-terminus is acidic and the last 40 residues of the C-terminus are neutral. This charge asymmetry is essential for guaranteeing the interaction with microtubules and others partners, for the internal protein folding and for the aggregation capacities<sup>44</sup>.

Tau protein is organized in four functional domains: the N-terminal region (NTR) or projection domain, the proline rich region (PRR), the microtubules binding domain (MTBD) and the C-terminal assembly region<sup>30</sup>. All these domains are not functionally independent but are dependent on their intramolecular interaction<sup>31</sup>.

The NTR domain projects away from the microtubules for interacting with other cytoskeletal and cytoplasmic proteins or organelles. This domain seems to be involved in tau subcellular distribution, signaling and aggregation. Since tau isoforms including E2 are specifically targeted to the nucleus, it was proposed that the NTR domain has a role in DNA, RNA and chromatin interaction<sup>45</sup>.

The PRR domain is highly enriched in proline residues conferring to this region rigidity and basicity<sup>46</sup>. This domain possesses several serine and threonine, important targets for kinases and phosphatases. The proline rich domain regulates tau phosphorylation promoting microtubules assembly and stability<sup>31</sup>. Being positively charged the MTBD makes electrostatic interactions with the negative charges of tubulin thus promoting microtubules stability, axonal transport and other important functions involving cytoskeleton such as cellular division and intracellular proteins and organelles trafficking<sup>32</sup>. MTBD is responsible for tau self-aggregation and polymerization in filaments and neurofibrillary tangles<sup>47</sup>. The C-terminal region contributes to microtubules binding and interacts with the N-terminal region, this interaction is crucial for tau physiological functions and prevents tau aggregation<sup>31</sup> (**Figure 3**).

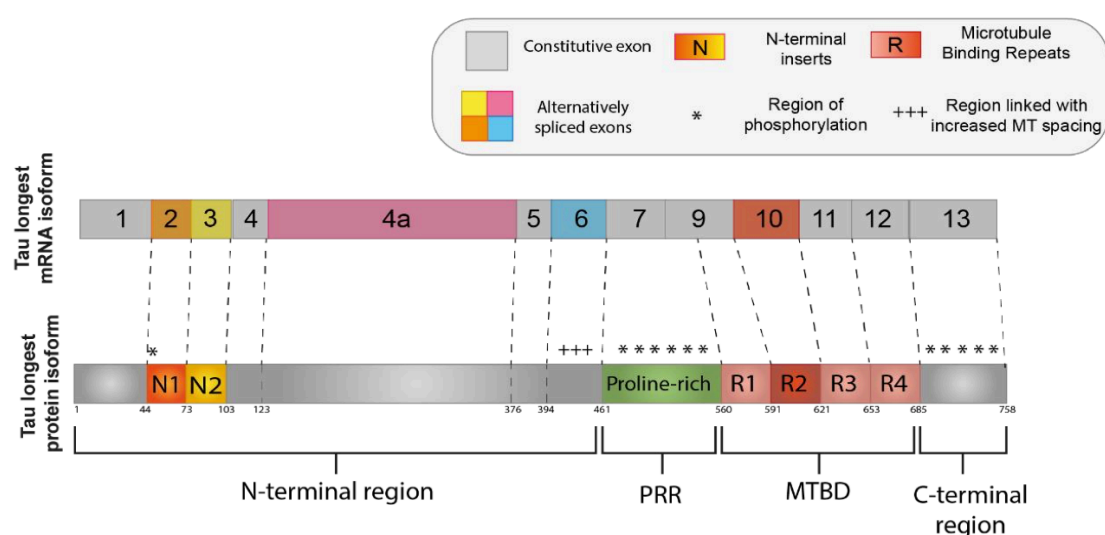


**Figure 3. Human tau mRNA and protein domains.** Modified from Corsi et al, 2022<sup>31</sup>

### ***Tau post-translational modifications***

Post-translational modifications (PTMs), especially on unfolded protein such as tau, are essential in determining the protein functionality, localization, and proteins-proteins interactions in physiological and in

pathological conditions. Importantly, PTMs can affect tau proteostasis and clearance subsequently influencing tau aggregation in diseases. Almost 35 % of the full length 2N4R tau is subjected to PTMs including phosphorylation, acetylation, ubiquitination, SUMOylation, methylation, glycosylation, truncation, protonation, nitration and oxidation<sup>48</sup>.

Tau contains 85 sites potentially subjected to phosphorylation: 45 serine, 35 threonine and 5 tyrosine residues<sup>49</sup>. Phosphorylation alters tau conformation by adding negative charges and this structural change is often associated with the appearance of pathological tau forms. Abnormal tau hyperphosphorylation leads to reduced microtubules binding affinity resulting in the formation of toxic aggregates. Importantly, tau phosphorylation is an event occurring as well in physiological conditions: in healthy brains almost 20 phosphorylated sites are observed<sup>50</sup>. In tauopathies 44 phosphorylated sites are identified; some of these sites are overlapping between controls and patients indicating that tau, during the disease course, is presenting an abnormal pattern of hyperphosphorylation rather than having specific pathological phosphorylation sites<sup>48</sup>. Transient serine and threonine phosphorylation represents the signaling motifs for tau degradation and if the degradation is blocked, these phosphorylations persist. The dynamic equilibrium of tau phosphorylation and dephosphorylation is guaranteed by different kinases and phosphatases<sup>50</sup>. Kinases can be classified in three main groups: **1)** proline-directed protein kinases (PDPK) which include mitogen-activated protein kinase (MAPK), glycogen synthase kinase-3 (GSK3), stress-activated protein kinase (SAPK) and cyclin-dependent kinases (cdK2 and cdk5), **2)** the non-PDPK including microtubule affinity-regulating kinase (MARK), Ca<sup>2+</sup>/calmodulin-dependent protein kinase II (CaMPK II), cAMP-dependent protein kinase A (PKA) and casein kinase II and **3)** tyrosine kinases such as FYN, SYK and SRC<sup>50</sup>. Tau dephosphorylation is mainly mediated by phosphatases and the protein phosphatase 2A (PP2A) accounts for almost 70% of tau dephosphorylation. Interestingly, PP2A activity is reduced by 50% in AD brains<sup>51</sup>. Overall, pathological tau hyperphosphorylation seems to be the result of a disequilibrium of the complex interplay between kinases and phosphatases activity. A degree of complexity is added considering that kinases and phosphatases can regulate multiples sites of tau, it is therefore complicated to identify which specific phosphorylation sites are responsible for the pathology.

10% of the full-length 2N4R tau is possibly subjected to acetylation. Incorporation of acetyl coenzyme-A on lysine residues neutralizes the positive charges of the protein leading to conformational changes. Tau acetylation is mediated mainly by the histone acetyl transferase CREB-binding protein (CBP) on the microtubule binding domain<sup>52</sup>. Histone deacetylase 6 (HDAC6) and the NAD<sup>+</sup>-dependent sirtuin 1 deacetylase (SIRT1) are the major tau deacetylases. SIRT1 has a protective role on tau aggregation whereas, on the contrary, HDAC6 contributes to increase tau aggregation<sup>52</sup>. While increase of CBP was observed in FTLD-tau patients, CBP levels and activity were found lower in the AD frontal cortex and hippocampus<sup>48</sup>, indicating that tau acetylation may vary between the different tauopathies. Importantly specific lysine residues acetylation can have precise effect on tau fate, for instance acetylation at residue K280 reduces tau affinity to microtubules destabilizing microtubules network and acetylation on K174 residue induces tau aggregation without affecting microtubule domain<sup>53</sup>.

Full length tau possesses 17 lysine residues sensitive to ubiquitination, these lysines are mainly located in the microtubule binding domain. Tau can be ubiquitinated by three E3 ligases: the C-terminus of Hsc70-interacting protein (CHIP), TNF receptor-associated factor 6 (TRAF6) and axotrophin/MARCH7. CHIP mediates proteasomal and autophagic-lysosomal clearance through K48 and K63 linkage, TRAF6 mainly ubiquitinates K63 degrading tau through the auto-lysosomal pathway<sup>48</sup>. Interestingly, ubiquitin has been found in aggregates

and insoluble forms of tau deriving from AD brain with modification at K48. These observations indicate that soluble and aggregated tau are degraded differentially<sup>54</sup>.

Tau can be SUMOylated at the N-terminus of lysine residues especially in the microtubule binding domain. Little is known about tau SUMOylation and its effects are controversial. For instance K340 SUMOylation inhibits tau ubiquitination and consequent proteasome-degradation resulting in aggregates formation<sup>48</sup>, however previous findings demonstrate that proteasome inhibition stimulates tau ubiquitination and subsequently eliminates SUMOylated tau via other degradative pathways. In fact, SUMOylated tau can be degraded via pathways involving autophagy: a recent study showed that SUMO1 lysosomes were enriched with tau aggregates in oligodendrocytes of PSP patients<sup>55</sup>.

Tau methylation occurs on lysine and arginine residues and tau methylation pattern seems to change especially during aging rather than disease progression. Methylation occurs mainly in the microtubule binding domain suppressing tau's microtubular functions<sup>56</sup>.

N-glycosylated tau was only found in AD brains, and it was suggested that N-glycosylation promotes tau hyperphosphorylation enhancing phosphorylation and suppressing dephosphorylation. On the contrary, specific tau O-glycosylation plays protective roles preventing tau phosphorylation by a competition mechanism, increasing tau affinity to microtubules and enhancing tau degradation<sup>57</sup>. Tau glycation was observed on lysine residues of the microtubule-binding domain of AD patients suggesting its potential detrimental role in disease progression<sup>48</sup>.

Tau can undergo proteolysis into smaller peptides through cytosolic proteases including caspases, calpains and thrombin<sup>58</sup>. Tau proteolysis can exert either a protective role promoting the removal of abnormal tau or being harmful favoring modified cleaved tau accumulation. Importantly, the toxic nature of tau fragments has not been demonstrated yet. Tau N-terminus truncation alters tau localization from cytosol to nucleus<sup>59</sup>.

Other additional important PTMs can affect tau fate: histidine protonation, cysteine oxidation, tyrosine nitration leading to changes in protein conformation, protein charge, protein solubility and stability consequentially affecting tau functionality<sup>44</sup>.

Overall, the combination of PTMs on tau in physiological and in pathological conditions makes very difficult to understand which tau PTMs have the highest impact on tau physiology and which specific PTMs represents the best candidate for being pharmacologically targeted.

## **Tau prion-like transmission**

Abnormally modified tau can spread from the original site of deposition to anatomically connected regions by a prion-like mechanism<sup>60</sup>. This propagation occurs transferring abnormal tau seeds, oligomers or aggregates able to self-replicate, from one donor cell to a recipient cell through the recruitment and conversion of physiological tau into new pathological tau forms. Propagation of pathological tau through a prion-like mechanism includes four main phases: 1) aberrant tau should be released from donor cells, 2) pathological tau must be uptaken by recipient cells 2) aberrant tau act as template and induce seeding in recipient cells and 3) the new pathological seeds are secreted and transferred intercellularly through synaptic and non-synaptic pathways like direct secretion or packed into extracellular vesicles<sup>61</sup>.

Aggregated tau can be taken up by several mechanisms including direct membrane fusion, clathrin-mediated endocytosis<sup>62</sup>, micropinocytosis<sup>60</sup>, heparan sulfate proteoglycans (HSPGs)-endocytosis<sup>63</sup>, extracellular

vesicles (exosomes and ectosomes) uptake<sup>64</sup>, through physical connections termed nanotubes<sup>65</sup> or via receptor mediated endocytosis. As illustrated in the study of Takahashi et al., endocytosis of hyperphosphorylated tau can occur through APP acting as a receptor in SH-SY5Y overexpressing cells<sup>66</sup>. Following the uptake, seeds must escape from the endocytic/lysosomal compartments and access to the cytosol. In the cytosol, antiparallel misfolded tau dimer containing  $\beta$ -sheets structures acts as a template and converts normal tau into amyloid-like fibrils<sup>62</sup>. Importantly, the aggregation competent portion of tau must include the microtubule binding domain as the fibrils formation is strictly dependent of the two hexapeptide motifs 275VQIINK<sub>280</sub> and 306VQIVYK<sub>311</sub> located at the beginning of the 2R or 3R respectively<sup>67</sup>. However, the minimal unit for seeding is still subjected to debate and most of the studies agreed that soluble tau oligomers are the most seeding prone species<sup>68</sup>. Under physiological conditions tau MTBD is positively charged, and it efficiently interacts with negative charged tubulin residues. When MTBD is modified, for example becoming more negatively charged through hyperphosphorylation, it is not able anymore to interact with tubulin and it detaches from microtubules. Reduced tau affinity to microtubules results in an increase of the free pool of soluble modified tau leading to a propensity of aggregates formation and higher probability to interact and convert the endogenous unmodified tau<sup>60</sup>. Interestingly polyanionic compounds such as RNA<sup>69</sup>, heparin or negative lipid micelles<sup>70</sup> can neutralize the positive charge of tau MTBD thus favoring tau aggregation. Importantly prion-like transmission relies on the templated seeding capacity, this means that morphologically distinct tau seeds induce the formation of aggregates that resemble the parental one<sup>71</sup>. This aspect is highly relevant especially considering the heterogeneity of human tauopathies. Supporting this idea several studies have demonstrated that injection of specific seeds deriving from determined tauopathies in the brain of mice expressing non aggregated tau led to the formation of the corresponding tauopathies inclusions<sup>72</sup>. It is important to highlight that in addition to the high seeds strains heterogeneity there are differences in the seeding competence of these different strains. For instance tau seeds extracted from brain homogenates are 10 fold more seeding capable than the equivalent aggregates produced *in vitro*<sup>73</sup>. Lastly, different pathological tau strains exert dissimilar mechanisms of toxicity, for example soluble hyperphosphorylated tau (monomeric or small oligomeric aggregates) causes neuronal dysfunction due to loss of functions effects like impairments in the cytoskeleton integrity, disrupted axonal transport and synaptic dysfunction. Tau oligomers and small fibrils, forms mainly involved in the prion-like propagation, are associated with toxicity due to a gain of toxic functions. In contrast the toxicity of larger insoluble oligomers and tangle-like structures is still debatable with some studies stating they are toxic and other protective<sup>74</sup>.

In human, tau prion-like propagation theory is highly supported by the anatomical evidences observed for instance during AD progression where at the beginning of the pathology neurofibrillary tangles are present in the hippocampus, basal nucleus of Meynert and the brainstem spreading progressively in interconnected regions like the neocortex. Importantly the spatio-temporal progression of the pathology correlates as well with the symptoms progression <sup>68</sup> (**Figure 4**).



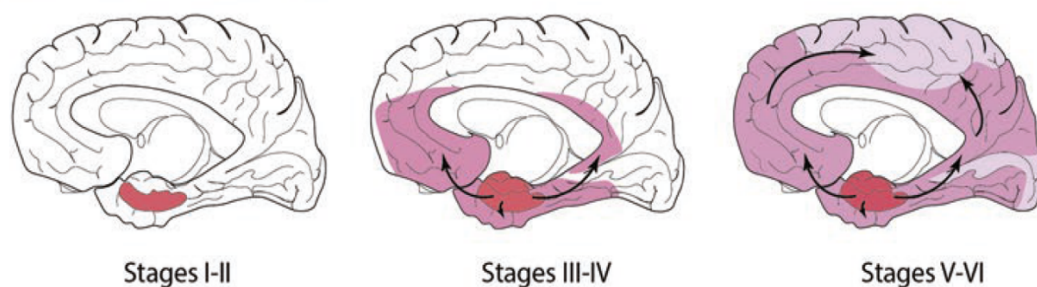


**Figure 4. Alzheimer's Disease prion-like propagation.** Modified from Takashima et al, 2019<sup>68</sup>

### **Extracellular vesicles (EVs) and neurodegeneration**

Signal sensing and delivery between cells is known as intercellular communication and comprises a range of molecular and biophysical mechanisms. Cells can interact through a direct contact between cellular membranes in which their surface proteins or glycoproteins can interact with the ligand-receptor specificities and the signals can be transduced. However, cells can communicate as well through indirect contacts relying on the secretion of factors diffusing in the extracellular medium. The secreted factors specialized in intercellular communication have been studied extensively and are categorized as hormones, cytokines, chemokines, growth factors, neurotransmitters, proteins, lipids, nucleic acids and carbohydrates eventually resulting in the alteration of the surrounding neighbor cells<sup>75</sup>. In the late 60's and 70's, extracellular vesicles (EVs), initially called "platelet dust", then "vesicles", then "exosomes", were observed in the extracellular medium and described as ways of disposal of undesired compounds for the cell<sup>76</sup>. After some years of research, besides this function, EVs were also recognized as a new type of messenger that allowed cells to communicate. EVs are a portion of the cytosol of the originating cells enclosed by a lipid bilayer deriving from the membrane of the same cell and then released to the external medium. Differently from other secreted factors, they are a nano- to micro-size packages of information, carrying a complex selection of lipids, proteins, genetic material and metabolites<sup>41</sup>. EVs are highly heterogenous in terms of composition and physicochemical properties, since their content and shape depend on the place where they originated: from which cell type, in which state they were and from which subcellular compartment the EV budded. Heterogeneity also arises from the mechanism of generation: several molecular mechanisms are described for the EVs biogenesis and they leave traces and make a selection of the components that the EV will carry<sup>77</sup>.

EVs play critical roles in physiological processes like synaptic transmission and nerve regeneration, however they are implicated as well in pathological processes like aberrant protein aggregates propagation resulting in the neurovegetative disease spread<sup>78</sup>. Importantly, there are still lacking clear evidences describing the exact molecular mechanisms regulating tau secretion into EVs and its consequent pathological effect on recipient cells<sup>79</sup>.

### **Canonical and non canonical tau seeding locations**

To propagate in a prion-like manner, tau aggregates must transit between cells and cross cell-limiting membranes, a process that is poorly understood. Tau uptake seems to be highly efficient, but importantly only 1-10% of internalized tau exhibits a seeding capacity<sup>80</sup>. One limiting step is that pathological tau has to encounter the endogenous tau and then induce its pathological conformational change. The mechanisms and

the subcellular localization underlying this contact are not still fully elucidated but the majority of the studies report the cytoplasm as main cellular site where seeding nucleation can occur<sup>81</sup>.

However, if tau seeds are internalized via an endocytic mechanisms before reaching the cytoplasm they are confined in endosomes and it was demonstrated that blocking endosomes maturation results in seeds trapping and consequent reduced tau seeds propagation<sup>82</sup>.

Overexpression of tau in rats increases LC3-II and tau accumulation in immature autophagic vacuoles. Additionally, it was observed that AD brains are enriched in autophagic vacuoles<sup>83</sup>. These observations suggest that autophagy is not merely deputed to tau aggregates clearance but in some cases enhanced autophagy and/or impaired autophagy completion may contribute to the disease progression. Lysosomes are degradative organelles thereby playing a role in tau aggregates clearance. However, a recent study reported that some specific lysosomal enzymes like cathepsin-L in N2A cells are enhancing aggregates formation promoting mutant  $\Delta$ K280 tau cleavage and favoring the formation of pro-aggregating fragments<sup>84</sup>. Additionally, we described that prion-like transmission of pathogenic forms of tau can occur in acidic organelles of cells. More precisely, exogenous pro-aggregating tau seeds transported by extracellular vesicles (EVs) induced tau accumulation in lysosomes of murine C17.2 cells<sup>42</sup>. Lastly, even the nucleus has been proposed as a new potential site for tau aggregation. In fact, the study of Montalbano et al. demonstrated that mutated tau interacts with the Musashi (MSI) RNA-binding leading to a shift in its localization and consequentially alter its function, triggering neurodegeneration and toxic tau aggregation<sup>85</sup>. All these studies highlight a high degree of complexity in the role of the autophagic compartments in the disease progression and they may indicate that the cytoplasm does not represent the unique site for pathological tau seeding.

## Degradative systems in neurodegeneration

Post-mitotic neurons are more sensitive to cytotoxic proteins accumulation due to several factors. Firstly, they cannot dilute toxic substances by cell division as compared to proliferating cells. Secondly, protein clearance in neurons is intrinsically more challenging due to the dendrites and axons in which protein aggregates need to be packaged into autophagic vacuoles and retrogradely transported to the cell body where lysosomes are mainly located<sup>86, 87</sup>. To maintain protein homeostasis, cells remove misfolded proteins using various proteolytic systems including ubiquitin (Ub)-proteasome system (UPS), chaperon mediated autophagy (CMA) and macroautophagy. Most misfolded proteins are degraded by the UPS in which Ub-conjugated substrates are deubiquitinated, unfolded and cleaved in small peptides<sup>88</sup>. CMA rely on the exposure of the substrates degradation motif KFERQ recognized by the heat shock chaperon 70 (Hsc70) and delivered to lysosomes where there are degraded by acidic hydrolases<sup>89</sup>. Substrates resistant to UPS and CMA can be degraded by macroautophagy in which cargoes are enclosed in autophagosomes before fusing with acidic lysosomes<sup>88</sup> (Figure 1).

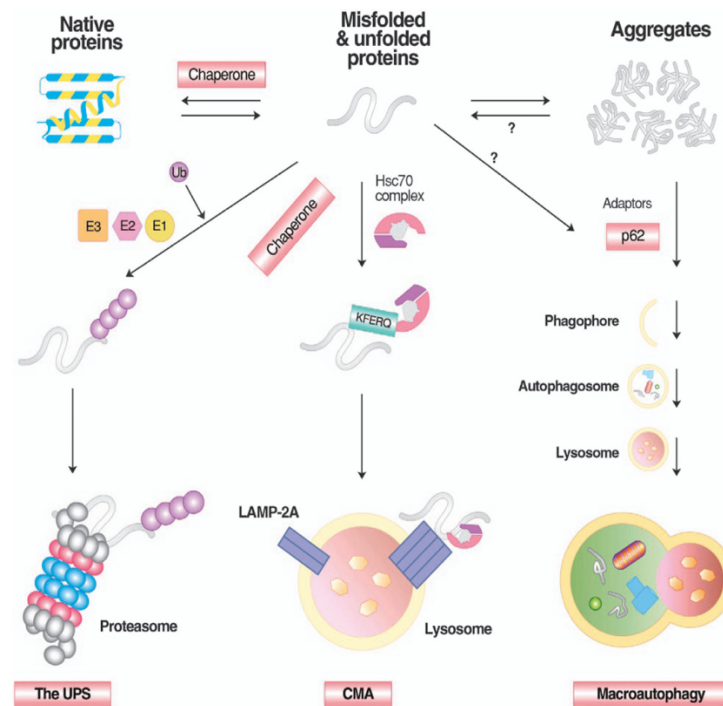


**Figure 1. Cellular proteolytic pathways for misfolded protein degradation.** Modified from Chiechanover and Kown, 2015<sup>88</sup>

Under stress conditions (for example starvation or elevated temperatures) intrinsically disordered soluble proteins undergo structural changes and self-assemble ultimately leading to their accumulation into insoluble deposits and cell death. Cellular cytotoxicity can be due to direct effects interfering with various cellular functions like for instance reducing the autophagic-lysosomal degradation capabilities or indirectly sequestering other proteins which play essential cellular functions<sup>8</sup>. Almost all the proteins can be efficiently removed from cells when misfolded, however a part of polypeptides especially post-translationally modified (such as hyperphosphorylated tau) or proteolytically cleaved (like amyloid  $\beta$  peptides) tend spontaneously to misfold and rapidly aggregate into oligomers enriched in  $\beta$ -sheet structures resistant to proteolytic degradation. The oligomers can further grow and form inclusion bodies or extracellular plaques characterized by fibrillary structures leading to consequent cytotoxicity and neuronal death<sup>90</sup>. The signal for targeting unfolded proteins to the UPS is the polyubiquitination. Polyubiquitination consists in adding to the lysine residues of the targeting protein four or more molecules of ubiquitin, containing itself seven lysines<sup>5</sup>. Proteins ubiquitination requires the coordination of different ubiquitin ligases E1, E2 and E3<sup>91</sup> and ubiquitin polyubiquitination at lysine (K48) represents the canonical signal for proteasomal degradation especially for short half-living proteins<sup>88</sup>. The polyubiquitinated protein is recognized by the proteasomal 26S barrel-shape structure containing a channel where the target protein is enzymatically processed. During the degradation ubiquitin is released by deubiquitinating enzymes and recycled<sup>92</sup>. The pathogenesis of neurodegenerative diseases is partially associated with downregulation of the UPS and one of the major risk factor for reduced UPS capabilities is aging<sup>5</sup>. In addition recent studies demonstrate that aggregates of many proteins can directly inhibit proteasome activity: for instance in AD aggregated tau can block the gate of the proteasome occupying its recognition site<sup>93</sup>. Autophagy consists in the degradation of cytoplasmic constituents by lysosomes and it can be divided mainly in microautophagy, chaperon mediated autophagy (CMA) and macroautophagy. Microautophagy relies

on the direct engulfment of the cytoplasmic cargo into lysosomes by a random process of lysosomal membrane invaginations. Recent studies have described two main microautophagic pathways: the fusion-type microautophagy requiring the autophagic machinery and the soluble N-ethylmaleimide-sensitive factor attachment proteins (SNARE) complex, and the most common fission-type microautophagy involving endosomal sorting complexes required for transport (ESCRTs) allowing membrane scission or budding<sup>94</sup>. The CMA consists in the selective exposure of the pentapeptide KFERQ that normally is hidden in properly folded proteins, once proteins start to unfold the KFERQ motif is exposed and recognized by the chaperone Hsc70 and additional cochaperones, delivered to the lysosomal membrane-associated protein 2A (LAMP2A) present on the lysosomal membrane successively translocated into the lysosome's lumen<sup>95</sup>. In macroautophagy, long half-life unfolded proteins and dysfunctional organelles are segregated in double membrane structures called autophagosomes and subsequently digested by lysosomal hydrolases. Neurons exhibit a high basal autophagic rate and autophagosomes turnover occurs rapidly; however in neurodegenerative diseases autophagic vesicles have the tendency to accumulate. It remains unclear whether autophagic vacuoles accumulation reflects an initial neuroprotective response or if it is the result of an autophagic dysfunction<sup>96</sup>. Macromolecules autophagy initiation requires the inhibition of the mechanistic target of rapamycin (mTOR), which normally suppresses ULK1 activity, and/or the activation of 5'AMP-activated protein kinase (AMPK) which in turn phosphorylates ULK1 complex allowing membrane nucleation, elongation and maturation<sup>97</sup>. Additionally, several observations have demonstrated that nutrients deprivation can induce autophagy via an independent-mTOR complex 1 inhibition pathway, through the nuclear translocation of the transcription factor EB (TFEB). TFEB is a master gene regulator involved in lysosomal biogenesis<sup>98</sup>. Importantly in SBMA, the mutated androgen receptor interferes with TFEB transactivation resulting in autophagy dysregulation<sup>96</sup>. The delivery of misfolded proteins to the autophagosomes requires specific adaptor p62/SQSTM-1/sequestosome. The ubiquitin binding protein p62 firstly interacts with the polyubiquitinated chain of misfolded proteins through its ubiquitin association domain and then the cargo is delivered to the active light chain 3-II (LC3-II) present on the membrane of autophagic structures<sup>88</sup>. Normally microtubule-associated 1A/1B-light chain (LC3) is a soluble protein and during autophagic processes a specific cytosolic LC3 form, termed LC3-I, binds to phosphatidylethanolamine to form LC3-phosphatidylethanolamine conjugate, LC3-II. LC3 lipidation is regulated by other cellular autophagic factors such as ATG5, ATG7 and ATG12 recruiting additional autophagosomal membranes forming autophagosomes that finally will fuse with lysosomes generating autolysosomes where the engulfed proteins, p62 and LC3-II will be degraded<sup>99</sup>. Importantly, mutation in p62 gene have been associated with the pathogenesis of familial and sporadic forms of ALS<sup>100</sup>. Extensive studies have shown that during aging many components of the UPS, CMA and macroautophagy display a reduced activity and are transcriptionally and translationally downregulated<sup>95, 97</sup>. Recent studies have shown that if cells accumulate excess of misfolded proteins they react in trying to temporally store them in specific cytosolic inclusions, termed aggresomes. In this process the histone deacetylase 6 and other chaperones bind the floating ubiquitinated aggresomes and deliver them via microtubules to cellular locations where their toxicity is minimized and can be degraded<sup>101</sup>. Overall, age-associated autophagy dysregulation possibly due to impaired lysosomal fusion and/or degradation is associated to cellular dysfunctions contributing to neurodegeneration.

## Neurodegeneration and lysosomal storage disorders

Lysosomal storage diseases (LSDs) are a group of metabolic diseases caused by inherited defects in lysosomal or non-lysosomal proteins leading to subsequent accumulation of undegraded substrate in lysosomes and global dysfunctions often associated with neurodegeneration<sup>102</sup>. Defective lysosomal storage typically occurs in many cell types and in particular in the nervous system, with the two third of LSD cases associated to major nervous system symptoms. LSDs linked with central nervous system (CNS) and peripheral nervous system (PNS) include Gaucher disease (GD), Krabbe disease (KD), Sandhoff disease (SD), Niemann-Pick type C (NPC), mucopolysaccharidoses and neuronal ceroid lipofuscinoses (NCLs rereferred as Batten disease)<sup>103</sup>. In LSD the mechanisms underlying neuronal degeneration are not completely understood. Initially it was thought that mainly defective biomolecule degradation was contributing to neuronal loss but recently new mechanisms have been identified like mitochondrial dysfunction<sup>104</sup>, calcium homeostasis perturbation<sup>105</sup>, astrocytosis<sup>106</sup> and axon demyelination<sup>107</sup>.

### Gaucher disease

Gaucher disease (GD) is a rare severe neurological sphingolipidosis with an incidence of 1:50'000 in the global population. GD is caused by recessive missense, nonsense and frameshift mutations in the glucocerebrosidase (*GBA1*) gene<sup>102</sup>. This gene is located in chromosome 1q21 neighbored by a pseudogene and it comprises 11 exons. It encodes for the lysosomal enzyme  $\beta$ -glucocerebrosidase (also called acid  $\beta$ -glucosidase, GCase or GBA1), a lysosomal enzyme fully active at acidic pH. GCase consists in 497 amino acids and 5 glycosylation sites. GCase catalyzes two main reactions 1) the hydrolysis of the  $\beta$ -glycosidic linkage of glucosylceramide (or glucocerebroside) into glucose and ceramide<sup>108</sup> or the hydrolysis of glucosylsphingosine into glucose and sphingosine (**Figure 5.**)<sup>109</sup>. Glucosylceramide is an intermediate glycolipid fundamental for cell membranes constitution<sup>110</sup>. Importantly the GCase activity is promoted by negative charged lipids and saposin C, an activator protein present in lysosomes<sup>108</sup>. In lysosomes, GCase has a short half-life due to its continuous proteolytic degradation mediated by lysosomal cathepsins<sup>111</sup>.

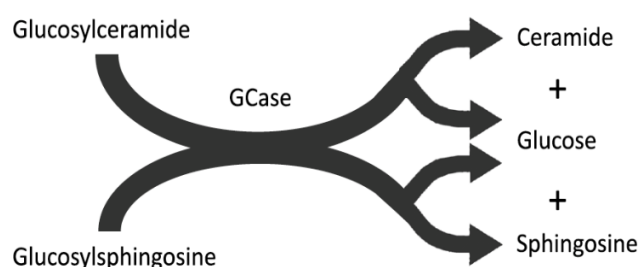


**Figure 5. GCase enzymatic reaction.** Modified from Do et al, 2019<sup>112</sup>.

While most of lysosomal hydrolases are transported to lysosomes by mannose-6-phosphate receptor, this is not the case of GCase. GCase folding occurs in the endoplasmic reticulum (ER) and there it binds to the lysosomal membrane protein 2 (LIMP2) and successively the GCase-LIMP2 complex is transported to lysosomes<sup>113</sup>. More recently, progranulin acting as chaperon was identified as additional factor facilitating GCase lysosomal transport<sup>114</sup>.

Gaucher disease is characterized by the progressive lysosomal accumulation of glucosylceramide and glucosylsphingosine especially in macrophages of bone, bone marrow, liver and spleen<sup>115</sup>. Importantly

glucosylceramide substrate accumulation indirectly leads to an increment of other secondary lipids such as: ceramide, di- and trihexosylceramide, phosphatidylglycerol and cholesterol<sup>116,117</sup>. Clinically GD patients manifest hepatosplenomegaly, hematological abnormalities, skeletal diseases and in some cases a very severe manifestation, termed collodion baby, impairing skin barriers<sup>118</sup>. GD is classified in three major phenotypic subcategories: a) Gaucher Type 1 constitutes 94% of the cases, with a late onset and considered non-neuronopathic b) Gaucher Type 2 accounts 1% of the cases, with an infantile or prenatal onset, neuronopathic and characterized with a short-life expectancy of 2-3 years c) Gaucher Type 3 accounts for 5% of the cases, with an early onset, neuronopathic with mild CNS manifestations and with a longer survival compared to Gaucher Type 2<sup>115</sup>.

The point mutations N370S and L444P are the most common mutations associated to GD. The N370S mutation, observed in Gaucher Type-1 patients, results in the production of mutant GCase enzyme with aberrant catalytic activity<sup>119</sup>. Instead, L444P mutation, probably arisen from homologous recombination of *GBA1* and its pseudogene, leads to GCase unfolding. The unfolded enzyme is retained in the ER and it triggers the unfolded protein response (UPR) leading to its ER degradation. In fact only 10% of the enzyme reaches the lysosomes<sup>120</sup>. Currently there are three therapies for GD: one relying on the enzyme replacement, the second aiming at decreasing substrate storage and the third using chemical chaperons for promoting proper enzyme folding<sup>121</sup>.

### **Gaucher disease and neurodegeneration**

In recent years heterozygous or biallelic *GBA1* mutations have been identified as key genetic risk factors for developing PD and related synucleopathies<sup>109</sup>. Importantly, *GBA1* homozygous carriers display between 6 to 11 years of earlier disease onset compared to heterozygous<sup>122</sup>. Most studies estimate that 5–15% of PD patients have *GBA1* mutations, and additionally patients affected by sporadic PD show a decreased glucocerebrosidase activity<sup>123</sup>. Despite *GBA1* mutations represent an increased risk factor for developing PD, only a minority of *GBA1* carriers develop PD. In *GBA1*-mutated PD brains it was possible to observe an increased  $\alpha$ -synuclein deposition. Possible explanations rely on gain and loss of function mechanisms. For the gain of function theory, it was shown that misfolded glucocerebrosidases induced lysosomal insufficiency by impairing autophagic process, resulting in an increased  $\alpha$ -synuclein aggregation in cultured neurons<sup>124</sup>. *In vitro* studies further demonstrated that overexpression of *GBA* mutants promoted  $\alpha$ -synuclein aggregation in a dose and time-dependent manner<sup>125</sup>. Loss of function theories are based on the accumulation of glucocerebrosidase substrates and other polyunsaturated lipids altering cell membrane sphingolipid composition. These membrane alterations consequentially favor  $\alpha$ -synuclein detachment from plasma membrane and increase its propensity to aggregate in the cytoplasm<sup>126</sup>. Recent observations highlight that toxic  $\alpha$ -synuclein trigger depletion of lysosomal *GBA1* resulting in a further  $\alpha$ -synuclein oligomers stabilization enhancing a self-propagating loop<sup>124</sup>.

The relationship between LSDs and tau aggregation has been less intensively investigated compared to  $\alpha$ -synuclein aggregation. However, recent studies highlight how LSDs can affect aggregation of other proteins. For instance, tau aggregates were detected in brain of mice modelling GD and other LSDs like Fabry disease and Hurler disease<sup>127</sup>. Interestingly, cultured wild-type cortical neurons treated with the *GBA1* irreversible inhibitor conduritol B epoxide (CBE) showed, in addition to glucosylceramide and glucosylsphingosine

substrate accumulation, the presence of  $\alpha$ -synuclein and APP aggregation<sup>128</sup>. It is therefore important to understand the link between LSDs and protein depositions as this knowledge could potentially allow to identify new therapies for treating neurodegenerative disease.

## RESULTS

### **Hypothesis and study design: *Tau Seeds in Extracellular Vesicles Induce Tau Accumulation in Degradative Organelles of Cells***

Extracellular vesicles (EVs) are lipid bilayer-delimited particles secreted by cells in the extracellular medium and have been identified as important mediators of intercellular communication and interactors with the surrounding extracellular matrix. EVs carry various cargoes, including proteins, that can deliver signals to induce physiological and pathological changes in recipient cells. Current research indicates that EVs are involved in the pathology of different neurodegenerative diseases such as AD, PD, HD and MS<sup>129</sup>. In proteinopathies, misfolded proteins spread in a prion-like manner from one original site to defined brain regions through different mechanisms not yet fully elucidated. Among them, one possible way of transmission relies on EVs<sup>130</sup>.

**We hypothesized that pro fibrillogenic forms of tau could spread from one cell to the other through EVs.** To study this transcellular propagation, we had firstly to establish a cellular system. We generated EVs overexpressing a pro aggregating tau fragment (TauMBD, the fragment encoding for the microtubule binding domain) isolated from donor murine neuronal progenitor C17.2 cells and successively incubated in recipient cells. In recipient cells, we investigated if EVs were internalized, if the content was released and which subcellular localization was involved in cargo unloading. We demonstrated that endogenous tau (2N4R/Tau 441) through autophagy modulation was encountering exogenous TauMBD carried by EVs in degradative organelles of cells and there starting to accumulate and switching phenotype through a more pathological one.

The following section will expose the study through the published manuscript entitled: ***Tau Seeds in Extracellular Vesicles Induce Tau Accumulation in Degradative Organelles of Cells***, in which I contribute mainly in the revision part and I am a co-author. I was mainly involved in the execution of experiments elucidating TFE3 role: experiments for evaluating TFE3 nuclear translocation and its transcription factors activation through qRT-PCR of Lamp1, p62 and RagC. Additionally, I generated the pseudo-lentivirus for knocking down (KD) ULK1 and performed the experiments modulating autophagy flux in this condition.



DNA AND CELL BIOLOGY  
Volume 40, Number 9, 2021  
© Mary Ann Liebert, Inc.  
Pp. 1185–1199  
DOI: 10.1089/dna.2021.0485

## Tau Seeds in Extracellular Vesicles Induce Tau Accumulation in Degradative Organelles of Cells

Giona Pedrioli,<sup>1,2</sup> Marialuisa Barberis,<sup>1</sup> Claudia Magrin,<sup>1,3</sup> Diego Morone,<sup>4,i</sup> Ester Piovesana,<sup>1,3</sup>  
Giorgia Senesi,<sup>1,5</sup> Martina Sola,<sup>1,3</sup> Stéphanie Papin,<sup>1</sup> and Paolo Paganetti<sup>1,3,ii</sup>

Clinical progression of tauopathies may result from transcellular propagation of pathogenic Tau seeds with the possible involvement of extracellular vesicles (EVs) as transport vectors. We established a cell model for investigating EV delivery of proteins, since the mechanism regulating EV cargo delivery to recipient cells is poorly understood. In our cell model, EVs are readily internalized and accumulate in degradative organelles (DOs). We then show for the first time that in this acidic compartment, profibrillogenic Tau delivered by EVs interacts with Tau expressed by the recipient cells and cause its accumulation by a process that involves the participation of autophagy. Thus, the degradative compartment of cells may represent the subcellular site initiating a cascade of events resulting in early hallmarks of tauopathies. These are characterized by seeded Tau accumulation, pathology-associated epitopes, DO stress, and cytotoxicity. The involvement of autophagy to this process and the relative accessibility of the degradative pathway for extracellular agents, support possible modes of intervention to slow down the progression of neurodegeneration.

**Keywords:** extracellular vesicles, degradative organelles, neurodegeneration, Tau

### Introduction

**T**AUOPATHIES ARE A group of progressive neurodegenerative diseases characterized by intracellular fibrillar Tau protein species ultimately deposited in neurofibrillary tangles as a disorder hallmark (Hardy and Selkoe, 2002; Serrano-Pozo *et al.*, 2011). Tangles appear first in disease-specific brain regions and then gradually spread along the neuronal connectivity invading the whole brain. Temporal and spatial tangle distributions correlate with the extent of neuronal loss and with the clinical disease stages (Braak and Braak, 1991). Because similar progressive pathological changes occur in most aging-associated neurodegenerative disorders, these are defined as proteinopathies characterized by disease-specific proteins acquiring gain of toxicity as a consequence of impaired protein homeostasis and accumulation (Freer *et al.*, 2016).

In tauopathies, propagation of Tau involves a prion-like course where pathogenic species self-spread through an unclarified protein-to-protein mechanism that also requires

transmission between cells (Clavaguera *et al.*, 2009; Frost *et al.*, 2009). Among the different means of transcellular transport of macromolecules, extracellular vesicles (EVs) represent paracrine vectors also involved in disease progression (Simons and Raposo, 2009). EVs are implicated in cancer (Kosaka *et al.*, 2010), inflammation (Zhang *et al.*, 2010), and neurodegeneration where EVs carrying replication-competent particles may contribute to brain pathology propagation (Fevrier *et al.*, 2004; Alais *et al.*, 2008).

EVs' communication relies on displaying or transferring cargo molecules produced by a donor cell to a recipient cell (Raposo *et al.*, 1996). RNAs are among the most studied luminal EV cargo molecules, whereby for example, in recipient cell mRNAs are translated into effector proteins or miRNAs regulate gene expression (Valadi *et al.*, 2007; Pegtel *et al.*, 2010; Zhang *et al.*, 2010; Zomer *et al.*, 2015). In contrast, the evidence for a biological function of proteins transported by EVs remains sparse (Skog *et al.*, 2008). The molecular mechanisms regulating EV's cargo delivery in

<sup>1</sup>Neurodegeneration Research Group, Laboratory for Biomedical Neurosciences, Neurocenter of Southern Switzerland, Ente Ospedaliero Cantonale, Lugano, Switzerland.

<sup>2</sup>Program of the Science Research, Biozentrum, University of Basel, Basel, Switzerland.

<sup>3</sup>Faculty of Biomedical Sciences, Università della Svizzera italiana (USI), Lugano, Switzerland.

<sup>4</sup>Faculty of Biomedical Sciences, Institute for Research in Biomedicine, Università della Svizzera italiana (USI), Lugano, Switzerland.

<sup>5</sup>Scienze Biomediche Biomolecolari, Università degli Studi di Pavia, Pavia, Italy.

<sup>i</sup>ORCID ID (<https://orcid.org/0000-0002-6847-3811>).

<sup>ii</sup>ORCID ID (<https://orcid.org/0000-0003-1896-6324>).

recipient cells remain unsatisfactorily understood (Pedrioli and Paganetti, 2020). Direct fusion at the plasma membrane represents the simplest route of delivery (Parolini *et al.*, 2009). Then again, EVs exploit the endocytic pathway as the main route for cell internalization (Mulcahy *et al.*, 2014; Heusermann *et al.*, 2016; Costa Verdera *et al.*, 2017) to reach, similar to nutrients, degradative organelles (DOs) for metabolism and recycling.

DOs represent an acidic subcellular compartment whose main function is the degradation of both intracellular and extracellular material, thus representing a crossroad for two major degradative pathways of the cell, endocytosis and macroautophagy (here referred to as autophagy) (Settembre *et al.*, 2013). Autophagy is a regulated degradation pathway for organelles, long-living cytosolic proteins and aggregates (Wang and Mandelkow, 2012; Lee *et al.*, 2013), and it requires the formation of double-bilayer autophagosomes that engulf and target intracellular material to DOs (Yang and Klionsky, 2010; Nikolettou *et al.*, 2015). Not surprisingly, DOs are key players in regulating cellular proteostasis, and age-associated DO's impairment is a pronounced feature of neurodegenerative diseases, linked to cell stress and death (Wang *et al.*, 2018; Malik *et al.*, 2019).

In this study, we report that DOs represent a subcellular site where a profibrillogenic Tau fragment transported by EVs interacts with, and may accelerate the accumulation of, an intracellular Tau pool. Under these conditions, a number of changes are observed in recipient cells such as acquisition of prepathologic Tau epitopes, DO stress, and cytotoxicity. Notably, our data are evidence that this adverse cascade of events may initiate within the acidic compartment of the host cell, with DOs representing a critical subcellular location for EVs' cargo delivery with disease relevance.

## Materials and Methods

### Cell culturing and plasmid transfections

C17.2 cells (ECACC 07062902) were grown at 37°C with saturated humidity and 5% CO<sub>2</sub> in Dulbecco's modified Eagle's medium (DMEM; Gibco, 61965-059) supplemented with 1% nonessential amino acids (Gibco; 11140035), 1% penicillin–streptomycin (Gibco; 15140122), 10% fetal bovine serum (FBS; Gibco, 10270106), and passaged at 90% confluency. Inducible cells were generated with the Flp-In T-Rex tetracycline-inducible cell system according to the manufacturer's instructions (Invitrogen; K650001) and maintained in the presence of 150 µg/mL hygromycin B (Invitrogen; 10687010) and 15 µg/mL blasticidin S (Gibco; A1113903). Gene expression was routinely induced in the presence of 60 ng/mL tetracycline. To induce autophagy by starvation, cells were washed three times with PBS and incubated at 37°C for 4 h in Hanks' Balanced Salt Solution (Gibco; 14025-050). Transfection of plasmids (Supplementary Data) were performed the day after cell plating with Lipofectamine 3000 (Invitrogen; L-3000-008), following the manufacturer's instructions.

### Coculture paradigms, flow cytometry, cell staining

For the analysis of transcellular transport of proteins, cells stably integrated with the LoxP-DsRed-LoxP-eGFP cassettes were cultured with cells that expressed the protein of

interest in an inducible manner for 72 h in an eight-well chamber (ibidi; 80826). Analysis of the cocultures were performed in-live by laser confocal microscopy, or with a benchtop flow cytometer (Beckman, CytoFLEX) after collecting cells with TrypLE™ (Gibco; 12604021) and resuspension in DMEM without phenol red (Gibco; 21063045) supplemented with 10% FBS. Immunostaining of the cells was performed with established procedures (Supplementary Data).

### Downregulation of ULK1 expression

The short hairpin RNA (shRNA) targeting *ULK1* was obtained from a commercial validated library (Sigma-Aldrich; NM\_009469). MISSION® pLKO.1-puro Non-Mammalian shRNA Control plasmid was used as negative control (Sigma-Aldrich; SHC002). Pseudolentiviral particles were produced in calcium phosphate-transfected (Foglieni *et al.*, 2017) cells (System Biosciences; HEK 293TN) with the pPACKH1 Kit (System Biosciences; LV500A-1). Particles were harvested 72 h post-transfection, concentrated on 30 kDa cutoff filters (Sigma-Aldrich; UFC903024). Aliquots were stored at –80°C until use.

### EV preparation

EVs were isolated from conditioned media by established procedures (Supplementary Data).

### Microscope image analysis

Fluorescence images were acquired with either a laser confocal microscope (Nikon C2) or a Lionheart FX automated microscope (BioTek). Image analysis and processing of the raw data were performed with the Gen5 (BioTek) or Fiji/ImageJ (1.51 g or later) software. Pearson's correlation coefficient (PCC) and Manders' overlapping coefficient (MOC, M1, & M2) were determined with the ImageJ JACoP plugin for dual-color colocalization or the Coloc 2 plugin when a cellular mask was required. For Tau puncta and nuclear TFE3 quantifications, automated analysis of DOs, correlative light-electron microscopy (CLEM), cytotoxicity, and tandem fluorescent-LC3 assay see Supplementary Data.

### Protein analysis

For western blot, total cell lysates were prepared from cells grown in 10 cm plates washed once in PBS and directly lysed in NaDodSO<sub>4</sub>-PAGE sample buffer (1.5% NaDodSO<sub>4</sub>, 8.3% glycerol, 0.005% bromophenol blue, 1.6% β-mercaptoethanol and 62.5 mM Tris pH 6.8), boiled at 96°C for 10 min. For the comparison of the amount of protein of interest in cells and in EVs, 1:20 of total cell lysate and the whole EV preparation in sample buffer were resolved by NaDodSO<sub>4</sub>-PAGE and transferred to PVDF membranes (Bio-Rad; 162-0177), blocked in Odyssey Blocking Buffer (LI-COR; 927-50000) and visualized by infrared on an Odyssey CLx device (LI-COR) using specific primary and secondary antibodies (Supplementary Data). AlphaLISA® was performed as described (Supplementary Data).

### Real-time quantitative polymerase chain reaction

Total RNA extraction (Qiagen RNeasy Micro 74004) and cDNA synthesis with random primers (Promega; GoScript Reverse Transcription A2800) were performed following

## SEEDED TAU ACCUMULATION IN DEGRADATIVE ORGANELLES

1187

the manufacturer's instructions. Amplification (Bio-Rad; SsoAdvanced Universal SYBR<sup>®</sup> Green Supermix 1725271) was performed by 43 cycles (95°C 5 s, 60°C 30 s, 60°C 1 min) with a thermocycler (CFX Connect Real-Time System, Bio-Rad) with specific primers (Supplementary Data). Relative mRNA expression was calculated using the comparative Ct method and normalized to the geometric mean of the *HPRT1* and *GAPDH* mRNAs (Schmittgen and Livak, 2008).

*Statistics and reproducibility*

All the experiments reported were repeated at least in three independent biological replicates. Differences between two means were assessed by two-tailed unpaired student's *t* test, differences between more than two means were tested by ordinary unpaired one-way ANOVA with Tukey's *post hoc* test comparing the mean of each column,  $\alpha=0.05$ , and differences between three groups, each with two conditions tested by unmatched two-way ANOVA corrected for multiple comparison for the mean of each column with Sidak,  $\alpha=0.05$ , if not otherwise indicated in figure legends. A *p*-value  $<0.05$  was applied to assess significances. Statistical analysis and graphs were generated with Prism (GraphPad software version 8).

*Data availability*

All raw data supporting the findings of the study are available from the corresponding author upon request.

**Results***Transport of proteins to DOs of recipient cells is mediated by EVs*

To study transcellular transport mediated by EVs, we opted for immortalized mouse cerebellar C17.2 cells (Ryder *et al.*, 1990), which display seed-induced aggregation of Tau (Frost *et al.*, 2009; Holmes *et al.*, 2013). To validate their competence in exchanging proteins, we generated stable lines expressing fluorescent proteins with different emissions to discriminate donor and recipient cells and the proteins exchanged (Fig. 1A). We established two donor lines with inducible expression of untargeted GFP ( $E_{m,max}=510$  nm) or GFP fused to CD63, an integral membrane tetraspanin efficiently targeted to EVs (Andreu and Yanez-Mo, 2014). GFP-CD63 cells displayed a slightly reduced median fluorescence intensity determined by flow cytometry when compared with GFP cells (Fig. 1B). Conversely, recipient cells expressed DsRed ( $E_{m,max}=583$  nm).

Coculture of donor and recipient cells at a 5:1 seeding ratio led to the appearance of double fluorescent cells when analyzed by flow cytometry (Fig. 1C). The recipient DsRed population showed a  $\sim 2$ -fold increase in GFP intensity in the presence of GFP-CD63 cells when compared with untargeted GFP cells (Fig. 1C). Orthogonal reconstruction of confocal microscopy images showed internalized GFP-CD63 fluorescence with a dot-like distribution in DsRed recipient cells, a pattern clearly distinct from the more homogeneous, cell membrane-associated distribution observed in the GFP-CD63 donor cells (Fig. 1D). We reasoned that the integral membrane protein CD63 was exchanged between cells in the C17.2 coculture paradigm.

To directly assess the involvement of EVs, these were enriched from the medium of donor cells by a standard centrifugation protocol (Gardiner *et al.*, 2016) and then incubated on recipient cells (Fig. 1E). The EV fraction was characterized for size and concentration by nanoparticle tracking analysis (Thery *et al.*, 2018). The GFP-CD63-EV population presented a mode diameter distribution of  $151 \pm 4$  nm (Fig. 1F) with  $\sim 10^9$  particles isolated routinely from a 10-cm dish after 3 days of medium conditioning. Western blot of  $10^9$  EVs showed the relative enrichment of the EV marker ALIX when compared with the mitochondrial marker TOMM20 (Fig. 1G). The targeting of GFP-CD63 to EVs appeared more efficient to that of endogenous ALIX when compared with the respective protein signal in donor cell lysates (Fig. 1G).

Recipient DsRed cells incubated with GFP-CD63-EVs showed the acquisition of GFP fluorescence when analyzed by flow cytometry (Fig. 1H). Internalized GFP-CD63-EVs colocalized with the lysosomal protein LAMP1 fused to mCherry suggesting accumulation within DOs of recipient cells (Fig. 1I), possibly by endocytosis as previously reported (Vogt *et al.*, 2019). Confirming internalization in an acidic compartment, recipient cells incubated with EVs loaded with the pH-sensitive biofluorescent protein pHluorin (Miesenbock *et al.*, 1998) ( $E_{m,max}=509$  nm) fused to CD63 (Fig. 1J, K), displayed increased fluorescence intensity when treated with the proton pump inhibitor bafilomycin A1 as compared with untreated conditions (Fig. 1L). In short, our C17.2 cell assay enabled monitoring transcellular transport and internalization of membrane-bound proteins transported by EVs.

*A profibrillogenic Tau fragment transported by EVs induces stress associated to DOs*

To study the transport of a soluble luminal EVs cargo, we fused GFP to a fragment of Tau matching the microtubule-binding domain with four repeats (GFP-MBD). The MBD fragment was utilized previously to induce transcellular Tau propagation because of its profibrillogenic activity (Frost *et al.*, 2009; Michel *et al.*, 2014). The EV fraction obtained from GFP-MBD cells displayed a mode diameter distribution of  $152 \pm 4$  nm (Fig. 2A). GFP-MBD was targeted less efficiently to EVs than the endogenous EV marker ALIX when comparing the respective EV/cell lysate ratios (Fig. 2B). GFP-MBD-EVs were incubated on recipient cells engineered to express full-length Tau (441 amino acid long) fused at the carboxyl end with mCherry, in the following referred to as Tau<sub>441</sub> (Fig. 2C). Analysis of the mCherry-positive cell population by flow cytometry showed EV-mediated transcellular transport of GFP-MBD to Tau<sub>441</sub> recipient cells (Fig. 2D).

To better support that GFP-MBD was incorporated within EVs, we first analyzed by size-exclusion chromatography (SEC) the P100 pellet isolated by the conclusive 100,000 *g* centrifugation of the EV enrichment protocol (Supplementary Fig. S1A). As expected, EVs detected by nanoparticle tracking analysis were mainly recovered in the early SEC fractions (Supplementary Fig. S1B), which were also enriched for the marker ALIX detected by western blot (Supplementary Fig. S1C). In contrast, the main pool of soluble proteins in the (EVs-depleted) S100 supernatant was

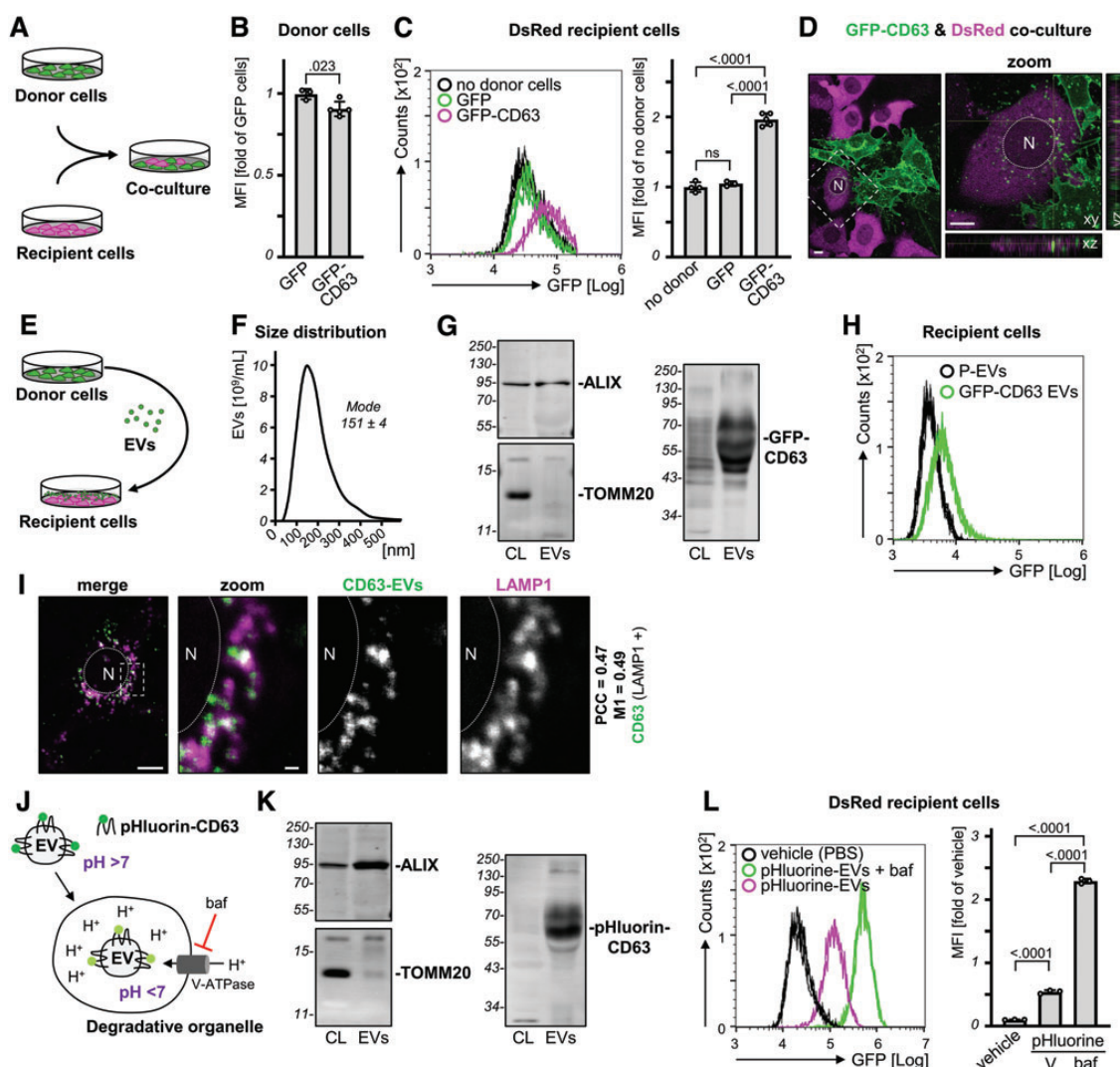


**FIG. 1.** Extracellular vesicle-mediated transcellular transport and internalization of CD63. **(A)** Scheme of coculture assay monitoring transcellular transport of GFP-CD63 protein (green) to DsRed cells (magenta). **(B)** MFI of GFP and GFP-CD63 cells; mean  $\pm$  SD,  $n \geq 3$ ,  $\geq 8 \times 10^3$  cells/replicate. **(C)** Plot of GFP-fluorescence intensity distribution by flow cytometry for DsRed cells alone (black), cocultured with GFP (green) or with GFP-CD63 (magenta);  $n \geq 3$ ,  $\geq 1.5 \times 10^3$  cells/replicate. MFI in DsRed cells cocultured as indicated; mean  $\pm$  SD,  $n \geq 3$ ,  $\geq 1.5 \times 10^3$  cells/replicate. **(D)** Fluorescent confocal image of DsRed (magenta) cells cultured with GFP-CD63 (green) cells for 3 days. The zoomed inset includes the orthogonal reconstruction of stacked z-planes showing internalized GFP in a DsRed cell. Scale bar 10  $\mu$ m. **(E)** Scheme of the GFP-CD63 (green) EVs assay on recipient DsRed (magenta) cells. **(F)** Size distribution of a representative GFP-CD63-EVs preparation by nanoparticle tracking analysis; mode  $\pm$  SD,  $n = 3$ ,  $\geq 1.8 \times 10^5$  particles/replicate. **(G)** Western blots for ALIX, TOMM20, or GFP-detecting GFP-CD63 of donor total CL and EVs (20 $\times$  the corresponding amount of CL). Molecular weight markers are given on the left in kDa. **(H)** Plot of GFP-fluorescence intensity distribution for parental cells incubated with  $1 \times 10^9$  parental-EVs (P-EVs, black) or GFP-CD63-EVs (green) for 1 day,  $n \geq 4$ ,  $\geq 4.4 \times 10^3$  cells/replicate. **(I)** Confocal image of a cell expressing LAMP1-mCherry (magenta) incubated for 1 day with  $1 \times 10^9$  GFP-CD63-EVs (green), co-emission of the two fluorophores shown in white pseudocolor indicates colocalization of GFP-CD63 within LAMP1 in DOs. Scale bar 10  $\mu$ m, 1  $\mu$ m for the zoomed inset. **(J)** Scheme of pHluorin-CD63-EVs (dark green) internalization in the acidic environment of DOs causing fluorescence quenching (light green). Acidification of DOs by the proton ( $H^+$ ) pump V-ATPase is inhibited by bafilomycin A1 (baf). **(K)** Western blots for ALIX, TOMM20, or GFP-detecting pHluorin-CD63 of donor total CL and EVs (20 $\times$  the corresponding amount of CL). Molecular weight markers are given on the left in kDa. **(L)** Plot of pHluorin-fluorescence intensity distribution and MFI of DsRed cells incubated with vehicle (black) or  $1 \times 10^9$  pHluorin-CD63-EVs for 16 h in the absence (green) or presence (magenta) of 25 nM bafilomycin-A1 (baf, added 4 h before analysis); mean  $\pm$  SD,  $n = 3$ ,  $\geq 1.5 \times 10^3$  cells/replicate. CL, cell lysates; DO, degradative organelle; EV, extracellular vesicle; MFI, median fluorescence intensity. Color images are available online.

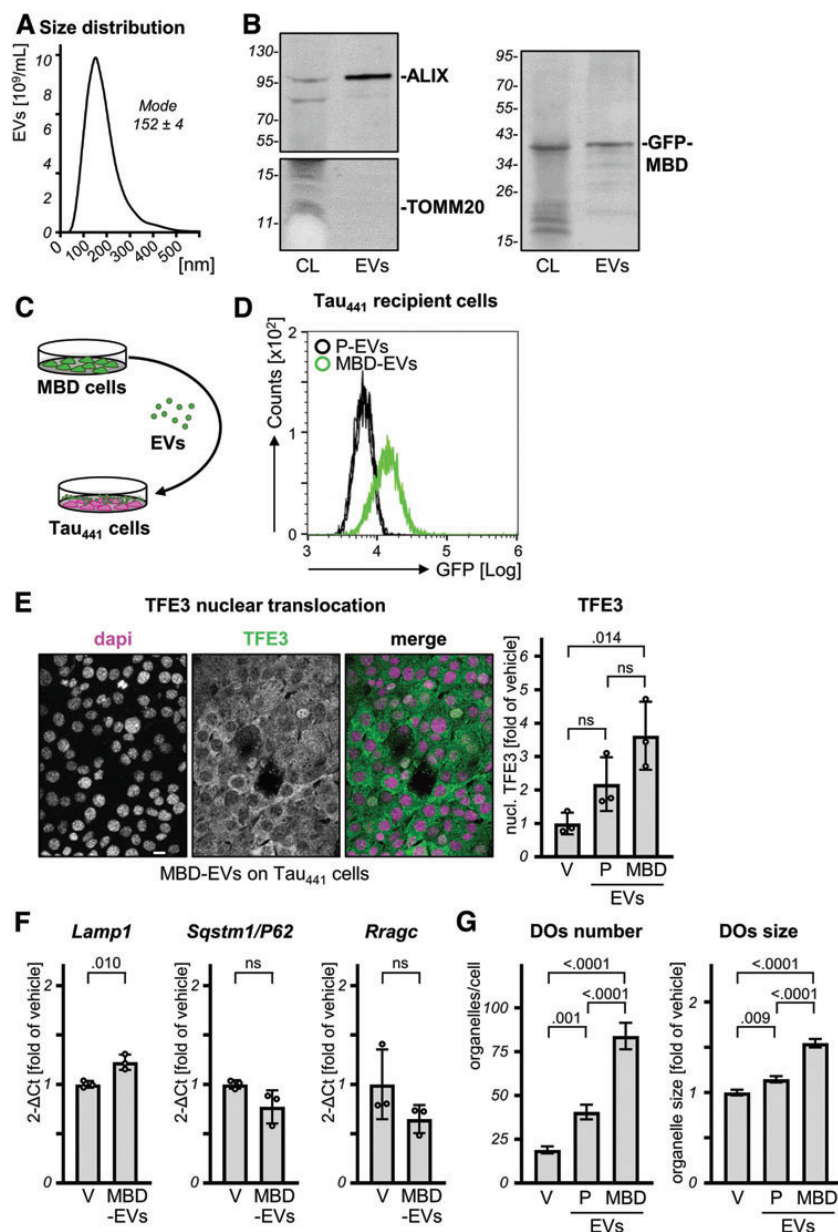


**FIG. 2.** The fibrillogenic Tau fragment MBD transported by extracellular vesicles induces cell stress associated to DOs. **(A)** Size distribution of a representative GFP-MBD-EVs preparation; mode ± SD,  $n = 3$ ,  $\geq 1.8 \times 10^5$  particles/replicate. **(B)** Western blots for ALIX, TOMM20, or GFP of total lysates from GFP-MBD cells (CL) and EVs (20× the corresponding amount of CL). Molecular weight markers are given on the left in kDa. **(C)** Scheme of the GFP-MBD-EVs (green) assay on recipient Tau<sub>441</sub>-mCherry (magenta) cells (Tau<sub>441</sub>). **(D)** Plot of fluorescence intensity distribution for Tau<sub>441</sub> cells incubated with  $1 \times 10^9$  P-EVs (black) or GFP-MBD-EVs (green) for 1 day,  $n = 3$ ,  $\geq 3.1 \times 10^3$  cells/replicate. **(E)** Confocal images of endogenous TFE3 (green) and dapi (magenta) in Tau<sub>441</sub>-mCherry cells incubated for 1 day with  $1 \times 10^9$  MBD-EVs, coemission of the two fluorophores when TFE3 is in the nucleus appears in white pseudocolor. Scale bar 10 μm. Quantification of cells with nuclear TFE3 (dapi mask) treated with vehicle (V),  $1 \times 10^9$  P-EVs or MBD-EVs; mean ± SD,  $n = 3$ ,  $\geq 1.2 \times 10^5$  cells/condition. **(F)** Quantification of transcript for the indicated TFE3 target genes in Tau<sub>441</sub>-mCherry cells incubated for 16 h with vehicle (V) or  $2 \times 10^9$  GFP-MBD-EVs by quantitative PCR; mean ± SD,  $n = 3$ . **(G)** Quantification of number/cell (left panel) and size (right panel) of LysoTracker-stained DOs in Tau<sub>441</sub>-mCherry cell treated for 1 day with vehicle (V),  $1 \times 10^9$  P-EVs or GFP-MBD-EVs; mean ± SEM,  $n = 3$ ,  $\geq 38$  cells/condition. ns, not significant,  $> .05$ . Color images are available online.

recovered in the slower migrating SEC fractions, in which only trace amounts of ALIX were found. When loading the EV pellet, GFP-MBD coenriched in the EV fractions when compared with the soluble protein fractions (Supplementary Fig. S1C). Resuspension of the P100 pellet in the presence of the nonionic detergent Tx-100 inverted this behavior, suggesting liberation of the EVs protein cargo containing ALIX and GFP-MBD (Supplementary Fig. S1C). Furthermore, GFP-MBD recovered in the EVs' P100 pellet was protected from trypsin digestion in contrast to the small amount of GFP-MBD present in the S100 supernatant (Supplementary Fig. S1C).

Considering that EVs were internalized and accumulated in DOs, we anticipated an adverse response in recipient cells incubated with EVs transporting profibrillogenic MBD. We assessed lysosomal stress by analyzing the nuclear translocation of TFE3, a master transcription factor regulating lysosomal biogenesis and macroautophagy (Settembre *et al.*, 2011; Martina *et al.*, 2014). Recipient cells treated with GFP-MBD-EVs displayed increased nuclear TFE3 when compared with cells treated with parental EVs (P-EVs; i.e., without the GFP-MBD-cargo) or with vehicle PBS (Fig. 2E). Nuclear translocation of TFE3 was accompanied by increased transcription of lysosomal *Lamp1* (Fig. 2F), a TFE3 target gene (Martina *et al.*, 2014). In contrast, no effect was observed for two autophagy-associated genes, *Sqstm1/P62* and *Rragc* (Fig. 2F); possibly indicative of a lack of autophagy stimulation by internalized MBD-EVs (see also Fig. 5I, J). Treatment with GFP-MBD-EVs increased number and size of LysoTracker-stained DOs in recipient cells (Fig. 2G), consistent with the lysosomal biogenesis TFE3 activity. A smaller effect was also obtained when cells were treated with P-EVs (Fig. 2G).

#### Profibrillogenic Tau transported by EVs induces *Tau<sub>441</sub>* accumulation in DOs

Extracellular MBD seeds were shown to induce the accumulation of Tau in cultured C17.2 cells (Frost *et al.*, 2009;

Holmes *et al.*, 2013). To assess whether a similar phenotype may be induced by GFP-MBD transported by EVs, we analyzed *Tau<sub>441</sub>* recipient cells by confocal microscopy and observed a four-fold increase in cells carrying Tau puncta when compared with cells treated with vehicle or P-EVs (Fig. 3A). Incubation with GFP-MBD-EVs also increased the number, area, and fluorescence intensity of Tau puncta analyzed at the single-cell level (Fig. 3B).

We showed that behavioral deficits induced by Tau overexpression in mice are reduced by the presence of two isoleucine to proline (2P)  $\beta$ -sheet-breaking mutations in the microtubule-binding domain of Tau (Lathuiliere *et al.*, 2017). Based on this study, we expressed 2P-mutated GFP-MBD in donor cells and isolated their EVs (Fig. 3C). The presence of the 2P mutation in GFP-MBD did not interfere with the incorporation of GFP-MBD into EVs (Fig. 3D). On the other hand, EVs carrying 2P-mutated GFP-MBD did not induce Tau puncta when compared with EVs isolated from parental cells (P-EVs), in contrast to EVs originating from cells expressing the wild-type sequence of GFP-MBD (Fig. 3E).

We then assessed whether the Tau puncta phenotype directly correlated with the nuclear translocation of TFE3. After exposure to MBD-EVs, about 11% of the cells displayed nuclear TFE3 and about 22% of the cells presented Tau puncta and these latter displayed increased nuclear TFE3 when compared with cells devoid of Tau puncta present in the same culture dish (Fig. 3F). While these data suggest that the aberrant TFE3 response is linked to Tau accumulation, whether GFP-MBD may influence subtle EV characteristics contributing to DO stress cannot be excluded.

Notably, a CLEM study demonstrated that Tau accumulation induced by GFP-MBD-EVs localized in characteristic DOs of the cell (Fig. 3G), which showed the accumulation of vesicles or degraded membranes. Confirming these data, *Tau<sub>441</sub>* accumulation colocalized by confocal microscopy with the ectopically expressed DO marker CD63 (Pols and Klumperman, 2009) fused to GFP as also determined by the

**FIG. 3.** The fibrillogenic Tau fragment MBD transported by extracellular vesicles induces Tau accumulation in DOs. (A) Fluorescent confocal image of *Tau<sub>441</sub>*-mCherry cells incubated for 1 day with  $1 \times 10^9$  GFP-MBD-EVs; scale bar 10  $\mu$ m,  $N$ =nucleus. Quantification of % cells with Tau puncta treated with vehicle (V), EVs obtained from parental cells (P-EVs) or from GFP-MBD cells (MBD-EVs); mean  $\pm$  s.d.,  $n=3$ ,  $\geq 295$  cells/replicate. (B) Single-cell analysis of Tau puncta phenotype in *Tau<sub>441</sub>*-mCherry cells incubated for 1 day with  $1 \times 10^9$  EVs isolated from parental (P-EVs) or GFP-MBD (MBD-EVs) cells. Quantification of Tau puncta number per cell; mean  $\pm$  SEM,  $N=16$ –21 cells in three replicates; area and fluorescence intensity of puncta; mean  $\pm$  SEM,  $n=480$ –1070 puncta in three replicates. (C) Scheme of the *Tau<sub>441</sub>* splice variant and the two microtubule-binding domain fragments (MBD) without or with the two Pro substitutions. (D) Western blots for ALIX or GFP of EVs obtained from parental (P), GFP-MBD<sub>2P</sub> (MBD<sub>2P</sub>), or GFP-MBD (MBD)-expressing cells. Molecular weight markers are given on the left in kDa. (E) Tau puncta per cell in *Tau<sub>441</sub>*-mCherry cells incubated for 1 day with  $1 \times 10^9$  EVs obtained from parental (P-EVs), GFP-MBD<sub>2P</sub>-EVs (MBD<sub>2P</sub>), or GFP-MBD (MBD-EVs) cells; mean  $\pm$  SD,  $n=3$ ,  $\geq 295$  cells/replicate. (F) Relative number of cells with nuclear TFE3 in Tau puncta-negative (–) or positive (+) *Tau<sub>441</sub>*-mCherry cells after incubation for 1 day with  $1 \times 10^9$  GFP-MBD-EVs; mean  $\pm$  SD,  $n=3$ ,  $\geq 342$  cells/replicate. (G) Correlative light-electron microscopy of *Tau<sub>441</sub>*-mCherry cells incubated for 1 day with  $1 \times 10^9$  GFP-MBD-EVs. Scale bar 1  $\mu$ m,  $N$ =nucleus. Insets 1–3 show zoomed images obtained by EM (left, A), confocal microscopy (middle, B), or the merging of the two (right, C). (H) Fluorescent confocal image of cells expressing *Tau<sub>441</sub>*-mCherry (magenta); without the T<sub>11</sub> tag and GFP-CD63 (green) incubated for 1 day with vehicle,  $1 \times 10^9$  P-EVs or nonfluorescent GFP<sub>1-10</sub>-MBD-EVs (MBD-EVs), colocalization of the two fluorophores appears in a white pseudocolor indicating the presence of *Tau<sub>441</sub>* within CD63-positive DOs; scale bar 10  $\mu$ m,  $N$ =nucleus. Determination of Pearson's correlation coefficient (PCC) for *Tau<sub>441</sub>* and CD63 in cells treated with vehicle (V), parental- (P-EVs) or GFP<sub>1-10</sub>-MBD-EVs (MBD-EVs);  $n=3$ , 29–34 cells; whiskers 1–99 percentiles, box 25–75 percentiles, horizontal bar median. (I) Fluorescent confocal image of a cell expressing *Tau<sub>441</sub>*-mCherry (magenta) and GFP-CD63 (green) incubated for 1 day with  $1 \times 10^9$  GFP<sub>1-10</sub>-MBD-EVs the image includes an orthogonal reconstruction of six focal z-planes, the zoomed insets show Z-representation of a single Tau puncta enclosed in CD63-positive membranes. Scale bar 10  $\mu$ m (1  $\mu$ m for the zoomed inset),  $N$ =nucleus. Scatter plot of *Tau<sub>441</sub>*- and CD63-fluorescence along the dotted-line in  $z=6$ . ns, not significant,  $>.05$ . Color images are available online.



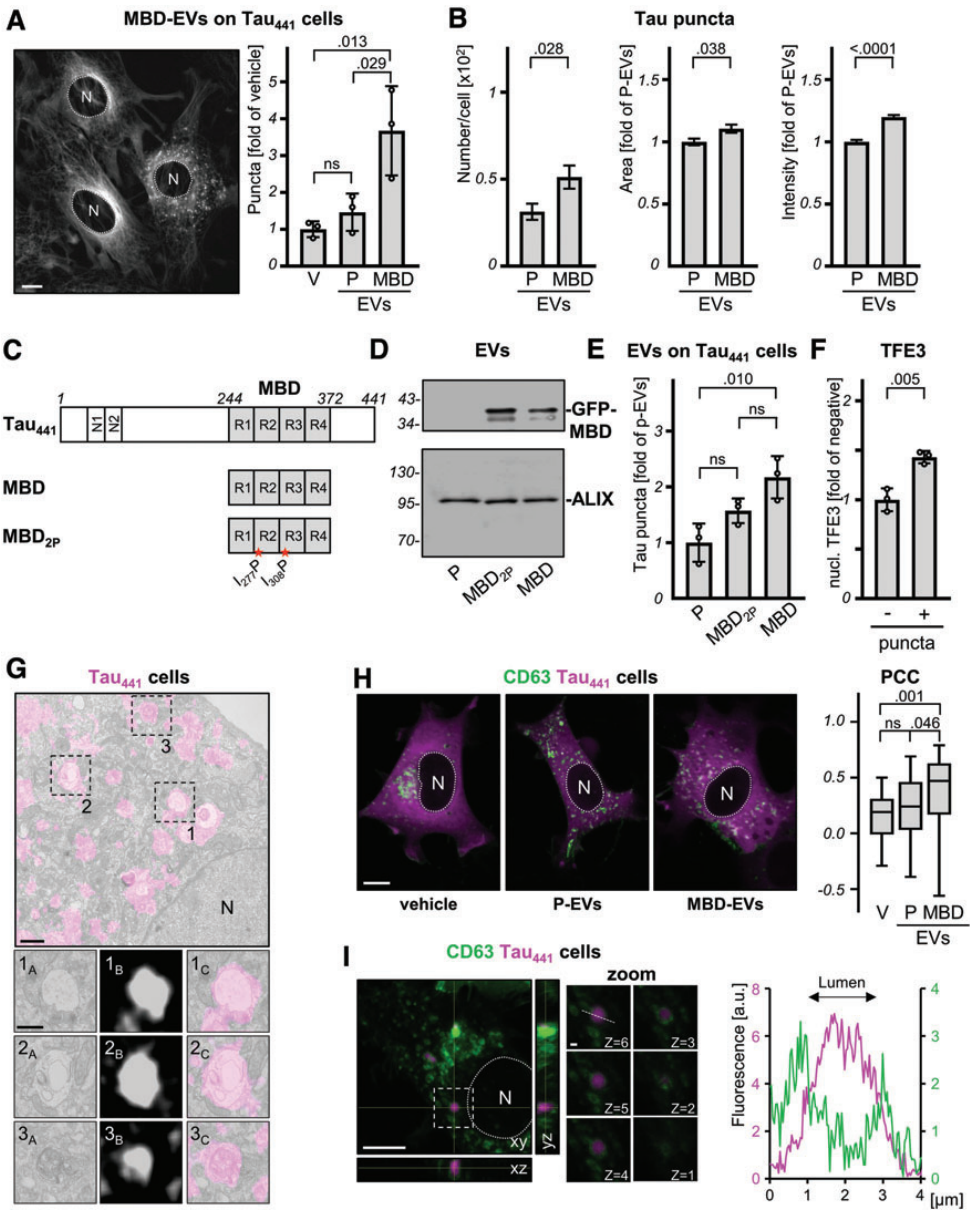
SEEDED TAU ACCUMULATION IN DEGRADATIVE ORGANELLES

1191

analysis of the PCC (Fig. 3H). This result was further substantiated by orthogonal reconstruction of stacked confocal planes demonstrating Tau<sub>441</sub> accumulation within the lumen of DOs identified by GFP-CD63 (Fig. 3I). The data were confirmed in a similar experiment performed in recipient cells transfected with LAMP1-GFP that, similar to CD63, is targeted to DO membranes with the GFP moiety pointing to the cytosol, or with acid-tolerant Gamillus (Em<sub>max</sub> = 519 nm) (Shinoda *et al.*, 2018) targeted to the DO lumen by fusion with LC3B (Supplementary Fig. S2).

*Internalized MBD-EVs does not cause DO leakage but interacts with cellular Tau within DOs*

To assess cytosolic targeting of a luminal protein transported by EVs under our experimental conditions, we selected as a model protein the Cre recombinase. Cre reagents were employed previously to detect with exquisite sensitivity *in vivo* the presence of this protein in cells expressing an adequate reporter cassette (Zomer *et al.*, 2015). To rapidly validate the assay, we first analyzed a coculture



paradigm made of a stable cell line with inducible Cre expression and a cell line with the integrated loxP-dependent red-to-green fluorescence reporter cassette (Fig. 4A). Flow cytometry analysis established that few recipient cells switched to green fluorescence as a consequence of transcellular transport of Cre produced by donor cells, although this was not dependent on the extent of Cre induction (Fig. 4B). The relative number of green-switched recipient cells increased gradually as a function of the donor-to-recipient cell ratio, reaching a maximal value of  $\sim 1.0\%$  at the ratio 25:1 (Fig. 4C).

Maximal Cre expression in donor cells was obtained by transient transfection and resulted in detectable amounts of Cre in the EVs' fraction (Fig. 4D). Incubation of these Cre-EVs led to the recombination of the red-to-green reporter with an efficiency close to that observed in the coculture model (Fig. 4E). In summary, the Cre-based cell assay showed high sensitivity for the cytosolic delivery of trace amounts of Cre transported by EVs. However, cytosolic delivery appeared as a function of the relative number of EVs delivered to recipient cells rather than of the relative amount of Cre targeted to EVs. Notably, cotreatment with GFP-MBD-EVs did not improve the cytosolic delivery of Cre (Fig. 4F), possibly indicating lack of a detectable DO leakage when cells were exposed to profibrillogenic Tau.

Instead, we observed that GFP-MBD transported by EVs colocalized with Tau<sub>441</sub> accumulating in recipient cells (Fig. 4G), suggesting the possibility of a direct protein encounter. We studied previously protein/protein interaction and its subcellular localization utilizing the bimolecular fluorescence complementation technology (biFC) (Foglieni *et al.*, 2017; Ulrich *et al.*, 2018) based on a predominantly monomeric GFP (Cabantous *et al.*, 2005). We applied the same approach to assess whether MBD transported by EVs may encounter Tau<sub>441</sub> expressed by the recipient cells. For this, we isolated EVs from cells expressing GFP<sub>1-10</sub> (cov-

ering the first 10  $\beta$ -strands of GFP) fused to MBD (GFP<sub>1-10</sub>-MBD-EVs) and delivered them on cells expressing Tau<sub>441</sub> fused at the amino terminus with the remaining 11<sup>th</sup>  $\beta$ -strand of GFP (T<sub>11</sub>-Tau<sub>441</sub>-mCherry) (Fig. 4H). Analysis by flow cytometry showed a positive biFC signal in recipient cells (Fig. 4I).

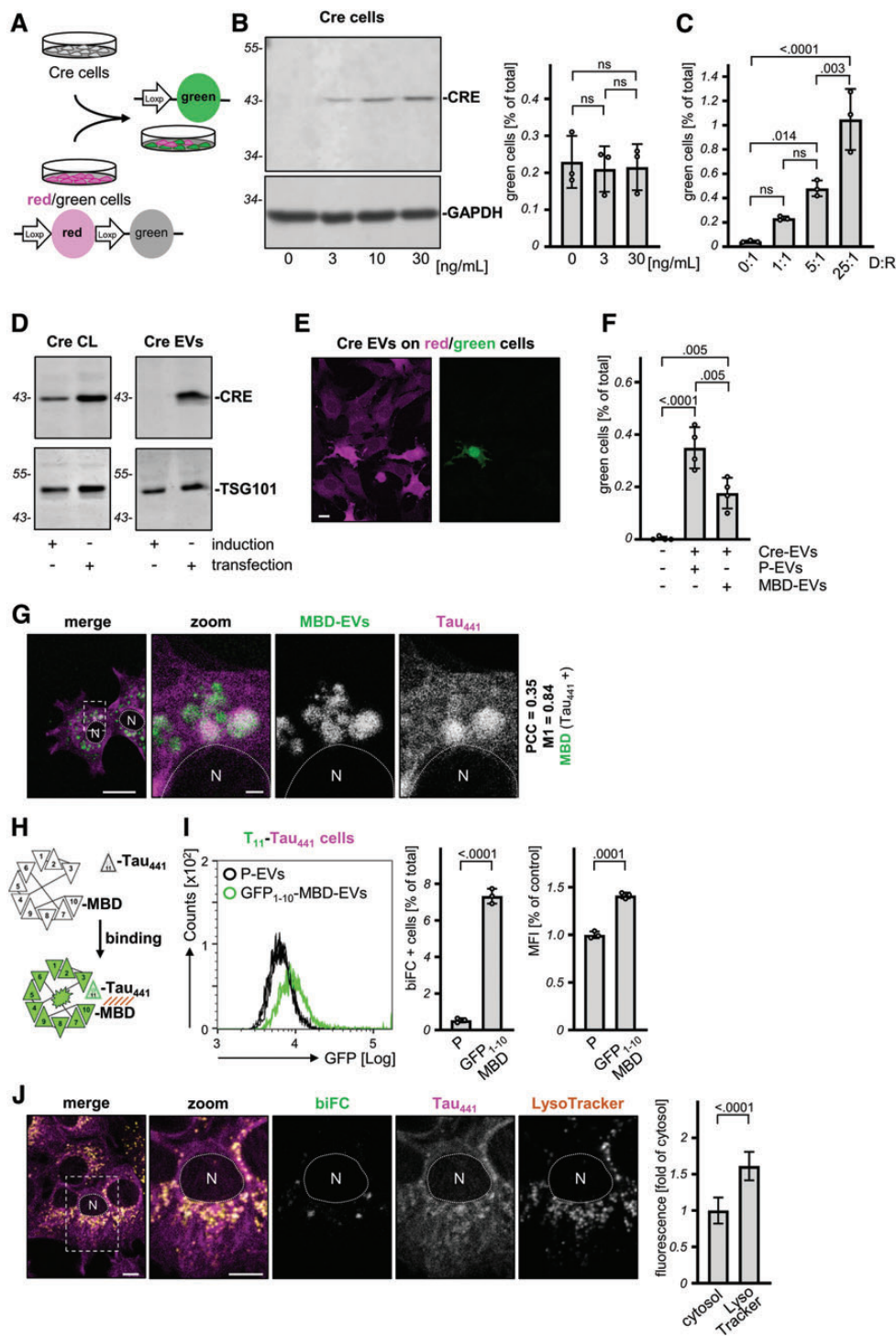
To identify the intracellular localization of biFC signal, we took advantage of the acidotropic fluorescent compound LysoTracker used as a tracer for acidic DOs. To exclude a possible interference of LysoTracker with DO acidification, the compound was added just before the analysis and after controlling that the biFC signal was already present in the cells. Confocal microscopy analysis showed that the interaction of EVs-MBD with cellular Tau<sub>441</sub>, utilizing biFC fluorescence as a proxy, occurred in LysoTracker-stained DOs displaying Tau accumulation (Fig. 4J). With an automated trained protocol (Morone *et al.*, 2020), we established that the mean biFC intensity in LysoTracker-positive DOs was higher than that measured in the cytosol (Fig. 4J). The suboptimal sensitivity of GFP fluorescence when exposed to acidic conditions may lead to an underestimation of cells positive for biFC. However, the 7% biFC-positive recipient cell population (Fig. 4I) was appreciably larger than the 0.2% cells displaying cytosolic release of Cre in the presence of GFP-MBD-EVs (Fig. 4F).

#### *Tau accumulation in DOs induced by profibrillogenic EV Tau involves autophagy*

The interaction between exogenous GFP-MBD and cellular Tau<sub>441</sub> and its accumulation within DOs hinted an autophagy-mediated transport of cytosolic Tau<sub>441</sub>, in agreement with the evidence that Tau is a substrate of autophagy (Wang *et al.*, 2009; Wang and Mandelkow, 2012; Moreau *et al.*, 2014; Silva *et al.*, 2020). In fact, nutrient-deprived Tau<sub>441</sub> cells, which displayed enhanced LC3

**FIG. 4.** The fibrillogenic Tau fragment MBD transported by extracellular vesicles interact with cellular Tau in DOs. (A) Scheme of assay to monitor transcellular transport of Cre recombinase to recipient cells expressing a floxed DsRed cassette (magenta) upstream of eGFP (green). (B) Western blot for Cre or GAPDH of lysates from inducible Cre cells incubated with the indicated tetracycline concentrations. Molecular weight markers are given on the left in kDa. Quantification by flow cytometry of percent recipient cells displaying Cre-dependent eGFP expression when cocultured for 3 days with Cre cells in the presence of the indicated tetracycline concentrations; mean  $\pm$  SD,  $n=3$ ,  $> 20 \times 10^3$  cells. (C) Cre-dependent eGFP-positive recipient cells (R) cocultured with donor Cre cells (D) at the indicated ratio for 3 days before analysis by flow cytometry; mean  $\pm$  SD,  $n=3$ ,  $> 20 \times 10^3$  cells. (D) Western blot for CRE or TSG101 of lysates obtained from donor cre cells (Cre CL) and their EVs (Cre EVs). Cre protein expression was induced with tetracycline or obtained by transient transfection as indicated. Molecular weight markers are shown on the left in kDa. (E) Fluorescence microscopy of recipient cells expressing the floxed DsRed cassette (magenta) upstream of eGFP (green) incubated for 3 days with  $1 \times 10^9$  Cre EVs. Scale bar 10  $\mu$ m. (F) Quantification by flow cytometry of percent recipient cells that underwent Cre-dependent recombination when incubated for 72 h with vehicle PBS or in the presence of  $1 \times 10^9$  EVs obtained from Cre cells (Cre-EVs), parental cells (P-EVs), or GFP-MBD cells (MBD-EVs) as indicated; mean  $\pm$  SD,  $n=4$ ,  $> 26 \times 10^3$  cells. (G) Confocal image of a Tau<sub>441</sub>-mCherry cell (magenta) incubated for 3 days with  $6 \times 10^9$  GFP-MBD-EVs (green), localization of GFP-MBD with Tau puncta results in a white pseudocolor. Scale bar 10  $\mu$ m, 1  $\mu$ m for zoomed inset. (H) Scheme of bimolecular fluorescence complementation (biFC). The first ten  $\beta$ -strands of GFP (GFP<sub>1-10</sub>) are fused to MBD and expressed in donor cells; the reconstituting 11th  $\beta$ -strand of GFP (T<sub>11</sub>) is fused to Tau<sub>441</sub>-mCherry and expressed in recipient cells. (I) Plot of biFC-fluorescence intensity distribution by flow cytometry for T<sub>11</sub>-Tau<sub>441</sub> cells incubated for 3 days with  $6 \times 10^9$  P-EVs (black) or GFP<sub>1-10</sub>-MBD-EVs (green);  $n=3$ ,  $3.1 \times 10^3$  cells/replicate. Quantification of percent biFC-positive cells (left panel) or of MDPI (right panel); mean  $\pm$  SD,  $n=3$ ,  $\geq 3.1 \times 10^3$  cells/replicate. (J) Fluorescent confocal images of a biFC-positive (green) T<sub>11</sub>-Tau<sub>441</sub>-mCherry cell (magenta) stained for LysoTracker (orange), the white pseudocolor indicates localization of biFC within LysoTracker-positive DOs containing Tau puncta. Scale bar 10  $\mu$ m. Quantification of biFC-fluorescence intensity in LysoTracker-positive DOs or in the cytosol; mean  $\pm$  SEM,  $n=193$  cells from three biological replicates. ns, not significant,  $>.05$ . Color images are available online.





1194

PEDRIOLI ET AL.

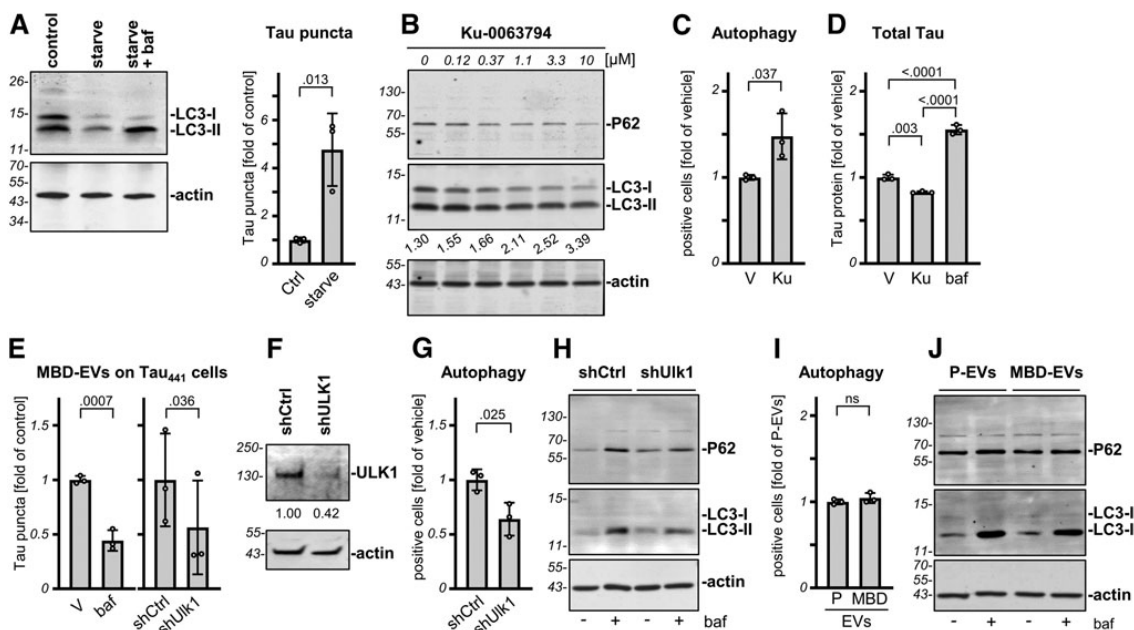


**FIG. 5.** Tau accumulation in degradative organelles involves autophagy. **(A)** Western blot for the LC3 isoforms or actin of lysates obtained from Tau<sub>441</sub> cells cultured in normal medium (control) or starved for 4 h in HBSS in the absence (starve) or presence of 25 nM bafilomycin A1 (starve + baf). Molecular weight markers are given on the left in kDa. Quantification of cells with a Tau puncta phenotype when cultured in normal medium (Ctrl) or for 4 h in HBSS (starve); mean  $\pm$  SD,  $n = 3$ ,  $> 1.3 \times 10^3$  cells. **(B)** Western blots for P62, LC3 isoforms, or actin of cell lysates obtained from Tau<sub>441</sub>-mCherry cells treated for 16 h with increasing concentrations of the catalytic mTOR inhibitor Ku-0063794. LC3 conversion is given as the ratio of LC3-II/LC3-I below the LC3 blot. Molecular weight markers are given on the left in kDa. **(C)** Quantification by flow cytometry of red fluorescent cells expressing the mRFP-GFP-LC3 reporter construct and treated with the vehicle DMSO (V) or 3.3  $\mu$ M Ku-0063794 (Ku) for 16 h; mean  $\pm$  SD,  $n = 3$ ,  $\geq 10^4$  cells/replicate. **(D)** Determination of cellular Tau protein by AlphaLISA<sup>®</sup> in Tau<sub>441</sub>-mCherry cells treated with the vehicle DMSO (V), 3.3  $\mu$ M Ku-0063794 (Ku) or 10 nM bafilomycin A1 (baf) for 16 h; mean  $\pm$  SD,  $n = 3$  from a representative experiment. **(E)** Determination of Tau puncta-positive cells after 1 day of treatment with GFP-MBD-EVs (MBD-EVs) and DMSO (V) or 10 nM bafilomycin A1 (baf) (left panel) or transduced for 3 days with a control shRNA (shCtrl) or a ULK1 shRNA (shULK1); mean  $\pm$  SD,  $n = 3$ ,  $\geq 392$  cells/replicate, paired *t* test. **(F)** Representative western blot for ULK1 or actin of lysates obtained from cells transduced for 3 days with a control shRNA (shCtrl) or a ULK1 shRNA (shULK1). The relative amount of ULK1 after normalization for actin is indicated below the blot. Molecular weight markers are given on the left in kDa. **(G)** Same as in (C) for cells transduced for 3 days with a control shRNA (shCtrl) or a ULK1 shRNA (shULK1); mean  $\pm$  SD,  $n = 3$ ,  $\geq 1.9 \times 10^3$  cells/replicate. **(H)** Western blot for P62, LC3 isoforms, or actin of lysates obtained from Tau<sub>441</sub>-mCherry cells treated with either shCtrl or shULK1 for 3 days and in the absence (–) or presence (+) of 25 nM bafilomycin A1 (baf) for the last 4 h. Molecular weight markers are given on the left in kDa. **(I)** Same as in (C) for cells treated for 1 day with P-EVs or GFP-MBD-EVs; mean  $\pm$  SD,  $n = 3$ ,  $\geq 1 \times 10^4$  cells/replicate. **(J)** Same as in (H) for cells treated for 1 day with  $2 \times 10^9$  P-EVs or GFP-MBD-EVs in the absence (–) or presence (+) of 25 nM bafilomycin A1 (baf) for the last 4 h. Molecular weight markers are given on the left in kDa. ns, not significant,  $> .05$ .

conversion, acquired a Tau puncta phenotype similar to that induced by MBD-EVs (Fig. 5A) in CD63-positive DOs (Supplementary Fig. S3).

To further corroborate the involvement of autophagy in the modulation of the amount of Tau present in cells, we first utilized the catalytic mTOR inhibitor Ku-0063794 (García-Martínez *et al.*, 2009) that we showed to stimulate autophagy in HN10 cells (Rosic *et al.*, 2011). We confirmed this observation in C17.2 cells by determining its dose-dependent activity in decreasing P62 and increasing LC3 conversion (defined as LC3-II/LC3-I ratio that gradually increases from 1.3 in the absence to 3.4 in the presence of 10  $\mu$ M compound) (Fig. 5B) as well as with the mRFP-GFP-LC3 assay mea-

suring active autophagic flux (Kimura *et al.*, 2007) (Fig. 5C). Autophagy stimulation with Ku-0063794 reduced the amount of Tau present in cells, whereas inhibition of DO's acidification and autophagosome maturation with bafilomycin A1 (Mauvezin and Neufeld, 2015) increased Tau when compared with untreated cells (Fig. 5D).

Notably, when compared with control conditions, bafilomycin A1 reduced by half the relative number of cells with Tau puncta induced by GFP-MBD-EVs, and this was reproduced by treatment with a shRNA specific for *ULK1* (*Atg1*, required for autophagosome biogenesis (Hurley and Young, 2017)) when compared with a control shRNA (Fig. 5E). Downregulation of ULK1 protein (Fig. 5F)

## SEEDED TAU ACCUMULATION IN DEGRADATIVE ORGANELLES

1195

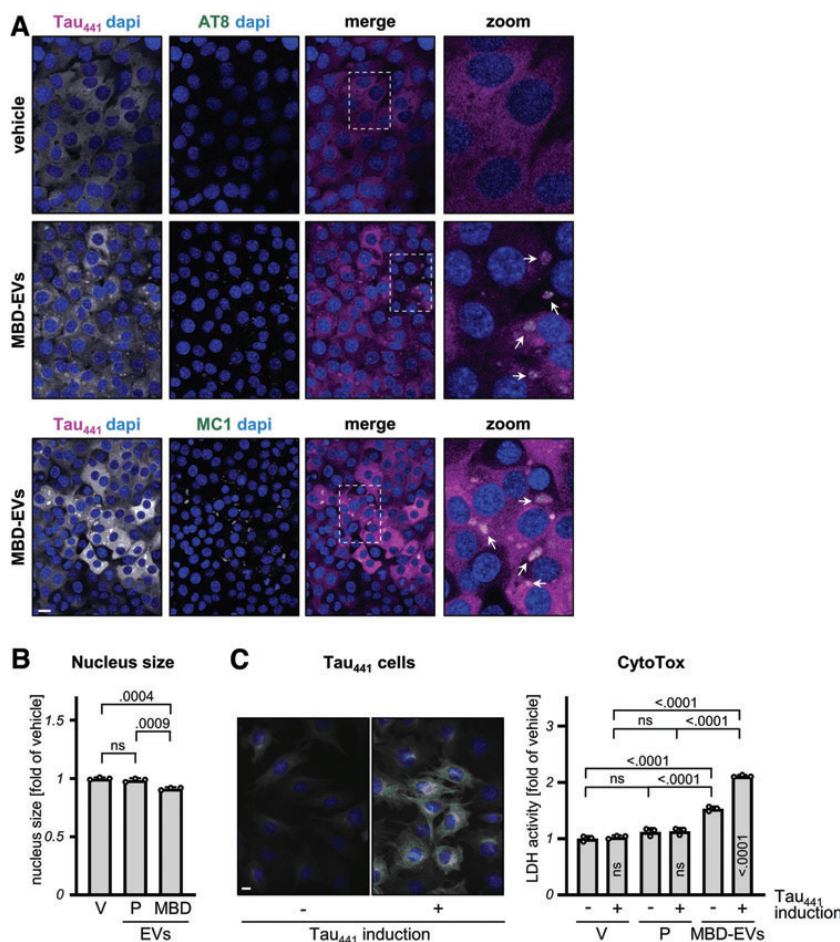


**FIG. 6.** Tau accumulation induced by extracellular vesicles carrying Tau-MBD causes the appearance of pathological Tau epitopes and cell toxicity. **(A)** Fluorescent confocal image of Tau<sub>441</sub>-mCherry cells (*magenta*) incubated for 3 days with vehicle or  $6 \times 10^9$  MBD-EVs and stained with the nuclear marker dapi and the Tau antibodies AT8 or MC1 (*green*), coemission of the two fluorophores shown in *white* pseudocolor indicates that Tau puncta are positive for AT8 and MC1. Scale bar 10  $\mu$ m. **(B)** Quantification of nuclear size (Hoechst mask) for cells treated for 1 day with vehicle PBS (V),  $1 \times 10^9$  P-EVs, or GFP-MBD-EVs (MBD-EVs); mean  $\pm$  SD,  $n = 3$ , with  $\geq 11.9 \times 10^3$  cells/condition. Fluorescent confocal images of cells noninduced or induced for 1 day with 60 ng/mL tetracycline for expression of Tau<sub>441</sub>-mCherry (*gray*), nuclei were counterstained with Hoechst (*blue*). Scale bar 10  $\mu$ m. **(C)** Endpoint LDH enzymatic activity in noninduced (–) and induced (+) Tau<sub>441</sub>-mCherry cells incubated for 1 day as in **(B)**; mean  $\pm$  SD,  $n = 3$ . ns, not significant,  $>.05$ . Color images are available online.

impaired the autophagic flux as determined with the mRFP-GFP-LC3 assay (Fig. 5G) and by determining P62 and LC3-II by western blot (Fig. 5H). As an additional control, we used these two latter assays to show that the treatment with GFP-MBD-EVs did not appear to affect autophagy when compared with parental EVs (Fig. 5I, J). Our data confirmed that cytosolic Tau represents a client protein of autophagy also in our cell system and, notably, highlighted the involvement of an active autophagic flux in the accumulation of cellular Tau in DOs in cells exposed to MBD-EVs. A possible interpretation of the data is that the presence of GFP-MBD transported by EVs to DOs affect the normal fate of Tau along the autophagic pathway.

#### Tau accumulation induced by MBD-EVs results in cytotoxic effects

Accumulation of Tau in DOs induced by MBD-EVs eventually resulted in the appearance of pathology-associated epitopes, namely the double phosphorylation at Ser202/Thr305 recognized by the AT8 antibody and the “paper clip” conformational recognized by the MC1 anti-

body (Fig. 6A). Both these Tau epitopes are absent in the Tau fragment MBD, but are present on abnormal species preceding fibril formation and neurofibrillary toxicity observed in the human brain (Jicha *et al.*, 1999). For our experiments, we choose an amount of EVs ( $\sim 10^9$ ) previously shown to be required for a functional activity in cultured cells (Valadi *et al.*, 2007). We also observed that incubation of recipient cells with GFP-MBD-EVs resulted in reduced nuclear size when compared with cells treated with vehicle or P-EVs (Fig. 6B), a phenotype suggesting an ongoing cytotoxic process (Cummings and Schnellmann, 2004). In fact, utilizing the LDH release assay, we show the occurrence of cytotoxicity in a manner that was dependent on the presence of GFP-MBD-EVs as well as the induction of Tau<sub>441</sub> expression (Fig. 6C).

#### Discussion

EVs-mediated transport of macromolecules is a route of cell-to-cell communication with implications in health and disease. While EVs’ biogenesis in donor cells has been extensively investigated, the elucidation of cellular mechanisms

involved in EVs' cargo delivery in recipient cells need further attention (Pedrioli and Paganetti, 2020). We focused our investigation on protein delivery mediated by EVs in the context of cell-to-cell propagation of Tau. For a luminal EVs protein it can be assumed that the main intracellular target site is the cytosol, consistent with the largely accepted notion that Tau aggregation occurs in the cytosol (Michel *et al.*, 2014). However, this latter would require a specific mechanism, for which experimental evidence is missing, which transfers the EVs cargo to the cytosol across two biological membranes, the EV lipid bilayer and the cell lipid bilayer.

In our cell model delivery of an EVs cargo to the cytosol occurs sporadically and a similar observation was made also *in vivo* (Zomer *et al.*, 2015). In contrast and in agreement with previous reports (Mulcahy *et al.*, 2014; Heusermann *et al.*, 2016; Costa Verdera *et al.*, 2017), EVs were efficiently internalized and delivered to DOs, similar to for example, high-density lipoproteins on their route to degradation (Miller *et al.*, 1977). Also, cytosolic proteins can be delivered to DOs by a ubiquitous process accomplished by different forms of autophagy.

Supported by these observations, we demonstrated herein for the first time that the initial encounter of a fibrillogenic Tau fragment transported by EVs with cellular Tau<sub>441</sub> occurred in DOs. This could represent the first step of transcellular propagation of protein seeds with pathogenic conformations, which is assumed to explain the progressive nature of proteinopathies. This prion-like mechanism appears to occur for most neurodegeneration-linked proteins propagating on normally functioning cognate proteins, and examples are A $\beta$ -peptides (Eisele *et al.*, 2010), Tau (Katsinelos *et al.*, 2018; Clavaguera *et al.*, 2020), huntingtin (Pecho-Vrieseling *et al.*, 2014),  $\alpha$ -synuclein, and TDP-43 (Peled *et al.*, 2017).

EVs may act as vectors of prion infectivity (Fevrier *et al.*, 2004; Alais *et al.*, 2008) and targeting of Tau in EVs contributing to pathology propagation is reported (Wang *et al.*, 2017; Pérez *et al.*, 2019). We now show that a fibrillogenic Tau fragment transported by EVs induces a number of hallmarks in host cells, such as Tau accumulation in DOs, acquisition of prepathologic Tau epitopes, DO stress, and cytotoxicity. Notably, our data are evidence that this adverse cascade of events may initiate within the acidic compartment of the host cell.

Turnover of cytosolic wild-type Tau, a long-lived protein, is mediated through the ubiquitin proteasome system and different forms of autophagy (Caballero *et al.*, 2018). The age-dependent decline in the activity of these pathways is considered as the main cause for the build-up of aberrant protein forms, which in turns is possibly accelerated by the presence of protein seeds (Nixon, 2013; Menzies *et al.*, 2015; Chen *et al.*, 2020). Increased DO number and aberrant DO storage in neurons are hallmarks of neurodegeneration (Nixon *et al.*, 2005). We observed that the neuronal progenitor C17.2 cells utilized for our study exhibit also under standard culture conditions a relatively robust autophagic activity, sufficient to cause the accumulation of Tau in DOs at basal conditions.

However, GFP-MBD-EV-induced Tau accumulation was accompanied by a response characterized by morphological changes in DOs and the activation of TFE3. This molecular signature is also observed in the postmortem human brain affected by neurodegeneration (Martini-Stoica *et al.*, 2016). Autophagy appears upregulated in early AD, possibly as a

response to protein accumulation, but then the increased levels of LC3, P62, and enlarged DOs as markers of autophagy flux become progressively impaired (Wong and Cuervo, 2010; Bordi *et al.*, 2016; Piras *et al.*, 2016). Moreover, DO markers are found enriched in brain protein deposits (Gowrishankar *et al.*, 2015; Hassiotis *et al.*, 2018). Considering the similarity with the observation made in our cell system, the effects reported herein may represent an underestimation of what may occur in nondividing postmitotic neurons, an aspect that merits future attention.

Autophagy stimulation is generally considered as a viable solution to protect neurons from harmful cytosolic protein aggregates (Yuan *et al.*, 2020). However, delivering Tau to DOs, which by itself may generate fibrillogenic Tau fragments (Wang *et al.*, 2009), may also increase the likelihood of an encounter with extracellular seeds. Considering that Tau is normally delivered to DOs (Vaz-Silva *et al.*, 2018; Ji *et al.*, 2019), our findings show that exogenous GFP-MBD transported by EVs binds and causes an aberrant Tau conformation in DOs ultimately leading to DO's impairment (Guix, 2020). Our data do not imply that exogenous Tau seeds are required for the formation and accumulation of toxic protein in DOs but, rather, they may contribute and accelerate the pathogenic process.

Interestingly, it has been shown that within DOs A $\beta$ -peptides (Brewer *et al.*, 2020) or  $\alpha$ -synuclein (Tsujimura *et al.*, 2015) form aggregates and the acidic environment of DOs may favor fibril formation (Uversky *et al.*, 2001; Pfefferkorn *et al.*, 2010; McGlinchey *et al.*, 2014; Moriarty *et al.*, 2017). Overall, our data support the involvement of DOs in the transcellular propagation of proteinopathies.

## Conclusions

Our investigation in cultured cells highlight that a luminal protein cargo of EVs can engage in a functionally relevant interaction in recipient cells. This may attain a specific significance for a whole class of progressive proteinopathies, exemplified herein by tauopathies. Our data suggest that autophagy inhibition may result in an approach to slow down intracellular Tau accumulation resulting from extracellular Tau seeds.

## Acknowledgments

The authors thank A. Raimondi from the ALEMBIC facility at the San Raffaele Scientific Institute, Milan, Italy for his support in the EM analysis; A. Spang, E. Pecho-Vrieseling, members of L. Barile's and M. Moretti's laboratory for discussions, critical advice, and support during this study.

## Authors' Contribution

Conceptualization and design of the project: P.P. and G.P. Methodologies and investigations: M.B., C.M., D.M., S.P., G.P., E.P., G.S., and M.S. Writing of original article: G.P. and P.P. Review, critical editing, and final approving: all co-authors. Supervision and financial support: P.P.

## Disclosure Statement

The authors declare no competing financial and non-financial interests. P.P. and S.P. worked for AC Immune

## SEEDED TAU ACCUMULATION IN DEGRADATIVE ORGANELLES

1197

SA and owns stock in the company. There are no patents, products in development, or marketed products to declare.

## Funding Information

This work was supported by grants from the Gelu Foundation, the Mecri Foundation, and the Swiss National Foundation for Research. No support was obtained from organizations that may gain or lose financially from publication of the article.

## Supplementary Material

Supplementary Data  
Supplementary Figure S1  
Supplementary Figure S2  
Supplementary Figure S3

## References

- Alais, S., Simoes, S., Baas, D., Lehmann, S., Raposo, G., Darlix, J.L., *et al.* (2008). Mouse neuroblastoma cells release prion infectivity associated with exosomal vesicles. *Biol Cell* **100**, 603–615.
- Andreu, Z., and Yanez-Mo, M. (2014). Tetraspanins in extracellular vesicle formation and function. *Front Immunol* **5**, 442.
- Bordi, M., Berg, M.J., Mohan, P.S., Peterhoff, C.M., Alldred, M.J., Che, S., *et al.* (2016). Autophagy flux in CA1 neurons of Alzheimer hippocampus: increased induction overburdens failing lysosomes to propel neuritic dystrophy. *Autophagy* **12**, 2467–2483.
- Braak, H., Braak, E. (1991). Neuropathological staging of Alzheimer-related changes. *Acta Neuropathol* **82**, 239–259.
- Brewer, G.J., Herrera, R.A., Philipp, S., Sosna, J., Reyes-Ruiz, J.M., Glabe, C.G. (2020). Age-related intraneuronal aggregation of amyloid-beta in endosomes, mitochondria, autophagosomes, and lysosomes. *J Alzheimer's Dis* **73**, 229–246.
- Caballero, B., Wang, Y., Diaz, A., Tasset, I., Juste, Y.R., Stiller, B., *et al.* (2018). Interplay of pathogenic forms of human tau with different autophagic pathways. *Aging Cell* **17**, e12692.
- Cabantous, S., Terwilliger, T.C., Waldo, G.S. (2005). Protein tagging and detection with engineered self-assembling fragments of green fluorescent protein. *Nat Biotechnol* **23**, 102–107.
- Chen, X., Li, Y., Wang, C., Tang, Y., Mok, S.A., Tsai, R.M., *et al.* (2020). Promoting tau secretion and propagation by hyperactive p300/CBP via autophagy-lysosomal pathway in tauopathy. *Mol Neurodegeneration* **15**, 2.
- Clavaguera, F., Bolmont, T., Crowther, R.A., Abramowski, D., Frank, S., Probst, A., *et al.* (2009). Transmission and spreading of tauopathy in transgenic mouse brain. *Nat Cell Biol* **11**, 909–913.
- Clavaguera, F., Duyckaerts, C., Haik, S. (2020). Prion-like properties of Tau assemblies. *Curr Opin Neurobiol* **61**, 49–57.
- Costa Verdera, H., Gitz-Francois, J.J., Schiffelers, R.M., Vader, P. (2017). Cellular uptake of extracellular vesicles is mediated by clathrin-independent endocytosis and macropinocytosis. *J Control Release* **266**, 100–108.
- Cummings, B.S., Schnellmann, R.G. (2004). Measurement of cell death in mammalian cells. *Curr Protoc Pharmacol* **Chapter 12**, Unit 12.8.
- Eisele, Y.S., Obermüller, U., Heilbronner, G., Baumann, F., Kaeser, S.A., Wolburg, H., *et al.* (2010). Peripherally applied Abeta-containing inoculates induce cerebral beta-amyloidosis. *Science (New York, NY)* **330**, 980–982.
- Fevrier, B., Vilette, D., Archer, F., Loew, D., Faigle, W., Vidal, M., *et al.* (2004). Cells release prions in association with exosomes. *Proc Natl Acad Sci U S A* **101**, 9683–9688.
- Foglieni, C., Papin, S., Salvade, A., Afroz, T., Pinton, S., Pedrioli, G., *et al.* (2017). Split GFP technologies to structurally characterize and quantify functional biomolecular interactions of FTD-related proteins. *Sci Rep* **7**, 14013.
- Freer, R., Sormanni, P., Vecchi, G., Ciryam, P., Dobson, C.M., Vendruscolo, M. (2016). A protein homeostasis signature in healthy brains recapitulates tissue vulnerability to Alzheimer's disease. *Sci Adv* **2**, e1600947.
- Frost, B., Jacks, R.L., Diamond, M.I. (2009). Propagation of tau misfolding from the outside to the inside of a cell. *J Biol Chem* **284**, 12845–12852.
- García-Martínez, J.M., Moran, J., Clarke, R.G., Gray, A., Cosulich, S.C., Chresta, C.M., *et al.* (2009). Ku-0063794 is a specific inhibitor of the mammalian target of rapamycin (mTOR). *Biochem J* **421**, 29–42.
- Gardiner, C., Di Vizio, D., Sahoo, S., Thery, C., Witwer, K.W., Wauben, M., *et al.* (2016). Techniques used for the isolation and characterization of extracellular vesicles: results of a worldwide survey. *J Extracell Vesicles* **5**, 32945.
- Gowrishankar, S., Yuan, P., Wu, Y., Schrag, M., Paradise, S., Grutzendler, J., *et al.* (2015). Massive accumulation of luminal protease-deficient axonal lysosomes at Alzheimer's disease amyloid plaques. *Proc Natl Acad Sci USA* **112**, E3699–E3708.
- Guix, F.X. (2020). The interplay between aging-associated loss of protein homeostasis and extracellular vesicles in neurodegeneration. *J Neurosci Res* **98**, 262–283.
- Hardy, J., Selkoe, D.J. (2002). The amyloid hypothesis of Alzheimer's disease: progress and problems on the road to therapeutics. *Science (New York, NY)* **297**, 353–356.
- Hassiotis, S., Manavis, J., Blumbergs, P.C., Hattersley, K.J., Carosi, J.M., Kamei, M., *et al.* (2018). Lysosomal LAMP1 immunoreactivity exists in both diffuse and neuritic amyloid plaques in the human hippocampus. *Eur J Neurosci* **47**, 1043–1053.
- Heusermann, W., Hean, J., Trojer, D., Steib, E., von Bueren, S., Graff-Meyer, A., *et al.* (2016). Exosomes surf on filopodia to enter cells at endocytic hot spots, traffic within endosomes, and are targeted to the ER. *The Journal of cell biology* **213**, 173–184.
- Holmes, B.B., DeVos, S.L., Kfoury, N., Li, M., Jacks, R., Yamamandra, K., *et al.* (2013). Heparan sulfate proteoglycans mediate internalization and propagation of specific proteopathic seeds. *Proc Natl Acad Sci U S A* **110**, E3138–E3147.
- Hurley, J.H., Young, L.N. (2017). Mechanisms of Autophagy Initiation. *Annu Rev Biochem* **86**, 225–244.
- Ji, C., Tang, M., Zeidler, C., Hohfeld, J., Johnson, G.V. (2019). BAG3 and SYNPO (synaptopodin) facilitate phospho-MAPT/Tau degradation via autophagy in neuronal processes. *Autophagy* **15**, 1199–1213.
- Jicha, G.A., Berenfeld, B., Davies, P. (1999). Sequence requirements for formation of conformational variants of tau similar to those found in Alzheimer's disease. *J Neurosci Res* **55**, 713–723.
- Katsinelos, T., Zeitler, M., Dimou, E., Karakatsani, A., Müller, H.M., Nachman, E., *et al.* (2018). Unconventional secretion mediates the trans-cellular spreading of tau. *Cell Rep* **23**, 2039–2055.
- Kimura, S., Noda, T., Yoshimori, T. (2007). Dissection of the autophagosome maturation process by a novel reporter protein, tandem fluorescent-tagged LC3. *Autophagy* **3**, 452–460.

- Kosaka, N., Iguchi, H., Yoshioka, Y., Takeshita, F., Matsuki, Y., Ochiya, T. (2010). Secretory mechanisms and intercellular transfer of microRNAs in living cells. *J Biol Chem* **285**, 17442–17452.
- Lathuiliere, A., Valdes, P., Papin, S., Cacquevel, M., Maclachlan, C., Knott, G.W., *et al.* (2017). Motifs in the tau protein that control binding to microtubules and aggregation determine pathological effects. *Sci Rep* **7**, 13556.
- Lee, M.J., Lee, J.H., Rubinshtein, D.C. (2013). Tau degradation: the ubiquitin-proteasome system versus the autophagy-lysosome system. *Prog Neurobiol* **105**, 49–59.
- Malik, B.R., Maddison, D.C., Smith, G.A., Peters, O.M. (2019). Autophagic and endo-lysosomal dysfunction in neurodegenerative disease. *Mol Brain* **12**, 100.
- Martina, J.A., Diab, H.I., Lishu, L., Jeong, A.L., Patange, S., Raben, N., *et al.* (2014). The nutrient-responsive transcription factor TFE3 promotes autophagy, lysosomal biogenesis, and clearance of cellular debris. *Sci Signal* **7**, ra9.
- Martini-Stoica, H., Xu, Y., Ballabio, A., Zheng, H. (2016). The autophagy-lysosomal pathway in neurodegeneration: a TFE3 perspective. *Trends Neurosci* **39**, 221–234.
- Mauvezin, C., Neufeld, T.P. (2015). Bafilomycin A1 disrupts autophagic flux by inhibiting both V-ATPase-dependent acidification and Ca-P60A/SERCA-dependent autophagosome-lysosome fusion. *Autophagy* **11**, 1437–1438.
- McGlinchey, R.P., Jiang, Z., Lee, J.C. (2014). Molecular origin of pH-dependent fibril formation of a functional amyloid. *ChemBiochem* **15**, 1569–1572.
- Menzies, F.M., Fleming, A., Rubinshtein, D.C. (2015). Compromised autophagy and neurodegenerative diseases. *Nat Rev Neurosci* **16**, 345–357.
- Michel, C.H., Kumar, S., Pinotsi, D., Tunnacliffe, A., St George-Hyslop, P., Mandelkow, E., *et al.* (2014). Extracellular monomeric tau protein is sufficient to initiate the spread of tau protein pathology. *J Biol Chem* **289**, 956–967.
- Miesenböck, G., De Angelis, D.A., Rothman, J.E. (1998). Visualizing secretion and synaptic transmission with pH-sensitive green fluorescent proteins. *Nature* **394**, 192–195.
- Miller, N.E., Weinstein, D.B., Steinberg, D. (1977). Binding, internalization, and degradation of high density lipoprotein by cultured normal human fibroblasts. *J Lipid Res* **18**, 438–450.
- Moreau, K., Fleming, A., Imarisio, S., Lopez Ramirez, A., Mercer, J.L., Jimenez-Sanchez, M., *et al.* (2014). PICALM modulates autophagy activity and tau accumulation. *Nat Commun* **5**, 4998.
- Moriarty, G.M., Olson, M.P., Atieh, T.B., Janowska, M.K., Khare, S.D., Baum, J. (2017). A pH-dependent switch promotes beta-synuclein fibril formation via glutamate residues. *J Biol Chem* **292**, 16368–16379.
- Morone, D., Marazza, A., Bergmann, T.J., Molinari, M. (2020). Deep learning approach for quantification of organelles and misfolded polypeptide delivery within degradative compartments. *Mol Biol Cell* **31**, 1512–1524.
- Mulcahy, L.A., Pink, R.C., Carter, D.R. (2014). Routes and mechanisms of extracellular vesicle uptake. *J Extracell Vesicles* **3**, 24641.
- Nikolopoulou, V., Papandreou, M.E., Tavernarakis, N. (2015). Autophagy in the physiology and pathology of the central nervous system. *Cell Death Differ* **22**, 398–407.
- Nixon, R.A., Wegiel, J., Kumar, A., Yu, W.H., Peterhoff, C., Cataldo, A., *et al.* (2005). Extensive involvement of autophagy in Alzheimer disease: an immuno-electron microscopy study. *J Neuropathol Exp Neurol* **64**, 113–122.
- Nixon, R.A. (2013). The role of autophagy in neurodegenerative disease. *Nat Med* **19**, 983–997.
- Parolini, I., Federici, C., Raggi, C., Lugini, L., Palleschi, S., De Mito, A., *et al.* (2009). Microenvironmental pH is a key factor for exosome traffic in tumor cells. *J Biol Chem* **284**, 34211–34222.
- Pecho-Vrieseling, E., Rieker, C., Fuchs, S., Bleckmann, D., Esposito, M.S., Botta, P., *et al.* (2014). Transneuronal propagation of mutant huntingtin contributes to non-cell autonomous pathology in neurons. *Nat Neurosci* **17**, 1064–1072.
- Pedrioli, G., Paganetti, P. (2020). Hijacking endocytosis and autophagy in extracellular vesicle communication: where the inside meets the outside. *Front Cell Dev Biol* **8**, 595515.
- Pegtel, D.M., Cosmopoulos, K., Thorley-Lawson, D.A., van Eijndhoven, M.A., Hopmans, E.S., Lindenberg, J.L., *et al.* (2010). Functional delivery of viral miRNAs via exosomes. *Proc Natl Acad Sci U S A* **107**, 6328–6333.
- Peled, S., Sade, D., Bram, Y., Porat, Z., Kreiser, T., Mimouni, M., *et al.* (2017). Single cell imaging and quantification of TDP-43 and alpha-synuclein intercellular propagation. *Sci Reports* **7**, 544.
- Pérez, M., Avila, J., Hernández, F. (2019). Propagation of tau via extracellular vesicles. *Front Neurosci* **13**, 698.
- Pfefferkorn, C.M., McGlinchey, R.P., Lee, J.C. (2010). Effects of pH on aggregation kinetics of the repeat domain of a functional amyloid, Pmel17. *Proc Natl Acad Sci USA* **107**, 21447.
- Piras, A., Collin, L., Grüniger, F., Graff, C., Rönnbäck, A. (2016). Autophagic and lysosomal defects in human tauopathies: analysis of post-mortem brain from patients with familial Alzheimer disease, corticobasal degeneration and progressive supranuclear palsy. *Acta Neuropathol Commun* **4**, 22.
- Pols, M.S., Klumperman, J. (2009). Trafficking and function of the tetraspanin CD63. *Exp Cell Res* **315**, 1584–1592.
- Raposo, G., Nijman, H.W., Stoorvogel, W., Liejendekker, R., Harding, C.V., Melief, C.J., *et al.* (1996). B lymphocytes secrete antigen-presenting vesicles. *J Exp Med* **183**, 1161–1172.
- Roscic, A., Baldo, B., Crochemore, C., Marcellin, D., Paganetti, P. (2011). Induction of autophagy with catalytic mTOR inhibitors reduces huntingtin aggregates in a neuronal cell model. *J Neurochem* **119**, 398–407.
- Ryder, E.F., Snyder, E.Y., Cepko, C.L. (1990). Establishment and characterization of multipotent neural cell lines using retrovirus vector-mediated oncogene transfer. *J Neurobiol* **21**, 356–375.
- Schmittgen, T.D., Livak, K.J. (2008). Analyzing real-time PCR data by the comparative C(T) method. *Nat Protocols* **3**, 1101–1108.
- Serrano-Pozo, A., Frosch, M.P., Masliah, E., Hyman, B.T. (2011). Neuropathological alterations in Alzheimer disease. *Cold Spring Harbor Perspect Med* **1**, a006189.
- Settembre, C., Di Malta, C., Polito, V.A., Garcia Arencibia, M., Vetrini, F., Erdin, S., *et al.* (2011). TFE3 links autophagy to lysosomal biogenesis. *Science (New York, NY)* **332**, 1429–1433.
- Settembre, C., Fraldi, A., Medina, D.L., Ballabio, A. (2013). Signals from the lysosome: a control centre for cellular clearance and energy metabolism. *Nat Rev Mol Cell Biol* **14**, 283–296.
- Shinoda, H., Ma, Y., Nakashima, R., Sakurai, K., Matsuda, T., Nagai, T. (2018). Acid-Tolerant Monomeric GFP from *Olindias formosa*. *Cell Chem Biol* **25**, 330–338.e7.



## SEEDED TAU ACCUMULATION IN DEGRADATIVE ORGANELLES

1199

- Silva, M.C., Nandi, G.A., Tentarelli, S., Gurrell, I.K., Jamier, T., Lucente, D., *et al.* (2020). Prolonged tau clearance and stress vulnerability rescue by pharmacological activation of autophagy in tauopathy neurons. *Nat Commun* **11**, 3258.
- Simons, M., Raposo, G. (2009). Exosomes—vesicular carriers for intercellular communication. *Curr Opin Cell Biol* **21**, 575–581.
- Skog, J., Würdinger, T., van Rijn, S., Meijer, D.H., Gainche, L., Sena-Esteves, M., *et al.* (2008). Glioblastoma microvesicles transport RNA and proteins that promote tumour growth and provide diagnostic biomarkers. *Nat Cell Biol* **10**, 1470–1476.
- Thery, C., Witwer, K.W., Aikawa, E., Alcaraz, M.J., Anderson, J.D., Andriantsitohaina, R., *et al.* (2018). Minimal information for studies of extracellular vesicles 2018 (MISEV2018): a position statement of the International Society for Extracellular Vesicles and update of the MISEV2014 guidelines. *J Extracell Vesicles* **7**, 1535750.
- Tsujimura, A., Taguchi, K., Watanabe, Y., Tatebe, H., Tokuda, T., Mizuno, T., *et al.* (2015). Lysosomal enzyme cathepsin B enhances the aggregate forming activity of exogenous  $\alpha$ -synuclein fibrils. *Neurobiol Dis* **73**, 244–253.
- Ulrich, G., Salvade, A., Boersema, P., Cali, T., Foglieni, C., Sola, M., *et al.* (2018). Phosphorylation of nuclear Tau is modulated by distinct cellular pathways. *Sci Rep* **8**, 17702.
- Uversky, V.N., Li, J., Fink, A.L. (2001). Evidence for a partially folded intermediate in alpha-synuclein fibril formation. *J Biol Chem* **276**, 10737–10744.
- Valadi, H., Ekstrom, K., Bossios, A., Sjostrand, M., Lee, J.J., Lotvall, J.O. (2007). Exosome-mediated transfer of mRNAs and microRNAs is a novel mechanism of genetic exchange between cells. *Nat Cell Biol* **9**, 654–659.
- Vaz-Silva, J., Gomes, P., Jin, Q., Zhu, M., Zhuravleva, V., Quintremil, S., *et al.* (2018). Endolysosomal degradation of Tau and its role in glucocorticoid-driven hippocampal malfunction. *EMBO J* **37**, e99084.
- Vogt, S., Stadlmayr, G., Grillari, J., Rüker, F., Wozniak-Knopp, G. (2019). Engineering of surface proteins in extracellular vesicles for tissue-specific targeting. In *Current Topics in Biochemical Engineering*. IntechOpen ed. Available at: <https://www.intechopen.com/chapters/65340>. Accessed January 15, 2020.
- Wang, C., Telpoukhovskaia, M.A., Bahr, B.A., Chen, X., Gan, L. (2018). Endo-lysosomal dysfunction: a converging mechanism in neurodegenerative diseases. *Curr Opin Neurobiol* **48**, 52–58.
- Wang, Y., Martinez-Vicente, M., Krüger, U., Kaushik, S., Wong, E., Mandelkow, E.M., *et al.* (2009). Tau fragmentation, aggregation and clearance: the dual role of lysosomal processing. *Hum Mol Genet* **18**, 4153–4170.
- Wang, Y., Mandelkow, E. (2012). Degradation of tau protein by autophagy and proteasomal pathways. *Biochem Soc Trans* **40**, 644–652.
- Wang, Y., Balaji, V., Kaniyappan, S., Krüger, L., Irsen, S., Teppe, K., *et al.* (2017). The release and trans-synaptic transmission of Tau via exosomes. *Mol Neurodegeneration* **12**, 5.
- Wong, E., Cuervo, A.M. (2010). Autophagy gone awry in neurodegenerative diseases. *Nat Neurosci* **13**, 805–811.
- Yang, Z., Klionsky, D.J. (2010). Mammalian autophagy: core molecular machinery and signaling regulation. *Curr Opin Cell Biol* **22**, 124–131.
- Yuan, Z., Yidan, Z., Jian, Z., Xiangjian, Z., Guofeng, Y. (2020). Molecular mechanism of Autophagy: its role in the therapy of Alzheimer's disease. *Curr Neuropharmacol* **18**, 720–739.
- Zhang, Y., Liu, D., Chen, X., Li, J., Li, L., Bian, Z., *et al.* (2010). Secreted monocytic miR-150 enhances targeted endothelial cell migration. *Mol cell* **39**, 133–144.
- Zomer, A., Maynard, C., Verweij, F.J., Kamermans, A., Schaffer, R., Beerling, E., *et al.* (2015). In Vivo imaging reveals extracellular vesicle-mediated phenocopying of metastatic behavior. *Cell* **161**, 1046–1057.

Address correspondence to:

Paolo Paganetti, PhD

Neurodegeneration Research Group

Laboratory for Biomedical Neurosciences

Neurocenter of Southern Switzerland

Ente Ospedaliero Cantonale

Via ai Söi 24

Bellinzona CH-6807

Switzerland

E-mail: paolo.paganetti@eoc.ch

Received for publication June 6, 2021; received in revised form June 23, 2021; accepted June 24, 2021.

### Supplementary Materials and Methods

**Plasmids.** The following plasmids were gifts obtained through Addgene: pCMV-lyso-pHluorin (RRID:Addgene\_70113, C. Rosenmund (Rost et al., 2015)), Gamillus-pcDNA3 (RRID:Addgene\_124837, T. Nagai (Shinoda et al., 2018)), pLAMP1-mCherry (RRID:Addgene\_45147, A. Palmer (Van Engelenburg and Palmer, 2010)), pLVCMV-LoxP-DsRed-LoxP-eGFP (RRID:Addgene\_65726, J. van Rheenen (Zomer et al., 2015)), mCherry-GFP-LC3 (RRID: Addgene\_110060, A. Brunet (Leeman et al., 2018)). The Cre plasmid was obtained by subcloning the PCR-amplified cDNA encoding for Cre (RRID:Addgene\_65727, J. van Rheenen (Zomer et al., 2015)) in the vector pcDNA5/FRT/TO downstream of the T11 sequence with primers containing EocRI and XhoI. The GFP plasmid was obtained by merging the cDNAs encoding for GFP1-10 with S11 (Foglieni et al., 2017) in the vector pcDNA5/FRT/TO with BamHI/XhoI. GFP-CD63 was obtained by sequential subcloning of the human CD63 cDNA in the vector pcDNA5/FRT/TO followed by in-frame 5'-insertion of the GFP cDNA with HindIII/BclI. A similar strategy was used to generate all the other organelle markers fused to GFP. GFP-MBD was generated by replacing the CD63 cDNA with that encoding for MBD with BamHI/XhoI. The GFP-MBD<sub>2P</sub> mutant was generated by introducing the I277P and I308P amino acid substitutions by two sequential rounds of site-directed mutagenesis PCR on the template GFP-MBD cDNA. Primers used were

for the I277P mutation: GGAAGGTGCAGCCAATTAATAAGAAGCTGG (forward) and CCAGCTTCTTATTAATTGGCTGCACCTTCC (reverse)

for the I308P mutation: GCAGTGTGCAACCAGTCTACAAACC (forward) and GGTGGTAGACTGGTTGCACACTGC (reverse)

The Tau<sub>441</sub>-mCherry cDNA was custom synthesized (Promogene, France) and subcloned in the vector pcDNA5/FRT/TO with BamHI/XhoI. For the split GFP, we added the first ten  $\beta$ -strands of GFP (GFP<sub>1-10</sub>) at the amino-terminus of MBD and the eleventh  $\beta$ -strand of GFP (T11) at the amino-terminus of Tau<sub>441</sub>-mCherry (Foglieni et al., 2017).



The sequences of the cDNAs generated for this study were the following:

aagcttaccATGGAGAAGAGGGACCACATGGTGCTGCTGGAGTACGTGACCGCCGCCGGCATCACCGACGCCT  
CGGGGGTACCAGTTTCAGAGTTCAGGCACGACAGCGGCGGACCCGGGAGCGGCGGTGAGGGCTCAGCCG  
GCGGAGGACCGGTGCGAGGCgcatccactagtaacggccgacgtgtgctgaattcacATGTCCAATTTACTGACCGTACAC  
CAAAATTTGCCTGCATTACCGGTGATGCAACGAGTGATGAGGTTGCGAAGAACCTGATGGACATGTTTCAGG  
GATCGCCAGGCGTTTTCTGAGCATACCTGGAAAATGCTTCTGTCCGTTTGCCGGTCGTGGGCGGCATGGTG  
CAAGTTGAATAACCGGAAATGGTTTCCCGCAGAACCTGAAGATGTTTCGCGATTATCTTCTATATCTTCAGGCG  
CGCGGTCTGGCAGTAAAACTATCCAGCAACATTTGGGCCAGCTAAACATGCTTCATCGTCGGTCCGGGCTG  
CCACGACCAAGTGACAGCAATGCTGTTTCACTGGTTATGCGGCGGATCCGAAAAGAAAACGTTGATGCCGGT  
GAACGTGCAAAACAGGCTCTAGCGTTCGAACGCACTGATTTGACCGAGTTCGTTCACTCATGAAAATAGC  
GATCGCTGCCAGGATATACGTAATCTGGCATTCTGGGGATTGCTTATAACACCCTGTTACGTATAGCCGAAA  
TTGCCAGGATCAGGGTTAAAGATATCTCAGTACTGACGGTGGGAGAATGTTAATCCATATTGGCAGAACGA  
AAACGCTGGTTAGCACCGCAGGTGTAGAGAAGGCACCTAGCCTGGGGGTAACATAACTGGTCGAGCGATGG  
ATTTCCGTCTCTGGTGTAGCTGATGATCCGAATAACTACCTGTTTTGCCGGGTCAGAAAAATGGTGTTGCCG  
CGCCATCTGCCACCAGCCAGCTATCAACTCGCGCCCTGGAAGGGATTTTTGAAGCAACTCATCGATTGATTT  
ACGGCGCTAAGGATGACTCTGGTCAGAGATACCTGGCCTGGTCTGGACACAGTGCCCGTGTGCGAGCCGC  
GCGAGATATGGCCCGCGCTGGAGTTTCAATACCGGAGATCATGCAAGCTGGTGGCTGGACCAATGTAAATA  
TTGTCATGAATATATCCGTAACCTGGATAGTGAAACAGGGGCAATGGTGCCTGCTGGAAGATGGCGATT  
AGctcgag (T11-Cre)

aagcttaccATGTCCAAAGGAGAAGAACTGTTTACCGGCGTGGTGCCAATTCTCGTGGAAGTGGATGGCGATGT  
GAATGGCCACAAATTTCTGTCTCAGAGGAGAGGGTGAAGGTGATGCCACAATCGGAAAGCTCACCTGAAATT  
CATCTGCACCACTGGAAAGCTCCCTGTGCCATGGCCAACACTGGTCACTACCCTGACCTACGGCGTGCAGT  
GCTTTTCCAGATACCCAGACCATATGAAGAGGCATGACTTTTTCAAGAGCGCCATGCCCGAGGGCTATGTGC  
AGGAGAGAACCATCTCTTTCAAAGATGACGGGAAATACAAGACCCGCGCTGTGGTCAAGTTCGAAGGAGAC  
ACACTGGTGAATAGAATCGAGTTGAAGGGCACAGACTTTAAGGAAGATGGAAACATTCTCGGCCACAAGCTG  
GAATACAACCTTAACTCCCACAATGTGTACATCACAGCCGACAAAGCAAAAGAATGGCATCAAGGCTAACTTCA  
CAGTCAGACACAACGTCGAGGATGGAAGCGTGACGCTGGCCGACCATTATCAACAGAACTCCAATCGGC  
GACGGCCCTGTGCTCCTCCAGACAACCATACCTGTCCACCCAGACAGTCTGAGCAAAGATCCAAATGAA  
AAACGGGACCACATGGTGTGCACGAGTACGTGAACGCCGCCGGCATCACAgGCTCAGCCGGCGGAGGAC  
CGGTGCGAGGCgcatccaccATGGCGGTGGAAGGAGGAATGAAATGTGTGAAGTTCTTGCTCTACGTCCTCCTG  
CTGGCCTTTTGCGCCTGTGCACTGGGACTGATTGCCGTGGGTGTGCGGGCACAGCTTGCTCTGAGTCAGAC  
CATAATCCAGGGGGTACCCCTGGCTCTCTGTTGCCAGTGGTCATCATCGAGTGGGTGTCTTCTCTCTCT  
GGTGGCTTTTGTGGGCTGCTGCGGGGCTGCAAGGAGAACTATTGTCTTATGATCACGTTTGCCATCTTTCT

GTCTCTTATCATGTTGGTGGAGGTGGCCGAGCCATTGCTGGCTATGTGTTTAGAGATAAGGTGATGTCAGA  
 GTTTAATAACAACCTCCGGCAGCAGATGGAGAATTACCCGAAAAACAACCACACTGCTTCGATCCTGGACAG  
 GATGCAGGCAGATTTTAAGTGTGTGGGGCTGCTAACTACACAGATTGGGAGAAAAATCCCTTCCATGTGCGAA  
 GAACCGAGTCCCCGACTCCTGTGTCATTAATGTTACTGTGGGCTGTGGGATTAATTTCAACGAGAAGGCGAT  
 CCATAAGGAGGGCTGTGTGGAGAAGATTGGGGGCTGGCTGAGGAAAAATGTGCTGGTGGTAGCTGCAGCA  
 GCCCTTGGAATTGCTTTTGTGAGGTTTTGGGAATTGCTTTGCCTGTGCCTCGTGAAGAGTATCAGAAAGTG  
 GCTACGAGGTGATGTAGaattc (GFP-CD63)

aagcttaccATGTCCAAAGGAGAAGAACTGTTTACCGGCGTGGTGCCAATTCTCGTGGAAGTGGATGGCGATGT  
 GAATGGCCACAAATTTTCTGTCTAGAGGAGAGGGTGAAGGTGATGCCACAATCGGAAAGCTCACCTGAAATT  
 CATCTGCACCACTGGAAAGCTCCCTGTGCCATGGCCAACACTGGTCACTACCCTGACCTACGGCGTGCAGT  
 GCTTTTCCAGATACCCAGACCATATGAAGAGGCATGACTTTTTCAAGAGCGCCATGCCGAGGGCTATGTGC  
 AGGAGAGAACCATCTCTTTCAAAGATGACGGGAAATACAAGACCCGCGCTGTGGTCAAGTTCAAGGAGAC  
 ACACTGGTGAATAGAATCGAGTTGAAGGGCACAGACTTTAAGGAAGATGGAAACATTCTCGGCCACAAGCTG  
 GAATACAACCTTAACCTCCACAATGTGTACATCACAGCCGACAAGCAAAAGAAATGGCATCAAGGCTAACTTCA  
 CAGTCAGACACAACGTCGAGGATGGAAGCGTGCAGCTGGCCGACCATTATCAACAGAACACTCCAATCGGC  
 GACGGCCCTGTGCTCCTCCAGACAACCATACCTGTCCACCCAGACAGTCTGAGCAAAGATCCAAATGAA  
 AAACGGGACCACATGGTGTGCACGAGTACGTGAACGCCGCCGCGCATCACAgggtcagccggcgaggaccggtcgga  
 ggcggatccACTAGCAGAAGCACAGCTAGGCCCAATGGGCAACCCAGGCCAGCAAAATTTGCCAGTTCAAATT  
 GGTCTGTGTGGAGAATCTGCAGTGGGAAAGTCAAGCCTGGTATTACGTTTTGTCAAAGGGCAGTTCCATGA  
 GTACCAGGAGAGCACCATTGGAGCGGCCTTCCTCACCCAGTCCGTTTGTCTAGATGACACAACAGTGAAGTT  
 TGAGATCTGGGACACAGCTGGGCAGGAGCGATATCACAGCTTAGCCCCCATGTACTACAGGGGTGCCCCAG  
 CTGCAATCGTGGTTTACGACATTACTAATCAGGAAACCTTTGCCGAGCAAAGACATGGGTGAAGGAACTAC  
 AGCGACAGGCCAGTCTAGCATCGTTATTGCCCTGGCAGGGAACAAAGCTGACCTGGCCAACAAACGTATG  
 GTGGAGTATGAAGAGGCCAGGCATATGCAGATGACAACAGCTTATTGTTTATGGAGACTTCAGCCAAGACA  
 GCTATGAACGTGAATGATCTCTTCTGGCAATAGCTAAGAAAGTTGCCAAAGAGTGAACCCAGAACTCTGGGA  
 GGTGCAGCAGGCCGAAGCCGGGTGTGGATCTCCATGAACAGTCCCAGCAGAACAAGAGCCAGTGTGTA  
 GCAACTGActcgagcatg (GFP-Rab5)

aattaagcttgacaccATGGCGGCCCCCGGCAGCGCCCGGCGACCCCTGCTGCTGCTACTGCTGTTGCTGCTGCT  
 CGGCCTCATGCATTGTGCGTCAGCAGCAATGTTTATGGTGAAAAATGGCAACGGGACCGCGTGATAATGG  
 CCAACTTCTCTGCTGCCTTCTCAGTGAACACGACACCAAGAGTGGCCCTAAGAACATGACCTTTGACCTGC  
 CATCAGATGCCACAGTGGTGTCAACCGCAGCTCCTGTGAAAAAGAGAACTTCTGACCCAGTCTCGTGA  
 TTGCTTTTGAAGAGGACATACACTCACTCTCAATTTACGAGAAATGCAACACGTTACAGCGTCCAGCTCAT  
 GAGTTTTGTTTATAACTTGTCTAGACACACACCTTTTCCCCAATGCGAGCTCAAAGAAATCAAGACTGTGGAA

TCTATAACTGACATCAGGGCAGATATAGATAAAAAATACAGATGTGTTAGTGGCACCCAGGTCCACATGAACA  
 ACGTGACCGTAACGCTCCATGATGCCACCATCCAGGCGTACCTTTCCAACAGCAGCTTCAGCAGGGGAGAG  
 ACACGCTGTGAACAAGACAGGCCTTCCCCAACACAGCGCCCCCTGCGCCACCCAGCCCCTCGCCCTCACC  
 CGTGCCCCAAGAGCCCCTCTGTGGACAAGTACAACGTGAGCGGCACCAACGGGACCTGCCTGCTGGCCAGC  
 ATGGGGCTGCAGCTGAACCTCACCTATGAGAGGAAGGACAACACGACGGTGACAAGGCTTCTCAACATCAA  
 CCCCACAAGACCTCGGCCAGCGGGAGCTGCGGCGCCACCTGGTGACTCTGGAGCTGCACAGCGAGGG  
 CACCACCGTCCTGCTCTTCCAGTTCGGGATGAATGCAAGTTCTAGCCGGTTTTTCTACAAGGAATCCAGTT  
 GAATACAATTCTTCTGACGCCAGAGACCCTGCCTTTAAAGCTGCCAACGGCTCCCTGCGAGCGCTGCAGG  
 CCACAGTCGGCAATTCTACAAGTGCAACGCGGAGGAGCACGTCCGTGTACGAAGGCGTTTTTCAGTCAAT  
 ATATTCAAAGTGTGGGTCCAGGCTTTCAAGGTGGAAGGTGGCCAGTTTGGCTCTGTGGAGGAGTGTCTGCT  
 GGACGAGAACAGCATGCTGATCCCCATCGCTGTGGGTGGTGCCCTGGCGGGGCTGGTCCCTCATCGTCCTCA  
 TCGCTACCTCGTCGGCAGGAAGAGGAGTCACGCAGGCTACCAGACTggggatccaccggtcgccaccATGGTGAGC  
 AAGGGCGAGGAGCTGTTACCGGGGTGGTGCCATCCTGGTCGAGCTGGACGGCGACGTAAACGGCCACA  
 AGTTACGCGTGTCCGGCGAGGGCGAGGGCGATGCCACCTACGGCAAGCTGACCCTGAAGTTTCACTGTGCAC  
 CACCGGCAAGCTGCCCGTGCCCTGGCCACCCCTCGTGACCACCCTGACCTACGGCGTGCAGTGTTCAGC  
 CGCTACCCCGACCACATGAAGCAGCAGACTTCTTCAAGTCCGCCATGCCGAAGGCTACGTCCAGGAGCG  
 CACCATCTTCTTCAAGGACGACGGCAACTACAAGACCCGCGCCGAGGTGAAGTTCGAGGGCGACACCCTGG  
 TGAACCGCATCGAGCTGAAGGGCATCGACTTCAAGGAGGACGGCAACATCCTGGGGCACAAGCTGGAGTAC  
 AACTACAACAGCCACAACGTCTATATCATGCGCGACAAGCAGAAGAACGGCATCAAGGTGAACCTTCAAGATC  
 CGCCACAACATCGAGGACGGCAGCGTGCAGCTCGCCGACCACTACCAGCAGAACACCCCCATCGGCGACG  
 GCCCCGTGCTGCTGCCCCGACAACCACTACCTGAGCACCCAGTCCGCCCTGAGCAAAGACCCCAACGAGAA  
 GCGCGATCACATGGTCTGCTGGAGTTCGTGACCGCCGCCGGGATCACTCTCGGCATGGACGAGCTGTACA  
 AGTAAagcgccgc (LAMP1-GFP)

aagcttaccATGGTGAGCAAGGGCGAGGAGGCATCTGGCAGAGCCCTGTTCCAGTACCCCATGACCAGCAAGAT  
 CGAGCTGAACGGCGAGATCAACGGCAAGAAATTCAGGTGGCCGGCGAGGGCTTACCCCCAGCAGCGGC  
 AGATTCAACATGCACGCCTACTGCACCACCGGCGACCTGCCTATGAGCTGGGTCGTGATTGCCAGCCCCCT  
 CCAGTACGGCTTCCACATGTTGCCCCACTACCCCGAGGACATCACACACTTTTTCCAGGAATGCTTCCCCGG  
 CAGCTACACCCTGGACCGGACCCTGAGAAATGGAAGGCGACGGCACCCTGACCACCCACCACGAGTACAGC  
 CTGGAGGACGGCTGCGTGACCTCCAAGACCACCCTGAATGCCAGCGGCTTCGACCCTAAGGGCGCCACCA  
 TGACCAAGAGCTTCGTGAAACAACCTGCCTAACGAGGTGAAGATCACCCCCACGGCCCCAACGGCATCAGA  
 CTGACCAGCACCGTGTGTACCTGAAGGAGGATGGCACCATCCAGATCGGCACCCAGGACTGCATCGTGAC  
 CCCTGTGGGCGGAAGGAAAGTGACCCAGCCCAAGGCCCACTTCTGCACACCCAGATCATCCAGAAGAAGG  
 ACCCCAACGACACCCGGGACCACATCGTGCAGACAGAAGTGGCCGTGGCCGGCAATCTGTGGCAGGGCAT  
 GGACGAGCTGTACAAGggaccggtcgagggcgatccCCGTGCGAGAAGACCTTCAAGCAGCGCCGCACCTTCGAA

CAAAGAGTAGAAGATGTCCGACTTATTCGAGAGCAGCATCCAACCAAAATCCCGGTGATAATAGAACGATAC  
 AAGGGTGAGAAGCAGCTTCCTGTTCTGGATAAAACAAAGTTCCCTGTACCTGACCATGTCAACATGAGTGAG  
 CTCATCAAGATAATTAGAAGGCGCTTACAGCTCAATGCTAATCAGGCCTTCTTCCTGTTGGTGAACGGACACA  
 GCATGGTCAGCGTCTCCACACCAATCTCAGAGGTGTATGAGAGTGAGAAAGATGAAGATGGATTCTCTGTACA  
 TGGTCTATGCCTCCCAGGAGACGTTCCGGGATGAAATTGTCAGTGTAActcgag (Gamillus-LC3)

aagcttaccATGTCCAAAGGAGAAGAAGTGTTCACCGGCGTGGTGCCAATTCTCGTGGAAGTGGATGGCGATGT  
 GAATGGCCACAAATTTTCTGTGTCAGAGGAGAGGGTGAAGGTGATGCCACAATCGGAAAGCTCACCTGAAATT  
 CATCTGCACCACTGGAAAGTCCCTGTGCCATGGCCAACACTGGTCACTACCCTGACCTACGGCGTGCAGT  
 GCTTTTCCAGATACCCAGACCATATGAAGAGGCATGACTTTTTCAAGAGCGCCATGCCCGAGGGCTATGTGC  
 AGGAGAGAACCATCTCTTTCAAAGATGACGGGAAATACAAGACCCGCGCTGTGGTCAAGTTCGAAGGAGAC  
 ACACTGGTGAATAGAATCGAGTTGAAGGGCACAGACTTTAAGGAAGATGGAAACATTCTCGGCCACAAGCTG  
 GAATACAACTTTAACTCCCAATGTGTACATCACAGCCGACAAGCAAAAGATGGCATCAAGGCTAACTTCA  
 CAGTCAGACACAACGTCGAGGATGGAAGCGTGCAGCTGGCCGACCATTATCAACAGAACTCCAAATCGGC  
 GACGGCCCTGTGCTCCTCCAGACAACCATTACCTGTCCACCCAGACAGTCTGAGCAAAGATCCAAATGAA  
 AAACGGGACCACATGGTGTGCACGAGTACGTGAACGCCGCCGGCATCACAgGCTCAGCCGGCGGAGGAC  
 CGGTCCGAGGCGgatccaccATGCAGACAGCCCCGTGCCATGCCAGACCTGAAGAATGTCAAGTCCAAGAT  
 CGGCTCCACTGAGAACCTGAAGCACCAGCCGGGAGGCGGGAAGGTGCAGATAATTAATAAGAGCTGGATC  
 TTAGCAACGTCCAGTCCAAGTGTGGCTCAAAGGATAATATCAAACACGTCCCGGAGGCGGCAGTGTGCAA  
 ATAGTCTACAAACCAGTTGACCTGAGCAAGGTGACCTCCAAGTGTGGCTCATTAGGCAACATCCATCATAAA  
 CCAGGAGGTGGCCAGGTGGAAGTAAATCTGAGAAGCTTGACTTCAAGGACAGAGTCCAGTCAAGATTGG  
 GTCCCTGGACAATATCACCCACGTCCCTGGCGGAGGAAATAAGATTGAATAActcgag (GFP-MBD)

aagcttaccATGTCCAAAGGAGAAGAAGTGTTCACCGGCGTGGTGCCAATTCTCGTGGAAGTGGATGGCGATGT  
 GAATGGCCACAAATTTTCTGTGTCAGAGGAGAGGGTGAAGGTGATGCCACAATCGGAAAGCTCACCTGAAATT  
 CATCTGCACCACTGGAAAGTCCCTGTGCCATGGCCAACACTGGTCACTACCCTGACCTACGGCGTGCAGT  
 GCTTTTCCAGATACCCAGACCATATGAAGAGGCATGACTTTTTCAAGAGCGCCATGCCCGAGGGCTATGTGC  
 AGGAGAGAACCATCTCTTTCAAAGATGACGGGAAATACAAGACCCGCGCTGTGGTCAAGTTCGAAGGAGAC  
 ACACTGGTGAATAGAATCGAGTTGAAGGGCACAGACTTTAAGGAAGATGGAAACATTCTCGGCCACAAGCTG  
 GAATACAACTTTAACTCCCAATGTGTACATCACAGCCGACAAGCAAAAGATGGCATCAAGGCTAACTTCA  
 CAGTCAGACACAACGTCGAGGATGGAAGCGTGCAGCTGGCCGACCATTATCAACAGAACTCCAAATCGGC  
 GACGGCCCTGTGCTCCTCCAGACAACCATTACCTGTCCACCCAGACAGTCTGAGCAAAGATCCAAATGAA  
 AAACGGGACCACATGGTGTGCACGAGTACGTGAACGCCGCCGGCATCACAgGCTCAGCCGGCGGAGGAC  
 CGGTCCGAGGCGgatccaccATGCAGACAGCCCCGTGCCATGCCAGACCTGAAGAATGTCAAGTCCAAGAT  
 CGGCTCCACTGAGAACCTGAAGCACCAGCCGGGAGGCGGGAAGGTGCAGCAATTAATAAGAGCTGGAT

CTTAGCAACGTCCAGTCCAAGTGTGGCTCAAAGGATAATATCAAACACGTCCCGGGAGGCGGCAGTGTGCA  
 ACCAGTCTACAAACCAGTTGACCTGAGCAAGGTGACCTCCAAGTGTGGCTCATTAGGCAACATCCATCATAA  
 ACCAGGAGGTGGCCAGGTGGAAGTAAATCTGAGAAGCTTGACTTCAAGGACAGAGTCCAGTCAAGATTG  
 GGTCCCTGGACAATATCACCCACGTCCCTGGCGGAGGAAATAAGATTGAATAActcgag (GFP-MBD<sub>2P</sub>)

aagcttaccATGTCCAAAGGAGAAGAACTGTTTACCGGCGTGGTGCCAATTCTCGTGGAAGTGGATGGCGATGT  
 GAATGGCCACAAATTTTCTGTCAGAGGAGAGGGTGAAGGTGATGCCACAATCGGAAAGCTCACCTGAAATT  
 CATCTGCACCACTGGAAAGCTCCCTGTGCCATGGCCAACACTGGTCACTACCCTGACCTACGGCGTGCAGT  
 GCTTTTCCAGATACCCAGACCATATGAAGAGGCATGACTTTTCAAGAGCGCCATGCCGAGGGCTATGTGC  
 AGGAGAGAACCATCTCTTTCAAAGATGACGGGAAATACAAGACCCGCGCTGTGGTCAAGTTCGAAGGAGAC  
 ACACTGGTGAATAGAATCGAGTTGAAGGGCACAGACTTTAAGGAAGATGGAACATTCTCGGCCACAAGCTG  
 GAATACAACTTTAACTCCACAATGTGTACATCACAGCCGACAAGCAAAGAATGGCATCAAGGCTAACTTCA  
 CAGTCAGACACAACGTGAGGATGGAAGCGTGCAGCTGGCCGACCATTATCAACAGAACACTCCAATCGGC  
 GACGGCCCTGTGCTCCTCCAGACAACCATTACCTGTCCACCCAGACAGTCTGAGCAAAGATCCAAATGAA  
 AAACGGGACCACATGGTGTGCACGAGTACGTGAACGCCGCGGCATCACAgGCTCAGCCGGCGGAGGAC  
 CGGTCCGAGGCGgatccaccATGCAGACAGCCCCGTGCCATGCCAGACCTGAAGAATGTCAAGTCCAAGAT  
 CGGCTCCACTGAGAACCTGAAGCACCAGCCGGGAGGCGGGAAGGTGCAGCCAATTAATAAGAAGCTGGAT  
 CTTAGCAACGTCCAGTCCAAGTGTGGCTCAAAGGATAATATCAAACACGTCCCGGGAGGCGGCAGTGTGCA  
 ACCAGTCTACAAACCAGTTGACCTGAGCAAGGTGACCTCCAAGTGTGGCTCATTAGGCAACATCCATCATAA  
 ACCAGGAGGTGGCCAGGTGGAAGTAAATCTGAGAAGCTTGACTTCAAGGACAGAGTCCAGTCAAGATTG  
 GGTCCCTGGACAATATCACCCACGTCCCTGGCGGAGGAAATAAGATTGAATAActcgag (GFP-MBD<sub>2P</sub>)

aagcttaccATGTCCAAAGGAGAAGAACTGTTTACCGGCGTGGTGCCAATTCTCGTGGAAGTGGATGGCGATGT  
 GAATGGCCACAAATTTTCTGTCAGAGGAGAGGGTGAAGGTGATGCCACAATCGGAAAGCTCACCTGAAATT  
 CATCTGCACCACTGGAAAGCTCCCTGTGCCATGGCCAACACTGGTCACTACCCTGACCTACGGCGTGCAGT  
 GCTTTTCCAGATACCCAGACCATATGAAGAGGCATGACTTTTCAAGAGCGCCATGCCGAGGGCTATGTGC  
 AGGAGAGAACCATCTCTTTCAAAGATGACGGGAAATACAAGACCCGCGCTGTGGTCAAGTTCGAAGGAGAC  
 ACACTGGTGAATAGAATCGAGTTGAAGGGCACAGACTTTAAGGAAGATGGAACATTCTCGGCCACAAGCTG  
 GAATACAACTTTAACTCCACAATGTGTACATCACAGCCGACAAGCAAAGAATGGCATCAAGGCTAACTTCA  
 CAGTCAGACACAACGTGAGGATGGAAGCGTGCAGCTGGCCGACCATTATCAACAGAACACTCCAATCGGC  
 GACGGCCCTGTGCTCCTCCAGACAACCATTACCTGTCCACCCAGACAGTCTGAGCAAAGATCCAAATGAA  
 AAAGGAACAgGCTCAGCCGGCGGAGGACCGGTGGAGGCgatccaccATGCAGACAGCCCCGTGCCATG  
 CCAGACCTGAAGAATGTCAAGTCCAAGATCGGCTCCACTGAGAACCTGAAGCACCAGCCGGGAGGCGGGAA  
 GGTGCAGATAATTAATAAGAAGCTGGATCTTAGCAACGTCCAGTCCAAGTGTGGCTCAAAGGATAATATCAA  
 CACGTCCCGGGAGGCGGCAGTGTGCAATAGTCTACAAACCAGTTGACCTGAGCAAGGTGACCTCCAAGTG

TGGCTCATTAGGCAACATCCATCATAAACCAGGAGGTGGCCAGGTGGAAGTAAATCTGAGAAGCTTGACTT  
 CAAGGACAGAGTCCAGTCCGAAGATTGGGTCCCTGGACAATATCACCCACGTCCCTGGCGGAGGAAATAAGA  
 TTGAATAActcgag (GFP1-10-MBD)

ggatccaccATGGCTGAGCCCCGCCAGGAGTTCGAAGTGATGGAAGATCACGCTGGGACGTACGGGTTGGGGG  
 ACAGGAAAGATCAGGGGGGCTACACCATGCACCAAGACCAAGAGGGTGACACGGACGCTGGCCTGAAAGA  
 ATCTCCCCTGCAGACCCCCACTGAGGACGGATCTGAGGAACCGGGCTCTGAAACCTCTGATGCTAAGAGCA  
 CTCCAACAGCGGAAGATGTGACAGCACCCCTTAGTGATGAGGGAGCTCCCGGCAAGCAGGCTGCCGCGCA  
 GCCCCACACGGAGATCCAGAAGGAACCACAGCTGAAGAAGCAGGCATTGGAGACACCCCCAGCCTGGAA  
 GACGAAGCTGCTGGTCACGTGACCCAAGCTCGCATGGTCAGTAAAAGCAAAGACGGGACTGGAAGCGATGA  
 CAAAAAGCCAAGGGGGCTGATGGTAAACGAAGATCGCCACACCGCGGGGAGCAGCCCCCTCAGGCCAG  
 AAGGGCCAGGCCAACGCCACCAGATTCCAGCAAAAACCCCGCCGCTCCAAAGACACCACCCAGCTCTG  
 GTGAACCTCCAAAATCAGGGGATCGCAGCGGCTACAGCAGCCCCGGCTCCCAGGCACTCCCGGCAGCCG  
 CTCCCGCACCCCGTCCCTTCCAACCCACCCACCCGGGAGCCCAAGAAGGTGGCAGTGGTCCGTACTCCA  
 CCCAAGTCGCCGTCTTCGCCAAGAGCCGCTGCAGACAGCCCCCGTGGCCATGCCAGACCTGAAGAATGT  
 CAAGTCCAAGATCGGCTCCACTGAGAACCTGAAGCACCAGCCGGGAGGCGGGAAGGTGCAGATAATTAATA  
 AGAAGCTGGATCTTAGCAACGTCCAGTCCAAGTGTGGCTCAAAGGATAATATCAAACACGTCCCGGGAGGC  
 GGCAGTGTCAAATAGTCTACAAACCAGTTGACCTGAGCAAGGTGACCTCCAAGTGTGGCTCATTAGGCAAC  
 ATCCATCATAAACCAGGAGGTGGCCAGGTGGAAGTAAATCTGAGAAGCTTGACTTCAAGGACAGAGTCCAG  
 TCGAAGATTGGGTCCCTGGACAATATCACCCACGTCCCTGGCGGAGGAAATAAAAAGATTGAAACCCACAAG  
 CTGACCTTCCGCGAGAACGCCAAAGCCAAGACAGACCAGGGGCGGAGATCGTGTACAAGTCGCCAGTGG  
 TGTCTGGGGACACGTCTCCACGGCATCTCAGCAATGTCTCTCCACCGGCAGCATCGACATGGTAGACTCG  
 CCCCAGCTCGCCACGCTAGCTGACGAGGTGTCTGCCTCCCTCGCGAAGCAGGGTTTGGTTTGAAGGGCGA  
 GGAGGATAACATGGCCATCATCAAGGAGTTCATGCGCTTCAAGGTGCACATGGAGGGTCCGTGAACGGCC  
 ACGAGTTCGAGATCGAGGGCGAGGGCGAGGGCCGCCCTACGAGGGCACCCAGACCAGCCGAAGCTGAAGG  
 TGACCAAGGGTGGCCCCCTACCTTCGCCTGGGACATCCTGTCCCTCAGTTCATGTACGGCTCCAAGGCC  
 TACGTGAAGCACCCCGCCGACATCCCCGACTACTTGAAGCTGTCTTCCCCGAGGGCTTCAAGTGGGAGCG  
 CGTGATGAACTTCGAGGACGGCGGCGTGGTGACCGTGACCCAGGACTCCTCCCTGCAGGACGGCGAGTTC  
 ATCTACAAGGTGAAGCTGCGCGGCACCAACTTCCCTCCGACGGCCCCGTAATGCAGAAGAAGACCATGGG  
 CTGGGAGGCCTCCTCCGAGCGGATGTACCCCGAGGACGGCGCCCTGAAGGGCGAGATCAAGCAGAGGCT  
 GAAGCTGAAGGACGGCGGCCACTACGACGCTGAGGTCAAGACCACCTACAAGGCCAAGAAGCCCGTGCAG  
 CTGCCCCGGCGCTACAACGTCAACATCAAGTTGGACATCACCTCCCACAACGAGGACTACACCATCGTGGA  
 ACAGTACGAACGCGCCGAGGGCCGCCACTCCACCGGCGGCATGGACGAGCTGTACAAGTAGctcgag  
 (Tau441-mCherry)

aagcttaccATGGAGAAGAGGGACCACATGGTGCTGCTGGAGTACGTGACCGCCGCCGGCATCACCGACGCCT  
CGGGGGTACCAGGTTTCAGAGTTCAGGCACGACAGCGGCGGACCCGGGAGCGGCGGTGAGGGCTCAGCCG  
GCGGAGGACCGGTTCGAGGCGgatccaccATGGCTGAGCCCCGCCAGGAGTTCGAAGTGATGGAAGATCACG  
CTGGGACGTACGGGTTGGGGGACAGGAAAGATCAGGGGGGCTACACCATGCACCAAGACCAAGAGGGTGA  
CACGGACGCTGGCCTGAAAGAATCTCCCCTGCAGACCCCCACTGAGGACGGATCTGAGGAACCGGGCTCT  
GAAACCTCTGATGCTAAGAGCACTCCAACAGCGGAAGATGTGACAGCACCCCTTAGTGATGAGGGAGCTCC  
CGGCAAGCAGGCTGCCGCGCAGCCCCACACGGAGATCCCAGAAGGAACACAGCTGAAGAAGCAGGCATT  
GGAGACACCCCCAGCCTGGAAGACGAAGCTGCTGGTCACGTGACCCAAGCTCGCATGGTCAGTAAAAGCAA  
AGACGGGACTGGAAGCGATGACAAAAAGCCAAGGGGGCTGATGGTAAAACGAAGATCGCCACACCGCGG  
GGAGCAGCCCCCTCAGGCCAGAAGGGCCAGGCCAACGCCACCAGGATTCCAGCAAAAACCCCGCCCGCTC  
CAAAGACACCCAGCTCTGGTGAACCTCCAAAATCAGGGGATCGCAGCGGCTACAGCAGCCCCGGCTCC  
CCAGGCACTCCCGGCAGCCGCTCCCGCACCCCGTCCCTTCCAACCCACCCACCCGGGAGCCCAAGAAGG  
TGGCAGTGGTCCGTACTCCACCCAAGTCGCCGTCTTCGCCAAGAGCCGCCTGCAGACAGCCCCCGTGCC  
CATGCCAGACCTGAAGAATGTCAAGTCCAAGATCGGCTCCACTGAGAACCTGAAGCACCAGCCGGGAGGCG  
GGAAGGTGCAGATAATTAATAAGAAGCTGGATCTTAGCAACGTCCAGTCCAAGTGTGGCTCAAAGGATAATA  
TCAAACACGTCCCGGGAGGCGGCAGTGTGCAAATAGTCTACAAACCAGTTGACCTGAGCAAGGTGACCTCC  
AAGTGTGGCTCATTAGGCAACATCCATCATAAACCAGGAGGTGGCCAGGTGGAAGTAAATCTGAGAAGCTT  
GACTTCAAGGACAGAGTCCAGTCAAGATTGGGTCCCTGGACAATATCACCCACGTCCCTGGCGGAGGAAA  
TAAAAAGATTGAAACCCACAAGCTGACCTTCCGCGAGAACGCCAAAGCCAAGACAGACCACGGGGCGGAGA  
TCGTGTACAAGTCGCCAGTGGTGTCTGGGGACACGTCTCCACGGCATCTCAGCAATGTCTCCTCCACCGGC  
AGCATCGACATGGTAGACTCGCCCCAGCTCGCCACGCTAGCTGACGAGGTGTCTGCCTCCCTCGCGAAGCA  
GGGTTTGGTTTCGAAGGGCGAGGAGGATAACATGGCCATCATCAAGGAGTTCATGCGCTTCAAGGTGCACA  
TGGAGGGCTCCGTGAACGGCCACGAGTTCGAGATCGAGGGCGAGGGCGAGGGCCGCCCTACGAGGGCA  
CCCAGACCGCCAAGCTGAAGGTGACCAAGGGTGGCCCCCTACCCTTCGCCTGGGACATCCTGTCCCCTCAG  
TTCATGTACGGCTCCAAGGCCTACGTGAAGCACCCCGCCGACATCCCCGACTACTTGAAGCTGTCTTCCCC  
GAGGGCTTCAAGTGGGAGCGCGTGATGAACTTCGAGGACGGCGGCGTGGTGACCGTGACCCAGGACTCCT  
CCCTGCAGGACGGCGAGTTCATCTACAAGGTGAAGCTGCGCGGCACCAACTTCCCTCCGACGGCCCCGTA  
ATGCAGAAGAAGACCATGGGCTGGGAGGCCTCCTCCGAGCGGATGTACCCCGAGGACGGCGCCCTGAAGG  
GCGAGATCAAGCAGAGGCTGAAGCTGAAGGACGGCGGCCACTACGACGCTGAGGTCAAGACCACCTACAA  
GGCCAAGAAGCCCGTGACGTGCCCCGGCGCCTACAACGTCAACATCAAGTTGGACATCACCTCCCACAACG  
AGGACTACACCATCGTGGAACAGTACGAACGCGCCGAGGGCCGCACTCCACCGGCGGCATGGACGAGCT  
GTACAAGTAGctcgag (T11-Tau441-mCherry)

aagcttaccATGGAGAAGAGGGACCACATGGTGCTGCTGGAGTACGTGACCGCCGCCGGCATCACCGACGCCT  
CGGGGGTACCAGGTTTCAGAGTTCAGGCACGACAGCGGCGGACCCGGGAGCGGCGGTGAGGGCTCAGCCG

GCGGAGGACCGGTCGGAGGCgcatccactagtaacggccgagtgctggaattcacATGTCCAATTTACTGACCGTACAC  
 CAAAATTTGCCTGCATTACCGGTCGATGCAACGAGTGATGAGGTTGCAAGAACCTGATGGACATGTTGAGG  
 GATCGCCAGGCGTTTTCTGAGCATACCTGGAAAATGCTTCTGTCCGTTTGCCGGTCGTGGGCGGCATGGTG  
 CAAGTTGAATAACCGGAAATGGTTTCCCGCAGAACCTGAAGATGTTGCGGATTATCTTCTATATCTTCAGGCG  
 CGCGGTCTGGCAGTAAAACTATCCAGCAACATTTGGGCCAGCTAAACATGCTTCATCGTCGGTCCGGGCTG  
 CCACGACCAAGTGACAGCAATGCTGTTTCACTGGTTATGCGGCGGATCCGAAAAGAAAACGTTGATGCCGGT  
 GAACGTGCAAAACAGGCTCTAGCGTTGCAACGCACTGATTCGACCAGGTTGTTCACTCATGGAATAAGC  
 GATCGCTGCCAGGATATACGTAATCTGGCATTCTGCGGATTGCTTATAACACCCTGTTACGTATAGCCGAAA  
 TTGCCAGGATCAGGGTTAAAGATATCTCACGTAAGTACGCTGCGGTTGGGAGAAATGTTAATCCATATTGGCAGAACGA  
 AAACGCTGGTTAGCACCGCAGGTGTAGAGAAGGCACCTAGCCTGGGGGTAACATAACTGGTCGAGCGATGG  
 ATTTCCGTCTCTGGTGTAGCTGATGATCCGAATAACTACCTGTTTTGCCGGGTCAGAAAAATGGTGTTGCCG  
 CGCCATCTGCCACCAGCCAGCTATCAACTCGCGCCCTGGAAGGGATTTTTGAAGCAACTCATCGATTGATTT  
 ACGGCGCTAAGGATGACTCTGGTCAGAGATACCTGGCCTGGTCTGGACACAGTGCCCGTGTGCGAGCCGC  
 GCGAGATATGGCCCGCGCTGGAGTTTCAATACCGGAGATCATGCAAGCTGGTGGCTGGACCAATGTAAATA  
 TTGTCATGAATATATCCGTAACCTGGATAGTGAAACAGGGGCAATGGTGCGCCTGCTGGAAGATGGCGATT  
 AGctcgag(T11-cre)

**Staining of cells and antibodies.** For immune fluorescence microscopy, cells routinely grown on poly-D-lysine coated 8-well chambers, were fixed in freshly diluted 4% formaldehyde (Sigma-Aldrich, F1635) for 15 min at room temperature (RT), washed twice with PBS supplemented with 100 mM glycine for 5 min and once with PBS. Cells were permeabilised in 0.05% saponin (Sigma-Aldrich, 84510) or 0.1% Triton X-100 (Sigma-Aldrich, X100) in PBS for 10 min and blocked with 5% normal goat serum (Biowest, S2000-500) in PBS for 30 min before incubation with primary antibodies for 1 h at RT in the permeabilisation buffer supplemented with 0.5% normal goat serum. Primary antibodies used were specific for TFE3 (0.6 µg/ml; Sigma-Aldrich, HPA023881), LAMP1 (1:50 conditioned medium of hybridoma cells; DSHB Hybridoma Product 1D4B was deposited by J.T. August), MC1 (1:100 conditioned medium of hybridoma cells; kindly provided by Prof. Peter Davies), AT8 (0.2 µg/ml, Thermo Fisher Scientific, MN1020). Detection was performed with 2 µg/mL secondary antibodies at RT in the dark for 1 h: α-mouse IgG AlexaFluor™ 350 (Thermo Fisher Scientific, A21049), α-rabbit IgG AlexaFluor™ 647 (Thermo Fisher Scientific, A21245), α-rabbit IgG AlexaFluor™ 488 (Thermo



Fisher Scientific, A11034) and  $\alpha$ -rat IgG AlexaFluor™ 647 (Thermo Fisher Scientific, A21247). Nuclei were counterstained with 0.5  $\mu$ g/mL DAPI (Sigma-Aldrich, D9542).

For the identification of acidic DOs, cells were incubated with 75 nM LysoTracker Red DND-99 or Deep Red (Thermo Fisher Scientific, L7528 and L12492) in complete medium at 37 °C for 30 min, washed with an excess of PBS and imaged live by laser confocal microscopy.

**Extracellular vesicle preparation.** C17.2 cells were first plated on 10 cm petri dishes (Corning, 353003) and grown to 80% confluency in complete medium before transient transfection with the plasmids of interest. Cells were then washed twice with PBS at 4 h post-transfection before switching to the serum-free conditions and incubation for 72 h. EVs were isolated from conditioned media by established procedures (Thery et al., 2006). In short, dead floating cells and cell debris were removed by centrifugation at 1'000 g for 20 min at 4°C. EVs were concentrated with 100 kDa cut-off filters (Sigma, UFC910096) at 3'000 g for 15 min at 4°C. The concentrated suspension was first cleared from large membrane vesicles by centrifugation at 10'000 g for 20 min at 4°C, followed by a centrifugation at 100'000 g for 120 min at 10 °C (Beckman fixed-angle TL110 rotor; Beckman Optima Max-TL ultracentrifuge). The so obtained P100 pellets, corresponding to the enriched EVs fraction, were re-suspended in 10  $\mu$ L ice-cold PBS. Size and concentration of EVs was determined through nanoparticle tracking analysis (NanoSight, LM10) with at least three repeated quantifications for each preparation. For routine cell uptake experiments, 15'000 cells/cm<sup>2</sup> in an 8-well chamber were incubated with 10<sup>9</sup> freshly enriched EVs for 16 h, unless differently specified in the figure legends.

For EVs purification by size-exclusion chromatography (SEC), P100 pellets or S100 supernatants obtained from the 100'000 g centrifugation were separated on a qEVOoriginal/70nm column (Izon Science, SP1) topped with 14 mL PBS. 500  $\mu$ L fractions were collected and fractions 7 to 24 were characterized by nanoparticle tracking analysis and for protein concentration. Fractions were then concentrated on 30 kDa cut-off filters (Sigma, UFC803024) and stored frozen at -20°C.

**Tau puncta quantification.** C17.2 cells expressing Tau<sub>441</sub> and incubated in culture medium supplemented with vehicle (PBS) or EVs were imaged by laser confocal microscopy. Acquisition settings were kept constant for all conditions analysed and acquired images were processed with the exact same parameters, including background subtraction, by applying a rolling bar radius of 50 pixels (ImageJ). Quantification of the percentage of cells with a Tau puncta phenotype was normalized with the total number of DAPI positive nuclei. Single Tau puncta were manually identified and analysed with the ImageJ software.

**Nuclear TFE3 quantification.** Cells were fixed, stained for TFE3 and imaged by laser confocal microscopy. A DAPI nuclear mask was applied to determine TFE3 fluorescence intensity within the nucleus and outside this mask. Quantification of the percentage of cells with a nuclear TFE3 phenotype was then determined applying an arbitrary threshold to the ratio between the two resulted masks. For the analysis of nuclear TFE3 translocation in cells presenting Tau puncta, cells were fixed and imaged by Lionheart FX automated microscope. After image acquisition on the channel relative to Tau<sub>441</sub>-mCherry, cells were stained for TFE3 (secondary antibody  $\alpha$ -rabbit IgG AlexaFluor™ 488) and imaged a second time by Lionheart FX automated microscope (ex. 488 nm) at the exact same x-y coordinates of the first acquisition. Alignment of Tau<sub>441</sub>-mCherry and TFE3 images was performed with the ImageJ DSH4 Image Alignment plugin. Single cell correlation of Tau puncta and TFE3 was then performed manually.

**Automated analysis of LysoTracker-stained DOs.** For the identification of acidic DOs, cells were stained live with LysoTracker. Images acquired at confocal microscopy were analysed with Fiji/ImageJ. Automatic segmentation of LysoTracker stained DOs was performed with a Weka machine learning approach (Morone et al., 2020). Training set comprised three images in which LysoTracker stained DOs and background regions were manually annotated. After balancing classes, Weka was trained with Gaussian Blur (sigma 1-16), Sobel filter, Hessian, Difference of Gaussians, Membrane projections and Lipschitz features. We then applied watershed filter to the output mask and filtered objects smaller than 0.2  $\mu\text{m}^2$  to generate a set of ROIs for LysoTracker positive DOs. Manual annotation of the cells of interest based on

Tau<sub>441</sub> were then used to create ROIs for the cytoplasm, by subtracting the combined ROIs of LysoTracker stained DOs from the ROI of the cell. LysoTracker positive DOs size and mean intensity were then quantified on biFC and Tau<sub>441</sub> channels using this set of ROIs.

**Correlative light-electron microscopy (CLEM).** After imaging, cells were fixed with 2.5% glutaraldehyde in 0.1M cacodylate buffer pH 7.4 for 1 h at RT. After several washes in cacodylate buffer, cells were post-fixed with 1% osmium tetroxide, 1.5% potassium ferrocyanide in 0.1M cacodylate buffer pH 7.4 for 1 h on ice. After rinsing in dH<sub>2</sub>O, samples were stained in 0.5% uranyl acetate overnight and dehydrated in increasing concentrations of ethanol and finally embedded in Epon. Samples were cured at 60°C in an oven for 48 h. Epon blocks were detached from dishes (Mattek, P35G-1.5-14-CGRD) by immersion in liquid nitrogen. The alphanumeric pattern imprinted on the resin surface was used to relocate the cells of interest. Epon blocks were sectioned using a Leica EM UC7 ultramicrotome (Leica Microsystems). 70 nm ultrathin sections were collected on formvar carbon coated slot grids, contrasted with 2% uranyl and lead citrate and observed with a TALOS L120C Transmission Electron Microscope (ThermoFisher Scientific). MAPS software (ThermoFisher Scientific) was used to relocate the cells of interest and to acquire large field of view by tile images acquisition and stitching. Fluorescent and EM images were aligned using midas software of IMOD package and the aligned EM and IF stacks images were overlaid using Fiji/ImageJ software.

**Tandem fluorescent-tagged LC3 assay.** C17.2 cells were grown on 24-well chambers until reaching 80% confluency, transiently transfected with the mCherry-GFP-LC3 plasmid and 4 h later treated with vehicle (DMSO for the compounds, PBS for the EVs), 10 nM bafilomycin A1, 3.3  $\mu$ M Ku-0063794; or  $2 \times 10^9$  EVs for 16 h. Transduction of shRNA viral particles was performed 48 h before plasmid transfection. Analysis was performed by flow cytometry following a previously established gating strategy (Zachari et al., 2020) using the FlowJo software v10.7.1 (BD Biosciences).

**Cell toxicity assays.** The nuclear area was analysed as a proxy for early cell toxicity events. Cells treated with EVs were stained with Hoechst at 37°C for 5 min, washed with PBS, fixed,

imaged at Lionheart microscope and analysed with the Gen5 software. LDH assay (ThermoFisher Scientific, 88954,) was performed following the manufacturer's instructions. In short, conditioned medium from cells was collected, processed and analysed by measuring the absorbance at 490 nm and 680 nm in an Infinite M Plex (Tecan).

**Antibodies for western blot.** Primary antibodies were incubated for 1 h at 37°C and were specific for ALIX (1 µg/mL; abcam, ab117600), TSG101 (1 µg/mL; abcam, ab30871), TOMM20 (0.8 µg/mL; abcam, ab78547), GFP and pHluorin (5 µg/mL; abcam, ab290), EEA1 (1/500; Thermo Fisher Scientific, MA5-14794), LC3B (1 µg/mL; Novus Biologicals, NB600-1384), P62/SQSTM1 (Cell Signaling, 88588), (TAU13 (0.2 µg/mL; Santa Cruz, sc-21796), ULK1 (1 µg/mL; Sigma-Aldrich, A7481), GAPDH (0.18 µg/mL; abcam, ab181602),  $\beta$ -actin (0.10 µg/mL; Sigma-Aldrich, A1978) and 2.3 µg/mL  $\beta$ 1 (Schrader-Fischer and Paganetti, 1996). Secondary antibodies were incubated for 1 h at 37°C and were  $\alpha$ -rabbit IgG coupled to IRDye 800CW (LI-COR) and  $\alpha$ -mouse IgG coupled to IRDye 680RD (LI-COR).

**AlphaLISA®.** Inducible C17.2 cells expressing Tau<sub>441</sub>-mCherry were grown on 24-well chambers in the presence of 60 ng/mL tetracycline to 80% confluency. Cells were treated with either vehicle (DMSO), 10 nM bafilomycin A1, or 3.3 µM Ku-0063794 for 16 h, washed twice with PBS and lysed in 1x AlphaLISA® Lysis Buffer (PerkinElmer, AL0035,) supplemented with inhibitor cocktails for proteases (Sigma-Aldrich, S8820) and phosphatases (Sigma-Aldrich, 04906845001). Cell lysates were gently mixed for 10 min at RT, centrifuged at 18'400 g for 2 min at 4°C and Tau was determined in the supernatants with a commercial kit (PerkinElmer, AL271C). For this, 5 µL/well of cell extracts diluted 1:30 in HiBlock Buffer (PerkinElmer, 10205589) were added to a 384-well plate (PerkinElmer, 6007290), supplemented with the same volume of HiBlock Buffer containing 1:50 diluted acceptor beads and biotinylated anti-Tau antibody. After 1 h incubation at RT in dark, 40 µL/well donor beads diluted 1:100 in HiBlock Buffer were added to each well, and incubated for additional 30 min prior to acquisition with a multi-plate reader (PerkinElmer, Victor Nivo). Data were analysed using the provided

software (PerkinElmer, Victor Nivo) and normalized for protein absorbance at 562 nm determined in the cell extracts a BCA protein assay (Thermo Fisher Scientific, 23225).

**Primers for real time quantitative PCR.** A primer pairs for RT-qPCR are specific for the mouse sequences (5'–3'):

LAMP1: TGTCAGCAAGATGCTCTCCCTC and ACCATCCTGAACACACTCTTCC

RRAGC: TGACCTTGCAGATGCTGGGCTA and GGTTTTCCAAAGTGGGCAGTTG

SQSTM: GGCTTCGGAAGCTGAAACATGG and ACATTGGGATCTTCTGGTGGAG

HPRT: TGCTCGAGATGTCATGAAGGA and TGTAATCCAGCAGGTCAGCA

GAPDH: TGGCAAAGTGGAGATTGTTGCC and AAGATGGTGATGGGCTTCCCG

## References

- Foglieni C, Papin S, Salvade A, Afroz T, Pinton S, Pedrioli G, et al. (2017) Split GFP technologies to structurally characterize and quantify functional biomolecular interactions of FTD-related proteins. *Sci Rep.* **7**:14013.
- Leeman DS, Hebestreit K, Ruetz T, Webb AE, McKay A, Pollina EA, et al. (2018) Lysosome activation clears aggregates and enhances quiescent neural stem cell activation during aging. *Science (New York, NY).* **359**:1277-83.
- Morone D, Marazza A, Bergmann TJ, Molinari M. (2020) Deep learning approach for quantification of organelles and misfolded polypeptide delivery within degradative compartments. *Molecular biology of the cell.* **31**:1512-24.
- Rost BR, Schneider F, Grauel MK, Wozny C, Bentz C, Blessing A, et al. (2015) Optogenetic acidification of synaptic vesicles and lysosomes. *Nature neuroscience.* **18**:1845-52.
- Schrader-Fischer G, Paganetti PA. (1996) Effect of alkalizing agents on the processing of the beta-amyloid precursor protein. *Brain research.* **716**:91-100.
- Shinoda H, Ma Y, Nakashima R, Sakurai K, Matsuda T, Nagai T. (2018) Acid-Tolerant Monomeric GFP from *Olindias formosa*. *Cell chemical biology.* **25**:330-8.e7.
- Thery C, Amigorena S, Raposo G, Clayton A. (2006) Isolation and characterization of exosomes from cell culture supernatants and biological fluids. *Current protocols in cell biology.* **Chapter 3**:Unit 3.22.

Van Engelenburg SB, Palmer AE. (2010) Imaging type-III secretion reveals dynamics and spatial segregation of Salmonella effectors. *Nature methods*. **7**:325-30.

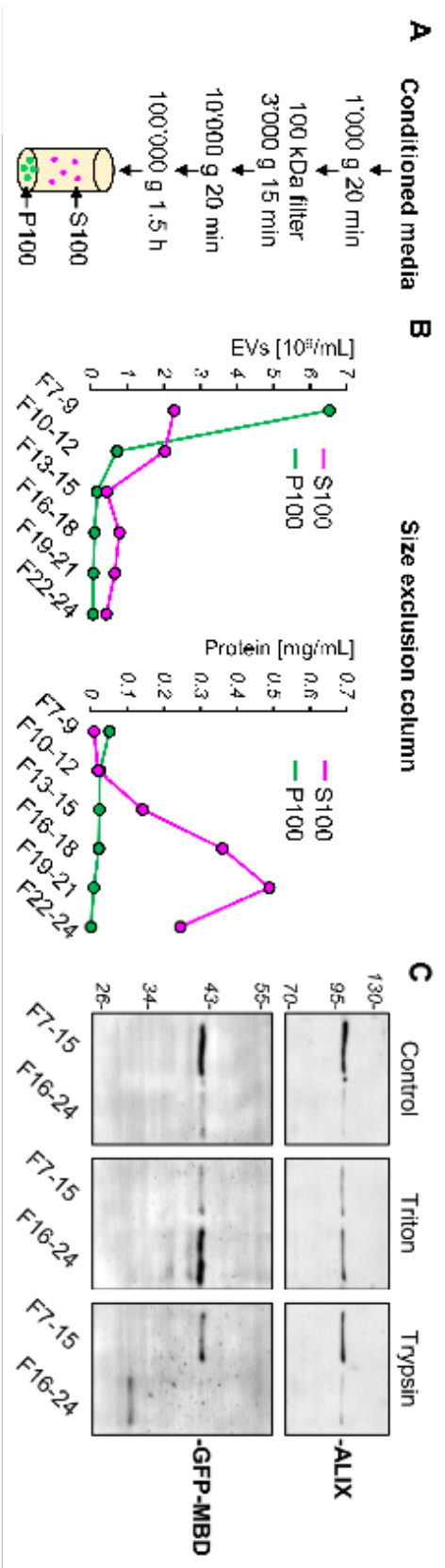
Zachari M, Longo M, Ganley IG. (2020) Aberrant autophagosome formation occurs upon small molecule inhibition of ULK1 kinase activity. *Life Science Alliance*. **3**:e202000815.

Zomer A, Maynard C, Verweij FJ, Kamermans A, Schafer R, Beerling E, et al. (2015) In Vivo imaging reveals extracellular vesicle-mediated phenocopying of metastatic behavior. *Cell*. **161**:1046-57.

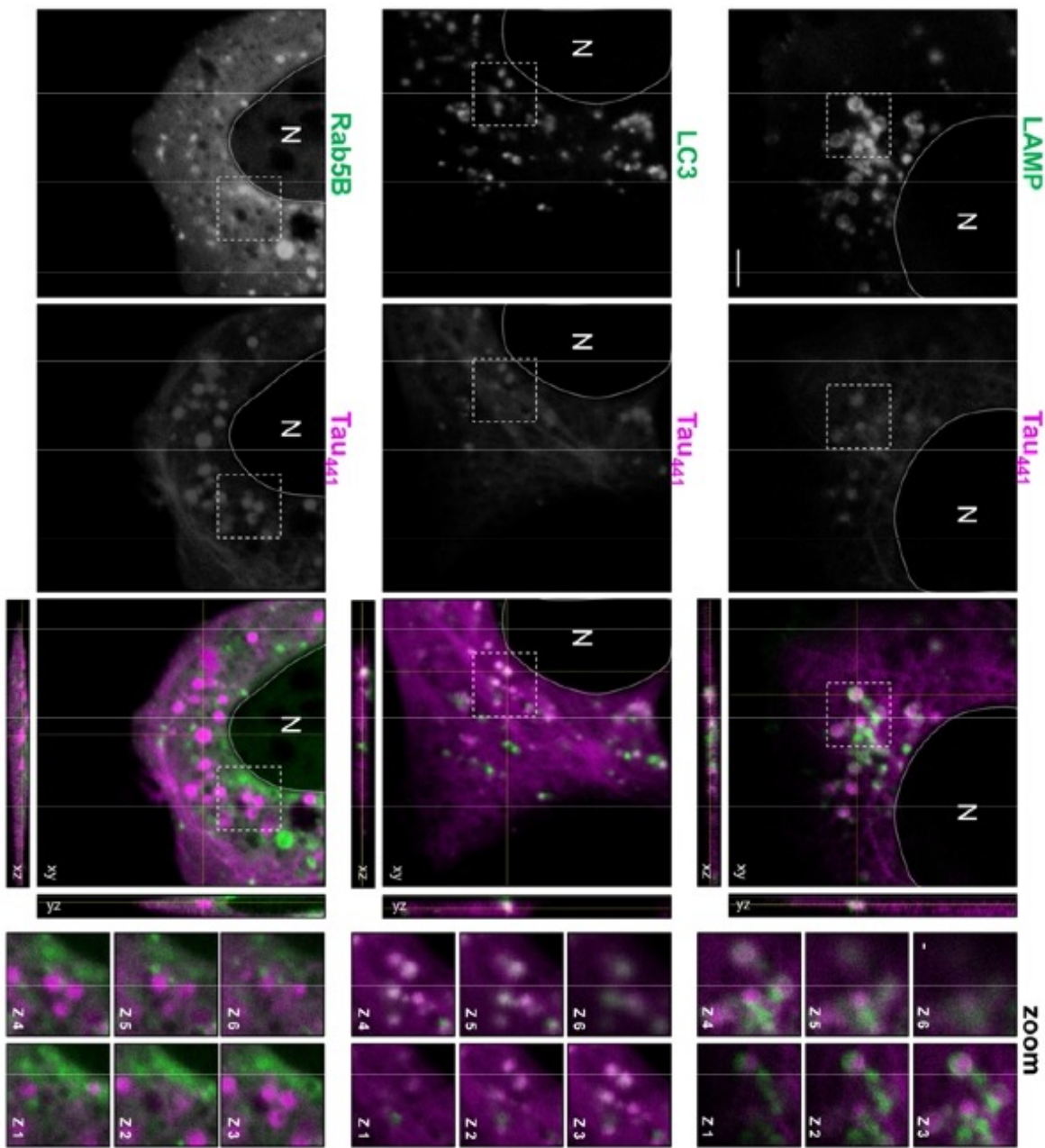
**Supplementary Figure 1 – Evidence for MBD transported in the lumen of extracellular vesicles.** **A.** Scheme of the serial centrifugation procedure for the enrichment of EVs from serum-free conditioned media of donor cells. P100 indicates the pellet fraction and S100 the supernatant of the last 100'000 x g centrifugation. **B.** Representative quantification of EVs concentration by nanoparticle tracking analysis (left panel) and determination of protein concentration (right panel) in the indicated pooled fractions of a size-exclusion chromatography (SEC) of S100 (magenta) or of P100 (green) samples obtained starting from  $\sim 50 \times 10^6$  C17.2 cells expressing GFP-MBD. **C.** Western blot for ALIX or GFP detecting GFP-MBD of pooled F7-F15 (containing EVs) or F16-F24 (free proteins) fractions obtained from  $10 \times 10^9$  GFP-MBD-EVs treated with PBS (Control), 0.1% Triton-X100 (Triton) or 0.1  $\mu\text{g/mL}$  trypsin (trypsin) before separation by SEC column. Molecular weight markers are given on the left in kDa.

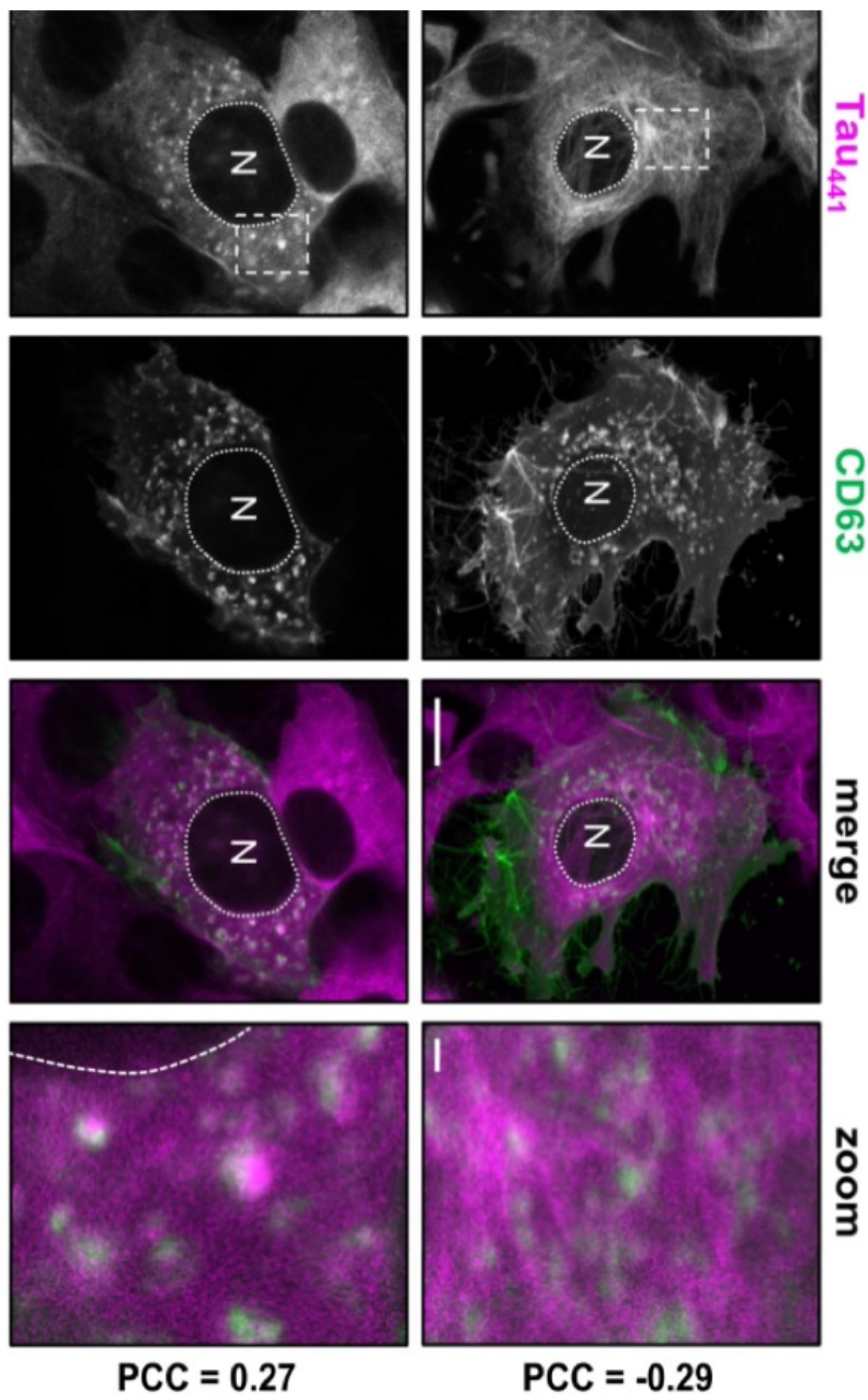
**Supplementary Figure 2 – Tau puncta co-localize with the DOs markers LAMP1 and LC3.** Fluorescent confocal images of a cell expressing Tau<sub>441</sub>-mCherry (magenta) and the indicated proteins fused to GFP. Cells were incubated for 1 d with  $1 \times 10^9$  GFP<sub>1-10</sub>-MBD-EVs. The merged images include an orthogonal reconstruction of stacked confocal planes, the zoomed insets show Z-representations of Tau puncta. Scale bar 10  $\mu\text{m}$  (1  $\mu\text{m}$  for the zoomed inset), N = nucleus.

**Supplementary Figure 3 – Induction of autophagy leads to Tau puncta accumulation in degradative organelles.** Fluorescent confocal images of cells expressing Tau<sub>441</sub>-mCherry (magenta) and GFP-CD63 (green) when cultured in normal medium (control) or starved for 4 h in HBSS (starvation), co-emission of the two fluorophores shown in white pseudo-colour indicates localisation of Tau<sub>441</sub> within CD63 positive DOs. Scale bar 10  $\mu\text{m}$  or 1  $\mu\text{m}$  for the zoomed inset, N = nucleus).









## RESULTS

### **Hypothesis and study design:** *Tau Accumulation in Degradative Organelles is Associated to Lysosomal Stress*

The aim of this study is to elucidate the implication of lysosomes in tau aggregation and vice-versa. It is well known that the autophagy-lysosomal pathway (ALP) is essential for the degradation of protein aggregates and that APL dysfunctions contributes to the development of neurodegenerative disease. We already reported (Chapter 2) that upon manipulation of the ALP system, tau accumulates in acidic degradative organelles (DOs) that may favor its pathologic conformational switch and spreading. **We hypothesized that tau accumulation in DOs may perturb lysosomal function, thereby mimicking lysosomal storage disorder (LSD) and that lysosomal deficiency may impact the accumulation of tau within acidic organelles.** To test this hypothesis, we used human primary fibroblasts overexpressing fluorescently-labelled tau and we studied lysosomal activity following the induction of tau accumulation in lysosomes through treatment with human AD brain-derived tau oligomers. On the contrary, we used an inhibitor of GCase, a key lysosomal enzyme mutated in Gaucher Disease, to address the impact of lysosomes deficiency on tau accumulation.

The following result section will present in detail the main findings of this study through the current version of the in-preparation manuscript entitled: ***Tau Accumulation in Degradative Organelles is Associated to Lysosomal Stress.***

### **Tau Accumulation in Degradative Organelles is Associated to Lysosomal Stress**

Ester Piovesana<sup>1,2</sup>, Claudia Magrin<sup>1,2</sup>, Matteo Ciccaldo<sup>3</sup>, Martina Sola<sup>1,2</sup>, Manolo Bellotto<sup>4</sup>, Maurizio Molinari<sup>3,5</sup>, Stéphanie Papin<sup>1</sup>, Paolo Paganetti<sup>1, 2, 6, \*</sup>

<sup>1</sup> Laboratory for Aging Disorders, Laboratories for Translational Research, Ente Ospedaliero Cantonale, Bellinzona, Switzerland

<sup>2</sup> PhD Program in Neurosciences, Faculty of Biomedical Sciences, Università della Svizzera Italiana, Lugano, Switzerland

<sup>3</sup> Institute for Research in Biomedicine, Faculty of Biomedical Sciences, Università della Svizzera italiana, Bellinzona, Switzerland

<sup>4</sup> GT Gain Therapeutics SA, Lugano, Switzerland

<sup>5</sup> School of Life Sciences, École Polytechnique Fédérale de Lausanne, Lausanne, Switzerland

<sup>6</sup> Neurocentro della Svizzera Italiana, Ente Ospedaliero Cantonale, Lugano, Switzerland

\* Corresponding author: Prof. Paolo Paganetti, Laboratories for Translational Research EOC, Room 102a, via Chiesa 5, CH-6500 Bellinzona, Switzerland  
phone +41 58 666 7103

email: [paolo.paganetti@eoc.ch](mailto:paolo.paganetti@eoc.ch) or [paolo.paganetti@usi.ch](mailto:paolo.paganetti@usi.ch)

**Abstract**

Neurodegenerative disorders are characterized by the brain deposition of insoluble amyloidogenic proteins, such as  $\alpha$ -synuclein or Tau, and the concomitant deterioration of cell functions such as the autophagy-lysosomal pathway (ALP). The ALP is involved in the degradation of intracellular macromolecules including protein aggregates. ALP dysfunction due to inherited defects in lysosomal or non-lysosomal proteins causes a group of diseases called lysosomal storage disorders (LSD) because of abnormal accumulation of lysosomal degradation substrates. Supporting the contribution of ALP defects in neurodegenerative diseases, deposition of amyloidogenic proteins occurs in LSD. Moreover, heterozygous mutations of several ALP genes represent risk factors for Parkinson's disease. The reciprocal contribution of  $\alpha$ -synuclein accumulation and lysosomal dysfunction have been extensively studied. However, whether this adverse crosstalk also embraces Tau pathology needs more investigation. Here, we show in human primary fibroblasts that Tau seeds isolated from the brain of Alzheimer's disease induce Tau accumulation in acidic degradative organelles and lysosomal stress. Furthermore, inhibition of glucocerebrosidase, a lysosomal enzyme mutated in Gaucher's disease and a main risk for Parkinson's disease, causes lysosomal dysfunction in primary fibroblasts and contributes to the accumulation of Tau. Considering the presence of Tau lesions in Parkinson's disease as well as in multiple neurodegenerative disorders including Alzheimer's disease, our data call for further studies on strategies to alleviate ALP dysfunction as new therapeutic opportunity for neurodegenerative diseases and LSD.

**Introduction**

A hallmark of neurodegenerative disorders is the deposition of insoluble protein aggregates composed of amyloidogenic proteins in the brain<sup>1</sup>. The most frequent neurodegenerative disorder is Alzheimer's disease (AD), characterized by the progressive formation of amyloid plaques composed of amyloid-beta peptides and of neurofibrillar hyperphosphorylated Tau protein aggregates<sup>2,3</sup>. In contrast,  $\alpha$ -synuclein deposition within Lewy bodies and neurites characterizes Parkinson's disease (PD),

which also presents Tau lesions<sup>4</sup>. Protein deposits are linked to a decline of cell functions culminating in cell death. However, cellular functions deteriorate at lower pace also during normal aging. An instance is the autophagy-lysosomal pathway (ALP), a cell process dedicated at the degradation of intracellular macromolecules and organelles<sup>5, 6</sup>. ALP can also eliminate protein aggregates and so, its dysfunction is proposed to contribute to the neurodegenerative process<sup>7, 8</sup>. In support of this is the evidence of increased deposition of amyloidogenic proteins in lysosomal storage disorders (LSD). LSD are caused by inherited defects in lysosomal or non-lysosomal proteins resulting in aberrant buildup of lysosomal substrates and deleterious ALP dysfunction<sup>9</sup>.

The correlation between protein accumulation and lysosomal dysfunction is better documented in PD compared to AD. Some mendelian forms of PD result from mutations in ALP genes e.g., *ATP13A2*<sup>10</sup>, *LRRK2*<sup>11</sup> or *VPS35*<sup>12</sup>. Also, monoallelic ALP gene mutations represent risk factors for PD but cause specific LSD in homozygote mutation carriers, validating the link between PD and LSD<sup>13, 14</sup>. Illustrative is the example of the *GBA* gene encoding for glucocerebrosidase (GCase), a lysosomal enzyme metabolizing glucosylceramide. Biallelic *GBA* mutation causes Gaucher's disease, mendelian disorders affecting several organs and tissues due to cells accumulating fatty substances. In contrast, monoallelic *GBA* mutations are present in ~10% of the patients affected by PD, representing thus the main genetic risk for PD and linking GCase dysfunction to  $\alpha$ -synuclein accumulation<sup>15</sup>.

Lower GCase activity and accumulation of glucosylceramide in lysosomes can inhibit autophagy<sup>16</sup> and favor the formation of soluble oligomeric  $\alpha$ -synuclein intermediates that can be converted into deposited amyloid fibrils<sup>17</sup>. Aggregation of  $\alpha$ -synuclein can impair the trafficking of newly synthesized GCase i.e., reducing the amount of GCase reaching its final destination in lysosomes. In addition, GCase can bind to  $\alpha$ -synuclein both in solution and on cell membranes<sup>18</sup>, which affects both GCase activity and the access to GCase substrates<sup>19</sup>. Therefore, the loss of functional GCase creates a noxious circle of glucosylceramide and  $\alpha$ -synuclein accumulation that ultimately leads to ALP dysfunction and neurodegeneration<sup>17</sup>. Despite similar aggregation and spreading properties, the relationship between Tau aggregation and ALP deficiency has been less intensively investigated so far. In the current study, we employed AD brain-derived Tau seeds together with a specific GCase inhibitor to describe that ALP

impairment contributes to Tau accumulation in degradative organelles of primary human fibroblasts.

## Results

**Generation and characterization of human fibroblast lines expressing Tau fused to fluorescent proteins.** To examine the subcellular distribution of Tau in primary human dermal fibroblasts, we fused in frame the cDNA of Tau<sub>2N4R</sub> either with that of mCherry or of Gamillus (**Figure 1A**), two differently emitting fluorescent proteins resistant to acidic pH<sup>20</sup>. A third cDNA construct was obtained by tagging Tau<sub>2N4R</sub> with both mCherry and GFP (tandem-Tau) (**Figure 1A**). This strategy takes advantage of the instability of GFP in an acidic environment exploited for monitoring LC3B subcellular distribution and autophagic flow<sup>21</sup>. The cDNAs were inserted into the pInducer20 vector for packaging into lentiviral pseudo particles<sup>22</sup>. Upon transduction for inducible expression of the single Tau variants, cells were characterized for Tau expression by confocal microscopy and flow cytometry. Protein expression was induced by cell treatment with doxycycline for two days. Doxycycline showed signs of cytotoxicity at concentrations above 2.5 µg/mL (**Figure 1B**). Upon induction with 0.3 µg/mL doxycycline, all three fluorescent Tau variants were found in a pattern of cytosolic distribution consistent with the association of Tau to the microtubule network (**Figure 1C**). Single cell analysis by flow cytometry showed a doxycycline dose-dependent increase in the amount of Tau present in the cell. Maximal induction levels were reached at about of 0.3 µg/mL doxycycline. In the geneticin-resistant cell populations, the percentage of positive cells varied from 75% for tandem-Tau to 89% and 94% for Tau-mCherry and Tau-Gamillus, respectively (**Figure 1C**). Only few cells expressed Tau in the absence of doxycycline indicating that the inducible system was not leaky. In the following experiments, Tau expression was routinely induced in the presence of 0.3 µg/ml doxycycline for two days.

### Tau localizes in DOs upon autophagy stimulation

Pharmacologic manipulation of the ALP system was performed to assess whether Tau may represent a substrate of autophagy<sup>23</sup> and be targeted to degradative organelles (DOs) of human fibroblasts.

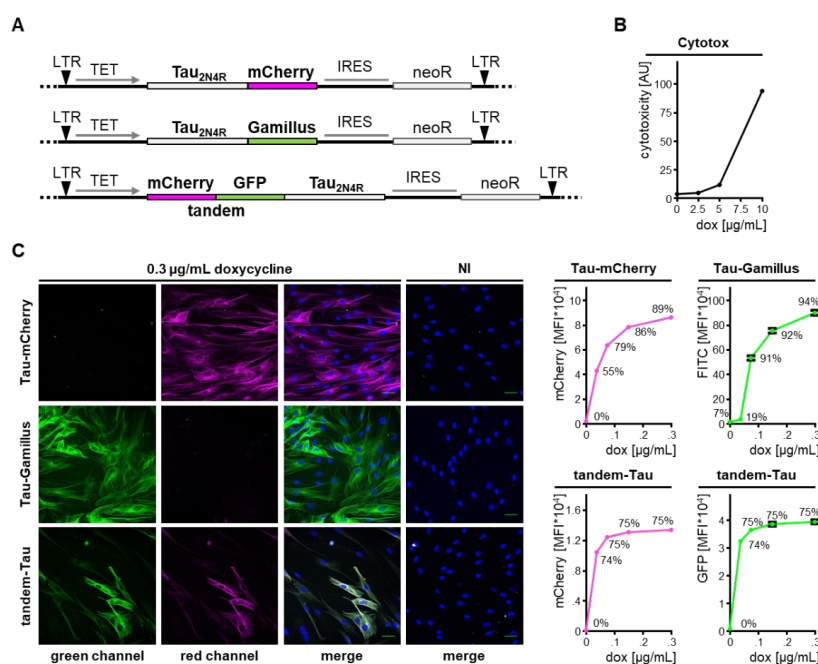


**Figure 1. Inducible Tau-expression in primary human fibroblasts.** **A.** Design of the lentiviral constructs driving the inducible expression of Tau-mCherry, Tau-Gamillus and tandem-Tau. **B.** Parental fibroblasts treated for 2 days with doxycycline were analyzed by cytofluorimetry, data are reported as geometric mean of fluorescence intensity. **C.** Cells were incubated in the presence or absence (not induced, NI) of 0.3 μg/mL doxycycline for 2 days and analyzed for Tau expression by laser confocal microscopy (representative images on the left, scale bar 40 μm). Mean fluorescence intensity (MFI ± sem) in the presence of increasing amounts of doxycycline was determined by cytofluorimetry (graphs on the right, percent positive cells is shown).

Autophagy was stimulated by mTOR inhibition with KU-0063794<sup>24</sup>, whereas autophagic flux and DO acidification were inhibited with the vacuolar proton pump blocker bafilomycin A1<sup>25</sup>. Acidic DOs in Tau-Gamillus fibroblasts were labelled with the acidotrophic marker LysoTracker Red emitting red fluorescence. KU-0063794 treatment strongly increased the number of LysoTracker positive DOs, consistent with its action as stimulator of autophagy (**Figure 2A**). Whereas under basal conditions Tau-Gamillus had a diffuse cytosolic pattern, the presence of KU-0063794 led to the formation of Tau-Gamillus puncta that appeared colocalized with LysoTracker-positive DOs (**Figure 2A**). In contrast, bafilomycin A1 eliminated the signal for the acidotrophic



LysoTracker Red signal and did not induce the formation of Tau-Gamillus puncta (**Figure 2A**). Quantitative laser confocal microscopy analysis proved that KU-0063794 increased the number and size of LysoTracker-positive DOs (**Figure 2B**), as well as the mean number of Tau-Gamillus puncta per cell (**Figure 2C**). Consistent results were obtained when analyzing Tau-mCherry fibroblasts with LysoTracker Green DND-26 (**Figure 2D**). We concluded that Tau is a likely target of the autophagic pathway when ectopically expressed in primary human dermal fibroblasts.

#### **AD-derived brain seeds induce Tau accumulation in DOs.**

We reported that fibrillogenic fragments of Tau carried by extracellular vesicles induced an aberrant accumulation of intracellular Tau within DOs of neuroblastoma cells<sup>23</sup>. So, next we studied whether Tau accumulation may occur also in DOs of human primary fibroblasts incubated with fibrillogenic seeds. We isolated Tau seeds from postmortem human AD brain. The presence of Tau lesions in the AD brain tissue used for the fractionation was first verified by immune fluorescence staining with antibodies for total Tau. This evidenced robust Tau pathology in the form of neurofibrillary tangles and neuropil threads that were also positive for the triply phospho-epitope of Tau recognized by the AT8 antibody<sup>26</sup> (**Figure 3A**). An established differential centrifugation protocol<sup>27, 28</sup> was implemented to enrich Tau seeds starting from 2 g AD brain wet tissue (**Figure 3B**). The initial P0 and S0 fractions accounted for ~120 mg and ~105 mg total protein, respectively, whereas the final S3 fraction contained ~1.7 mg total protein. The main fractions obtained were analyzed by western blot. The final supernatant S3 contained the largest relative amount of AT8-positive phosphorylated Tau when compared to the other fractions, although 10-time lower amounts of S3 protein were loaded on the gel (**Figure 3C**), showing at least a 1000-fold enrichment of Tau seeds following this protocol.

Overnight addition of the Tau seeds to the culture medium of doxycycline-induced fibroblasts, resulted in the robust accumulation of Tau-mCherry puncta in cells (**Figure 3D**). Interestingly, also the number per cell of LysoTracker-positive DOs was increased (**Figure 3E**). However, the effect of Tau seeds on DO number was not affected by the expression of Tau, indicating a lysosomal stress response caused by the treatment. In contrast, the increase of DO mean size required the presence of Tau (**Figure 3E**), suggesting that intracellular Tau accumulation contributed to seed-induced lysosomal stress.

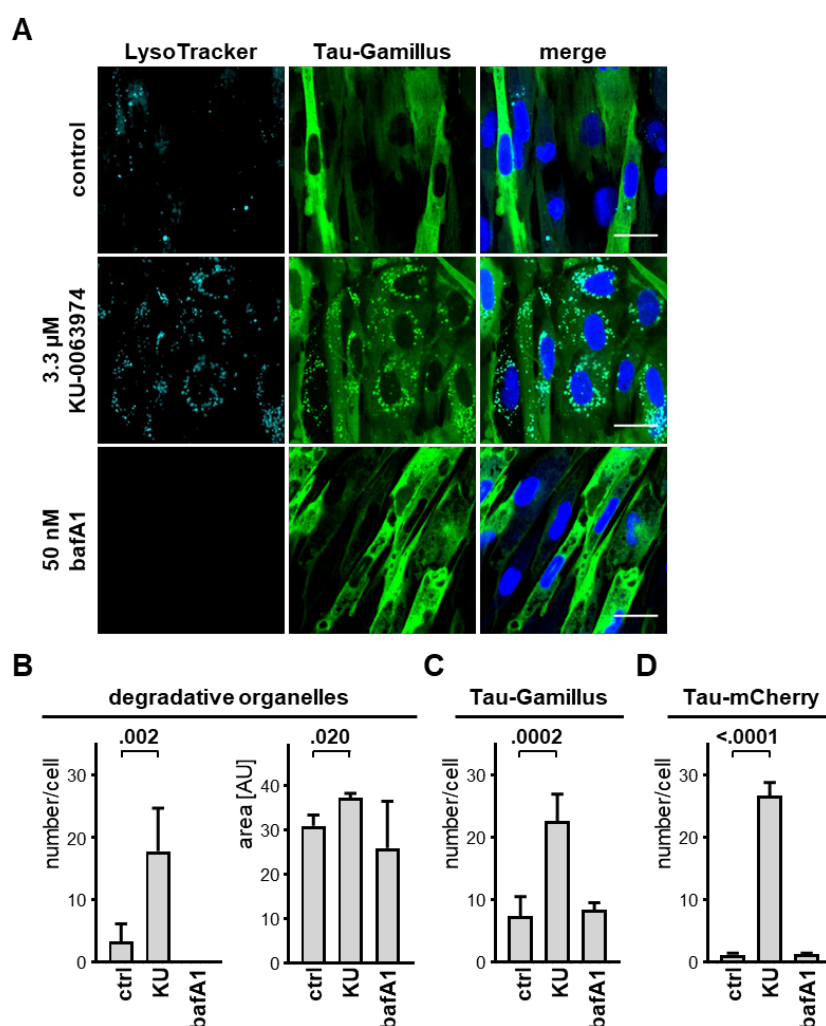


**Figure 2. Tau is a target of the autophagic pathway.** **A.** Representative images by laser confocal microscopy of Tau-Gamillus fibroblasts cultured with 0.3 μg/mL doxycycline for 2 days and treated overnight with 3.3 μM of KU-0063974 (KU), 50 nM bafilomycin A1 (BafA1), or left untreated (control). Cells were stained with LysoTracker Red and Hoechst. Scale bar 47 μm. **B.** Quantitative analysis of LysoTracker-positive DOs is shown in terms of DO number per cell (left graph, mean ± SD) and DO size (area, right graph, mean ± sem). **C.** Quantitative analysis of Tau-Gamillus puncta number (mean ± SD) per cell expressing Tau-Gamillus. **D.** Quantitative analysis of Tau-mCherry puncta number (mean ± SD) per cell expressing Tau-mCherry. Ordinary one-way ANOVA and Sidak's multiple comparison test.

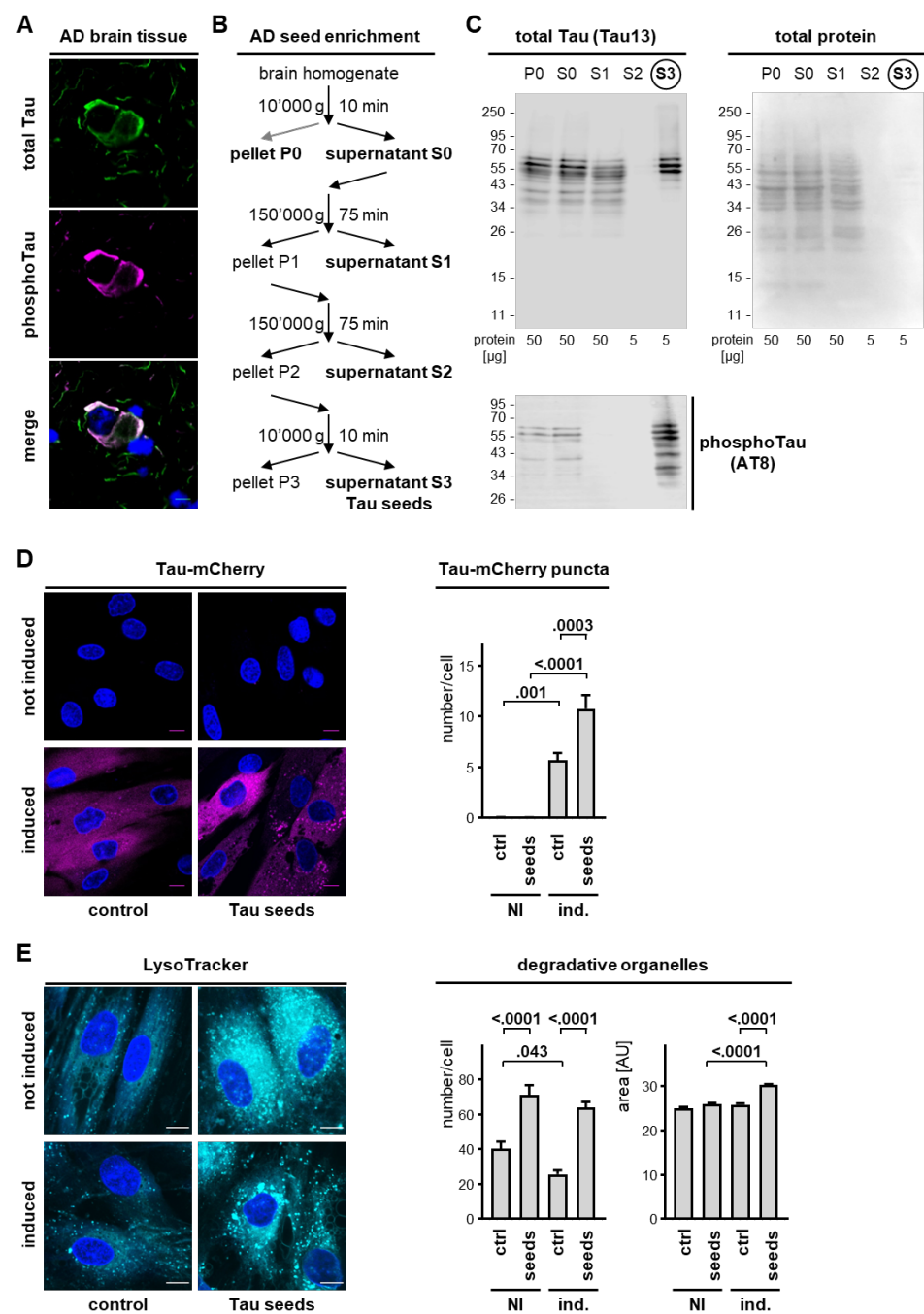


**Figure 3. AD brain-derived Tau seeds induce Tau accumulation and lysosomal stress response.** *A.* Representative images by laser confocal microscopy of frozen AD brain sections stained for total Tau (revealed with anti-rabbit-AlexaFluor488

secondary antibody, in green) and for AT8 phosphoTau (revealed with anti-mouse-AlexaFluor594 secondary antibody, in magenta). Nuclear counterstaining with DAPI, scale bar 10  $\mu$ m. **B.** Scheme of the procedure used for enriching Tau seeds from frozen AD brain. **C.** The indicated enrichment fractions were analyzed by western blot with the Tau13 antibody against total Tau or the AT8 antibody against phosphoTau. Primary antibodies were revealed with anti-mouse-IRDye800CW secondary antibody. Shown is also total protein staining with Ponceau S. **D.** Representative images by laser confocal microscopy of Tau-mCherry fibroblasts cultured with (induced) or without (not induced) 0.3  $\mu$ g/mL doxycycline for a total of 3 days, whereby the last day cells were treated in the absence (control) or presence of AD brain-derived Tau seeds. Nuclei were counterstained with Hoechst, scale bar 30  $\mu$ m. Shown is also the quantification of Tau-mCherry puncta number per cell (mean  $\pm$  SD). **E.** As in **D.** but DOs were stained with LysoTracker. Shown is the DO number per cell (mean  $\pm$  SD) and the DO size (mean  $\pm$  sem). Ordinary one-way ANOVA and Sidak's multiple comparison test.

To further document Tau accumulation in DOs, we took advantage of the tandem-Tau system. Due to the instability of GFP in an acidic environment, we predicted that upon entry into acidic DOs, GFP emission would be lost but mCherry emission preserved (**Figure 4A**), similarly to what described for the autophagy receptor LC3B<sup>21</sup>. Under control conditions, and upon induction of tandem-Tau expression with doxycycline, cells displayed GFP (in green) and mCherry (in magenta) fluorescence along the microtubule network (**Figure 4B**). Treatment of the cells with the autophagy stimulator KU-0063794 again led to tandem-Tau accumulation in puncta that, yet, lacked GFP emission (**Figure 4B**). Determination of the mCherry/GFP emission ratio for tandem-Tau puncta or for whole cells by quantitative laser confocal microscopy confirmed this property of tandem-Tau (**Figure 4C**). Based on this observation, and to obtain more quantitative data, we next evaluated the use of cytofluorimetry as a mean to quantify the localization of Tau in acidic DOs. In the presence of KU-0063794, we observed a small, but statistically significant shift of the ratio of mean mCherry fluorescence over mean green fluorescence (**Figure 4D**) by cytofluorimetry. The relatively small effect determined with this assay was possibly explained by double-fluorescent Tau present in the cytoplasm, which was partially masking the shift to mCherry fluorescence when Tau reached acidic DOs.

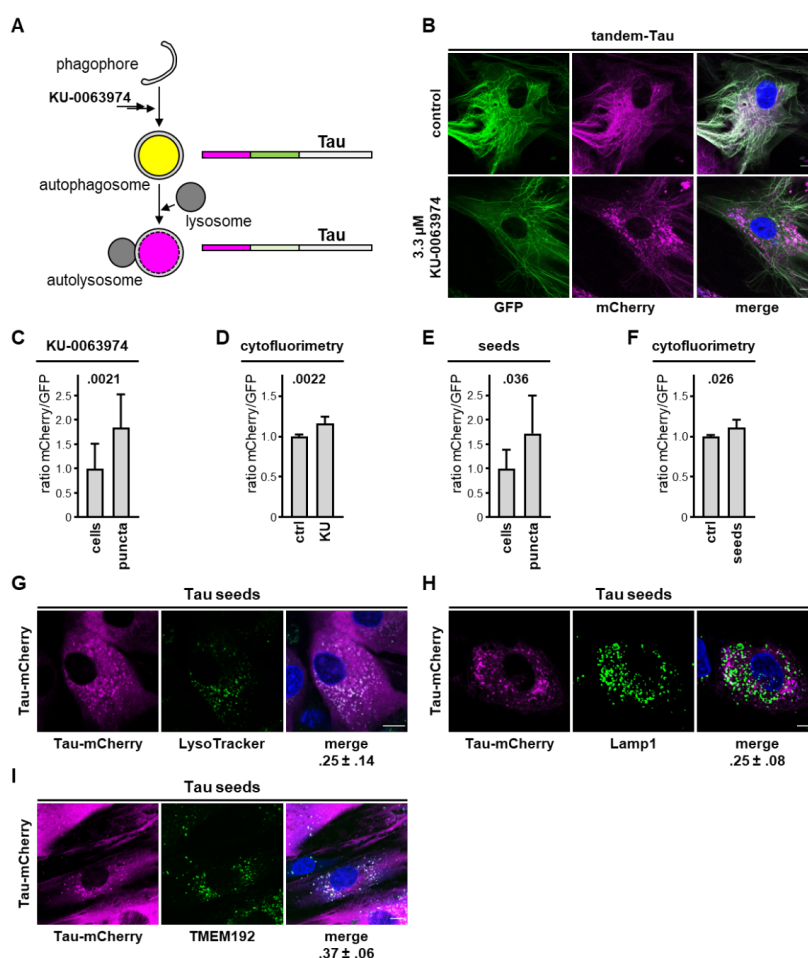


**Figure 4. Tau accumulation occurs in DOs.** **A.** Principle of the tandem-Tau assay. **B.** Representative images by laser confocal microscopy prior to fixation of Tandem-Tau fibroblasts induced with 0.3  $\mu\text{g/mL}$  doxycycline for 2 days and then treated overnight in the absence (control) or presence of 3.3  $\mu\text{M}$  of the autophagy stimulator KU-0063974. Nuclei were counterstained with Hoechst, scale bar 20  $\mu\text{m}$ . **C.** Ratio of mCherry over GFP fluorescence (mean  $\pm$  SD) calculated from confocal images utilizing a total cell mask (defined with an overlay of two emissions) or a tandem-Tau puncta mask (mCherry emission). **D.** Ratio of mCherry over GFP (geometric mean fluorescence  $\pm$  SD) determined by cytofluorimetry. **E-F.** 2 days-induced tandem-Tau fibroblasts were treated overnight in the absence or presence of Tau seeds and analyzed as in C-D. **C-F.** Unpaired Mann Whitney *t*-test. **G-H.** Representative laser confocal microscope images of mCherry-Tau fibroblasts (mCherry fluorescence in

*magenta) treated with Tau-seeds and stained (G) with LysoTracker (in green, nuclei counterstained with Hoechst in blue), or (H) with a LAMP1 antibody and a secondary anti-mouse AlexaFluor 488 antibody (in green, nuclei counterstained with DAPI in blue). I. Representative images of doxycycline induced mCherry-Tau fibroblasts transduced for Gamillus-TMEM192 and incubated with Tau seeds overnight (TMEM192 in green, nuclei counterstained with Hoechst in blue). G-I. Scale bar 30  $\mu$ m. Under the merged images, the Pearson coefficient of colocalization is shown.*

Prompted by the data obtained, we assessed the effect of Tau seeds when supplemented to tandem-Tau cells. We found that also in this case Tau seed-induced tandem-Tau puncta displayed increased mCherry/GFP emission ratio when analyzed by confocal microscopy (**Figure 4E**) or by cytofluorimetry (**Figure 4F**). These data indicated that Tau accumulation in fibroblasts occurred mainly in acidic DOs when induced by autophagy stimulation of treatment with extracellular Tau seeds. Consistent with this, accumulation of Tau co-localized with DOs positive for LysoTracker (**Figure 4G**), for DOs stained with LAMP1 antibodies (**Figure 4H**), and for DOs positive for the ectopic expression of TMEM192 (**Figure 4I**). Overall, our data demonstrated aberrant accumulation of Tau in acidic DOs of primary human fibroblasts.

#### **Inhibition of GCase activity induces an increase of Tau accumulation in DOs.**

We rationalized that lysosomal stress, such as due to GCase impairment, may impact on the accumulation of Tau in DOs. So, we cultured the cells in the presence of conduritol- $\beta$ -epoxide (CBE), an irreversible inhibitor of GCase (**Figure 5A**). We first showed that one hour treatment with CBE blocked GCase activity in fibroblasts. For this we used a cytofluorimetric assay for GCase activity with PFD-F d $\beta$ GluP, a modified substrate of GCase that becomes fluorescent once metabolized by GCase (**Figure 5B**). Overnight CBE treatment of fibroblasts expressing Tau-mCherry ultimately caused a cell response in terms of increased number of LysoTracker-positive DOs (**Figure 5C**). In absence of Tau induction, we did not observe a statistically significant effect of CBE on DO number, thereby demonstrating a synergistic effect on the number of LysoTracker-positive DOs, a surrogate marker of lysosomal stress, due to the concomitant inhibition of GCase and the presence of Tau.

GCase impairment affects lipid metabolism in lysosomes<sup>29, 30</sup>. Indeed, CBE treatment led to the appearance of DOs positive for BODIPY FL C<sub>5</sub>-lactosylceramide (**Figure**

**5D**). However, the increase in glycosphingolipid-positive DOs following inhibition of GCase occurred in a similar way in fibroblasts with or without induction of Tau expression. These data allowed us to conclude that in our cellular model GCase inhibition was linked to abnormal lipid metabolism and DOs function. Importantly, CBE-mediated GCase impairment promoted Tau-mCherry puncta formation (**Figure 5D**), indicating that lysosomal dysfunction caused Tau accumulation.

**Seeded Tau accumulation in lysosomes induce lysosomal dysfunction/stress.**

Next, we assessed the possible association of GCase inhibition to seed-induced Tau accumulation in DOs. First, we found that the addition of Tau seeds to Tau-mCherry expressing fibroblasts, but not in the absence of Tau expression induction, increased the formation of DOs positive for BODIPY FL C5-lactosylceramide. Again, Tau seeds promoted the accumulation of Tau-mCherry in puncta, which appeared to colocalize with the BODIPY FL C5-lactosylceramide positive DOs (**Figure 6A**). These data indicated that Tau accumulation in the presence of extracellular AD brain seeds, induced a lysosomal dysfunction in terms of lipid metabolism as shown by the concomitant accumulation of BODIPY FL C5-lactosylceramide (**Figure 6A**). A surrogate marker of lysosomal stress response is the nuclear translocation of TFE3, a master regulator potentiating lysosomal biogenesis and autophagic activity e.g., following treatment with the mTOR inhibitor KU-0063794 (**Figure 6B**). Nuclear translocation of TFE3 was also observed when cells were incubated with Tau seeds, whereas Tau expression and Tau accumulation further increased this cell response. These data demonstrated that Tau accumulation in DOs contributed to a lysosomal stress response in primary fibroblasts.

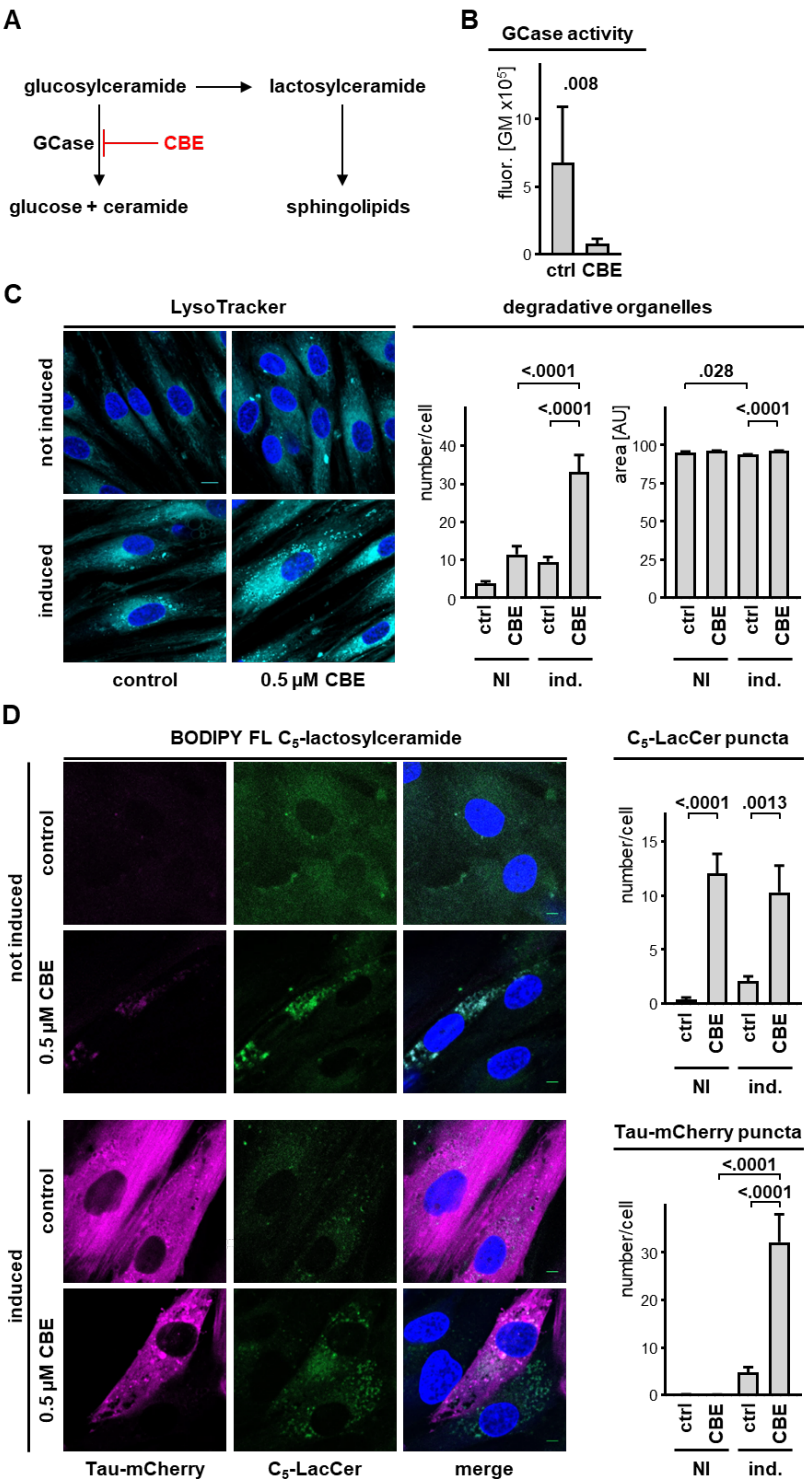




**Figure 5. GCase inhibition promotes Tau accumulation and lysosomal stress.** **A.** Simplified scheme of glucosylceramide metabolism. **B.** Human primary fibroblasts were treated in the absence or presence of 1 mM GCase inhibitor CBE for 1.5 h. The GCase substrate PFB-FDGlu was added at 0.075 mM final concentration before analysis by cytofluorimetry for the determination of geometric mean fluorescence generated by the cleaved GCase substrate ( $\pm$  SD). Unpaired Mann Whitney t-test. **C.** Representative laser confocal microscope images (left) of 2 days-induced Tau-mCherry fibroblasts treated with 0.5  $\mu$ M CBE overnight and stained with LysoTracker and Hoechst prior to fixation, scale bar 20  $\mu$ m. Reported is the number per cells and size of LysoTracker-positive DOs (mean  $\pm$  sem). Ordinary one-way ANOVA and Sidak's multiple comparison test. **D.** Tau-mCherry fibroblasts cultured in the absence (not induced) or presence (induced) of 0.3  $\mu$ g/mL doxycycline were treated with 0.5  $\mu$ M CBE overnight, incubated with 3.5  $\mu$ M BODIPY FL C<sub>5</sub>-lactosylceramide for 15 min, and a day later analyzed by laser confocal microscopy. Representative images of Tau in magenta, C<sub>5</sub>-LacCer in green, and Hoechst in blue, scale bar 20  $\mu$ m. Quantification of number per cell of C<sub>5</sub>-LacCer and Tau-mCherry puncta (mean  $\pm$  sem). Ordinary one-way ANOVA and Sidak's multiple comparison test.

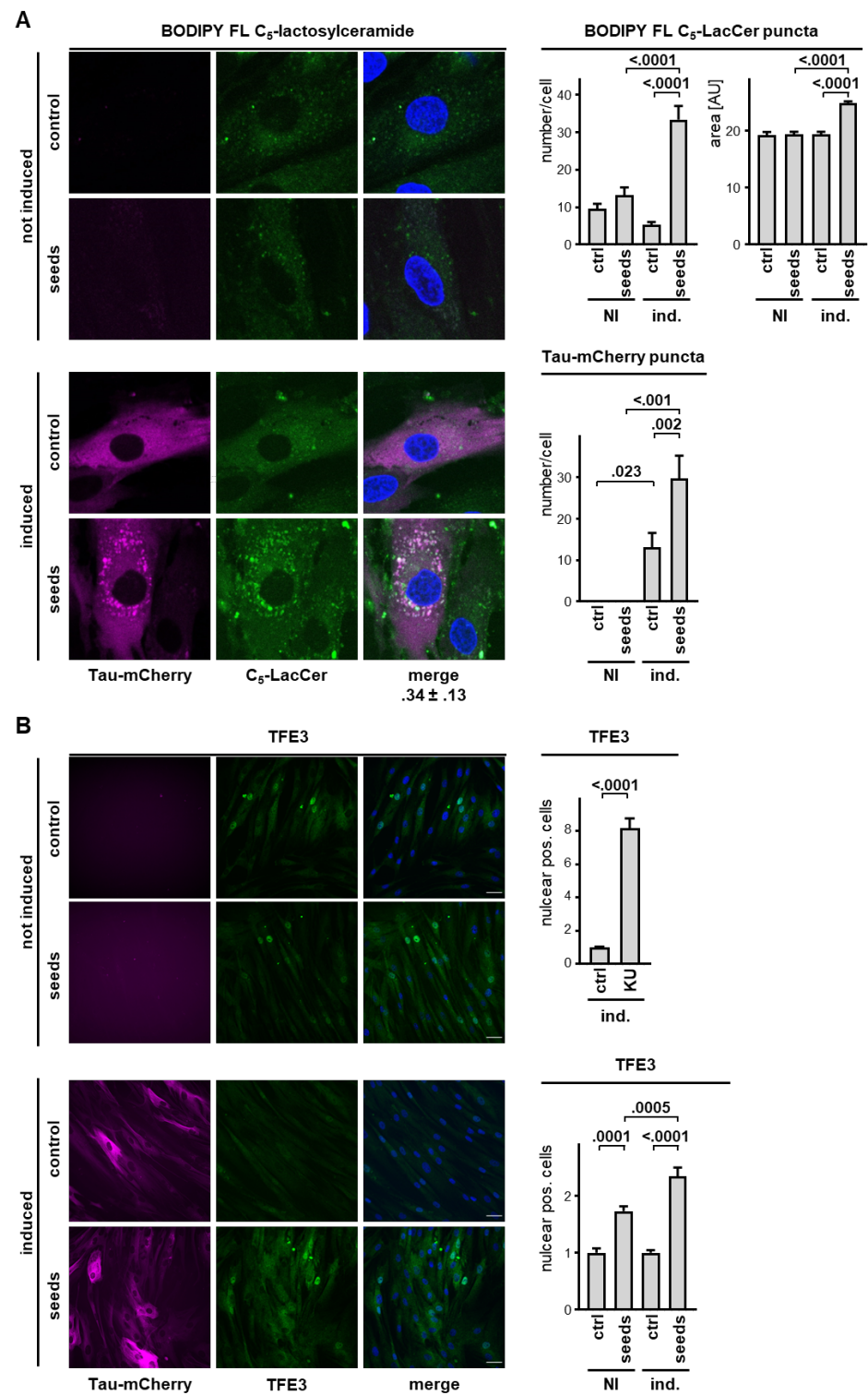


**Figure 6. Seed-induced Tau accumulation is linked to lysosomal stress.** *Tau-mCherry fibroblasts cultured in the absence (not induced) or presence (induced) of 0.3 µg/mL doxycycline for 2 days were treated with Tau seeds overnight. A. Representative images by laser confocal microscopy of cells (left) analyzed one day after incubation with 3.5 µM BODIPY FL C<sub>5</sub>-lactosylceramide for 15 min. Scale bar 20 µm. Shown under the merged image is the Pearson coefficient of colocalization. Quantification (right) of C<sub>5</sub>-LacCer puncta number per cell and size, and Tau-mCherry puncta number per cell (mean ± sem). Ordinary one-way ANOVA and Sidak's multiple comparison test. B. Representative images (left) of cells stained with a TFE3 antibody and a secondary anti-mouse AlexaFluor 488 antibody. Nuclei were counterstained with DAPI, scale bar 40 µm. Quantification (right) of percent cells with positive nuclear TFE3 after overnight incubation in the absence (ctrl) or presence of 3.3 µM KU-0063974 (upper graph, mean ± sem, unpaired Mann Whitney t-test), or Tau seeds (lower graph, mean ± sem, ordinary one-way ANOVA and Sidak's multiple comparison test).*

## Discussion

We found evidence of aberrant Tau accumulation linked to lysosomal stress in primary human fibroblasts expressing various fluorescent forms of Tau. This adverse process was promoted by the presence of AD brain-derived Tau seeds or upon treatment with CBE: a cell-active pharmacologic irreversible inhibitor of lysosomal GCCase. Tau was found to be a target for the autophagic pathway and Tau accumulation was colocalized with DO markers (LAMP1, TMEM192), the acidophilic compound LysoTracker, and showed a specific loss of GFP emission characteristic of an acidic environment. Based on our data, we propose that lysosomal dysfunction and the presence of internalized Tau seeds may cause, through an unknown mechanism, the accumulation of Tau on route to degradation within DOs. Similar results were described in murine cells incubated with exosomes containing a fibrillogenic fragment of Tau<sup>23</sup>. Tau accumulation in DOs was associated to increased lactosylceramide and lysosomal stress, indicating that seeded accumulation of Tau and impairment of lysosomal function and lipid metabolism are reciprocally engaged in a sequence of harmful events.

CBE has been used to generate research models of GCase deficiency in LSD because the extent of GCase inactivation can be adjusted by variation in the inhibitor concentration and/or exposure time in cultured cells and mice<sup>31</sup>. Using a short overnight CBE treatment of human fibroblasts expressing Tau, we observed an accumulation of lactosylceramide and an increase of lysosome number and size. These data are in agreement with previous data reported in two neuronal models of GCase deficiency following a two weeks CBE treatment that led to degeneration linked to increased glucosylceramide and glucosylsphingosine, nuclear translocation of TFE3, LAMP1 upregulation, enhanced lysosome size, number and exocytosis<sup>32</sup>. Also, SH-SY5Y cells treated with CBE presented abnormalities in autophagic flux, ALP, and mitochondrial activity<sup>33, 34</sup>. We monitored Tau-dependent lipid accumulation and lysosomal dysfunction in primary fibroblasts and found that CBE-mediated lactosylceramide accumulation was independent on the presence of Tau. However, the increase of lysosome number and size, indicative of lysosomal stress, resulted from the concomitant accumulation of ectopically expressed Tau. Possibly because of the short treatment, the inhibition of GCase by CBE had a relatively weak effect on Tau accumulation, but showed, for the first time, a direct link between GCase dysfunction and Tau accumulation in acidic DOs. Accumulation of soluble and insoluble forms of  $\alpha$ -synuclein following CBE treatment has been reported<sup>33, 35, 36</sup> with some exceptions<sup>37</sup>.

The association between lysosomal impairment and accumulation of pathologic forms of Tau (aggregated and phosphorylated Tau) may contribute to pathology. Indeed, Tau lesions are present in a mouse model of Gaucher's disease<sup>38</sup>, and other LSD such as Niemann–Pick<sup>39</sup>, Sanfilippo syndrome type B<sup>40</sup>, Christianson syndrome<sup>41</sup> and Fabry's disease<sup>42</sup>. Restoring mutated GCase activity with the chaperone Ambroxol<sup>43</sup> or through ectopic expression of wild-type GCase<sup>44</sup> delayed Tau and  $\alpha$ -synuclein accumulation. These data support the importance of pharmacologic strategies aimed at increasing GCase activity for providing innovative, disease-modifying therapies for  $\alpha$ -synucleinopathies and tauopathies.

ALP impairment as a consequence of protein aggregation may generate a vicious cycle boosting proteotoxicity in neurodegenerative disorders<sup>9</sup>. In addition, this may contribute to disease progression by favoring the transcellular spreading of pathogenic protein forms<sup>45</sup> along neuro-anatomical connections by a prion-like mechanisms<sup>46</sup>. Indeed, injection of extracellular protein seeds *in vivo* induces intraneuronal

pathology<sup>47</sup> by a mechanism that hitherto remains a matter of debate<sup>48</sup>. Proposed are several mediators such as extracellular vesicles<sup>49–50</sup>, of synaptic vesicle release<sup>51</sup>, membrane translocation<sup>52</sup>, clathrin-dependent endocytosis<sup>53</sup>, or transport of lysosome-associated aggregates through tunneling nanotubes<sup>54, 55</sup>. A role of lysosomes in the propagation of pathogenic  $\alpha$ -synuclein and Tau forms is supported by several studies<sup>54, 56–58</sup>, emphasizing the need to better understand the link between (age-related) DOs dysfunction and protein aggregation. Our study supports a tight crosstalk between GCase activity, DOs dysfunction and aberrant Tau accumulation in DOs, offering new clues for treatment of tauopathies and LSD.

## Materials and Methods

### Cell culture

Human primary dermal fibroblasts were isolated from a skin biopsy<sup>59</sup> obtained from a healthy 30-year-old female. Fibroblasts were cultured in DMEM (61965–059, Gibco) supplemented with 15% FBS (F7524, BCBZ9153, Sigma), 1% non-essential amino acids (NEAA, 11140035, Gibco), 1% penicillin-streptomycin (P/S, 15140122, Gibco) and maintained at 37°C in humidified atmosphere with 5% CO<sub>2</sub>. Cells were cultured for not more than one month. Human HEK293FT cells (gently provided by Prof. Barile, University of Southern Switzerland, Switzerland) were cultured in DMEM with 10% FBS (F7524, 0001643900 Sigma), 1% NEAA and 1% P/S.

### DNA plasmids

The plasmid pInducer20, a gift from Stephen Elledge (Addgene plasmid # 44012), was the vector for tet-on inducible expression of Tau<sub>2N4R</sub> in human primary fibroblasts. The cDNAs (**Supplementary Table 1**) were amplified by the polymerase chain reaction (PCR) using human full-length templates and specific oligonucleotide primers from parental plasmids already available in the laboratory<sup>23</sup>. The cDNAs were first inserted in the pENTRY4 backbone (A10561, Invitrogen) before recombination with Gateway LR Clonase II (11791-020, Invitrogen) following the instructions of the manufacturer.

### Pseudoviral particle production and transduction

Pseudolentiviral particles were produced by transient transfection of HEK293FT cells with 2  $\mu$ g of the desired pInducer plasmid and 8  $\mu$ g packaging plasmid mix (pPACKH1-

XL, LV510A-1, SBI). Cell conditioned medium was collected 2 days after transfection and cleared by centrifugation at 300 g for 5 min, 4°C. Pseudo-lentiviruses were 20-fold concentrated with centrifugal filters (MWCO 30 kDa, UFC903024, Amicon) at 3'000 g for 30-45 min, 4°C, aliquoted and stored at -80°C.

Human primary fibroblasts ( $6-8 \times 10^5$ ) were seeded into a 10 cm plate coated with poly-D-lysine (p6407, Sigma) one day before pseudolentiviral particle transduction. One day later, cells were supplemented with fresh complete medium and selected in the presence of 0.5 mg/mL geneticin (G418, 11811-031, Gibco) for two weeks.

### Drugs and cell treatments

Tau expression was induced with doxycycline (D9891, Sigma) for at least 2 days. Final drug concentrations were 3.3  $\mu$ M for the mTORC1/mTORC2 complex inhibitor KU-0063794<sup>24</sup> (HY-50710, Sigma), 20 nM for the lysosomal proton pump inhibitor bafilomycin A1 (BafA1, B1795, Sigma) and 0.5  $\mu$ M for the lysosomal GCCase inhibitor conduritol-beta-epoxide<sup>60</sup> (CBE, 6090-95-5, Medchem).

### GCCase activity

Human primary fibroblasts ( $3-5 \times 10^5$ ) were seeded on poly-D-lysine coated MW6 or MW12, respectively. A day later cells were treated with 5-(pentafluorobenzoylamino) fluorescein di- $\beta$ -D-glucopyranoside (PFB-FDGlu, P11947, Invitrogen) at 0.075 mM for 30 min, 37°C. Cells were then gently washed with PBS and resuspended in 100-150  $\mu$ L MACS buffer (PBS, 2% FBS, 2 mM EDTA) in a U bottom MW96. 100'000 cells were analyzed by cytofluorimetry.

### Cell and tissue histology

Cells expressing fluorescent Tau forms were seeded on poly-D-lysine coated 8 well microscope slides (80826-IBI, Ibidi). Nuclei were stained with 2.5  $\mu$ g/mL Hoechst (H3570, Invitrogen) for 10 min, 37°C, followed by gently washes in complete medium and PBS. Cells were fixed in 100% methanol for 20 min, -20°C and washed with PBS. Analysis and images were acquired on a microscope (ImageXpress 4 Micro, Molecular Devices). mCherry (ex: 587 nm, em: 610 nm) was visualized on the Texas Red channel (ex: 560/32 nm, em: 624/40 nm), GFP (ex: 488 nm, em: 507 nm) and Gamillus (ex: 504 nm, em 519) on the FITC channel (ex: 475/34 nm, em: 515/520 nm), and Hoechst (ex: 352 nm, em: 455 nm) with the DAPI channel (ex: 377/50, em: 461 nm).

For nuclear TFE3 analysis, Tau expression was first analyzed in live. Then, 4% formaldehyde fixed cells were stained with 0.3 µg/mL TFE3 antibody (HPA023881, Sigma), 2 µg/mL anti-rabbit IgG-Alexa488 antibody, nuclei were counterstained with DAPI. Analysis and images were acquired on the ImageXpress 4 Micro microscope. A DAPI nuclear mask was applied to determine the mean fluorescence intensity of nuclear TFE3 and outside the mask. Percentage of cells with a nuclear TFE3 phenotype was determined by applying an arbitrary threshold between the two masks. Total cell number was determined by counting the nuclei stained with DAPI for each image.

For LysoTracker staining, cells in poly-D-lysine 8 well slides were incubated with 0.25 µM LysoTracker (L7528 or L12492, ThermoFisher Scientific; 8783S, Cell Signaling) for 10 min, 37°C followed by nuclear Hoechst counterstaining.

3.5 µM BODIPY FL C5-lactosylceramide complexed to BSA (B34402, Invitrogen) in ice-cold EBSS (24010-043, Gibco) was incubated on cells for 15 min, 4°C. Cells were washed three times with ice-cold EBSS and then incubated in complete medium overnight, 37°C. Before analysis, cells were fixed in 2% formaldehyde (F1635-4L, Sigma), and washed with 10 mM glycine in PBS.

For Lamp1 staining, cells were fixed in 4% formaldehyde for 5 min, 37°C followed by 50% methanol for 10 min, room temperature. Cells were permeabilized and blocked with phosphate buffer, 10% normal goat serum, 15 mM glycine, 0.001% saponin (84510-100G, Sigma), 10 mM HEPES (15630-656, Gibco) for 1 h, room temperature. Cells were incubated in 0.2 µg/mL Lamp1 antibody (sc20011, Santa Cruz) for 1 h, 2 µg/mL anti-mouse IgG-Alexa488 antibody and DAPI.

Alzheimer's disease frontal cortex samples were obtained from The Netherlands Brain Bank, Netherlands Institute for Neuroscience, Amsterdam ([www.brainbank.nl](http://www.brainbank.nl)). All anonymized donors signed a written informed consent for brain autopsy and further use of tissue and clinical information for research purpose. Based on local guidelines for research on anonymized samples, ethic committee authorization was not required. For immune staining, frozen tissue was cut in 5 µm sections with a cryostat (Cryostar NX50). Sections were fixed in 100% methanol (32213-5L, Sigma) for 15 min, -20°C. Fixed sections were incubated for 60 min in PBS with 5% normal goat serum (16210064, ThermoFisher Scientific) and 0.3% Triton X-100 (X100, Sigma-Aldrich).

The sections were incubated overnight at 4°C with 0.2 µg/mL TauAS rabbit antiserum or 0.4 µg/mL AT8 (MN1020, ThermoFisher Scientific) followed by 2 µg/mL secondary antibodies anti-rabbit IgG-Alexa488 (A-11034, ThermoFisher Scientific) or anti-mouse IgG-Alexa594 (A-11032) for 60 min, room temperature. Nuclei were counterstained with 0.5 µg/mL DAPI (D9542, Sigma-Aldrich) for 5 min, room temperature.

Images were acquired on a fluorescent laser confocal microscope (C2, Nikon) by sequential excitations (line-by-line scan) with the 405 nm laser (464/40 nm emission filter), the 488 nm laser (525/50 nm filter), and the 561 nm laser (561/LP nm filter).

### **Enrichment of Tau seeds from AD brain tissue**

Brain tissue pooled from 4-5 AD donors was homogenized on ice in ~9 volumes) of filtered PHF buffer (10 mM Tris pH 7.4, 10% sucrose, 0.8 M NaCl and 0.1% sarkosyl, L9150-50G, Sigma) supplemented with protease and phosphatase inhibitor cocktails (S8820 & 04906845001, Sigma) in a glass Dounce homogenizer. Brain homogenates were briefly cleared by a centrifugation at 10'000 g for 10 min, 4°C. Sarkosyl was added to a 1% final concentration to the first supernatant (S0) and incubated for 90 min, room temperature, under agitation, before ultracentrifugation at 150'000 g for 75 min, 10°C. To remove sarkosyl, the P1 pellet was gently washed with cold PBS before repeating the ultracentrifugation. The P2 pellet was resuspended in 200 µl PBS supplemented with protease and phosphatase inhibitor cocktails and sonicated. The S2 supernatant was centrifuged at 10'000 g for 10 min, 4°C, and the Tau seed fraction S3 collected and stored frozen in aliquots. Total protein concentration was determined with the Pierce BCA protein assay kit (23227, ThermoFisher Scientific).

### **Cell sorting and flow cytometry**

For enrichment of double positive mCherry-GFP-Tau fibroblasts, 2 day-induced cells ( $3.5 \times 10^6$ ) were first stained with 1/200 viability Aqua Dye (ex: 381 nm, em: 511 nm) (L34957, ThermoFisher Scientific) for 20 min, 37°C. Cells were then washed, filtered through a 40 µm cell strainer (15-1040-2, Biologix) and resuspended in 1 mL cold MACS buffer before sorting (FACSymphony S6, BD Biosciences). Live cells were gated using DAPI channel (ex: 350 nm, em: 460 nm). Successively, selected live double positive cells were sorted for mCherry using the PECF594 channel (ex: 566 nm, em: 610 nm) and for GFP using the BB515 channel (ex: 490 nm, em: 515 nm).



For the GCase activity assay, cytofluorimetry (CytoFLEX, Beckman Coulter) was performed with the 488 nm excitation laser and 525/40 nm emission.

For the cytotoxicity assay, Aqua Dye-stained cells were analyzed by cytofluorimetry with 405 nm excitation laser and 450/45 nm emission.

For Tau expression, cytofluorimetry was acquired either with ex: 561 nm and em: 610/20 nm, or ex: 488 nm and em: 525/40 nm.

Data analysis was performed with the software FloJow (V 10.6.2, BD Biosciences). Values collected included total single cell number, gated cell number and geometric mean fluorescence.

### Western blot

Samples were diluted to 1x SDS-PAGE sample buffer (1.5% SDS, 8.3% glycerol, 0.005% bromophenol blue, 1.6%  $\beta$ -mercaptoethanol, 62.5 mM Tris pH 6.8) and boiled for 10 min before 12% polyacrylamide gel electrophoresis. Resolved proteins were semi-dry transferred on a PVDF membrane, followed by incubation in 3% blocking buffer (Blocking Solution, 927-60001, Licor) in TBS for 1 h, room temperature. Primary antibodies were incubated overnight, 4°C: 0.2  $\mu$ g/mL Tau13-AlexaFluor (sc-21796 AF680, Santa Cruz) or 0.2  $\mu$ g/mL AT8 (MN1020, ThermoFisher Scientific) and revealed with anti-mouse IgG IRDye RD 680 (Licor Biosciences, 926-68070) on an infrared imaging scanner (Licor Biosciences, Odyssey CLx 9140).

### Statistics and reproducibility

Statistical analysis was performed with GraphPad Prism version 8.4 with at least three independent biological replicates. Most quantifications are reported as fold over control/untreated conditions unless otherwise indicated in the graphs. Representative western blots and microscopic images are shown.

### References

1. Chiti, F. & Dobson, C.M. Protein Misfolding, Amyloid Formation, and Human Disease: A Summary of Progress Over the Last Decade. *Annu Rev Biochem* **86**, 27-68 (2017).
2. Goedert, M. & Spillantini, M.G. A century of Alzheimer's disease. *Science* **314**, 777-781 (2006).
3. Nisbet, R.M. & Götz, J. Amyloid- $\beta$  and Tau in Alzheimer's Disease: Novel Pathomechanisms and Non-Pharmacological Treatment Strategies. *J Alzheimers Dis* **64**, S517-s527 (2018).
4. Spillantini, M.G. & Goedert, M. Neurodegeneration and the ordered assembly of  $\alpha$ -synuclein. *Cell Tissue Res* **373**, 137-148 (2018).

5. Giovedi, S., Ravanelli, M.M., Parisi, B., Bettegazzi, B. & Guarnieri, F.C. Dysfunctional Autophagy and Endolysosomal System in Neurodegenerative Diseases: Relevance and Therapeutic Options. *Frontiers in Cellular Neuroscience* **14** (2020).
6. Finkbeiner, S. The Autophagy Lysosomal Pathway and Neurodegeneration. *Cold Spring Harb Perspect Biol* **12** (2020).
7. Nixon, R.A. The role of autophagy in neurodegenerative disease. *Nat Med* **19**, 983-997 (2013).
8. Fraldi, A., Klein, A.D., Medina, D.L. & Settembre, C. Brain Disorders Due to Lysosomal Dysfunction. *Annu Rev Neurosci* **39**, 277-295 (2016).
9. Monaco, A. & Fraldi, A. Protein Aggregation and Dysfunction of Autophagy-Lysosomal Pathway: A Vicious Cycle in Lysosomal Storage Diseases. *Frontiers in Molecular Neuroscience* **13** (2020).
10. Dehay, B. *et al.* Loss of P-type ATPase ATP13A2/PARK9 function induces general lysosomal deficiency and leads to Parkinson disease neurodegeneration. *Proceedings of the National Academy of Sciences* **109**, 9611-9616 (2012).
11. Madureira, M., Connor-Robson, N. & Wade-Martins, R. "LRRK2: Autophagy and Lysosomal Activity". *Front Neurosci* **14**, 498 (2020).
12. Zavodszky, E. *et al.* Mutation in VPS35 associated with Parkinson's disease impairs WASH complex association and inhibits autophagy. *Nature Communications* **5**, 3828 (2014).
13. Shachar, T. *et al.* Lysosomal storage disorders and Parkinson's disease: Gaucher disease and beyond. *Movement Disorders* **26**, 1593-1604 (2011).
14. Robak, L.A. *et al.* Excessive burden of lysosomal storage disorder gene variants in Parkinson's disease. *Brain* **140**, 3191-3203 (2017).
15. Behl, T. *et al.* Cross-talks among GBA mutations, glucocerebrosidase, and  $\alpha$ -synuclein in GBA-associated Parkinson's disease and their targeted therapeutic approaches: a comprehensive review. *Translational Neurodegeneration* **10**, 4 (2021).
16. Du, T.T. *et al.* GBA deficiency promotes SNCA/ $\alpha$ -synuclein accumulation through autophagic inhibition by inactivated PPP2A. *Autophagy* **11**, 1803-1820 (2015).
17. Mazzulli, J.R. *et al.* Gaucher disease glucocerebrosidase and  $\alpha$ -synuclein form a bidirectional pathogenic loop in synucleinopathies. *Cell* **146**, 37-52 (2011).
18. Yap, T.L. *et al.* Alpha-synuclein interacts with Glucocerebrosidase providing a molecular link between Parkinson and Gaucher diseases. *J Biol Chem* **286**, 28080-28088 (2011).
19. Muñoz, S.S., Petersen, D., Marlet, F.R., Küçüköke, E. & Galvagnion, C. The interplay between Glucocerebrosidase,  $\alpha$ -synuclein and lipids in human models of Parkinson's disease. *Biophys Chem* **273**, 106534 (2021).
20. Shinoda, H. *et al.* Acid-Tolerant Monomeric GFP from *Olindias formosa*. *Cell chemical biology* **25**, 330-338.e337 (2018).
21. Kimura, S., Noda, T. & Yoshimori, T. Dissection of the autophagosome maturation process by a novel reporter protein, tandem fluorescent-tagged LC3. *Autophagy* **3**, 452-460 (2007).
22. Meerbrey, K.L. *et al.* The pINDUCER lentiviral toolkit for inducible RNA interference in vitro and in vivo. *Proceedings of the National Academy of Sciences of the United States of America* **108**, 3665-3670 (2011).
23. Pedrioli, G. *et al.* Tau Seeds in Extracellular Vesicles Induce Tau Accumulation in Degradative Organelles of Cells. *DNA Cell Biol* **40**, 1185-1199 (2021).
24. García-Martínez, J.M. *et al.* Ku-0063794 is a specific inhibitor of the mammalian target of rapamycin (mTOR). *The Biochemical journal* **421**, 29-42 (2009).
25. Mauvezin, C. & Neufeld, T.P. Bafilomycin A1 disrupts autophagic flux by inhibiting both V-ATPase-dependent acidification and Ca-P60A/SERCA-dependent autophagosome-lysosome fusion. *Autophagy* **11**, 1437-1438 (2015).
26. Malia, T.J. *et al.* Epitope mapping and structural basis for the recognition of phosphorylated tau by the anti-tau antibody AT8. *Proteins* **84**, 427-434 (2016).
27. Li, L. *et al.* Alzheimer's disease brain contains tau fractions with differential prion-like activities. *Acta neuropathologica communications* **9**, 28 (2021).

28. Xu, H. *et al.* In vitro amplification of pathogenic tau conserves disease-specific bioactive characteristics. *Acta neuropathologica* **141**, 193-215 (2021).
29. Chen, C.S., Patterson, M.C., Wheatley, C.L., O'Brien, J.F. & Pagano, R.E. Broad screening test for sphingolipid-storage diseases. *Lancet (London, England)* **354**, 901-905 (1999).
30. Silience, D.J. *et al.* Glucosylceramide modulates membrane traffic along the endocytic pathway. *Journal of lipid research* **43**, 1837-1845 (2002).
31. Vardi, A. *et al.* Delineating pathological pathways in a chemically induced mouse model of Gaucher disease. *The Journal of Pathology* **239**, 496-509 (2016).
32. Lunghi, G. *et al.*  $\beta$ -Glucocerebrosidase Deficiency Activates an Aberrant Lysosome-Plasma Membrane Axis Responsible for the Onset of Neurodegeneration. *Cells* **11**, 2343 (2022).
33. Cleeter, M.W.J. *et al.* Glucocerebrosidase inhibition causes mitochondrial dysfunction and free radical damage. *Neurochemistry International* **62**, 1-7 (2013).
34. Magalhaes, J. *et al.* Autophagic lysosome reformation dysfunction in glucocerebrosidase deficient cells: relevance to Parkinson disease. *Human Molecular Genetics* **25**, 3432-3445 (2016).
35. Rocha, E.M. *et al.* Sustained Systemic Glucocerebrosidase Inhibition Induces Brain  $\alpha$ -Synuclein Aggregation, Microglia and Complement C1q Activation in Mice. *Antioxidants & Redox Signaling* **23**, 550-564 (2015).
36. Manning-Boğ, A.B., Schüle, B. & Langston, J.W. Alpha-synuclein-glucocerebrosidase interactions in pharmacological Gaucher models: A biological link between Gaucher disease and parkinsonism. *NeuroToxicology* **30**, 1127-1132 (2009).
37. Gegg, M.E., Verona, G. & Schapira, A.H.V. Glucocerebrosidase deficiency promotes release of  $\alpha$ -synuclein fibrils from cultured neurons. *Human Molecular Genetics* **29**, 1716-1728 (2020).
38. Sardi, S.P. *et al.* Augmenting CNS glucocerebrosidase activity as a therapeutic strategy for parkinsonism and other Gaucher-related synucleinopathies. *Proc Natl Acad Sci U S A* **110**, 3537-3542 (2013).
39. Pacheco, C.D., Elrick, M.J. & Lieberman, A.P. Tau normal function influences Niemann-Pick type C disease pathogenesis in mice and modulates autophagy in NPC1-deficient cells. *Autophagy* **5**, 548-550 (2009).
40. Ohmi, K. *et al.* Sanfilippo syndrome type B, a lysosomal storage disease, is also a tauopathy. *Proc Natl Acad Sci U S A* **106**, 8332-8337 (2009).
41. Fernandez, M.A. *et al.* Loss of endosomal exchanger NHE6 leads to pathological changes in tau in human neurons. *Stem Cell Reports* **17**, 2111-2126 (2022).
42. Clarke, J., Kayatekin, C., Viel, C., Shihabuddin, L. & Sardi, S.P. Murine Models of Lysosomal Storage Diseases Exhibit Differences in Brain Protein Aggregation and Neuroinflammation. *Biomedicines* **9** (2021).
43. Yang, S.Y., Taanman, J.-W., Gegg, M. & Schapira, A.H.V. Ambroxol reverses tau and  $\alpha$ -synuclein accumulation in a cholinergic N370S GBA1 mutation model. *Human Molecular Genetics* **31**, 2396-2405 (2022).
44. Bae, E.-J. *et al.* Glucocerebrosidase depletion enhances cell-to-cell transmission of  $\alpha$ -synuclein. *Nature Communications* **5**, 4755 (2014).
45. Victoria, G.S. & Zurzolo, C. The spread of prion-like proteins by lysosomes and tunneling nanotubes: Implications for neurodegenerative diseases. *J Cell Biol* **216**, 2633-2644 (2017).
46. Frost, B. & Diamond, M.I. Prion-like mechanisms in neurodegenerative diseases. *Nat Rev Neurosci* **11**, 155-159 (2010).
47. Polymenidou, M. & Cleveland, D.W. Prion-like spread of protein aggregates in neurodegeneration. *J Exp Med* **209**, 889-893 (2012).
48. Davis, A.A., Leyns, C.E.G. & Holtzman, D.M. Intercellular Spread of Protein Aggregates in Neurodegenerative Disease. *Annual Review of Cell and Developmental Biology* **34**, 545-568 (2018).

49. Natale, F., Fusco, S. & Grassi, C. Dual role of brain-derived extracellular vesicles in dementia-related neurodegenerative disorders: cargo of disease spreading signals and diagnostic-therapeutic molecules. *Translational Neurodegeneration* **11**, 50 (2022).
50. Minakaki, G. *et al.* Autophagy inhibition promotes SNCA/alpha-synuclein release and transfer via extracellular vesicles with a hybrid autophagosome-exosome-like phenotype. *Autophagy* **14**, 98-119 (2018).
51. Yamada, K. & Iwatsubo, T. Extracellular  $\alpha$ -synuclein levels are regulated by neuronal activity. *Molecular Neurodegeneration* **13**, 9 (2018).
52. Ahn, K.J., Paik, S.R., Chung, K.C. & Kim, J. Amino acid sequence motifs and mechanistic features of the membrane translocation of alpha-synuclein. *J Neurochem* **97**, 265-279 (2006).
53. Rodriguez, L., Marano, M.M. & Tandon, A. Import and Export of Misfolded  $\alpha$ -Synuclein. *Front Neurosci* **12**, 344 (2018).
54. Dilsizoglu Senol, A. *et al.*  $\alpha$ -Synuclein fibrils subvert lysosome structure and function for the propagation of protein misfolding between cells through tunneling nanotubes. *PLoS Biol* **19**, e3001287 (2021).
55. Abounit, S., Wu, J.W., Duff, K., Victoria, G.S. & Zurzolo, C. Tunneling nanotubes: A possible highway in the spreading of tau and other prion-like proteins in neurodegenerative diseases. *Prion* **10**, 344-351 (2016).
56. Xie, Y.X. *et al.* Lysosomal exocytosis releases pathogenic  $\alpha$ -synuclein species from neurons in synucleinopathy models. *Nature Communications* **13**, 4918 (2022).
57. Bayati, A. *et al.* Rapid macropinocytic transfer of  $\alpha$ -synuclein to lysosomes. *Cell Reports* **40**, 111102 (2022).
58. Kolay, S. *et al.* The dual fates of exogenous tau seeds: Lysosomal clearance *versus* cytoplasmic amplification. *Journal of Biological Chemistry* **298** (2022).
59. Vacchi, E. *et al.* Tau protein quantification in skin biopsies differentiates tauopathies from alpha-synucleinopathies. *Brain : a journal of neurology* **145**, 2755-2768 (2022).
60. Hughes, L.P., Halliday, G.M. & Dzamko, N. Flow Cytometry Measurement of Glucocerebrosidase Activity in Human Monocytes. *Bio-protocol* **10**, e3572 (2020).

**Acknowledgments**

We thank the whole laboratory for support and advice during this study. We thank the Microscopy and Flow Cytometry facilities of the Bellinzona Institutes of Science (BIOS+) for support during the executions and analysis of the experiments. Research was mainly supported by the Innovation Project 35449.1 IP-LS from the Swiss Innovation Agency. The Paganetti's lab is founded by the Gelu Foundation, the Mecri Foundation and The Charitable Gabriele Foundation.

**Author contributions**

Conceptualization: EP, MM, MB, SP, PP

Methods and investigations: EP, CM, MC, MS

Supervision: SP, PP

Writing (original draft): EP, SP

Writing (review & editing): all co-authors

**Competing interests:** The authors declare no competing interest. Manolo Bellotto is an employee of GT Gain Therapeutics SA

**Data and materials availability:** all raw data can be found in the supplementary material.

**Supplementary Table 1: cDNA sequences**

Protein	cDNA sequence
<i>Tau-mCherry</i>	ATGGCTGAGCCCCGCCAGGAGTTCGAAGTGATGGAAGATCACGCTGGGACGTACGGGTGGG GGGACAGGAAAGATCAGGGGGGCTACACCATGCACCAAGACCAAGAGGGTGACACGGACGC TGGCCTGAAAGAATCTCCCCTGCAGACCCCCACTGAGGACGGATCTGAGGAACCGGGCTCT GAAACCTCTGATGCTAAGAGCACTCCAACAGCGGAAGATGTGACAGCACCTTAGTGGATG AGGGAGCTCCCGGCAAGCAGGCTGCCGCGCAGCCCCACACGGAGATCCCAGAAGGAACCAC AGCTGAAGAAGCAGGCATTGGAGACACCCCCAGCCTGGAAGACGAAGCTGCTGGTCACGTG ACCCAAGCTCGCATGGTCAGTAAAGCAAAGACGGGACTGGAAGCGATGACAAAAAGCCA AGGGGGCTGATGGTAAACGAAGATCGCCACACCGGGGAGCAGCCCCCAGGCCAGAA GGGCCAGGCCAACGCCACCAGGATTCCAGCAAAAACCCCGCCGCTCCAAGACACCACCC AGCTCTGGTGAACCTCCAAATCAGGGGATCGCAGCGGTACAGCAGCCCCGGCTCCCCAG GCACTCCCGGCAGCCGCTCCCGCACCCCGTCCCTTCCAACCCACCCACCCGGGAGCCCAA GAAGGTGGCAGTGGTCCGTACTCCACCCAAGTCGCCGTCTTCGCCAAGAGCCGCTGCAG ACAGCCCCCGTGCCCATGCCAGACCTGAAGAATGTCAAGTCCAAGATCGGCTCCACTGAGA ACCTGAAGCACCAGCCGGGAGGCGGGAAGGTGCAGATAATTAATAAGAAGCTGGATCTTAG CAACGTCCAGTCCAAGTGTGGCTCAAAGGATAATATCAAACACGTCCCGGGAGGCGGCAGT GTGCAAATAGTCTACAAACCAGTTGACCTGAGCAAGGTGACCTCCAAGTGTGGCTCATTAG GCAACATCCATCATAAACCAGGAGGTGGCCAGGTGGAAGTAAAATCTGAGAAGCTTGACTT CAAGGACAGAGTCCAGTCAAGATTGGGTCCCTGGACAATATCACCCACGTCCCTGGCGGA GGAAATAAAAAGATTGAAACCCACAAGCTGACCTTCCGCGAGAACGCCAAGCCAAAGACAG ACCACGGGGCGGAGATCGTGTAAGTCGCCAGTGGTGTCTGGGGACACGTCTCCACGGCA TCTCAGCAATGTCTCTCCACCGGCAGCATCGACATGGTAGACTCGCCCCAGCTCGCCACG CTAGCTGACGAGGTGTCTGCCTCCCTCGGAAGCAGGGTTTGGTTTCGAAGGGCGAGGAGG ATAACATGGCCATCATCAAGGAGTTCATGCGCTTCAAGGTGCACATGGAGGGCTCCGTGAA CGGCCACGAGTTCGAGATCGAGGGCGAGGGCGAGGGCCGCCCTACGAGGGCACCCAGACC GCCAAGCTGAAGGTGACCAAGGGTGGCCCCCTACCCTTCGCCTGGGACATCCTGTCCCCTC AGTTCATGTACGGCTCCAAGGCCTACGTGAAGCACCCCGCCGACATCCCCGACTACTTGAA GCTGTCTTCCCGAGGGCTTCAAGTGGGAGCGCGTGATGAACCTCGAGGACGGCGGCGTG GTGACCGTGACCCAGGACTCTCCCTGCAGGACGGCGAGTTCATCTACAAGGTGAAGCTGC GCGGCACCAACTTCCCCTCCGACGGCCCCGTAATGCAGAAGAAGACCATGGGCTGGGAGGC CTCCTCCGAGCGGATGTACCCCGAGGACGGCGCCCTGAAGGGCGAGATCAAGCAGAGGCTG AAGCTGAAGGACGGCGGCCACTACGACGCTGAGGTCAAGACCACCTACAAGGCCAAGAAGC CCGTGCAGCTGCCCCGGCGCCTACAACGTCAACATCAAGTTGGACATCACCTCCACAACGA GGACTACACCATCGTGGAACAGTACGAACGCGCCGAGGGCCGCCACTCCACCGCGGCATG GACGAGCTGTACAAGTAG
<i>Tau-Gamillus</i>	ATGGCTGAGCCCCGCCAGGAGTTCGAAGTGATGGAAGATCACGCTGGGACGTACGGGTGGG GGGACAGGAAAGATCAGGGGGGCTACACCATGCACCAAGACCAAGAGGGTGACACGGACGC TGGCCTGAAAGAATCTCCCCTGCAGACCCCCACTGAGGACGGATCTGAGGAACCGGGCTCT

	<p>GAAACCTCTGATGCTAAGAGCACTCCAACAGCGGAAGATGTGACAGCACCCCTAGTGGATG  AGGGAGCTCCCGGCAAGCAGGCTGCCGCGCAGCCCCACACGGAGATCCCAGAAGGAACCAC  AGCTGAAGAAGCAGGCATTGGAGACACCCCCAGCCTGGAAGACGAAGCTGCTGGTCACGTG  ACCCAAGCTCGCATGGTCAGTAAAAGCAAAGACGGGACTGGAAGCGATGACAAAAAAGCCA  AGGGGGCTGATGGTAAAACGAAGATCGCCACACCGCGGGGAGCAGCCCCCTCAGGCCAGAA  GGGCCAGGCCAACGCCACCAGGATTCCAGCAAAAACCCGCCCCGCTCCAAGACACCACCC  AGCTCTGGTGAACCTCCAAAATCAGGGGATCGCAGCGGCTACAGCAGCCCCGGCTCCCCAG  GCACTCCCGGCAGCCGCTCCCGCACCCCGTCCCTTCCAACCCACCCACCCGGGAGCCCAA  GAAGGTGGCAGTGGTCCGTACTCCACCCAAGTCGCCGTCTTCCGCCAAGAGCCGCTGCAG  ACAGCCCCCGTCCCATGCCAGACCTGAAGAATGTCAAGTCCAAGATCGGCTCCACTGAGA  ACCTGAAGCACCAGCCGGGAGGCGGAAGGTGCAGATAATTAATAAGAAGCTGGATCTTAG  CAACGTCCAGTCCAAGTGTGGCTCAAAGGATAATATCAAACACGTCCCGGGAGGCGGCAGT  GTGCAAAATAGTCTACAAACAGTTGACCTGAGCAAGGTGACCTCCAAGTGTGGCTCATTAG  GCAACATCCATCATAAACCAGGAGGTGGCCAGGTGGAAGTAAAATCTGAGAAGCTTGACTT  CAAGGACAGAGTCCAGTCGAAGATTGGGTCCCTGGACAATATCACCCACGTCCCTGGCGGA  GGAAATAAAAAGATTGAAACCCACAAGCTGACCTTCCGCGAGAACGCCAAGCCAAAGACAG  ACCACGGGGCGGAGATCGTGTACAAGTCGCCAGTGGTGTCTGGGGACACGTCTCCACGGCA  TCTCAGCAATGTCTCCTCCACCGGCAGCATCGACATGGTAGACTCGCCCCAGCTCGCCACG  CTAGCTGACGAGGTGTCTGCCTCCCTCGGAAGCAGGGTTTGCTCGAGATGGTGAGCAAGG  GCGAGGAGGCATCTGGCAGAGCCCTGTTCCAGTACCCCATGACCAGCAAGATCGAGCTGAA  CGGCGAGATCAACGGCAAGAAATTCAAGGTGGCCGGCGAGGGCTTACCCCCAGCAGCGGC  AGATTCAACATGCACGCCTACTGCACCACCGGCGACCTGCCTATGAGCTGGGTCTGTATTG  CCAGCCCCCTCCAGTACGGCTTCCACATGTTGCGCCACTACCCCGAGGACATCACACACTT  TTTCCAGGAATGCTTCCCCGGCAGCTACACCCTGGACCGGACCCCTGAGAATGGAAGGCGAC  GGCACCTGACCACCCACCACGAGTACAGCCTGGAGGACGGCTGCGTGACCTCCAAGACCA  CCCTGAATGCCAGCGGCTTCGACCCTAAGGGCGCCACCATGACCAAGAGCTTCGTGAAACA  ACTGCCTAACGAGGTGAAGATCACCCCCACGGCCCCAACGGCATCAGACTGACCAGCACC  GTGCTGTACCTGAAGGAGGATGGCACCATCCAGATCGGCACCCAGGACTGCATCGTGACCC  CTGTGGGCGGAAGGAAAGTGACCCAGCCCAAGGCCCACTTCTGCACACCCAGATCATCCA  GAAGAAGGACCCCAACGACACCCGGGACCACATCGTGCAGACAGAAGTGGCCGTGGCCGGC  AATCTGTGGCACGGCATGGACGAGCTGTACAAG</p>
<i>tandem-Tau</i>	<p>ATGGCTGAGCCCCGCCAGGAGTTCGAAGTGATGGAAGATCACGCTGGGACGTACGGGTGG  GGGACAGGAAAGATCAGGGGGGTACACCATGCACCAAGACCAAGAGGGTGACACGGACGC  TGGCCTGAAAGAATCTCCCCTGCAGACCCCCACTGAGGACGGATCTGAGGAACCGGCTCT  GAAACCTCTGATGCTAAGAGCACTCCAACAGCGGAAGATGTGACAGCACCCCTAGTGGATG  AGGGAGCTCCCGGCAAGCAGGCTGCCGCGCAGCCCCACACGGAGATCCCAGAAGGAACCAC  AGCTGAAGAAGCAGGCATTGGAGACACCCCCAGCCTGGAAGACGAAGCTGCTGGTCACGTG  ACCCAAGCTCGCATGGTCAGTAAAAGCAAAGACGGGACTGGAAGCGATGACAAAAAAGCCA  AGGGGGCTGATGGTAAAACGAAGATCGCCACACCGCGGGGAGCAGCCCCCTCAGGCCAGAA  GGGCCAGGCCAACGCCACCAGGATTCCAGCAAAAACCCGCCCCGCTCCAAGACACCACCC</p>

	AGCTCTGGTGAACCTCCAAAATCAGGGGATCGCAGCGGCTACAGCAGCCCCGGCTCCCCAG GCACTCCCGGCAGCCGCTCCCGCACCCCGTCCCTTCCAACCCACCCACCCGGGAGCCCAA GAAGGTGGCAGTGGTCCGTACTCCACCCAAGTCGCCGTCTCCGCCAAGAGCCGCTGCAG ACAGCCCCCGTGCCCATGCCAGACCTGAAGAATGTCAAGTCCAAGATCGGCTCCACTGAGA ACCTGAAGCACCAGCCGGGAGCGGGAAGGTGCAGATAATTAATAAGAAGCTGGATCTTAG CAACGTCCAGTCCAAGTGTGGCTCAAAGGATAATATCAAACACGTCCCGGGAGGCGGCAGT GTGCAAATAGTCTACAAACCAGTTGACCTGAGCAAGGTGACCTCCAAGTGTGGCTCATTAG GCAACATCCATCATAAACCAGGAGGTGGCCAGGTGGAAGTAAAACTGAGAAGCTTGACTT CAAGGACAGAGTCCAGTGAAGATTGGGTCCCTGGACAATATCACCCACGTCCCTGGCGGA GGAAATAAAAAGATTGAAACCCACAAGCTGACCTTCCGCGAGAACGCCAAAGCCAAGACAG ACCACGGGGCGGAGATCGTGTACAAGTCGCCAGTGGTGTCTGGGGACACGTCTCCACGGCA TCTCAGCAATGTCTCCTCCACCGGCAGCATCGACATGGTAGACTCGCCCCAGCTCGCCACG CTAGCTGACGAGGTGTCTGCCTCCCTCGCGAAGCAGGGTTTGCTCGAGATGGTGAAGCAAGG GCGAGGAGGCATCTGGCAGAGCCCTGTTCAGTACCCCATGACCAGCAAGATCGAGCTGAA CGGCGAGATCAACGGCAAGAAATTCAAGGTGGCCGGCGAGGGCTTACCCCCAGCAGCGGC AGATTCAACATGCACGCCTACTGCACCACCGGCACCTGCCTATGAGCTGGGTCTGTATTG CCAGCCCCCTCCAGTACGGCTTCCACATGTTGCCCCACTACCCCGAGGACATCACACACTT TTTCCAGGAATGCTTCCCCGGCAGCTACACCCTGGACCGGACCTGAGAATGGAAGGCGAC GGCACCTGACCACCCACCACGAGTACAGCCTGGAGGACGGCTGCGTGACCTCCAAGACCA CCCTGAATGCCAGCGGCTTCGACCCTAAGGGCGCCACCATGACCAAGAGCTTCGTGAAACA ACTGCCTAACGAGGTGAAGATCACCCCCACGGCCCCAACGGCATCAGACTGACCAGCACC GTGCTGTACCTGAAGGAGGATGGCACCATCCAGATCGGCACCCAGGACTGCATCGTGACCC CTGTGGGCGGAAGGAAAGTGACCCAGCCCAAGGCCCACTTCCTGCACCCAGATCATCCA GAAGAAGGACCCCAACGACACCCGGGACCACATCGTGCAGACAGAAGTGGCCGTGGCCGGC AATCTGTGGCACGGCATGGACGAGCTGTACAAG
<i>Gamillus- TMEM192-3HA</i>	ATGGCTGAGCCCCGCCAGGAGTTTGAAGTGATGGAAGATCAGCTGGGACGTACGGGTGG GGGACAGGAAAGATCAGGGGGGTACACCATGCACCAAGACCAAGAGGGTGACACGGACGC TGGCCTGAAAGAATCTCCCTGCAGACCCCCACTGAGGACGGATCTGAGGAACCGGGCTCT GAAACCTCTGATGCTAAGAGCACTCCAACAGCGGAAGATGTGACAGCACCTTAGTGGATG AGGGAGCTCCCGGCAAGCAGGCTGCCGCGCAGCCCCACACGGAGATCCCAGAAGGAACCAC AGCTGAAGAAGCAGGCATTGGAGACACCCCCAGCCTGGAAGACGAAGCTGCTGGTCACGTG ACCCAAGCTCGCATGGTCAGTAAAGCAAAGACGGGACTGGAAGCGATGACAAAAAGCCA AGGGGGCTGATGGTAAACGAAGATCGCCACACCGGGGAGCAGCCCCCTCAGGCCAGAA GGGCCAGGCCAACGCCACCAGGATTCCAGCAAAAACCCGCCCCGTCCAAGACACCACCC AGCTCTGGTGAACCTCCAAAATCAGGGGATCGCAGCGGCTACAGCAGCCCCGGCTCCCCAG GCACTCCCGGCAGCCGCTCCCGCACCCCGTCCCTTCCAACCCACCCACCCGGGAGCCCAA GAAGGTGGCAGTGGTCCGTACTCCACCCAAGTCGCCGTCTCCGCCAAGAGCCGCTGCAG ACAGCCCCCGTGCCCATGCCAGACCTGAAGAATGTCAAGTCCAAGATCGGCTCCACTGAGA ACCTGAAGCACCAGCCGGGAGGCGGGAAGGTGCAGATAATTAATAAGAAGCTGGATCTTAG CAACGTCCAGTCCAAGTGTGGCTCAAAGGATAATATCAAACACGTCCCGGGAGGCGGCAGT



	<div>GTGCAAATAGTCTACAAACCAGTTGACCTGAGCAAGGTGACCTCCAAGTGTGGCTCATTAG</div> <div>GCAACATCCATCATAAACCAGGAGGTGGCCAGGTGGAAGTAAAAATCTGAGAAGCTTGACTT</div> <div>CAAGGACAGAGTCCAGTCCAAGATTGGGTCCCTGGACAATATCACCCACGTCCCTGGCGGA</div> <div>GGAAATAAAAAGATTGAAACCCACAAGCTGACCTTCCGCGAGAACGCCAAAGCCAAGACAG</div> <div>ACCACGGGGCGGAGATCGTGTACAAGTCGCCAGTGGTGTCTGGGGACACGTCTCCACGGCA</div> <div>TCTCAGCAATGTCTCTCCACCGGCAGCATCGACATGGTAGACTCGCCCCAGCTCGCCACG</div> <div>CTAGCTGACGAGGTGTCTGCCTCCCTCGCGAAGCAGGGTTTGCTCGAGATGGTGAGCAAGG</div> <div>GCGAGGAGGCATCTGGCAGAGCCCTGTTCCAGTACCCCATGACCAGCAAGATCGAGCTGAA</div> <div>CGGCGAGATCAACGGCAAGAAATTCAAGGTGGCCGGCGAGGGCTTCACCCCGAGCAGCGGC</div> <div>AGATTCAACATGCACGCCTACTGCACCACCGCGACCTGCCTATGAGCTGGGTCTGTATTG</div> <div>CCAGCCCCCTCCAGTACGGCTTCCACATGTTGCCCCACTACCCCGAGGACATCACACACTT</div> <div>TTTCCAGGAATGCTTCCCCGGCAGCTACACCCTGGACCGGACCCTGAGAATGGAAGGCGAC</div> <div>GGCACCCCTGACCACCCACCACGAGTACAGCCTGGAGGACGGCTGCGTGACCTCCAAGACCA</div> <div>CCCTGAATGCCAGCGGCTTCGACCCTAAGGGCGCCACCATGACCAAGAGCTTCGTGAAACA</div> <div>ACTGCCTAACGAGGTGAAGATCACCCCCACGGCCCCAACGGCATCAGACTGACCAGCACC</div> <div>GTGCTGTACCTGAAGGAGGATGGCACCATCCAGATCGGCACCCAGGACTGCATCGTGACCC</div> <div>CTGTGGGCGGAAGGAAAGTGACCCAGCCCAAGGCCCACTTCCTGCACCCAGATCATCCA</div> <div>GAAGAAGGACCCCAACGACACCCGGGACCACATCGTGCAGACAGAACTGGCCGTGGCCGGC</div> <div>AATCTGTGGCACGGCATGGACGAGCTGTACAAG</div>
--	---

## DISCUSSION AND FUTURE PERSPECTIVES

Pathological aging is often associated with neurodegenerative diseases like PD, AD and other tauopathies<sup>131</sup>. These proteinopathies affect the brain, resulting in cognitive impairments and severe motor dysfunctions that strongly impact the quality of life. As discussed in the introduction, the exact causes of these diseases are not fully understood, and multiple factors appeared to be involved in the disease onset and progression. It is therefore important to understand the exact pathological mechanisms underlying these diseases to develop preventive and curative therapies<sup>132</sup>.

The first part of my research conducted in murine neuronal progenitor cells C17.2 revealed a novel cellular mechanism for the paracrine signaling mediated by EVs. In particular, we demonstrated the interplay between two well-known cellular pathways: endocytosis and autophagy favor target engagement between fibrillogenic tau loaded in EVs and its cytosolic cellular tau counterpart located in degradative organelles of recipient cells. EVs loaded with either GFP fused to the tetraspanin CD63 or with the tau-MTBD were internalized through an endocytic mechanism by recipient cells overexpressing DsRed or overexpressing full-length tau fused to mCherry. Our observations were consistent with other studies reported in literature demonstrating that CD63 EVs uptake occurs preferentially via endocytosis<sup>133, 134</sup>. We demonstrated that, in recipient cells, cytosolic proteins including tau, are delivered to lysosomes through autophagy to be degraded. Thus, we showed that the lysosome represents the subcellular location where the exogenous material meets the endogenous one. A recent study conducted in Hela cells showed that EVs loaded with CD63 fused to nanoluciferase were uptaken with a low yield (about 1%). The delivery of EVs content was measured by luciferase activity in recipient cells. The authors demonstrated that the delivery of EVs cargo was controlled by the acidic endo-lysosomal pH, triggering endosomal acidification and fusion with lysosomes and subsequent cytosolic release (about 30%)<sup>135</sup>. In our cellular model we did not assess quantitatively the rate of EVs uptake and content delivery, this would require further investigations. In addition, EVs uptake and content delivery are highly variable depending on several factors such as the cell type, the EVs surface composition, the internalization mechanism (via direct membrane fusion or endocytosis) and the activation state of the recipient cells<sup>136, 137</sup>. Another finding of our work was that the encounter of the pro-aggregating tau from EVs and the endogenous tau-mCherry was promoting tau accumulation in acidic organelles and this accumulation of lysosomal tau was associated with disease hallmarks such as lysosomal stress (increased DOs number/area and TFE3 nuclear translocation), pathological tau forms (AT8 and MC1 positive puncta) and cytotoxicity (decrease in nuclear size and increase of LDH activity). It is not still clear if autophagy is playing a harmful or protective role in neuronal homeostasis. In PD, AD and HD brains an increased number of autophagic vacuoles and markers has been reported<sup>138</sup>. Enhanced autophagy can contribute to neuronal death or represent a compensatory cellular response triggered to eliminate protein aggregates which are resistant to other degradative system such as the UPS<sup>139</sup>. Collectively it is believed that UPS and ALP stimulation represent good therapeutic strategy to remove proteins aggregates and consequentially being beneficial for AD and other tauopathies<sup>140, 141</sup>. However, even opposite outcomes were documented as, for instance, in our work we suggested that autophagy inhibition may be more appropriate to avoid tau prion-like propagation. Other studies demonstrated that, in flies treated with A $\beta$ 1-42, autophagy stimulation with rapamycin, resulted in increased toxicity and shortened life span<sup>142</sup>, indicating that autophagy modulation is more complex than initially thought. These controversial outcomes can be partially explained by the use of different animal and cellular model, the

experimental paradigm and by the fact that the different model systems represent different stages of the pathology<sup>140</sup>. Interestingly, low pH typical in acidic organelles seems to play a role in aggregates formation. For instance, an *in vitro* study demonstrated that low pH was inducing tau unfolding and favoring the formation of ordered conformers which may precede the formation of pathological aggregates<sup>143</sup>. One possible cause of lysosomal defects induced by protein misfolding and/or accumulation is that protein aggregates are targeted by the ALP for degradation but the lysosomes fail to degrade them and start to be dysfunctional and subsequently favor further protein aggregation<sup>144, 145</sup>. In our cellular system we observed, upon treatment with EVs carrying the pro-aggregating tau, a nuclear translocation of TFE3, a transcription factor involved in lysosomal biogenesis. We speculate that this cellular response represents a compensatory mechanism in which the cell tries to eliminate tau aggregates through lysosomes and autophagy stimulation. In accordance with our results other groups demonstrated beneficial effects of TFEB or TFE3 overexpression<sup>146</sup>. A study conducted in neurons proposed that TFEB, another member of the TFE family, plays an active role in the secretion of a mutated form of tau without affecting the secretion of wild-type tau. In the same study authors confirmed similar behaviors using conditional TFEB KO PS19 transgenic mice for the active secretion of aberrant tau showing increased tau pathology respect to controls. The authors demonstrated that TFEB forms a complex with the lysosomal Ca<sup>2+</sup> channel TRPML1 mediating exocytosis of lysosomes containing aberrant tau resulting in an enhanced cellular clearance<sup>147</sup>. Overall, our study conducted in neuronal progenitor C17.2 cells further strengthen that lysosomes are not only degradative organelles but structures also important in more complex cellular functions.

The second part of my research project aimed at investigating in more details the implications of lysosomes in tauopathies. It is well documented that during normal and even more pathologic aging lysosomes number and functionality are reduced<sup>148</sup>. Thus, we exploit the use of an *in vitro* model mimicking the lysosomal storage disorder Gaucher disease, a rare genetic disorder affecting lysosomal GCase leading to the tissue accumulation of glucosylceramide and glucosylsphingosine. This model consists in the use of CBE, an irreversible GCase inhibitor, to treat human primary fibroblasts expressing, in an inducible manner, tau fused to different fluorophores. We demonstrated that upon treatment with CBE, tau accumulates in DOs, partially colocalizing with lysosomal markers (Lamp1, TMEM192 and LysoTracker). Additional co-localization studies with other lysosomal (Lamp2, Limp2), autophagic (LC3, p62) or endosomal (Rab5, Rab7, Rab11) markers may allow to better characterize the DOs in which tau accumulates.

To further investigate the effect of tau pathologic accumulation on lysosomes function, we used human AD brain-derived tau seeds to show that these seeds also favor tau accumulation in lysosomes. Tau accumulation in DOs correlated as well with lysosomal stress (DOs number and area increase, TFE3 nuclear translocation and lactosylceramide puncta accumulation), suggesting that tau accumulation mediated by seeds and CBE impairs lysosomal function and lipid metabolism. Lysosomal functional assays such as evaluation of pH, lysosomal membrane integrity (galectin-3) or lysosomal activity (cathepsin B) may help to better understand the impact of tau accumulation on lysosomal functions. Similarly, it would be relevant to characterize the PTMs of tau in DOs to understand if it associates with a pathological signature.

It is well known that mutations in *GBA1*,  $\alpha$ -synuclein (*SNCA*) and leucine-rich repeat kinase 2 (*LRRK2*) represent the most common genetic risk-factors for sporadic PD and dementia with Lewy Bodies<sup>149</sup>. Several studies investigated the link between  $\alpha$ -synuclein and GCase impairment whereas the link between tau and GCase dysfunction has not been documented. GCase KO HEK293-FT cells displayed an accumulation of  $\alpha$ -synuclein

and impaired ALP represented by an increment of autophagic substrates like p62, Lamp2 and LC3<sup>150</sup>. Several studies conducted in PD mouse models demonstrated that TFE3 plays essential roles in regulating the ALP axis resulting in dopaminergic neuronal survival<sup>151</sup>. Importantly TFE3 nuclear translocation can occur as well upon ER stress<sup>152</sup>. Some Gaucher disease mutations like the L444P lead to misfolded GCase, unfolded enzyme ER retention and consequent ER stress<sup>153</sup>. It is tempting to speculate that persistent mutant misfolded GCase inducing ER stress could affect TFE3 subcellular localization. Lactosylceramide is an active sphingolipid and has been described in LSD to accumulate especially in neurons of Niemann-Pick disease type C (NPC) and with a lower extent as well in Gaucher disease cells<sup>154</sup>. Additional *in vitro* studies demonstrated that fibroblasts treated with GCase inhibitor led to the lactosylceramide accumulation in lysosomes<sup>154</sup>. Aberrant intracellular LacCer localization is associated with abnormal cholesterol accumulation, membranes dysfunctions and cell membrane trafficking impairments<sup>155</sup>.

For the first time we demonstrated a bidirectional link between GCase dysfunctions and tau accumulation in degradative organelles in human primary fibroblasts therefore indicating that GCase impairments not only affect  $\alpha$ -synuclein biology but also other proteinopathies. However, further studies are needed to elucidate the role of tau accumulation on GCase activity and vice-versa in more relevant neuronal models or in patient derived samples. In addition, our study may provide new therapeutic insights for neurodegeneration: increasing GCase activity and/or reducing its substrates accumulation, autophagic impairments and/or lysosomal stress may be beneficial as well for the treatment of tauopathies. In GCase deficient cells modelling PD and DLB, inhibition of acid ceramidase with carmofur, restoring ceramide levels, led to a reduction of intracellular  $\alpha$ -synuclein accumulation and improving dysregulated secretory autophagic pathways<sup>150</sup>.

In our study, we used dermal fibroblasts that may not represent the most suitable *in vitro* system to investigate tau pathology. However, we decided to use these primary cells envisioning the possibility to obtain by a simple non-invasive skin biopsy patient-derived cells<sup>156</sup> carrying different LSD mutations. Fibroblasts derived from patients affected by GD and carrying mutations in GCase are available from biobanks like the Coriell Institute for Medical Research. We identified several deposited fibroblasts carrying hetero or homozygous *GBA1* mutations and we purchased four cell lines with L444P biallelic mutation. The most frequent *GBA1* mutations associated to PD are the L444P and N370S<sup>157</sup>. Future experiments will aim at investigating tau accumulation in degradative organelles of *GBA1* mutated fibroblasts. We would expect that our data obtained with GCase pharmacological inhibition recapitulate what it is occurring in patient's mutated cells. We decided to use dermal fibroblasts for their potential to be directly transdifferentiated in induced neurons (iNs)<sup>158, 159</sup>. Direct conversion of somatic cells into human neuronal cells requires the activation of neuronal-fate determining genes, chemical modulation of key signaling pathways and subsequent donor cell identity repression<sup>160</sup>. Transdifferentiation consists in a direct cell fate reprogramming and it does not require passing through a pluripotent intermediate<sup>161</sup>. Importantly during transdifferentiation cell identity is maintained and the epigenetic signatures are more conserved compared to the differentiation achieved through induced pluripotent stem cells (iPSC)<sup>162</sup>. The direct reprogrammed neurons preserve their epigenetic age as demonstrated in a study where neurons obtained by direct reprogramming of HD patient fibroblasts were forming aberrant huntingtin aggregates<sup>163</sup>. This study empathized the importance of cellular age in modeling late-onset neurological disorders. Reprogrammed cells are very heterogenous in term of genetics, epigenetics and phenotypes compared to iPSC<sup>162</sup> and if this represent an advantage or disadvantage depends on the studied disease. For the study of neurodegenerative diseases being characterized by complex cellular heterogeneity iNs represent the most

suitable cellular model. Unfortunately, transdifferentiation presents some limitations such as the fact that not all somatic cells can be directly reprogrammed, the conversion efficiency is quite low, the reprogramming is technically challenging and requires a long time<sup>164</sup>. In addition, iNs are not proliferating cells consequentially there is a restricted cell scalability and more importantly for the clinical use of iNs in regenerative medicine additional studies are required to evaluate adverse effects due to viral transduction, a procedure that often is used for the first phases of reprogramming<sup>165</sup>.

## CONCLUSIONS

My studies conducted in murine neuronal progenitor cells and human primary fibroblasts demonstrated that extracellular pathological tau forms, either transported by EVs or endocytosed, encounter endogenous wild-type tau in acidic structures of recipient cells. We demonstrated that ALP stimulation is involved in the endogenous tau transport to lysosomes and may favor the pathological switch of physiological tau into aggregated tau. Furthermore, we observed that tau accumulation in DOs correlates with lysosomal stress and that inhibition of GCase leads to tau accumulation and lysosomal dysfunction. These results suggest that lysosomal impairments due to genetic factor such as mutations occurring in LSD or aging-dependent deterioration of lysosomes may represent a risk factor for the propagation of pathogenic tau in neurodegenerative diseases (**Figure 6.**).

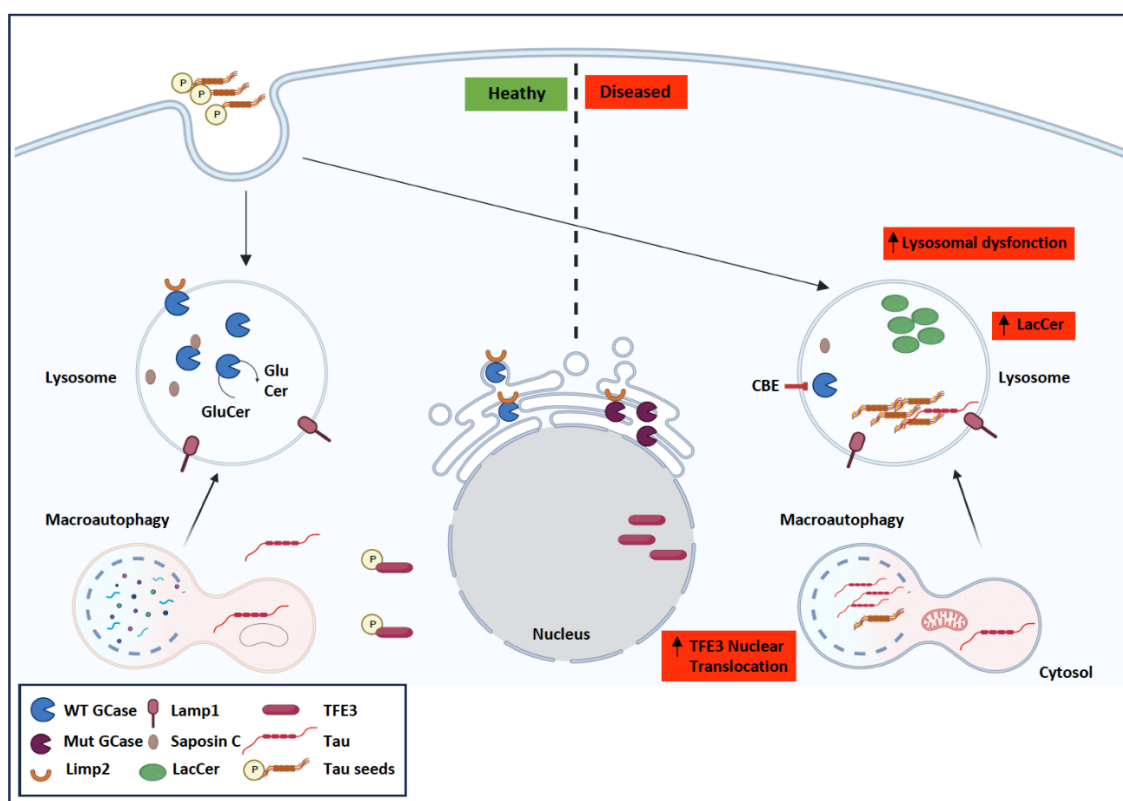


**Figure 6.** Graphical abstract of our paper finding (Drawn using Biorender 2023)

## BIBLIOGRAPHY

1. Manuscript A. Alzheimer ' s Disease: The Challenge of the Second Century. 2012;3(77):1-35. doi:10.1126/scitranslmed.3002369.Alzheimer
2. Mhatre V. Ho, Ji-Ann Lee and KCM, Dien et al. 2013. 基因的改变NIH Public Access. *Bone*. 2008;23(1):1-7. doi:10.3233/JAD-2010-1221.Alzheimer
3. Leroy M, Bertoux M, Skrobala E, et al. Characteristics and progression of patients with frontotemporal dementia in a regional memory clinic network. *Alzheimer's Res Ther*. 2021;13(1):1-11. doi:10.1186/s13195-020-00753-9
4. Hergesheimer RC, Chami AA, De Assis DR, et al. The debated toxic role of aggregated TDP-43 in amyotrophic lateral sclerosis: A resolution in sight? *Brain*. 2019;142(5):1176-1194. doi:10.1093/brain/awz078
5. Brandt R, Trushina NI, Bakota L, et al. Protein Aggregation and Dysfunction of Autophagy-Lysosomal Pathway: A Vicious Cycle in Lysosomal Storage Diseases. *Hum Mol Genet*. 2022;17(1):1-13. doi:10.3389/fnmol.2020.00037
6. Daldin M, Fodale V, Cariulo C, et al. Polyglutamine expansion affects huntingtin conformation in multiple Huntington's disease models. *Sci Rep*. 2017;7(1):1-15. doi:10.1038/s41598-017-05336-7
7. Young JE, Garden GA, Martinez RA, et al. Polyglutamine-expanded androgen receptor truncation fragments activate a Bax-dependent apoptotic cascade mediated by DP5/Hrk. *J Neurosci*. 2009;29(7):1987-1997. doi:10.1523/JNEUROSCI.4072-08.2009
8. Monaco A, Fraldi A. Protein Aggregation and Dysfunction of Autophagy-Lysosomal Pathway: A Vicious Cycle in Lysosomal Storage Diseases. *Front Mol Neurosci*. 2020;13(March):1-8. doi:10.3389/fnmol.2020.00037
9. Zhang Y, Wu KM, Yang L, Dong Q, Yu JT. Tauopathies: new perspectives and challenges. *Mol Neurodegener*. 2022;17(1):1-29. doi:10.1186/s13024-022-00533-z
10. Bang J, Spina S, Miller BL. Non-Alzheimer's dementia 1. 2018;386(10004):1672-1682. doi:10.1016/S0140-6736(15)00461-4.Non-Alzheimer
11. Greaves C V., Rohrer JD. An update on genetic frontotemporal dementia. *J Neurol*. 2019;266(8):2075-2086. doi:10.1007/s00415-019-09363-4
12. Lowe J, Errington DR, Lennox G, et al. Ballooned neurons in several neurodegenerative diseases and stroke contain  $\alpha\beta$  crystallin. *Neuropathol Appl Neurobiol*. 1992;18(4):341-350. doi:10.1111/j.1365-2990.1992.tb00796.x
13. Reid MJ, Beltran-Lobo P, Johnson L, Perez-Nievas BG, Noble W. Astrocytes in Tauopathies. *Front Neurol*. 2020;11(September):1-9. doi:10.3389/fneur.2020.572850
14. Dickson DW, Yen H, Suzuki KI, Davies P, Gareia JH, Hirano A. Nkta. 1986:216-223.
15. Josephs KA, Whitwell JL, Parisi JE, et al. Argyrophilic grains: A distinct disease or an additive pathology? *Neurobiol Aging*. 2008;29(4):566-573. doi:10.1016/j.neurobiolaging.2006.10.032
16. Chung D eun C, Roemer S, Petrucelli L, Dickson DW. Cellular and pathological heterogeneity of primary tauopathies. *Mol Neurodegener*. 2021;16(1):1-20. doi:10.1186/s13024-021-00476-x
17. Ghetti B, Oblak AL, Boeve BF, Johnson KA, Dickerson BC, Goedert M. Invited review: Frontotemporal dementia caused by microtubule-associated protein tau gene (MAPT) mutations: A chameleon for neuropathology and neuroimaging. *Neuropathol Appl Neurobiol*. 2015;41(1):24-46. doi:10.1111/nan.12213
18. Strang KH, Golde TE, Giasson BI. MAPT mutations, tauopathy, and mechanisms of neurodegeneration. *Lab Invest*. 2019;99(7):912-928. doi:10.1038/s41374-019-0197-x

19. Drummond E, Nayak S, Pires G, Ueberheide B, Wisniewski T. Isolation of amyloid plaques and neurofibrillary tangles from archived alzheimer's disease tissue using laser-capture microdissection for downstream proteomics. *Methods Mol Biol.* 2018;1723:319-334. doi:10.1007/978-1-4939-7558-7\_18
20. Weller RO, Massey A, Kuo YM, Roher AE. Cerebral amyloid angiopathy: Accumulation of A $\beta$  in interstitial fluid drainage pathways in Alzheimer's disease. *Ann N Y Acad Sci.* 2000;903(3):110-117. doi:10.1111/j.1749-6632.2000.tb06356.x
21. Lopez OL, Dekosky ST. Alzheimer ' s disease Clinical symptoms in Alzheimer ' s disease. *Handb Clin Neurol.* 2008;89.
22. Crespo-Biel N, Theunis C, Van Leuven F. Protein Tau: Prime cause of synaptic and neuronal degeneration in alzheimer's disease. *Int J Alzheimers Dis.* 2012;2012. doi:10.1155/2012/251426
23. Liu CC, Kanekiyo T, Xu H BG. Nat Rev Neurol. *Nat Rev Neurosci.* 2013;9(2):106-118. doi:10.1038/nrneurol.2012.263.Apolipoprotein
24. Brinckerhoff CE. Historical Perspective. *Matrix Met Heal Dis Sculpt Hum Body.* 2017;13(1):13-30. doi:10.1142/9789813207554\_0002
25. Ricciarelli R, Fedele E. The Amyloid Cascade Hypothesis in Alzheimer's Disease: It's Time to Change Our Mind. *Curr Neuroparmacol.* 2017;15(6):926-935. doi:10.2174/1570159x15666170116143743
26. Morris GP, Clark IA, Vissel B. Inconsistencies and Controversies Surrounding the Amyloid Hypothesis of Alzheimer's Disease. *Acta Neuropathol Commun.* 2014;2(1):1-21. doi:10.1186/s40478-014-0135-5
27. Braak H, Braak E. Staging of alzheimer's disease-related neurofibrillary changes. *Neurobiol Aging.* 1995;16(3):271-278. doi:10.1016/0197-4580(95)00021-6
28. Gonzalez C, Armijo E, Bravo-Alegria J, Becerra-Calixto A, Mays CE, Soto C. Modeling amyloid beta and tau pathology in human cerebral organoids. *Mol Psychiatry.* 2018;23(12):2363-2374. doi:10.1038/s41380-018-0229-8
29. van der Kant R, Goldstein LSB, Ossenkoppele R. Amyloid- $\beta$ -independent regulators of tau pathology in Alzheimer disease. *Nat Rev Neurosci.* 2020;21(1):21-35. doi:10.1038/s41583-019-0240-3
30. Barbier P, Zejneli O, Martinho M, et al. Role of tau as a microtubule-associated protein: Structural and functional aspects. *Front Aging Neurosci.* 2019;10(JUL):1-14. doi:10.3389/fnagi.2019.00204
31. Corsi A, Bombieri C, Valenti MT, Romanelli MG. Tau Isoforms: Gaining Insight into MAPT Alternative Splicing. *Int J Mol Sci.* 2022;23(23). doi:10.3390/ijms232315383
32. Wang Y, Mandelkow E. Tau in physiology and pathology. *Nat Rev Neurosci.* 2016;17(1):5-21. doi:10.1038/nrn.2015.1
33. Sündermann F, Fernandez MP, Morgan RO. An evolutionary roadmap to the microtubule-associated protein MAP Tau. *BMC Genomics.* 2016;17(1):1-16. doi:10.1186/s12864-016-2590-9
34. Wu L, Wang Z, Lad S, et al. Selective Detection of Misfolded Tau From Postmortem Alzheimer's Disease Brains. *Front Aging Neurosci.* 2022;14(July):1-14. doi:10.3389/fnagi.2022.945875
35. Bachmann S, Bell M, Klimek J, Zempel H. Differential Effects of the Six Human TAU Isoforms: Somatic Retention of 2N-TAU and Increased Microtubule Number Induced by 4R-TAU. *Front Neurosci.* 2021;15(May):1-10. doi:10.3389/fnins.2021.643115
36. Kenner L, El-Shabrawi Y, Hutter H, et al. Expression of three- and four-repeat tau isoforms in mouse liver. *Hepatology.* 1994;20(4):1086-1089. doi:10.1002/hep.1840200442
37. Gu Y, Oyama F, Ihara Y.  $\tau$  Is widely expressed in rat tissues. *J Neurochem.* 1996;67(3):1235-1244. doi:10.1046/j.1471-4159.1996.67031235.x



38. Trabzuni D, Wray S, Vandrovcsa J, et al. MAPT expression and splicing is differentially regulated by brain region : relation to genotype and implication for tauopathies. 2012;21(18):4094-4103. doi:10.1093/hmg/dds238
39. Maina MB, Al-Hilaly YK, Serpell LC. Nuclear tau and its potential role in alzheimer's disease. *Biomolecules*. 2016;6(1):2-20. doi:10.3390/biom6010009
40. Sultan A, Nesslany F, Violet M, et al. Nuclear Tau, a key player in neuronal DNA protection. *J Biol Chem*. 2011;286(6):4566-4575. doi:10.1074/jbc.M110.199976
41. Pedrioli G, Piovesana E, Vacchi E, Balbi C. Extracellular vesicles as promising carriers in drug delivery: Considerations from a cell biologist's perspective. *Biology (Basel)*. 2021;10(5). doi:10.3390/biology10050376
42. Pedrioli G, Barberis M, Magrin C, et al. Tau Seeds in Extracellular Vesicles Induce Tau Accumulation in Degradative Organelles of Cells. 2021;40(9):1185-1199. doi:10.1089/dna.2021.0485
43. Mandelkow EM, Mandelkow E. Biochemistry and cell biology of Tau protein in neurofibrillary degeneration. *Cold Spring Harb Perspect Med*. 2012;2(7):1-26. doi:10.1101/cshperspect.a006247
44. Guo T, Noble W, Hanger DP. Roles of tau protein in health and disease. *Acta Neuropathol*. 2017;133(5):665-704. doi:10.1007/s00401-017-1707-9
45. Ruiz-Gabarre D, Carnero-Espejo A, Ávila J, García-Escudero V. What's in a Gene? The Outstanding Diversity of MAPT. *Cells*. 2022;11(5). doi:10.3390/cells11050840
46. Brandt R, Trushina NI, Bakota L. Much More Than a Cytoskeletal Protein: Physiological and Pathological Functions of the Non-microtubule Binding Region of Tau. *Front Neurol*. 2020;11(October):1-14. doi:10.3389/fneur.2020.590059
47. Goedert M, Spillantini MG. Propagation of Tau aggregates Tim Bliss. *Mol Brain*. 2017;10(1):1-9. doi:10.1186/s13041-017-0298-7
48. Alquezar C, Arya S, Kao AW. Tau Post-translational Modifications: Dynamic Transformers of Tau Function, Degradation, and Aggregation. *Front Neurol*. 2021;11(January):1-24. doi:10.3389/fneur.2020.595532
49. Hanger DP, Anderton BH, Noble W. Tau phosphorylation: the therapeutic challenge for neurodegenerative disease. *Trends Mol Med*. 2009;15(3):112-119. doi:10.1016/j.molmed.2009.01.003
50. Morishima-Kawashima M, Hasegawa M, Takio K, et al. Proline-directed and non-proline-directed phosphorylation of PHF-tau. *J Biol Chem*. 1995;270(2):823-829. doi:10.1074/jbc.270.2.823
51. Iqbal K, Del C. Alonso A, Chen S, et al. Tau pathology in Alzheimer disease and other tauopathies. *Biochim Biophys Acta - Mol Basis Dis*. 2005;1739(2):198-210. doi:10.1016/j.bbdis.2004.09.008
52. Wipt P, George KM. 基因的改变NIH Public Access. *Bone*. 2008;23(1):1-7. doi:10.1016/j.neuron.2010.08.044.Acetylation
53. Irwin DJ, Cohen TJ, Grossman M, et al. Acetylated tau, a novel pathological signature in Alzheimer's disease and other tauopathies. *Brain*. 2012;135(3):807-818. doi:10.1093/brain/aws013
54. Morishima-Kawashima M, Hasegawa M, Takio K, Suzuki M, Titani K, Ihara Y. Ubiquitin is conjugated with amino-terminally processed tau in paired helical filaments. *Neuron*. 1993;10(6):1151-1160. doi:10.1016/0896-6273(93)90063-W
55. Takamura H, Nakayama Y, Ito H, Katayama T, Fraser PE, Matsuzaki S. SUMO1 Modification of Tau in Progressive Supranuclear Palsy. *Mol Neurobiol*. 2022;59(7):4419-4435. doi:10.1007/s12035-022-02734-5
56. Balmik AA, Chinnathambi S. Methylation as a key regulator of Tau aggregation and neuronal health in Alzheimer's disease. *Cell Commun Signal*. 2021;19(1):1-13. doi:10.1186/s12964-021-00732-z
57. Mhatre V. Ho, Ji-Ann Lee and KCM, Dien et al. 2013. 基因的改变NIH Public Access. *Bone*. 2008;23(1):1-7.

doi:10.1146/annurev-biochem-060608-102511.Cross

58. Quinn JP, Corbett NJ, Kellett KAB, Hooper NM. Tau Proteolysis in the Pathogenesis of Tauopathies: Neurotoxic Fragments and Novel Biomarkers. *J Alzheimers Dis.* 2018;63(1):13-33. doi:10.3233/JAD-170959
59. Paholikova K, Salingova B, Opattova A, et al. N-terminal truncation of microtubule associated protein tau dysregulates its cellular localization. *J Alzheimer's Dis.* 2015;43(3):915-926. doi:10.3233/JAD-140996
60. Ayers JI, Giasson BI, Borchelt DR. Prion-like Spreading in Tauopathies. 2019;83(4):337-346. doi:10.1016/j.biopsych.2017.04.003.Prion-like
61. Gibbons GS, Lee VMY, Trojanowski JQ. Mechanisms of Cell-to-Cell Transmission of Pathological Tau: A Review. *JAMA Neurol.* 2019;76(1):101-108. doi:10.1001/jamaneurol.2018.2505
62. Hasegawa M. Molecular mechanisms in the pathogenesis of alzheimer's disease and Tauopathies-Prion-Like seeded aggregation and phosphorylation. *Biomolecules.* 2016;6(2). doi:10.3390/biom6020024
63. Holmes BB, Devos SL, Kfoury N, et al. Heparan sulfate proteoglycans mediate internalization and propagation of specific proteopathic seeds. 2013. doi:10.1073/pnas.1301440110
64. Winston CN, Aulston B, Rockenstein EM, et al. Mouse Neurons in vivo. 2021;67(2):541-553. doi:10.3233/JAD-180776.Neuronal
65. Abounit S, Wu JW, Duff K, Soraya G. Tunneling nanotubes : A possible highway in the spreading of tau and other prion-like proteins in neurodegenerative diseases. 2016;35(19):344-351. doi:10.1080/19336896.2016.1223003
66. Takahashi M, Miyata H, Kametani F, Nonaka T. Extracellular association of APP and tau fibrils induces intracellular aggregate formation of tau. 2015:895-907. doi:10.1007/s00401-015-1415-2
67. Mukrasch MD, Von Bergen M, Biernat J, et al. The 'jaws' of the tau-microtubule interaction. *J Biol Chem.* 2007;282(16):12230-12239. doi:10.1074/jbc.M607159200
68. Wolozin B. *Tau Biology.*
69. Zwierzchowski-Zarate AN, Mendoza-Oliva A, Kashmer OM, Collazo-Lopez JE, White CL, Diamond MI. RNA induces unique tau strains and stabilizes Alzheimer's disease seeds. *J Biol Chem.* 2022;298(8):1-11. doi:10.1016/j.jbc.2022.102132
70. Bok E, Leem E, Lee BR, et al. Role of the Lipid Membrane and Membrane Proteins in Tau Pathology. *Front Cell Dev Biol.* 2021;9(April):1-14. doi:10.3389/fcell.2021.653815
71. Scialò C, De Cecco E, Manganotti P, Legname G. Prion and prion-like protein strains: Deciphering the molecular basis of heterogeneity in neurodegeneration. *Viruses.* 2019;11(3):1-37. doi:10.3390/v11030261
72. Robert A, Schöll M, Vogels T. Tau seeding mouse models with patient brain-derived aggregates. *Int J Mol Sci.* 2021;22(11). doi:10.3390/ijms22116132
73. Mudher A, Colin M, Dujardin S, et al. What is the evidence that tau pathology spreads through prion-like propagation ? 2017:1-20. doi:10.1186/s40478-017-0488-7
74. Goedert M, Spillantini MG, Jakes R, Rutherford D, Crowther RA. Multiple isoforms of human microtubule-associated protein tau: sequences and localization in neurofibrillary tangles of Alzheimer's disease. *Neuron.* 1989;3(4):519-526. doi:10.1016/0896-6273(89)90210-9
75. Freed JK, Gutterman DD. Communication Is Key: Mechanisms of Intercellular Signaling in Vasodilation. *J Cardiovasc Pharmacol.* 2017;69(5):264-272. doi:10.1097/FJC.0000000000000463
76. Merchant ML, Rood IM, Deegens KJ, Klein JB. Isolation and characterization of urinary extracellular vesicles: Implications for biomarker discovery. *Nat Rev Nephrol.* 2017;13(12):731-749. doi:10.1038/nrneph.2017.148

77. Willms E, Cabañas C, Mäger I, Wood MJA, Vader P. Extracellular vesicle heterogeneity: Subpopulations, isolation techniques, and diverse functions in cancer progression. *Front Immunol.* 2018;9(APR). doi:10.3389/fimmu.2018.00738
78. Ruan Z. Extracellular vesicles drive tau spreading in Alzheimer's disease. *Neural Regen Res.* 2022;17(2):328-329. doi:10.4103/1673-5374.317975
79. Pérez M, Avila J, Hernández F. Propagation of tau via extracellular vesicles. *Front Neurosci.* 2019;13(JUL):1-7. doi:10.3389/fnins.2019.00698
80. Kolay S, Vega AR, Dodd DA, et al. The dual fates of exogenous tau seeds: Lysosomal clearance versus cytoplasmic amplification. *J Biol Chem.* 2022;298(6):102014. doi:10.1016/j.jbc.2022.102014
81. Jiang S, Bhaskar K. Degradation and Transmission of Tau by Autophagic-Endolysosomal Networks and Potential Therapeutic Targets for Tauopathy. *Front Mol Neurosci.* 2020;13(October):1-19. doi:10.3389/fnmol.2020.586731
82. Ugbo C, Fort-Aznar L, Sweeney ST. Leaky endosomes push tau over the seed limit. *J Biol Chem.* 2019;294(50):18967-18968. doi:10.1074/jbc.H119.011687
83. Feng Q, Luo Y, Zhang XN, et al. MAPT/Tau accumulation represses autophagy flux by disrupting IST1-regulated ESCRT-III complex formation: a vicious cycle in Alzheimer neurodegeneration. *Autophagy.* 2020;16(4):641-658. doi:10.1080/15548627.2019.1633862
84. Wang Y, Martinez-Vicente M, Krüger U, et al. Tau fragmentation, aggregation and clearance: The dual role of lysosomal processing. *Hum Mol Genet.* 2009;18(21):4153-4170. doi:10.1093/hmg/ddp367
85. Montalbano M, McAllen S, Puangmalai N, et al. RNA-binding proteins Musashi and tau soluble aggregates initiate nuclear dysfunction. *Nat Commun.* 2020;11(1):1-16. doi:10.1038/s41467-020-18022-6
86. Gordon-Weeks PR. The ultrastructure of the neuronal growth cone: New insights from subcellular fractionation and rapid freezing studies. *Electron Microsc Rev.* 1988;1(2):201-219. doi:10.1016/0892-0354(88)90002-0
87. Larsen KE, Sulzer D. Autophagy in neurons: A review. *Histol Histopathol.* 2002;17(3):897-908. doi:10.14670/HH-17.897
88. Ciechanover A, Kwon YT. Degradation of misfolded proteins in neurodegenerative diseases: therapeutic targets and strategies. *Exp Mol Med.* 2015;47(3). doi:10.1038/EMM.2014.117
89. Alfaro IE, Albornoz A, Molina A, et al. Chaperone mediated autophagy in the crosstalk of neurodegenerative diseases and metabolic disorders. *Front Endocrinol (Lausanne).* 2019;10(JAN):1-13. doi:10.3389/fendo.2018.00778
90. Chen GF, Xu TH, Yan Y, et al. Amyloid beta: Structure, biology and structure-based therapeutic development. *Acta Pharmacol Sin.* 2017;38(9):1205-1235. doi:10.1038/aps.2017.28
91. Mhatre V, Ho, Ji-Ann Lee and KCM, Dien et al. 2013. 基因的改变 NIH Public Access. *Bone.* 2008;23(1):1-7. doi:10.4172/jpb.1000091.Defining
92. Takalo M, Salminen A, Soininen H, Hiltunen M, Haapasalo A. Protein aggregation and degradation mechanisms in neurodegenerative diseases. *Am J Neurodegener Dis.* 2013;2(1):1-14.
93. Tydlacka S, Wang CE, Wang X, Li S, Li XJ. Differential activities of the ubiquitin-proteasome system in neurons versus glia may account for the preferential accumulation of misfolded proteins in neurons. *J Neurosci.* 2008;28(49):13285-13295. doi:10.1523/JNEUROSCI.4393-08.2008
94. Wang L, Klionsky DJ, Shen HM. The emerging mechanisms and functions of microautophagy. *Nat Rev Mol Cell Biol.* 2023;24(3):186-203. doi:10.1038/s41580-022-00529-z
95. Auzmendi-Iriarte J, Matheu A. Impact of Chaperone-Mediated Autophagy in Brain Aging: Neurodegenerative

- Diseases and Glioblastoma. *Front Aging Neurosci.* 2021;12(January):1-17. doi:10.3389/fnagi.2020.630743
96. Cortes CJ, Miranda HC, Frankowski H, et al. HHS Public Access. 2015;17(9):1180-1189. doi:10.1038/nn.3787.Polyglutamine-expanded
  97. Aman Y, Schmauck-Medina T, Hansen M, et al. Autophagy in healthy aging and disease. *Nat Aging.* 2021;1(8):634-650. doi:10.1038/s43587-021-00098-4
  98. Settembre C, Di Malta C, Polito VA, et al. Europe PMC Funders Group Europe PMC Funders Author Manuscripts TFEB Links Autophagy to Lysosomal Biogenesis. *Science (80- ).* 2011;332(6036):1429-1433. doi:10.1126/science.1204592.TFEB
  99. Runwal G, Stamatakou E, Siddiqi FH, Puri C, Zhu Y, Rubinsztein DC. LC3-positive structures are prominent in autophagy-deficient cells. *Sci Rep.* 2019;9(1):1-14. doi:10.1038/s41598-019-46657-z
  100. Teyssou E, Takeda T, Lebon V, et al. Mutations in SQSTM1 encoding p62 in amyotrophic lateral sclerosis: Genetics and neuropathology. *Acta Neuropathol.* 2013;125(4):511-522. doi:10.1007/s00401-013-1090-0
  101. Ouyang H, Ali YO, Ravichandran M, et al. Protein aggregates are recruited to aggresome by histone deacetylase 6 via unanchored ubiquitin C termini. *J Biol Chem.* 2012;287(4):2317-2327. doi:10.1074/jbc.M111.273730
  102. Onyenwoke RU, Brenman JE. Lysosomal Storage Diseases — Regulating Neurodegeneration. 2015;9:81-91. doi:10.4137/JEN.S25475.TYPE
  103. Vieira SRL, Schapira AHV. Glucocerebrosidase mutations: A paradigm for neurodegeneration pathways. *Free Radic Biol Med.* 2021;175(August):42-55. doi:10.1016/j.freeradbiomed.2021.08.230
  104. Saffari A, Kölker S, Hoffmann GF, Ebrahimi-Fakhari D. Linking mitochondrial dysfunction to neurodegeneration in lysosomal storage diseases. *J Inherit Metab Dis.* 2017;40(5):631-640. doi:10.1007/s10545-017-0048-0
  105. Vitner EB, Platt FM, Futerman AH. Common and uncommon pathogenic cascades in lysosomal storage diseases. *J Biol Chem.* 2010;285(27):20423-20427. doi:10.1074/jbc.R110.134452
  106. Rama Rao K V., Kielian T. Astrocytes and lysosomal storage diseases. *Neuroscience.* 2016;323(June):195-206. doi:10.1016/j.neuroscience.2015.05.061
  107. Tomonaga T. HActa europatholog : ca. *J Neurol.* 1990:689-691.
  108. Boer DEC, van Smeden J, Bouwstra JA, Aerts JMFG. Glucocerebrosidase: Functions in and beyond the lysosome. *J Clin Med.* 2020;9(3). doi:10.3390/jcm9030736
  109. Do J, McKinney C, Sharma P, Sidransky E. Glucocerebrosidase and its relevance to Parkinson disease. 2019:1-16.
  110. Fredj Ben B, Artola M, Overkleeft HS, Ubbink M, Johannes MFGA. Distinguishing the differences in -glycosylceramidase folds, dynamics, and actions informs therapeutic uses. *J Lipid Res.* 2018;59(12):2262-2276. doi:10.1194/jlr.R086629
  111. Ben Bdira F, Kallemeyjn WW, Oussoren S V., et al. Stabilization of Glucocerebrosidase by Active Site Occupancy. *ACS Chem Biol.* 2017;12(7):1830-1841. doi:10.1021/acscchembio.7b00276
  112. Do J, McKinney C, Sharma P, Sidransky E. Glucocerebrosidase and its relevance to Parkinson disease. *Mol Neurodegener.* 2019;14(1):1-16. doi:10.1186/s13024-019-0336-2
  113. Gegg ME, Schapira AHV. The role of glucocerebrosidase in Parkinson disease pathogenesis. *FEBS J.* 2018;285(19):3591-3603. doi:10.1111/febs.14393
  114. Jian J, Hettinghouse A, Liu C ju. Progranulin acts as a shared chaperone and regulates multiple lysosomal enzymes. *Genes Dis.* 2017;4(3):125-126. doi:10.1016/j.gendis.2017.05.001

115. Rosenbloom BE, Weinreb NJ. Gaucher disease: A comprehensive review. *Adv Gauch Dis Basic Clin Perspect*. 2013;18(3):27-49. doi:10.2217/EBO.12.198
116. Hein LK, Meikle PJ, Hopwood JJ, Fuller M. Secondary sphingolipid accumulation in a macrophage model of Gaucher disease. *Mol Genet Metab*. 2007;92(4):336-345. doi:10.1016/j.ymgme.2007.08.001
117. Sillence DJ. Glucosylceramide modulates endolysosomal pH in Gaucher disease. *Mol Genet Metab*. 2013;109(2):194-200. doi:10.1016/j.ymgme.2013.03.015
118. Low ZX, Hariharan G. Gaucher Disease – A Rare Cause of Collodion. *Indian J Pediatr*. 2020;87(1):82. doi:10.1007/s12098-019-03072-6
119. Salvioli R, Tatti M, Scarpa S, et al. The N370S (Asn370 → Ser) mutation affects the capacity of glucosylceramidase to interact with anionic phospholipid-containing membranes and saposin C. *Biochem J*. 2005;390(1):95-103. doi:10.1042/BJ20050325
120. Bendikov-Bar I, Ron I, Filocamo M, Horowitz M. Characterization of the ERAD process of the L444P mutant glucocerebrosidase variant. *Blood Cells, Mol Dis*. 2011;46(1):4-10. doi:10.1016/j.bcmd.2010.10.012
121. Bennett LL, Fellner C. Pharmacotherapy of gaucher disease: Current and future options. *P T*. 2018;43(5):274-281.
122. Levy O, Waters C, Fahn S, et al. NIH Public Access. 2015;71(6):752-757. doi:10.1001/jamaneurol.2014.313.Comparison
123. Kinghorn KJ, Asghari AM, Castillo-quan JI, Kinghorn KJ, Ph D. The emerging role of autophagic-lysosomal dysfunction in Gaucher disease and Parkinson ' s disease. 2017;12(3). doi:10.4103/1673-5374.202934
124. Mazzulli JR, Xu Y, Sun Y, et al. NIH Public Access. 2012;146(1):37-52. doi:10.1016/j.cell.2011.06.001.Gaucher
125. Papadopoulos VE, Nikolopoulou G, Antoniadou I, et al. Modulation of b -glucocerebrosidase increases a -synuclein secretion and exosome release in mouse models of Parkinson ' s disease. 2018;27(10):1696-1710. doi:10.1093/hmg/ddy075
126. Marlet FR, Cerri S, Schapira AH V, Blandini F, Monte DA Di. Sphingolipid changes in Parkinson L444P GBA mutation fibroblasts promote a -synuclein aggregation. 2022:1038-1051.
127. Clarke J, Kayatekin C, Viel C, Shihabuddin L, Sardi SP. Murine models of lysosomal storage diseases exhibit differences in brain protein aggregation and neuroinflammation. *Biomedicines*. 2021;9(5). doi:10.3390/biomedicines9050446
128. Xu YH, Xu K, Sun Y, et al. Multiple pathogenic proteins implicated in neuronopathic Gaucher disease mice. *Hum Mol Genet*. 2014;23(15):3943-3957. doi:10.1093/hmg/ddu105
129. Lee JY, Kim HS. Extracellular Vesicles in Neurodegenerative Diseases: A Double-Edged Sword. *Tissue Eng Regen Med*. 2017;14(6):667-678. doi:10.1007/s13770-017-0090-x
130. Hill AF, Fowler CD. Dual Perspectives Dual Perspectives Companion Paper: Extracellular Vesicles and Neurodegenerative Diseases, by NeuroEVs: Characterizing Extracellular Vesicles Generated in the Neural Domain. 2019;39(47):9269-9273. <https://doi.org/10.1523/JNEUROSCI.0146-18.2019>.
131. Ho YS, So KF, Chang RCC. Anti-aging herbal medicine-How and why can they be used in aging-associated neurodegenerative diseases? *Ageing Res Rev*. 2010;9(3):354-362. doi:10.1016/j.arr.2009.10.001
132. Medeiros R, Baglietto-Vargas D, Laferla FM. The Role of Tau in Alzheimer's Disease and Related Disorders. *CNS Neurosci Ther*. 2011;17(5):514-524. doi:10.1111/j.1755-5949.2010.00177.x
133. Joshi BS, de Beer MA, Giepmans BNG, Zuhorn IS. Endocytosis of Extracellular Vesicles and Release of Their Cargo from Endosomes. *ACS Nano*. 2020;14(4):4444-4455. doi:10.1021/acsnano.9b10033
134. Mulcahy LA, Pink RC, Carter DRF. Routes and mechanisms of extracellular vesicle uptake. *J Extracell Vesicles*.

- 2014;3(1):1-14. doi:10.3402/jev.v3.24641
135. Bonsergent E, Grisard E, Buchrieser J, Schwartz O, Théry C, Lavieu G. Quantitative characterization of extracellular vesicle uptake and content delivery within mammalian cells. *Nat Commun.* 2021;12(1):1-11. doi:10.1038/s41467-021-22126-y
  136. Liu YJ, Wang C. A review of the regulatory mechanisms of extracellular vesicles-mediated intercellular communication. *Cell Commun Signal.* 2023;21(1):77. doi:10.1186/s12964-023-01103-6
  137. Kwok ZH, Wang C, Jin Y. Extracellular Vesicle Transportation and Uptake by Recipient Cells: A Critical Process to Regulate Human Diseases. 2021;9(2):1-22. doi:10.3390/pr9020273.Extracellular
  138. Atpa K. © 2012 Landes Bioscience . Do not distribute . © 2012 Landes Bioscience . Do not distribute . 2012;(June):987-988.
  139. Article RW. The role of autophagy-lysosome pathway in neurodegeneration associated with Parkinson ' s disease. 2008. doi:10.1093/brain/awm318
  140. Funderburk SF, Marcellino BK, Yue Z. Mechanism in Alzheimer ' s Disease. 2010:59-68. doi:10.1002/MSJ
  141. Han DH, Na H, Choi WH, et al. to delay tau aggregation. *Nat Commun.* 2014. doi:10.1038/ncomms6633
  142. Ling D, Song H, Garza D, Neufeld TP, Salvaterra PM. Abeta42-Induced Neurodegeneration via an Age-Dependent Autophagic-Lysosomal Injury in Drosophila. 2009;4(1). doi:10.1371/journal.pone.0004201
  143. Jebarupa B, Muralidharan M, Arun A, Mandal AK, Mitra G. Conformational heterogeneity of tau: Implication on intrinsic disorder, acid stability and fibrillation in Alzheimer's disease. *Biophys Chem.* 2018;241:27-37. doi:10.1016/j.bpc.2018.07.005
  144. Lamark T, Johansen T. Aggrephagy: Selective disposal of protein aggregates by macroautophagy. *Int J Cell Biol.* 2012;2012. doi:10.1155/2012/736905
  145. Hoffmann AC, Minakaki G, Menges S, et al. Extracellular aggregated alpha synuclein primarily triggers lysosomal dysfunction in neural cells prevented by trehalose. *Sci Rep.* 2019;9(1):1-18. doi:10.1038/s41598-018-35811-8
  146. Raben N, Puertollano R. TFEB and TFE3: Linking Lysosomes to Cellular Adaptation to Stress\*. *Annu Rev Cell Dev Biol.* 2016;32(May):255-278. doi:10.1146/annurev-cellbio-111315-125407
  147. Xu Y, Du S, Marsh JA, et al. TFEB regulates lysosomal exocytosis of tau and its loss of function exacerbates tau pathology and spreading. 2021;26(10):5925-5939. doi:10.1038/s41380-020-0738-0.TFEB
  148. Guerrero-Navarro L, Jansen-Dürr P, Cavinato M. Age-Related Lysosomal Dysfunctions. *Cells.* 2022;11(12):1-20. doi:10.3390/cells11121977
  149. Smith LJ, Lee CY, Menozzi E, Schapira AHV. Genetic variations in GBA1 and LRRK2 genes: Biochemical and clinical consequences in Parkinson disease. *Front Neurol.* 2022;13(3). doi:10.3389/fneur.2022.971252
  150. Kim MJ, Jeon S, Burbulla LF, Krainc D. Acid ceramidase inhibition ameliorates  $\alpha$ -synuclein accumulation upon loss of GBA1 function. *Hum Mol Genet.* 2018;27(11):1972-1988. doi:10.1093/hmg/ddy105
  151. He X, Xie Y, Zheng Q, et al. TFE3-Mediated Autophagy is Involved in Dopaminergic Neurodegeneration in Parkinson's Disease. *Front Cell Dev Biol.* 2021;9(November):1-13. doi:10.3389/fcell.2021.761773
  152. Martina JA, Diab HI, Brady OA, Puertollano R. TFEB and TFE 3 are novel components of the integrated stress response . *EMBO J.* 2016;35(5):479-495. doi:10.15252/embj.201593428
  153. Maor G, Rencus-Lazar S, Filocamo M, Steller H, Segal D, Horowitz M. Unfolded protein response in Gaucher disease: From human to Drosophila. *Orphanet J Rare Dis.* 2013;8(1):1. doi:10.1186/1750-1172-8-140
  154. Hůlková H, Ledvinová J, Asfaw B, Koubek K, Kopřiva K, Elleder M. Lactosylceramide in lysosomal storage

- disorders. A comparative immunohistochemical and biochemical study. *Virchows Arch.* 2005;447(1):31-44. doi:10.1007/s00428-005-1246-y
155. Ballabio A, Gieselmann V. Lysosomal disorders: From storage to cellular damage. *Biochim Biophys Acta - Mol Cell Res.* 2009;1793(4):684-696. doi:10.1016/j.bbamcr.2008.12.001
  156. Vacchi E, Lazzarini E, Pinton S, et al. Tau protein quantification in skin biopsies differentiates tauopathies from alpha-synucleinopathies. *Brain.* 2022;145(8):2755-2768. doi:10.1093/brain/awac161
  157. Ran C, Brodin L, Forsgren L, et al. Strong association between glucocerebrosidase mutations and Parkinson's disease in Sweden. *Neurobiol Aging.* 2016;45:212.e5. doi:10.1016/j.neurobiolaging.2016.04.022
  158. Yang Y, Chen R, Wu X, et al. Rapid and Efficient Conversion of Human Fibroblasts into Functional Neurons by Small Molecules. *Stem Cell Reports.* 2019;13(5):862-876. doi:10.1016/j.stemcr.2019.09.007
  159. Zhao Z, Xu M, Wu M, Tian X, Zhang C, Fu X. Transdifferentiation of fibroblasts by defined factors. *Cell Reprogram.* 2015;17(3):151-159. doi:10.1089/cell.2014.0089
  160. Carter JL, Halmai JANM, Fink KD. The iNs and Outs of Direct Reprogramming to Induced Neurons. *Front Genome Ed.* 2020;2(September). doi:10.3389/fgeed.2020.00007
  161. Wang H, Yang Y, Liu J, Qian L. Direct cell reprogramming: approaches, mechanisms and progress. 2022;22(6):410-424. doi:10.1038/s41580-021-00335-z.Direct
  162. Samoylova EM, Baklaushev VP. Cell Reprogramming Preserving Epigenetic Age : 2020;85(9).
  163. Victor MB, Richner M, Olsen HE, et al. *Striatal Neurons Directly Converted from Huntington's Disease Patient Fibroblasts Recapitulate Age-Associated Disease Phenotypes.* Vol 21.; 2018. doi:10.1038/s41593-018-0075-7.Striatal
  164. Access O. Limitations and challenges of direct cell reprogramming. 2022:723-737. doi:10.14670/HH-18-458
  165. Grath A, Dai G. Direct cell reprogramming for tissue engineering and regenerative medicine. 2019;9:1-15.

## ABBREVIATIONS

**A $\beta$** : Amyloid Beta

**AD**: Alzheimer Disease

**AGD**: Argyrophilic Grain Disease

**ALP**: Autophagy Lysosomal Pathway

**ALS**: Amyotrophic Lateral Sclerosis

**APOE**: Apolipoprotein E

**APP**: Amyloid Precursor Protein

**ATG**: Autophagy-Related Gene or Protein

**CBD**: Corticobasal Degeneration

**CBE**: conduritol  $\beta$  Epoxide

**cDNA**: Complementary DNA

**CMA**: Chaperon Mediated Autophagy

**CNS**: Central Nervous System

**DBL**: Dementia with Lewy Bodies

**Da**: Dalton

**DOs**: Degradative Organelles

**ER**: Endoplasmic Reticulum

**ERAD**: Endoplasmic Reticulum Associated Protein Degradation

**ESCRT**: Endosomal-Sorting Complex Required for Transport

**EVs**: Extracellular Vesicles

**FTD**: Frontotemporal Dementia

**GBA1**: Glucosylceramidase 1 Gene

**GCase**: Glucosylceramidase, Glucocerebrosidase, Acid- $\beta$ -Glucosidase, D-Glucosyl-N-Acylsphingosine or Glucosylhydrolase

**GD**: Gaucher Disease

**GAPDH**: Glyceraldehyde 3-Phosphate Dehydrogenase

**GFP**: Green Fluorescence Protein

**H**: Hours

**HD**: Huntington Disease

**KO**: Knockout

**K18**: Truncated Tau Isoform Containing 4 Microtubules Binding Repeat

**LacCer**: Lactosylceramide

**LAMP1**: Lysosomal Associated Membrane Protein 1

**LAMP2**: Lysosomal Associated Membrane Protein 2

**Limp2**: Lysosomal Integral Membrane Protein 2

**LC3**: MAP1LC3, Microtubule Associated Proteins 1A/1B light Chain 3B

**LSD**: Lysosomal Storage Disorder

**MAPT**: Microtubule Associated Protein Tau gene

**MAPK**: Mitogen-Activated Protein Kinase



**Min:** Minutes  
**MTBD:** Microtubule Binding Domain  
**mTOR:** Mammalian Target of Rapamycin  
**MTs:** Microtubules  
**MVBs:** Multivesicular Bodies  
**NFTs:** Neurofibrillary Tangles  
**PD:** Parkinson Disease  
**PiD:** Pick Disease  
**PHFs:** Paired Helical filaments  
**PNS:** Peripheral Nervous system  
**PrP:** Prion Protein  
**PSP:** Progressive Supranuclear Palsy  
**PTMs:** Post translational Modifications  
**RT:** Room Temperature  
**SBMA:** Spino and Bulbar Amyotrophy  
**SFs:** Straight Filaments  
**Tau441:** Tau isoform (441 amino acids long) also referred as variant 2N4R, 4 microtubule binding repeats (R) and 2 amino terminal inserts (N)  
**TauMBD:** Microtubule Binding Domain of Tau  
**TDP43:** Transactive Response DNA Binding Protein 43  
**TFEB:** Transcription Factor EB  
**TFE3:** Transcription Factor E3  
**UPR:** Unfolded Protein Response  
**UPS:** Ubiquitin Proteasome System

## ANNEXES

In this section are reported as annexes the works that I conducted in my previous laboratory in France head by Prof. Dr. Clotilde Théry at the Institut Curie. These works were finalized and published during these last three years. The first article in which I am co-first author was published in 2020 entitled: *Extracellular Vesicles containing ACE2 efficiently prevent infection by Sars-CoV-2 Spike protein-containing virus*, the work illustrates how vesicles can be used as therapeutic decoy agents to reduce viral infection. The second manuscript in which I am a co-author released in 2023 of the title *Efficient cell death mediated by bioengineered killer extracellular vesicles*, shows how extracellular vesicles containing diphtheria toxin induce cell death and could potentially be used as tool for designing new anti-cancer treatments.

# Extracellular vesicles containing ACE2 efficiently prevent infection by SARS-CoV-2 Spike protein-containing virus

Federico Coccozza<sup>1,2,\*</sup> | Nathalie Névo<sup>1,\*</sup> | Ester Piovesana<sup>1,2,\*</sup> | Xavier Lahaye<sup>1</sup> | Julian Buchrieser<sup>3</sup> | Olivier Schwartz<sup>3</sup> | Nicolas Manel<sup>1</sup> | Mercedes Tkach<sup>1,†</sup> | Clotilde Théry<sup>1,†</sup> | Lorena Martin-Jaular<sup>1,†</sup>

<sup>1</sup> INSERM U932, Institut Curie Centre de Recherche, PSL Research University, Paris, France

<sup>2</sup> Université de Paris, Paris, France

<sup>3</sup> Virus and Immunity Unit, Institut Pasteur and CNRS UMR 3569, Paris, France

## Correspondence

Mercedes Tkach, INSERM U932, Institut Curie Centre de Recherche, PSL Research University, Paris 75005, France  
Email: [mercedes.tkach@curie.fr](mailto:mercedes.tkach@curie.fr)  
Clotilde Théry, INSERM U932, Institut Curie Centre de Recherche, PSL Research University, Paris 75005, France  
Email: [clotilde.thery@curie.fr](mailto:clotilde.thery@curie.fr)  
Lorena Martin-Jaular, INSERM U932, Institut Curie Centre de Recherche, PSL Research University, Paris 75005, France  
Email: [lorena.martin-jaular@curie.fr](mailto:lorena.martin-jaular@curie.fr)

\* Federico Coccozza, Nathalie Névo, and Ester Piovesana are co-first authors.

† Mercedes Tkach, Clotilde Théry, and Lorena Martin-Jaular are co-last authors.

## Funding information

Institut Curie, INSERM, CNRS; H2020-MSCA-ITN, Grant/Award Numbers: 722148, TRAIN-EV; ARC, Grant/Award Number: RF20180206962; INCA, Grant/Award Number: 11548; LABEX DCBIOL, Grant/Award Numbers: ANR-10-IDEX-0001-02 PSL\*, ANR-11-LABX-0043; LABEX VRI, Grant/Award Number: ANR-10-LABX-77; ANRS, Grant/Award Numbers: ECTZ36691, ECTZ71745; Sidaction, Grant/Award Number: 17-1-AAE-11097-2; ANR, Grant/Award Numbers: ANR-19-CE15-0018-01, ANR-18-CE92-0022-01; DIMIHEALTH

## Abstract

SARS-CoV-2 entry is mediated by binding of the spike protein (S) to the surface receptor ACE2 and subsequent priming by host TMPRSS2 allowing membrane fusion. Here, we produced extracellular vesicles (EVs) exposing ACE2 and demonstrate that ACE2-EVs are efficient decoys for SARS-CoV-2 S protein-containing lentivirus. Reduction of infectivity positively correlates with the level of ACE2, is much more efficient than with soluble ACE2 and further enhanced by the inclusion of TMPRSS2.

## KEYWORDS

ACE2, EV therapy, SARS-CoV-2, TMPRSS2

## 1 | INTRODUCTION

SARS-CoV-2 is the infectious causative agent of the COVID-19 pandemic (Zhou et al., 2020). Viral entry into host cells is mediated by the interaction of the spike (S) protein on the surface of SARS-CoV-2 with the surface receptor angiotensin-converting enzyme 2 (ACE2) (Walls et al., 2020). After binding to ACE2, the S protein is cleaved by Transmembrane protease serine 2 (TMPRSS2) and becomes fusogenic thus allowing viral entry (Hoffmann et al., 2020).

This is an open access article under the terms of the [Creative Commons Attribution](https://creativecommons.org/licenses/by/4.0/) License, which permits use, distribution and reproduction in any medium, provided the original work is properly cited.

© 2020 The Authors. *Journal of Extracellular Vesicles* published by Wiley Periodicals, LLC on behalf of the International Society for Extracellular Vesicles

ACE2 is expressed at the surface of pneumocytes and intestinal epithelial cells which are potential target cells for infection (Ziegler et al., 2020). A soluble form of the ACE2 ectodomain can be released after cleavage by ADAM10 or ADAM17 in different physiological conditions (Jia et al., 2009). In addition, TMPRSS2 can compete with the metalloproteases for ACE2 cleavage (Heurich et al., 2014). Soluble recombinant ACE2 neutralizes SARS-CoV-2 by binding the S protein and has been proven to reduce entry of SARS-CoV-2 into Vero-E6 cells and engineered human organoids (Monteil et al., 2020). ACE2, however, is synthesized as a transmembrane protein, like TMPRSS2. We postulate that ACE2 could be present on the surface of extracellular vesicles (EVs), which could result in better efficacy as a decoy to capture SARS-CoV-2. Furthermore, concomitant presence of an active serine-protease TMPRSS2 on the same EVs could further interfere with viral infectivity, by forcing viral fusion on the EV membrane, rather than on target cells.

EVs are lipid bilayer-enclosed structures containing transmembrane proteins, membrane-associated proteins, cytosolic proteins and nucleic acids that are released into the environment by different cell types (Mathieu et al., 2019). Since EVs have the same membrane orientation as cells, they expose at their surface the extracellular domains of transmembrane proteins that can bind to nearby or long-distance targets. By specifically binding to different proteins and protein-containing structures, EVs can act as a decoy for virus (De Carvalho et al., 2014) and bacterial toxins (Keller et al., 2020), thus suggesting a potential role as therapeutic agents.

## 2 | RESULTS

In order to explore the hypothesis that EVs can be used as SARS-CoV-2 decoy agents, we first assessed whether ACE2 can be present in EVs from cell lines derived from tissues expressing ACE2. As cell lines endogenously expressing ACE2, we used the human lung epithelial cell line Calu-3 and the epithelial colorectal cell line Caco-2 which are known targets for SARS-CoV-2 infection (Hoffmann et al., 2020). In a pilot experiment, Calu-3 and Caco-2 were cultured in medium without fetal bovine serum (FBS) for 24 h and EVs were isolated from the cell conditioned medium (CCM) by size-exclusion chromatography (SEC). This technique allows the separation of EVs from soluble proteins (Figure 1a). We analysed side-by-side fractions enriched in EVs (pooled fractions 7–11), in soluble factors (pooled fractions 17–21), and the fractions in-between (pooled fraction 12–16) (Figure 1a). Particle quantification by nanoparticle tracking analysis (NTA) confirmed that the majority of particles released by Calu-3 and Caco-2 cells were isolated in EV-containing fractions (Supplementary Figure A). In this experiment, Caco-2 cells released less EVs but of similar mode size than Calu-3 (Figure 1b). These EVs contained ACE2 protein as well as known EV markers (CD63, CD81 ADAM10) (Figure 1c). In addition, although Caco-2 and Calu-3 expressed TMPRSS2, this protease was not released in EVs (Figure 1c). To obtain EVs with high amounts of ACE2 and TMPRSS2 to be tested as decoy agents, we switched to 293FT cells that could be easily genetically-edited. We transduced 293FT cells with lentivirus containing ACE2 alone (293FT-ACE2) or in combination with TMPRSS2 (293FT-ACE2-TMPRSS2). 293FT cells transduced with lentivirus containing empty plasmids were used as a control (293FT-mock). The three 293FT cell lines were cultured in FBS-containing EV-depleted medium and EVs were isolated from concentrated CCM by SEC. We observed a high count of particles with comparable mode sizes in EV fractions from all 293FT cell lines (Figure 1d, Supplementary Figure A) coincident with the presence of CD63, CD81, ADAM10 and HSP70 EV markers (Figure 1e). Overexpression of ACE2 in 293FT cells led to the incorporation of this molecule into EVs (Figure 1e) with higher levels found on EVs from 293FT-ACE2 than from 293FT-ACE2-TMPRSS2 (Supplementary Figure B). 293FT-mock and 293FT-ACE2 cells expressed TMPRSS2, but the predicted full-length 54 kDa form was not detected in their EVs: a 30 kDa N-terminal fragment devoid of the serine protease domain (Zmora et al., 2015) was mainly detected, together with a low level of the glycosylated full-length 70 kDa form. Importantly, EVs from 293FT cells overexpressing TMPRSS2 contained higher levels of the full-length TMPRSS2 protein and less of a cleaved form than EVs from 293FT-mock or 293FT-ACE2 cells (Figure 1e, Supplementary Figure C) (Afar et al., 2001). Since the ACE2 ectodomain can be released after cleavage (Jia et al., 2009), we evaluated whether cells overexpressing ACE2 release soluble ACE2 in addition to EV-associated ACE2. To do this, we analysed the presence of ACE2, the EV marker CD81 and the non-EVs component AChE (Liao et al., 2019) by WB on EV fractions ( $1 \times 10^9$  particles) and the intermediate and soluble fractions obtained from the same amount of CCM. We detected some particles in intermediate and soluble fractions from the three 293FT cell lines, that probably came from the depleted medium since they did not contain EV markers by WB (Supplementary Figure A, D, E). AChE was enriched in soluble fractions whereas CD81 was mainly found in EV fractions validating our isolation protocol for EVs and soluble components (Figure 1f). Importantly, ACE2 was found as a full-length transmembrane form in the EV fractions, as two shorter cleaved forms in the soluble fractions, and a mixture of all forms in the intermediate fractions (Figure 1f). Intermediate fractions thus represent a mixture of EVs and soluble proteins and for this reason were not further analysed. Low levels of ACE2 were found in the soluble SEC fractions of 293FT-ACE2 cells when compared to the levels present on the EV-containing fraction (Figure 1f, 1g). By contrast, 293FT-ACE2-TMPRSS2 cells released similar amounts of EV-associated as of soluble ACE2 (Figure 1f, 1g), suggesting that the overexpression of the protease cleaves ACE2 as previously described (Heurich et al., 2014), favouring its secretion to the extracellular space as a soluble protein instead of associated to EVs.

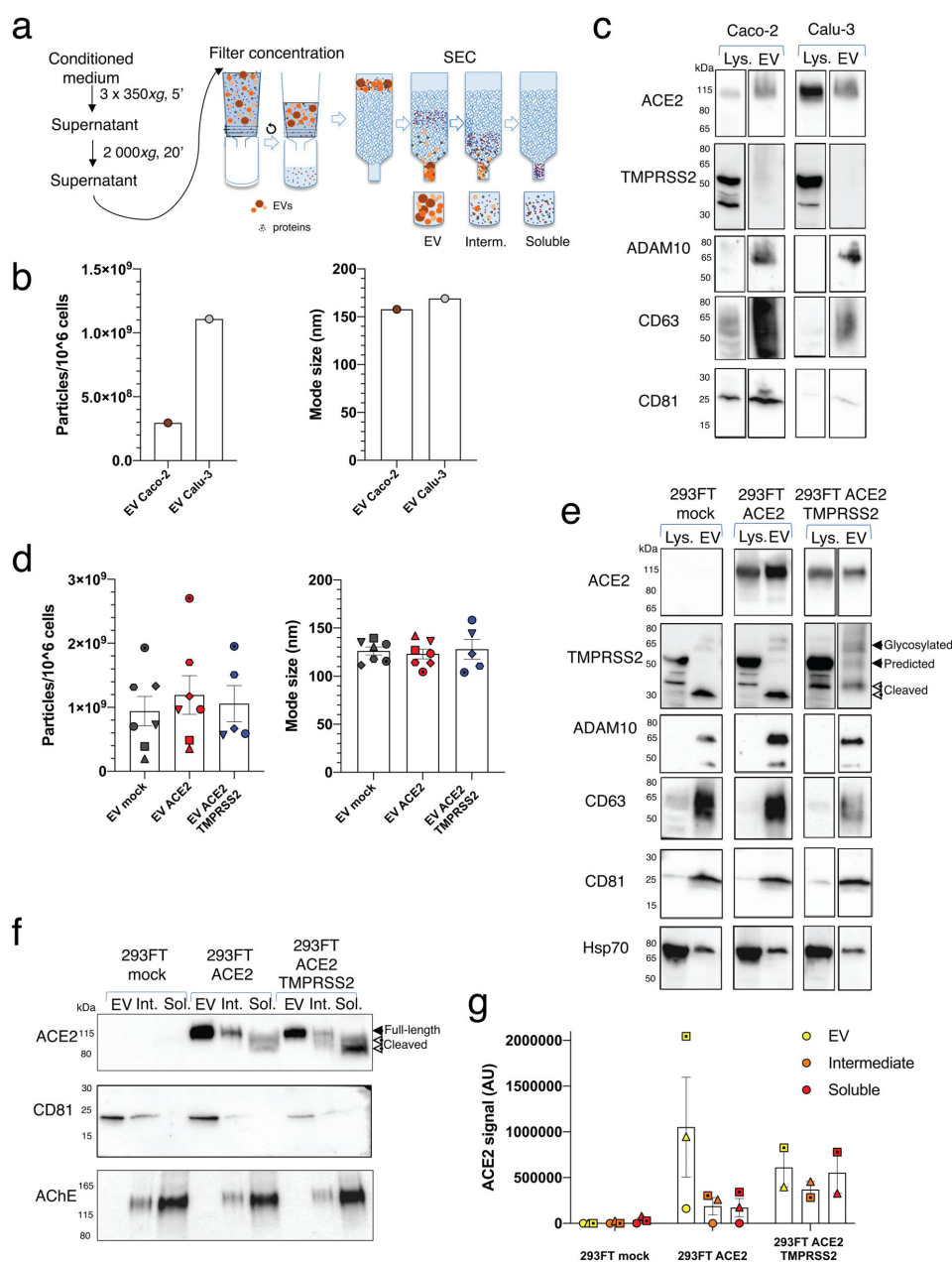


**FIGURE 1** Isolation and characterization of EVs containing ACE2 and TMPRSS2. (a) Scheme of EV isolation and separation from soluble components by SEC. (b) NTA quantification and mode size of the particles in EV-containing SEC fractions obtained from Caco-2 and Calu-3 cells. (c) WB analysis of ACE2, TMPRSS2 and different EV markers in lysates from  $4 \times 10^5$  cells and  $1 \times 10^{10}$  2020 (Caco-2) or  $0.5 \times 10^{10}$  2020 (Calu-3) particles obtained from EV SEC fractions. One experiment. (d) NTA quantification and mode size of the particles in EV-containing fractions obtained from 293FT-mock, 293FT-ACE2 and 293FT-ACE2-TMPRSS2 cell lines. Different symbols correspond to independent experiments. Error bars indicate SEM. (e) WB analysis of ACE2, TMPRSS2 and different EV markers in lysates from  $4 \times 10^5$  cells and  $1 \times 10^{10}$  2020 particles from EV SEC fractions obtained from the three 293FT cell lines. (f-g) WB analysis of ACE2, CD81 and AChE on EV, intermediate and soluble fractions from the three 293FT cell lines.  $1 \times 10^9$  particles from the EV fraction or material recovered from the same corresponding volume of CCM, for the intermediate or soluble fractions, were loaded on the gel. (f) Representative WB. (g) Quantification of ACE2 signal (pooled full-length and cleaved forms) in 2–3 independent WB

We then analysed the capacity of ACE2- and ACE2-TMPRSS2-containing EVs to reduce the infection of target cells by a lentivirus containing SARS-CoV-2-S protein. The virus used in this study was produced using an HIV packaging vector pseudotyped with SARS-CoV-2 Spike protein and including a GFP-coding sequence, which is expressed in infected cells. A variant of SARS-CoV-2 Spike protein bearing a region of the tail of the HIV gp41, instead of the Spike tail, previously shown to enhance infection of pseudotyped virus (Moore et al., 2004) was used. First, we determined the infectivity of the target cells Caco-2, Calu-3 and 293FT-ACE2 by SARS-CoV-2-S-pseudotyped lentivirus and observed that each of these cell lines is infected similarly in a concentration-dependent manner (Figure 2a). To assess the ability of ACE2-containing EVs to decrease virus infectivity *in vitro*, we infected target cells with SARS-CoV-2-S-pseudotyped virus in the presence or the absence of EVs isolated from 293FT-mock (mock-EVs) or 293FT-ACE2 (ACE2-EVs) or 293FT-ACE2-TMPRSS2 cells (ACE2-TMPRSS2-EVs) (Figure 2b). Infection of 293FT-ACE2 cells in the presence of ACE2-EVs and ACE2-TMPRSS2-EVs was reduced while infection remained unaffected by mock-EVs (Figure 2c and quantification in 2d). Importantly, this inhibition was dependent on the dose of EVs (Figure 2d). Caco-2 infection was also reduced in the presence of ACE2-EVs and ACE2-TMPRSS2-EVs (Figure 2e). We then quantified by enzyme-linked immunosorbent assay (ELISA) the amount of ACE2 released by these cell lines. As previously documented by western blot (Figure 1f and 1g), we observed that 293FT-ACE2 cells released high levels of ACE2 mainly associated with EVs while 293FT-ACE2-TMPRSS2 cells released lower ACE2 levels that were equally distributed between EV and soluble fractions (Figure 2f). Strikingly, ACE2 in the soluble fractions from these latter cells could not inhibit SARS-CoV-2-S-pseudotyped virus infection as compared to a comparable amount of ACE2 associated with EVs (Figure 2g). When re-plotting the results obtained in Figure 2d as a function of the absolute amount of ACE2 measured for these same samples by ELISA (Figure 2f), we observed that EVs from cells overexpressing the full length TMPRSS2 together with ACE2 were more efficient at inhibiting SARS-CoV-2-S-pseudotyped viral infection than those from cells overexpressing ACE2 alone (Figure 2h). Moreover, to achieve similar levels of inhibition of lentiviral infection as those observed with ACE2- or ACE2-TMPRSS2-EVs, 500 to 1500 times more of the soluble recombinant human ACE2 had to be used (Figure 2h) in accordance with previous publications (Monteil et al., 2020). Altogether, these findings highlight the increased efficiency of EVs containing full-length ACE2 to inhibit SARS-CoV-2-S-pseudotyped viral entry when compared to the soluble protein alone. The enhanced efficiency of EVs from cells overexpressing TMPRSS2 could be due to the presence of TMPRSS2 together with ACE2, leading to fusion of the virus with the EV thus impairing their capacity to infect cells, and/or to other modifications of the EV composition induced by overexpression of TMPRSS2 in the EV-secreting cells.

### 3 | DISCUSSION

Our data demonstrate that EVs containing ACE2, alone or in combination with TMPRSS2, block SARS-CoV-2 Spike-dependent infection in a much more efficient manner than soluble ACE2. Thus, ACE2-EVs represent a potential versatile therapeutic tool to block not only SARS-CoV-2 infection but also other coronavirus infections that use the ACE2 receptor for host cell entry, such as SARS-CoV (Li et al., 2003) and NL63 (H et al., 2005). Further studies to determine the efficacy of the ACE2/TMPRSS2-EVs in experimental models of SARS-CoV-2 virus need to be conducted to validate their therapeutic use for COVID-19, but also the lack of side-effects. The use of engineered EVs as therapeutic agents has been proposed several years ago and is currently being explored in humans (Wiklander et al., 2019), suggesting that well-designed EV therapeutics against COVID-19 may be feasible to prevent initial infection or further internal dissemination of the virus, and thus reducing the virus burden and disease severity. However, as recently highlighted by the International Societies for EV (ISEV) and for Cellular Therapies (ISCT) (Börger et al., 2020), despite the urgency induced by the current pandemic, EV-based therapeutic developments for COVID-19 will have to meet as strong criteria of manufacturing processes, quality controls and compliance to safety regulation as any other therapies, before they can be implemented in human subjects.

Note: a speculative article discussing the idea that we demonstrate experimentally here was published while we were preparing this article, thus showing concomitant emergence of similar scientific ideas (Inal, 2020).

### 4 | METHODS

#### 4.1 | Cells

Human Caco-2 (HTB-37) and Calu-3 (HTB-55) were purchased from ATCC and maintained at 37°C in a humidified atmosphere with 5% CO<sub>2</sub>. Caco-2 and Calu-3 cells were cultured in DMEM (Thermo Fisher Scientific) supplemented with 10% FBS (Gibco), 100 U/ml penicillin-streptomycin (Thermo Fisher Scientific) and 1% non-essential amino acids (Thermo Fisher Scientific). For Calu-3 cells the medium was also supplemented with 1 mM sodium pyruvate (Thermo Fisher Scientific) and 10 mM HEPES (Thermo Fisher Scientific). 293FT cells were cultured in DMEM medium (Thermo Fisher Scientific) supplemented with 10% FBS (Eurobio) and 100 U/ml penicillin-streptomycin (Thermo Fisher Scientific). 293FT-mock, 293FT-ACE2 and 293FT-ACE2-TMPRSS2 cells were generated by stable double transduction with pTRIP-SFFV-tagBFP-2A and

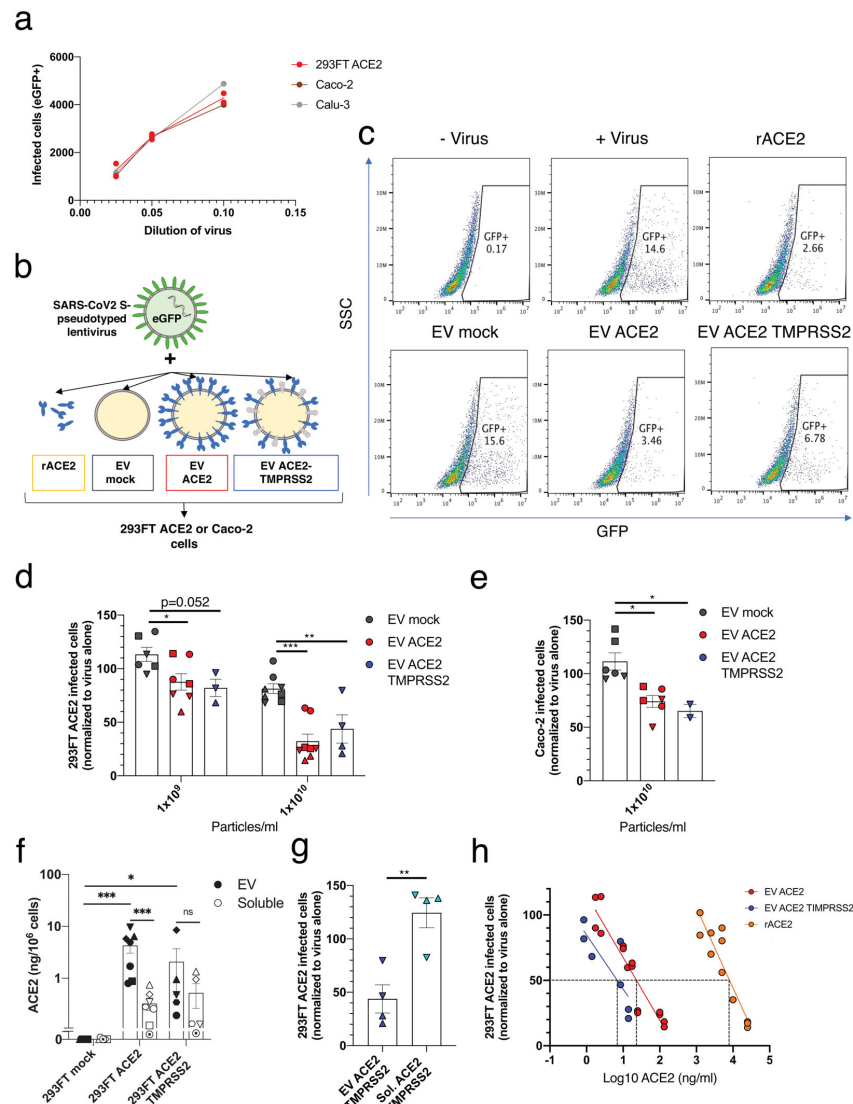


**FIGURE 2** Inhibition of SARS-CoV-2-S-pseudotyped virus infection with ACE2 EVs. (a) Infection of 293FT-ACE2, Caco-2 and Calu-3 cells with different dilutions of a SARS-CoV-2-S-pseudotyped lentivirus encoding for eGFP. The number of infected cells was calculated by multiplying the percentage of GFP-positive cells by the initial number of cells. (b) Scheme of the infectivity assay with different treatments. (c) Dot plots showing the percentage of infected (= eGFP+) 293FT-ACE2 cells obtained after incubation with viruses alone (0.05 dilution), in combination with  $1 \times 10^{10}$  2020 EVs from the different 293FT cell lines or in combination with rACE2 (25  $\mu$ g/ml). This rACE2 level represents 250 and 2960 times more ACE2 than the one contained in ACE2-EVs and ACE2-TMPRSS2-EVs, respectively, measured by ELISA. (d) Quantification of the number of infected 293FT-ACE2 cells in the presence of EVs. The percentage of eGFP+ cells was measured by FACS and normalized to infection with the virus alone (100%). Results from three independent experiments are shown. All replicates from each experiment are included. \* $P < 0.05$ ; \*\* $P < 0.01$ ; \*\*\* $P < 0.001$  (Dunnett's test). (e) Caco-2 infection in the presence of ACE2-EVs and ACE2-TMPRSS2-EVs. \* $P < 0.05$  (Dunnett's test). (f) ACE2 quantification by ELISA in EV and soluble fractions obtained from the three different 293FT cell lines. Results are expressed as ng per million of secreting cells. \* $P < 0.05$ ; \*\*\* $P < 0.001$  (non-parametric ANOVA with Kruskal-Wallis test for comparison among all groups). \*\*\* $P < 0.001$  (Mann-Whitney test for comparison among EV vs soluble for each cell line). (g) Comparison of the effect on 293T-ACE2 infection of  $1 \times 10^{10}$  EVs and soluble fractions from an equivalent volume of CCM of 293FT-ACE2-TMPRSS2 cells. \*\* $P < 0.01$  (t-test) (h) Percentage of infectivity from Figure 2d related to the amount of EV-associated ACE2, quantified by ELISA in Figure 2f. As a comparison, cell infection rates in the presence of increasing amount of recombinant ACE2 (rACE2) were also determined ( $n = 4$ ). Lines represent results of linear regression analysis. Comparison of slopes and intercepts using Prism indicated that the three regression lines are distinct but parallels. ACE2-TMPRSS2 is different from ACE2 ( $P = 0.0017$ ) and rACE2 is different from ACE2-TMPRSS2 ( $P < 0.0001$ ) and from ACE2 ( $P < 0.0001$ )



pTRIP-SFFV-TagRFP657-2A, pTRIP-SFFV-tagBFP-2A-hACE2 and pTRIP-SFFV-TagRFP657-2A, or pTRIP-SFFV-tagBFP-2A-hACE2 and pTRIP-SFFV-TagRFP657-2A-TMPRSS2, respectively.

## 4.2 | Plasmids

The plasmids psPAX2, CMV-VSVG, pTRIP-SFFV-tagBFP-2A (Cerboni et al., 2017) and pTRIP-SFFV-eGFP-NLS (Raab et al., 2016) were previously described. pTRIP-SFFV-TagRFP657-2A was generated by PCR from a synthetic gene coding for TagRFP657. pTRIP-SFFV-tagBFP-2A-hACE2 and pTRIP-SFFV-TagRFP657-2A-TMPRSS2 constructs were obtained by PCR from pLenti6-hACE2-BSD (hACE2 sequence from Addgene #1786 subcloned into pLenti6-BSD) and pCSDest-TMPRSS2 (Addgene #53887) respectively. A codon optimized version of the SARS-CoV-2 S gene (GenBank: QHD43416.1) was transferred into the pCMV backbone (GenBank: AJ318514), by replacing the VSV-G gene (pCMV-SARS-CoV-2-Spike) (Grzelak et al., 2020). pCMV-SARS-CoV-2-S-H2 was obtained by PCR from pCMV-SARS-CoV-2-Spike in order to include the membrane-proximal region of the cytoplasmic domain of HIV-1 gp160 (NRVRQGYs, amino acid sequence) (Mammano et al., 1995) after residue 1246 of the S protein (Moore et al., 2004).

## 4.3 | Preparation of EV-depleted medium

EV-depleted medium was obtained by overnight ultracentrifugation of DMEM supplemented with 20% FBS at 100,000  $\times g$  in a Type 45 Ti rotor (Beckman Coulter, K-factor 1042.2). After ultracentrifugation, EV-depleted supernatant was carefully pipetted from the top and leaving 7 ml in the bottom. Supernatant was filtered through a 0.22  $\mu m$  bottle filter (Millipore) and additional DMEM and antibiotics were added to prepare complete medium (10% EV-depleted FBS medium).

## 4.4 | EV isolation by size-exclusion chromatography

239FT-mock, 293FT-ACE2 and 293FT-ACE2-TMPRSS2 cells were cultured in FBS EV-depleted medium for 24 h. Caco-2 and Calu-3 cells were cultured in FBS-free DMEM for 24 h. Cell conditioned medium (CCM) was harvested by pelleting cells at 350 $\times g$  for 5 min at 4°C three times. Supernatant was centrifuged at 2,000 $\times g$  for 20 min at 4°C to discard 2K pellet and concentrated on a Millipore Filter (MWCO = 10 kDa, UCF701008) to obtain concentrated CCM. Medium was concentrated to 1 ml from 12 to 41 ml for Caco-2 and Calu-3 and from 75 ml for 293FT cells and overlaid on a 70 nm qEV size-exclusion column (Izon, SP1). 0.5 ml fractions were collected and EVs were recovered in fractions 7 to 11 following manufacturer's instructions. We additionally collected intermediate fractions 12 to 16 and soluble factors in fractions 17 to 21. The three pools of fractions were concentrated using 10 kDa filter (Amicon, UCF801024) to reach a final volume of approximately 100  $\mu l$ . Samples were stored aliquoted at -80°C.

We have submitted all relevant data of our experiments to the EV-TRACK knowledgebase (EV-TRACK ID: EV200117) (Van Deun et al., 2017).

## 4.5 | Nanoparticle tracking analysis

NTA was performed to analyse EV fractions, intermediate fractions and soluble fractions using ZetaView PMX-120 (Particle Metrix) with software version 8.04.02. The instrument was set a sensitivity 77 and shutter of 70. Measurements were done at 11 different positions (three cycles per position) and frame rate of 30 frames per second.

## 4.6 | Western blotting (WB)

Cell lysate was prepared using lysis buffer (50 mM Tris, 150 mM NaCl, 1% Triton, pH 8) supplemented with Protease Inhibitor Cocktail (Sigma) at a concentration of  $4 \times 10^6$  cells in 100  $\mu l$  of buffer. After incubation for 20 min on ice, samples were centrifuged at  $18,500 \times g$  for 20 min. The pellet was discarded and the supernatant was kept for further analysis. Cell lysates, EVs and the other SEC fractions were resuspended in Laemmli Sample Buffer (Bio-Rad). Cells lysates corresponding to  $4 \times 10^5$  cells, the number of particles indicated in figures legends for EV fractions and the intermediate and soluble fractions obtained from the same volume of conditioned medium were loaded on 4%–15% Mini-Protean TGX Stain-Free gels (Bio-Rad), under non-reducing conditions. Transferred membranes (Immuno-Blot PVDF Bio-Rad) were incubated with antibodies and developed using Clarity Western ECL substrate (Bio-Rad) and the ChemiDoc Touch imager (Bio-Rad). Antibodies for WB were anti-human: ACE2 (clone EPR4435 against extracellular domain, Abcam 108252), TMPRSS2 (clone EPR3681 against cytoplasmic domain, Abcam 92323), ADAM10 (clone 163003, R&D Systems MAB1427), CD63 (clone H5C6, BD Bioscience 556019), Syntenin-1 (clone C2C3,



Genetex GTX10847), CD81 (clone 5A6, Santa Cruz sc-23692), HSP70 (clone C92F3A-5, Enzo LifeScience, ADI-SPA-810-D) and AChE (Abcam, ab31276). Secondary antibodies included HRP-conjugated goat anti-rabbit IgG (H+L) (Jackson 111-035-144), goat anti-mouse IgG (H+L) (Jackson 111-035-146) and donkey anti-goat IgG (Jackson, 705-035-147).

#### 4.7 | Viral production

SARS-CoV-2-S-pseudotyped lentiviruses were produced by transient transfection of 293FT cells in 150 cm<sup>2</sup> flask with 5 µg phCMV-SARS-CoV-2-S-H2, 13 µg psPAX2 and 20 µg pTRIP-SFFV-eGFP-NLS and 114 µl of TransIT-293 (Mirus Bio). SARS-CoV-2-S-pseudotyped viruses' supernatant was centrifuged at 300xg for 5 min to remove dead cells, filtered with a 0.45 µm filter (Millipore) and loaded on top of a 20% sucrose gradient for concentration. Viral concentration was achieved by ultracentrifugation at 120,000 x g for 1 h 30 min at 4 °C in a SW32i rotor. The pellet containing concentrated SARS-CoV-2 S-pseudotyped virus from three 150 cm<sup>2</sup> flasks was resuspended in 1 ml EV-depleted DMEM and 100 µl aliquots were stored at -80 °C.

#### 4.8 | Infectivity assay

20,000 Caco-2 or Calu-3 cells or 10,000 293FT-ACE2 cells were seeded in a 96 well plate 6 h before infection with SARS-CoV-2 S-pseudotyped virus. Infection was performed in the absence or in the presence of different amount of EVs or human recombinant ACE2 (Abcam, 151852) by spinoculation at 1200 x g for 1 h 30 min at 25 °C. 48 h after infection, cells were washed, trypsinized and fixed. Infection was measured by analysing eGFP expression using a CytoFLEX LX cytometer. Data were analysed using FlowJo software.

#### 4.9 | ACE2 enzyme-linked immunosorbent assay

Quantification of the amount of human ACE2 in the different EV preparations and other SEC fractions was done using the human ACE2 ELISA kit (Abcam, ab235649) following manufacturer's instructions.

#### ACKNOWLEDGMENTS

This work was supported by Institut Curie, INSERM, CNRS, grants H2020-MSCA-ITN (722148, TRAIN-EV), INCa (11548) and Fondation ARC (PGA1 RF20180206962) to C Théry, LABEX DCBIOL (ANR-10-IDEX-0001-02 PSL\* and ANR-11-LABX-0043) to C. Théry and N. Manel, LABEX VRI (ANR-10-LABX-77), ANRS (France Recherche Nord & Sud Sida-HIV Hépatites; ECTZ36691, ECTZ71745), Sidaction (17-1-AAE-11097-2), ANR (ANR-19-CE15-0018-01, ANR-18-CE92-0022-01), DIMIHEALTH to N Manel. N Manel thanks Mutuelle Bleue for support. We thank Eugene Diatloff for critically reading the manuscript.

#### AUTHOR CONTRIBUTIONS

Federico Coccozza, Ester Piovesana, Nathalie Névo, Xavier Lahaye performed the experiments. Federico Coccozza, Ester Piovesana, Mercedes Tkach, Lorena Martin-Jaular, Clotilde Théry analysed the data. Lorena Martin-Jaular, Clotilde Théry, Mercedes Tkach designed the experiments. Ester Piovesana, Federico Coccozza, Mercedes Tkach, Clotilde Théry, Lorena Martin-Jaular wrote the paper. Xavier Lahaye, Nicolas Manel, Julian Buchrieser, Olivier Schwartz designed plasmids. Xavier Lahaye, Nicolas Manel generated cells overexpressing ACE2 and TMPRSS2 and developed the infection assay.

#### ORCID

Federico Coccozza  <https://orcid.org/0000-0003-4311-3083>

Nathalie Névo  <https://orcid.org/0000-0001-6350-7122>

Ester Piovesana  <https://orcid.org/0000-0002-4983-7819>

Xavier Lahaye  <https://orcid.org/0000-0001-7124-1707>

Julian Buchrieser  <https://orcid.org/0000-0003-4790-7577>

Olivier Schwartz  <https://orcid.org/0000-0002-0729-1475>

Nicolas Manel  <https://orcid.org/0000-0002-1481-4430>

Mercedes Tkach  <https://orcid.org/0000-0002-8011-9444>

Clotilde Théry  <https://orcid.org/0000-0001-8294-6884>

Lorena Martin-Jaular  <https://orcid.org/0000-0002-1511-8576>

#### REFERENCES

- Afar, D. E. H., Vivanco, I., Hubert, R. S., Kuo, J., Chen, E., Saffran, D. C., Raitano, A. B., & Jakobovits, A. et al. (2001). Catalytic Cleavage of the Androgen-regulated TMPRSS2 Protease Results in Its Secretion by Prostate and Prostate Cancer Epithelia. *Cancer Research*, 59, 6015–6022.
- Börger, V., Weiss, D. J., Anderson, J. D., Borrás, F. E., Bussolati, B., Carter, D. R. F., Dominici, M., Falcón-Pérez, J. M., Gimona, M., Hill, A. F., Hoffman, A. M., de Kleijn, D., Levine, B. L., Lim, R., Lötvall, J., Mitsialis, S. A., Monguió-Tortajada, M., Muraca, M., Nieuwland, R. ... Giebel, B. (2020). International Society

- for Extracellular Vesicles and International Society for Cell and Gene Therapy statement on extracellular vesicles from mesenchymal stromal cells and other cells: Considerations for potential therapeutic agents to suppress coronavirus disease-19. *Cytotherapy*, 22, 482–485
- Cerboni, S., Jeremiah, N., Gentili, M., Gehrmann, U., Conrad, C., Stolzenberg, M. C., Picard, C., Neven, B., Fischer, A., Amigorena, S., Rieux-Laucat, F., & Manel, N. (2017). Intrinsic antiproliferative activity of the innate sensor STING in T lymphocytes. *Journal of Experimental Medicine*, 214, 1769–1785
- De Carvalho, J. V., De Castro, R. O., Da Silva, E. Z. M., Silveira, P. P., Da Silva-Januario, M. E., Arruda, E., Jamur, M. C., Oliver, C., Aguiar, R. S., & Dasilva, L. L. P. (2014). Nef Neutralizes the Ability of Exosomes from CD4+ T Cells to Act as Decoys during HIV-1 Infection. *Plos One*, 9, e113691
- Grzelak, L., Temmam, S., Planchais, C., Demeret, C., Huon, C., Guivel-Benhassine, F., Staropoli, I., Chazal, M., Dufloo, J., Planas, D., Buchrieser, J., Michael Rajah, M., Robinot, R., Porrot, F., Albert, M., Chen, K.-Y., Crescenzo, B., Donati, F., Anna, F., ... van der Werf, S. (2020). SARS-CoV-2 serological analysis of COVID-19 hospitalized patients, pauci-symptomatic individuals and blood donors. medRxiv 2020.04.21.20068858. <https://doi.org/10.1101/2020.04.21.20068858>
- Heurich, A., Hofmann-Winkler, H., Gierer, S., Liepold, T., Jahn, O., & Pöhlmann, S. (2014). TMPRSS2 and ADAM17 cleave ACE2 differentially and only proteolysis by TMPRSS2 augments entry driven by the severe acute respiratory syndrome coronavirus spike protein. *Journal of Virology*, 88, 1293–1307
- Hofmann, H., Pyrc, K., van der Hoek, L., Geier, M., Berkhout, B., Pöhlmann, S. (2005). Human coronavirus NL63 employs the severe acute respiratory syndrome coronavirus receptor for cellular entry. *Proceedings of the National Academy of Sciences of the United States of America*, 102, 7988–7993
- Hoffmann, M., Kleine-Weber, H., Schroeder, S., Krüger, N., Herler, T., Erichsen, S., Schiergens, T. S., Herrler, G., Wu, N.-H., Nitsche, A., Müller, M. A., Drosten, C., & Pöhlmann, S. (2020). SARS-CoV-2 cell entry depends on ACE2 and TMPRSS2 and is blocked by a clinically proven protease inhibitor. *Cell*, 181, 271–280.e8
- Inal, J. M. (2020). Decoy ACE2-expressing extracellular vesicles that competitively bind SARS-CoV-2 as a possible COVID-19 therapy. *Clinical Science*, 134, 1301–1304
- Jia, H. P., Look, D. C., Tan, P., Shi, L., Hickey, M., Gakhar, L., Chappell, M. C., Wohlford-Lenane, C., & Mccray, P. B. (2009). Ectodomain shedding of angiotensin converting enzyme 2 in human airway epithelia. *American Journal of Physiology. Lung Cellular and Molecular Physiology*, 297, L84–L96
- Keller, M. D., Ching, K. L., Liang, F. X., Dhabaria, A., Tam, K., Ueberheide, B. M., Unutmaz, D., Torres, V. J., & Cadwell, K. (2020). Decoy exosomes provide protection against bacterial toxins. *Nature*, 579, 260–264
- Li, W., Moore, M. J., Vasilieva, N., Sui, J., Wong, S. K., Berne, M. A., Somasundaran, M., Sullivan, J. L., Luzuriaga, K., Greenough, T. C., Choe, H., & Farzan, M. (2003). Angiotensin-converting enzyme 2 is a functional receptor for the SARS coronavirus. *Nature*, 426, 450–454
- Liao, Z., Jaular, L. M., Soueidi, E., Jouve, M., Muth, D. C., Schøyen, T. H., Seale, T., Haughey, N. J., Ostrowski, M., Théry, C., & Witwer, K. W. (2019). Acetylcholinesterase is not a generic marker of extracellular vesicles. *Journal of Extracellular Vesicles*, 8, 1628592
- Mammano, F., Kondo, E., Sodroski, J., Bukovsky, A., & Göttlinger, H. G. (1995). Rescue of human immunodeficiency virus type 1 matrix protein mutants by envelope glycoproteins with short cytoplasmic domains. *Journal of Virology*, 69, 3824–3830
- Mathieu, M., Martin-Jaular, L., Lavieu, G., & Théry, C. (2019). Specificities of secretion and uptake of exosomes and other extracellular vesicles for cell-to-cell communication. *Nature Cell Biology*, 21, 9–17
- Monteil, V., Kwon, H., Prado, P., Hagelkrüys, A., Wimmer, R. A., Stahl, M., Leopoldi, A., Garreta, E., Hurtado Del Pozo, C., Prosper, F., Romero, J. P., Wirnsberger, G., Zhang, H., Slutsky, A. S., Conder, R., Montserrat, N., Mirazimi, A., & Penninger, J. M. (2020). Inhibition of SARS-CoV-2 infections in engineered human tissues using clinical-grade soluble human ACE2. *Cell*, 181, 905–913.e7
- Moore, M. J., Dorfman, T., Li, W., Wong, S. K., Li, Y., Kuhn, J. H., Coderre, J., Vasilieva, N., Han, Z., Greenough, T. C., Farzan, M., & Choe, H. (2004). Retroviruses pseudotyped with the severe acute respiratory syndrome coronavirus spike protein efficiently infect cells expressing angiotensin-converting enzyme 2. *Journal of Virology*, 78, 10628–10635
- Raab, M., Gentili, M., De Belly, H., Thiam, H.-R., Vargas, P., Jimenez, A. J., Lautenschlaeger, F., Voituriez, R., Lennon-Dumenil, A.-M., Manel, N., & Piel, M. (2016). ESCRT III repairs nuclear envelope ruptures during cell migration to limit DNA damage and cell death. *Science*, 352, 359–362
- Van Deun, J., Mestdagh, P., Agostinis, P., Akay, Ö., Anand, S., Anckaert, J., Martinez, Z. A., Baetens, T., Beghein, E., Bertier, L., Berx, G., Boere, J., Boukouris, S., Bremer, M., Buschmann, D., Byrd, J. B., Casert, C., Cheng, L., Cmocho, A., ... Hendrix, A. (2017). EV-TRACK: Transparent reporting and centralizing knowledge in extracellular vesicle research. *Nature Methods*, 14, 228–232
- Walls, A. C., Park, Y.-J., Tortorici, M. A., Wall, A., McGuire, A. T., & Veesler, D. (2020). Structure, function, and antigenicity of the SARS-CoV-2 spike glycoprotein. *Cell*, 181, 281–292.e6
- Wiklander, O. P. B., Brennan, M. Á., Lötvall, J., Breakefield, X. O., & El Andaloussi, S. (2019). Advances in therapeutic applications of extracellular vesicles. *Science Translational Medicine*, 11, eaav8521
- Zhou, P., Yang, X.-L., Wang, X.-G., Hu, B., Zhang, L., Zhang, W., Si, H.-R., Zhu, Y., Li, B., Huang, C.-L., Chen, H.-D., Chen, J., Luo, Y., Guo, H., Jiang, R.-D., Liu, M.-Q., Chen, Y., Shen, X.-R., Wang, X., ... Shi, Z.-L. (2020). A pneumonia outbreak associated with a new coronavirus of probable bat origin. *Nature*, 579, 270–273
- Ziegler, C. G. K., Allon, S. J., Nyquist, S. K., Mbanjo, I. M., Miao, V. N., Tzouanas, C. N., Cao, Y., Yousif, A. S., Bals, J., Hauser, B. M., Feldman, J., Muus, C., Wadsworth, M. H., Kazer, S. W., Hughes, T. K., Doran, B., Gatter, G. J., Vukovic, M., Taliaferro, F., ... Zhang, K. (2020). SARS-CoV-2 receptor ACE2 Is an interferon-stimulated gene in human airway epithelial cells and is detected in specific cell subsets across tissues. *Cell*, 181, 1016–1035.e19
- Zmora, P., Moldenhauer, A. S., Hofmann-Winkler, H., & Pöhlmann, S. (2015). TMPRSS2 Isoform 1 Activates Respiratory Viruses and Is Expressed in Viral Target Cells. *Plos One*, 10, e0138380

## SUPPORTING INFORMATION

Additional supporting information may be found online in the Supporting Information section at the end of the article.

**How to cite this article:** Cocozza F, Névo N, Piovesana E, et al. Extracellular vesicles containing ACE2 efficiently prevent infection by SARS-CoV-2 Spike protein-containing virus. *J Extracell Vesicles*. 2020;10:e12050. <https://doi.org/10.1002/jev2.12050>



# OPEN Efficient cell death mediated by bioengineered killer extracellular vesicles

Julia Dancourt<sup>1✉</sup>, Ester Piovesana<sup>2</sup> & Gregory Lavieu<sup>1✉</sup>

Extracellular vesicles (EVs) are biological vehicles that are thought to mediate cell–cell communication via the transfer of biomolecules from donor to acceptor cells. Repurposing those natural vesicles into therapeutics delivery vectors is a high priority challenge for translational science. Here we engineer donor cells to produce copious amount of fusogenic EVs loaded with the catalytic domain of the Diphtheria Toxin, known to trigger cell death through protein synthesis inhibition. We show that, when incubated with cancer acceptor cells, these Killer EVs block protein synthesis and lead to cell death. This proof of concept establishes the efficacy of Killer EVs *in vitro*, and suggests that further development may lead to tumor ablation *in vivo*, expanding the existing cancer therapeutics arsenal.

Extracellular Vesicles, hereafter named EVs, are virtually secreted by all kind of cells/tissues and circulate in bodily fluids<sup>1</sup>. EVs have been associated with a broad spectrum of physiological functions<sup>2</sup>. They contain cargoes such as nucleotides and proteins, which are protected by a lipid bilayer from the extracellular environment, and have been proposed to mediate cargo transfer from acceptor to donor cells. Although the systematic occurrence of EV cargo delivery is still debated, several studies, including ours<sup>3–5</sup>, formally demonstrated that EV cargo release within the cytosol of acceptor cells does occur. Quantification of the process however suggests that EV delivery is a relatively low yield process<sup>4</sup>. Nevertheless, the uptake/delivery capacity of EVs appears to be superior to that of liposomes, commonly used in therapies<sup>6</sup>.

This reinforces the long-standing interest in utilizing and capitalizing on EV properties to develop novel vectors dedicated to therapeutics delivery. This line of research has been extensively investigated, especially towards the delivery of nucleotides<sup>7</sup>. Delivery of protein-based therapeutics through EVs has however been neglected, although several lethal toxins have been the objects of intensive translational research, especially in the context of cell/tissue ablation. This is particularly relevant to the field of cancer, in which those toxins have long been contenders to promote tumor ablation<sup>8,9</sup>.

Diphtheria toxin is one of the most potent toxins known and its biology is well characterized<sup>10</sup>. It belongs to the A-B toxin family, for which the B-domain enables cell surface binding, internalization followed by membrane penetration and cytosolic liberation of the catalytic A-domain (DTA), responsible, in the case of DTA, for protein synthesis blockade through inhibition of the elongation factor eIF2. The inhibitory action of DTA on eIF2 occurs through the specific ADP-ribosylation of a diphtamide-modified histidine residue on eIF2<sup>11</sup>. Enzymes DPH1-5 are required for the biosynthesis of diphtamide and depletion of any of these proteins abolishes DTA-sensitivity<sup>12,13</sup>.

Importantly, DTA on its own is not capable of penetrating the cell even at a high concentration in the extracellular media<sup>14</sup>. However, expression of DTA alone in the cytoplasm is sufficient to ultimately kill cells through protein translation blockage. This makes DTA a suitable candidate for EV-mediated delivery.

In the past, liposome-mediated DTA delivery has been tested but led to poor efficiency<sup>15</sup>. More recently, DTA-expressing lentiviruses emanating from DPH-depleted cells have been shown to trigger the death of infected wildtype cells<sup>16</sup>, but lentiviruses come with high safety constraints when considered for therapeutic applications.

Here we tested the capacity of EVs to deliver lethal DTA to acceptor cells, in a virus-free context. First, we engineered DPH2KD donor cells that are DTA-resistant and can thus express detectable amounts of the toxin. Secondly, we added of a palmitoylation motif to DTA, which enabled its reversible membrane anchoring and its efficient loading into EVs, while maintaining its capacity to abolish protein synthesis. Treatment of acceptor cells with DTA-containing EVs show modest but measurable protein synthesis inhibition, that is dose-dependent.

<sup>1</sup>Université Paris Cité, INSERM U1316, UMR 7057/CNRS, Paris, France. <sup>2</sup>Present address: Laboratory for Aging Disorders, Laboratories for Translational Research, EOC Bellinzona (Bios+), Bellinzona, Switzerland. ✉email: julia.dancourt@ext.inserm.fr; gregory.lavieu@inserm.fr

**Figure 1.** DTA-resistant donor cells. (A) Parent HeLa cells were infected with a lentivirus encoding a shRNA targeting the DPH2 gene to generate DPH2KD cells. DPH2 knockdown was confirmed by qRT-PCR. \*\*\*\*:  $p < 0.0001$ . (B) Parent or DPH2KD cells were co-transfected with NLuc-Hsp70 along with a mock plasmid or a plasmid encoding DTA-HA. 30 h post-transfection, the percentage of protein synthesis in cells co-transfected with a DTA-HA plasmid was calculated as the percentage of NanoLuciferase activity in these cells relative to mock-transfected cells. \*\*\*\*:  $p < 0.0001$ . (C) A plasmid encoding DTA-HA and/or a plasmid encoding mCherry were transfected into parent or DPH2KD cells. 36 h post-transfection, equal protein amounts of each sample were analyzed by western blot. (D) EVs were prepared from parent or DPH2KD cells and analyzed by western blot along with total cell lysates (CL). The same amount of protein was loaded for each sample. (E) Particle metrics for EVs in D. (F) EVs from NLuc-Hsp70-expressing parent or DPH2KD cells were incubated on acceptor (parent HeLa) cells for 24 h. EV uptake was calculated as percent of input material. (G) EVs were obtained from DPH2KD cells transfected with a plasmid encoding DTA-HA. Total cell lysates (CL) and EV proteins were analyzed by western blot. The same amount of protein was loaded for each sample.

When equipped with the VSV-G fusogenic protein, DTA-containing EVs show a five-fold increase in protein synthesis inhibition towards the treated acceptor cells, which led to massive cell death.

This proof of concept demonstrates that Killer EVs are potent in vitro to trigger protein translation inhibition followed by cell death and suggest that the next generation of Killer EVs may trigger specific tumor ablation in vivo.

## Results

**Engineering DTA-containing EVs.** Our goal was to generate EV donor cells that would secrete potent DTA-containing EVs. First, in order to express DTA in donor cells, we'd have to render them resistant to the toxin. We thus generated, through RNA interference, stable donor HeLa cells knocked down for DPH2, an enzyme responsible for dipeptidyl synthesis which is absolutely required for DTA sensitivity<sup>12</sup>. DPH2 expression was assessed by qRT-PCR, which showed a 65% ( $\pm 5\%$ ) knockdown efficiency in the selected DPH2KD cells (Fig. 1A).

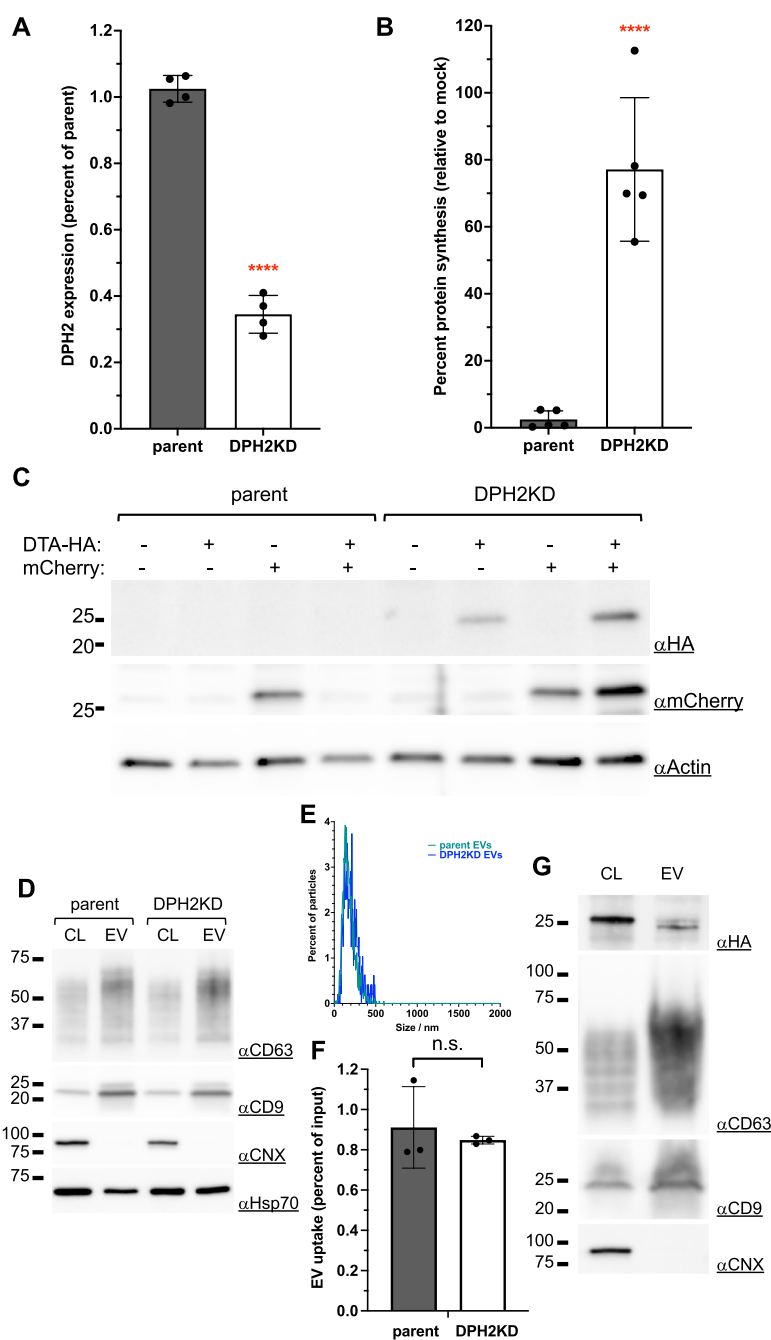
To study whether the DPH2KD cells were indeed DTA-resistant, we assessed their protein synthesis activity using a NanoLuciferase (NLuc)-encoding plasmid as a reporter. Parent and DPH2KD cells were co-transfected with the NLuc-plasmid and with either an empty plasmid (mock) or with a plasmid encoding HA-tagged DTA (DTA-HA). We measured the luminescence activity 30 h post-transfection. Co-transfection with DTA completely abolished NLuc expression within parent cells (less than 3% of control protein synthesis activity), whereas DPH2KD cells retained more than 75% of protein synthesis activity in the same conditions (Fig. 1B). This demonstrated that DTA-HA expression efficiently blocked protein synthesis in parent cells, and that DPH2KD cells were DTA resistant.

We confirmed these data by co-transfecting parent or DPH2KD cells with plasmids encoding mCherry as a reporter and plasmids expressing either mock or DTA-HA. We assessed protein expression by western blot 36 h post-transfection. The mCherry protein was detected in parent cells when co-transfected with a mock plasmid but was absent from cells co-transfected with DTA-HA (Fig. 1C). Note that DTA-HA is not detectable in those cells either, suggesting that DTA-HA is so efficient at turning off protein synthesis that an undetectable amount of the toxin is enough to inhibit its own expression. Only long-lived proteins such as actin remained detectable in these conditions. On the other end, both mCherry and DTA-HA were detectable in DPH2KD cells when co-expressed (Fig. 1C). This independently confirmed our previous results and demonstrated that DTA-HA could be expressed in detectable amounts in DPH2KD cells.

Although DPH2 knockdown has been shown to lead to decreased cellular fitness<sup>16</sup>, we showed here that these cells are able to produce natural EVs that are similar to EVs produced from parent cells, both in terms of composition and size (Fig. 1D, E). Moreover, the EVs produced by DPH2KD cells are as uptake-competent as wildtype EVs (Fig. 1F).

Since DTA-HA could be expressed in DPH2KD cells (Fig. 1C), we hypothesized that it could be passively loaded into EVs. Indeed, it has been shown that abundant endogenous cytosolic protein such as actin or chaperones (such as Hsp70, Fig. 1D), as well as overexpressed cytosolic proteins can be found in EVs<sup>17</sup>. We therefore tested the presence of DTA-HA in EVs emanating from DTA-HA-transfected DPH2KD cells. 36 h post transfection, we isolated EVs through sequential centrifugation, and tested their contents by western blot. Although the EV fraction was enriched in classical EV markers (Hsp70, high molecular weight CD63 and CD9) and depleted of an endoplasmic reticulum marker (Calnexin), suggesting efficient and specific EV isolation, DTA-HA could not or only barely be detected (Fig. 1G). We concluded that DTA-HA was not passively loaded into EVs (even depleted when compared to total cell lysate), and that we needed to increase its loading efficiency.

Myristoylation and palmitoylation consensus signals are often used to force cargo loading into EVs through membrane association<sup>18,19</sup>. While palmitoylation is a reversible process (Fig. 2A), myristoylation is not and seems incompatible with putative downstream EV-mediated delivery of such a modified cargo. We therefore reasoned that fusing a well-characterized palmitoylation motif<sup>20</sup> to DTA-HA might better serve our purposes. We therefore engineered a Palm-DTA-HA encoding plasmid and first tested if this protein was prominently associated with membranes. DPH2KD cells expressing Palm-DTA-HA were first submitted to mechanical disruption, and cytosolic and membrane fractions were separated by ultracentrifugation. Palm-DTA-HA was enriched in the membrane fraction (Fig. 2B), which also contained the endoplasmic reticulum marker calnexin, but was strongly depleted of HSP70, a cytosolic protein. On the contrary, the cytosolic fraction, highly enriched in HSP70, but depleted of calnexin, only contained a very low amount of Palm-DTA-HA, as well as a smaller species, probably



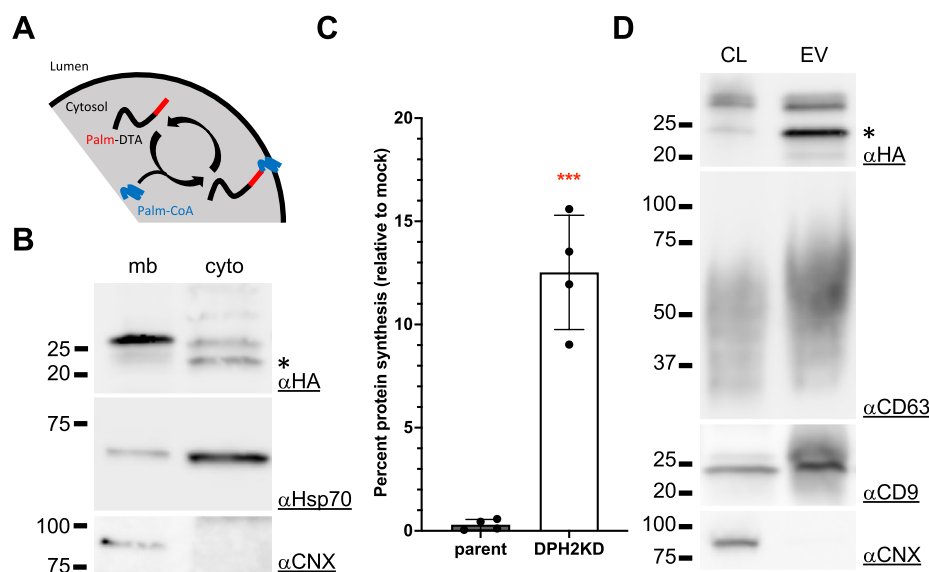


**Figure 2.** Palm-DTA loading into EVs. (A) Scheme of Palm-DTA association with membranes. (B) DPH2KD cells were transfected with a plasmid encoding Palm-DTA-HA and subjected to cytosol / membrane fractionation 36 h after transfection. \*: de-palmitoylated form of the protein. (C) Parent or DPH2KD cells were co-transfected with NanoLuc-Hsp70 along with a mock plasmid or a plasmid encoding Palm-DTA-HA. 30 h post-transfection, the percentage of protein synthesis in cells co-transfected with a Palm-DTA-HA plasmid was calculated as the percentage of NanoLuciferase activity in these cells relative to mock-transfected cells. \*\*\*:  $p < 0.001$ . (D) EVs were prepared from DPH2KD cells transfected with a plasmid encoding Palm-DTA-HA. Total cell lysates (CL) and EV proteins were analyzed by western blot. The same amount of protein was loaded for each sample.

representing de-palmitoylated Palm-DTA-HA (marked with an asterisk in Fig. 2B). Such a palmitoylation-induced size shift have been shown for other proteins<sup>20,21</sup>. In the absence of a palmitoylation signal, DTA-HA is exclusively found in the cytosolic fraction (Fig. S1A). This validated the membrane association of Palm-DTA-HA.

We then tested the efficacy of Palm-DTA-HA towards protein synthesis inhibition to ensure that the motif did not alter the toxin activity. Using the aforementioned luminescent assay, we showed that Palm-DTA-HA completely abolished protein expression within parent cells (less than 0.3% of control activity), whereas DPH2KD cells showed significant resistance as they retained more than 12% of control activity (Fig. 2C). Note that Palm-DTA-HA resistance of DPH2KD cells was lower than the one for soluble DTA-HA. This suggests that Palm-DTA-HA had a higher toxin potency in our system, probably due to higher expression levels in cells (DTA-HA and Palm-DTA-HA are expressed from different plasmid backbones). This could also be due to membrane anchoring that may stabilize the protein. Moreover, this difference in toxin potency between DTA-HA and Palm-DTA-HA has little impact on donor cell viability at the time of conditioned medium harvest for EV preparation (Fig. S1B). EV preparation was indeed performed from cells that are > 80% viable. This observation is obviously not a handicap, is fully compatible with our goals, and might even serve our interests by enhancing the impact on acceptor cells. It however means that, in its current form, this system requires continuous transfection of new cells for EV production.

Next, we tested if Palm-DTA-HA was efficiently loaded into EVs. DPH2KD cells were transfected with Palm-DTA-HA and conditioned medium was harvested 36 h post-transfection. EVs were, once again, isolated through sequential ultracentrifugation. The EV fraction was positive for HSP70, high molecular weight CD63 and CD9 and negative for Calnexin, as expected. Satisfyingly, we found that Palm-DTA-HA was efficiently loaded into EVs (Fig. 2D). Interestingly, we note that the de-palmitoylated form of Palm-DTA-HA is consistently more prominent in EVs than in the cell lysate (although to varying degrees, Figs. 2D and S1C), suggesting that net de-palmitoylation occurs after EV loading.

**Testing the potency of DTA-containing EVs in vitro.** With our new tools in hand, we decided to test the potency of Palm-DTA-HA-containing EVs on acceptor HT1080 cells, a well-established experimental model that is genetically less aberrant than HeLa cells and highly compatible with future hypothetical genetic screening. To assess the protein synthesis activity in these acceptor cells, we stably equipped them with GFP-PEST<sup>22</sup>, a short half-life version of the Green Fluorescent Protein that gives adequate sensitivity and time resolution and enables single-cell studies by flow cytometry. We previously demonstrated that EV content delivery is a low



yield process<sup>4</sup> and anticipated that natural Palm-DTA-HA-containing EVs might be too limited to dramatically impact protein synthesis in acceptor cells. We therefore decided to also generate, in parallel, Palm-DTA-HA-loaded EVs decorated with VSV-G, a viral fusogen, known to dramatically increase EV content delivery through fusion with the endosomal membranes<sup>23</sup>. Although there is a semantic debate whether VSV-G-bearing EVs should still be called EVs (they have been called Virus-Like Particles, gesicles, gectosomes in the literature), we chose to keep this denomination below as they were found to be indistinguishable by size or marker content from regular EVs (Fig. 3A,B).

We isolated EVs from mock-transfected DPH2KD cells, or DPH2KD cells expressing Palm-DTA-HA with or without VSV-G. EVs were isolated again through sequential ultracentrifugation and characterized by western blot (Fig. 3A) and nanoparticle tracking (Fig. 3B). All EVs showed similar profiles in terms of marker protein content and size distribution. Note that VSV-G is so enriched in EVs that it is barely detectable in total cell lysates.

We then showed that our GFP-PEST-expressing HT1080 clonal cell line would allow us to monitor a putative effect of Palm-DTA-HA EVs on protein synthesis. We showed that, in these cells, green fluorescence has a half-life of about 4,5 h (compared to more than 24 h for wildtype GFP<sup>24</sup> (Fig. S1C,D), and that these cells are sensitive to DTA activity. Indeed, 24 h of transfection of DTA-HA drastically reduces green fluorescence intensity, as measured by FACS (Fig. S1E,F).

Next, we investigated the effect of EV treatment on these cells. GFP-PEST expression level of untreated acceptor cells was assessed by FACS and compared with signals from cells treated for 24 h with a single dose of either mock EVs, Palm-DTA-HA-containing EVs, or Palm-DTA-HA-VSVG<sup>+</sup> EVs (hereafter named Killer EVs). Palm-DTA-HA EVs triggered a modest but detectable decrease of GFP-PEST signal (about 15% when considering the mean fluorescence intensity, Fig. 3C,D). Killer EVs, on the other hand, triggered a massive decrease of GFP-PEST signal within acceptor cells (more than 75% when considering the mean fluorescence intensity, Fig. 3C,D). Importantly, we established that Palm-DTA-HA-mediated protein synthesis inhibition is dose dependent for both types of EVs, with again a superior effect of Killer EVs (Fig. 3E). To evaluate cell death induced by Killer EVs over time, we performed a quantitative viability assay on acceptor cells and observed that, after 3 days of incubation with a single dose of EVs, Killer EVs led to important (> 90%), dose-dependent, cell death (Fig. 3F). Moreover, we monitored acceptor cells by fluorescence microscopy in the same conditions and observed that mock EVs-treated cells expanded and maintained their fluorescent signal, while viable acceptor green cells were virtually absent in samples treated with Killer EVs (Fig. 3G). This establishes the lethal potency of Killer EVs on our GFP-PEST-expressing HT1080 clonal cell line. To test whether this effect was transposable to other acceptor cell lines, we performed a cell viability assay on HeLa cells treated with either mock EVs, or Killer EVs for 3 days. Results showed that Killer EVs also had a dose-dependent killing activity on HeLa acceptors (Fig. S1H). This suggests that Killer EVs could be potent on multiple types of acceptor cells.

## Discussion

The aim of this study was to engineer toxin-loaded EVs that would efficiently kill target cells, we named them Killer EVs. We succeeded by (a) engineering EV donor cells that are toxin-resistant and thus can express high amounts of it; (b) engineering an active toxin that is efficiently loaded into EVs; (c) engineering fusogenic EVs to increase their content delivery into acceptor cells.

We chose DTA as a toxin candidate because of its known exceptional potency<sup>14</sup> and its well-characterized mode of action<sup>10</sup>. Although in vitro DTA-resistance of DPH2KD cells has been characterized before; we further investigated these cells here and observed that they were able to produce EVs that showed most hallmarks of the natural EVs produced in parent cells, including similar uptake efficiency (Fig. 1).

In order to efficiently load DTA into EVs, we appended a palmitoylation signal to its N-terminus (Fig. 2). Although we cannot say whether it's the palmitoylated, membrane-bound, form of the protein that is active or the reversibly-formed de-palmitoylated, cytosolic form, we showed that Palm-DTA-HA retains DTA's ability to inhibit protein translation.

The fact that Palm-DTA-HA EVs were able to have an effect, although modest, on acceptor cells suggest that natural EVs deliver their content into the cytoplasm of acceptor cells to a detectable level, which has been debated over recent years. Nevertheless, expressing the VSV-G fusogen on Palm-DTA-HA EVs dramatically increase (fivefold increase) their content delivery into acceptor cells, leading to protein synthesis inhibition and cell death (Fig. 3).

All the EVs produced in this study are expected to be an heterogenous mix including exosomes, ectosomes and exomeres. Although careful characterization of Killer EVs will be needed in the future to better their development, the scope of this proof-of-concept study remains to show their efficiency.

For this study, we chose to work with a heterologous system where the EV donor cells (derived from HeLa) and the EV acceptor cells (derived from HT1080) are of different origin. This was motivated by the will to show the flexibility of the system, but in the future, one can envision using a homologous system, which may or may not be more efficient, but which may be better tolerated in the context of autologous EV therapy for instance. With this in mind, we validated that at least the HeLa donor / HeLa acceptor homologous system is efficient (Fig. S1H).

Our Killer EVs are not artificially targeted, which again has the advantage of flexibility, but also the disadvantage of possible high toxicity as they potentially target all cells indiscriminately. If our Killer EVs were to be used for tumor ablation, one could envision intra-tumoral injection. EVs have indeed been shown to passively target tumor cells through the Enhanced Permeability and Retention (EPR) effect<sup>25</sup>. In the near future, we however plan to equip a new version of Killer EVs with targeting signals and/or other fusogens to increase specificity and tolerability of these new potential therapeutics. VSV-G has indeed been shown to trigger rejection response to lentiviral therapeutics<sup>26</sup>. Humanized fusogens could be envisioned instead.

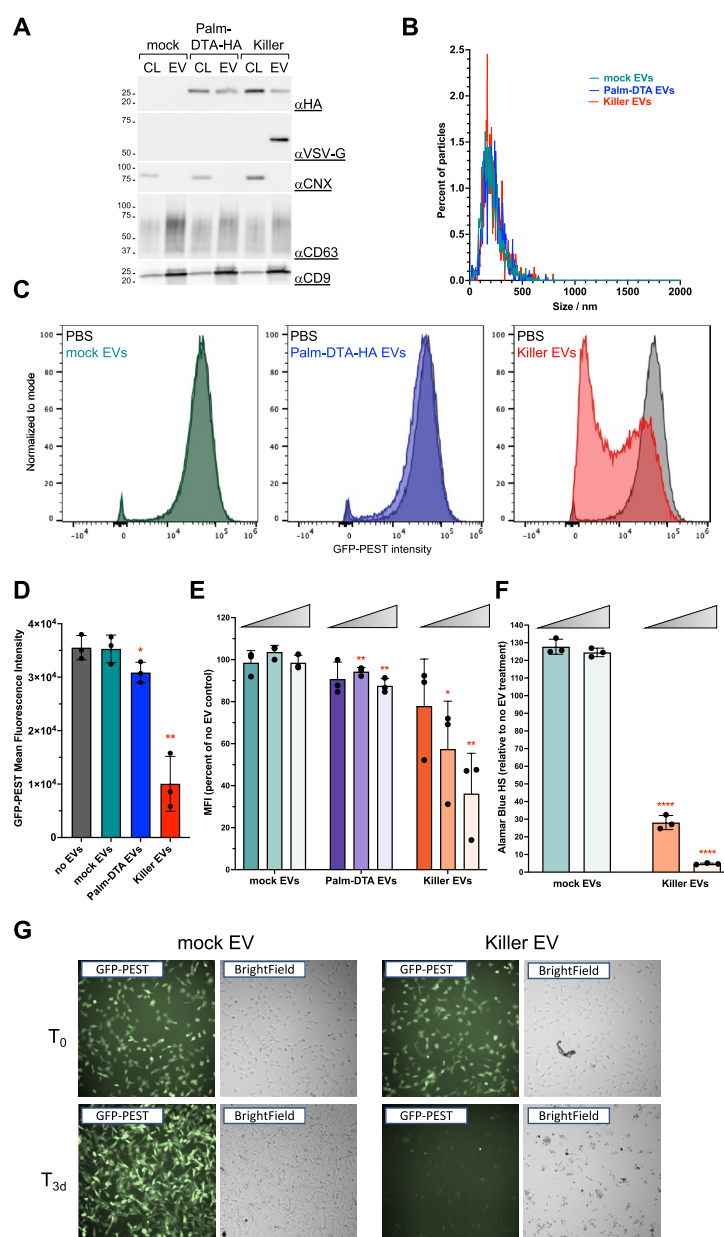


**Figure 3.** Killer EVs are potent in vitro. (A) Western blot characterization of EVs generated from DPH2KD cells transfected with plasmids encoding either Palm-DTA-HA, Palm-DTA-HA + VSV-G (Killer EVs), or a mock plasmid. The same amount of protein was loaded for each sample. (B) Particle metrics obtained for the EVs in A. (C) 100  $\mu$ g/mL of the indicated EVs (or DPBS) were incubated for 24 h on GFP-PEST-expressing HT1080 cells. After incubation, green fluorescence was analyzed by FACS and data for each EV-treated sample was plotted against DPBS-treated cells. (D) Quantification of data obtained as in panel C. Plotted are the geometric mean of green fluorescence intensity (MFI) for each sample, each data point represents an independent experiment (including independent EV preparation). \*:  $p < 0.1$ ; \*\*:  $p < 0.01$ . (E) 10, 20, or 50  $\mu$ g/mL of the indicated EVs (or DPBS) were incubated for 24 h on GFP-PEST-expressing HT1080 cells. After incubation, cells were analyzed by FACS and the geometric mean of green fluorescence intensity for each sample was obtained and plotted as the percentage of the one obtained for DPBS-treated cells (set at 100%). Each data point represents an independent experiment (including independent EV preparation). \*:  $p < 0.1$ ; \*\*:  $p < 0.01$ . (F) A cell viability assay was performed on GFP-PEST-expressing HT1080 cells incubated with the indicated EVs (20 or 50  $\mu$ g/mL) for 3 days. \*\*\*\*:  $p < 0.0001$ . (G) Microscopic observation of GFP-PEST-expressing HT1080 cells incubated with 100  $\mu$ g/mL Killer EVs indicates a total loss of cells after 3 days.



Finally, EVs seem like an ideal candidate for DTA delivery. DT has indeed long been considered for tumor or tissue ablation<sup>27</sup>, in the form of immunotoxins or through other vehicles (liposomes, viruses), but a few hurdles impeded the success of these endeavors (production, purification, formulation, administration route, immunogenicity). One of the issues related to immunotoxins is the preexisting DT immunity due to existing immunization schemes (> 80% babies in the world have been vaccinated in 2020). EV-mediated delivery of DTA would avoid this issue. Moreover, EV-encapsulated DTA would also be protected from circulating decoy exosomes<sup>28</sup>. EVs also represent a more natural toxin delivery system<sup>29</sup> than liposomes or viruses, thus less prone to rejection.

The results presented here demonstrate the potency of killer EVs and suggest that further development involving specific targeting and humanized fusogens may lead to novel treatments towards tumor or specific cell/tissue ablation.

## Material and methods

**Cell culture.** HeLa and HT1080 cells (ATCC, Virginia, U.S.A.) and their transgenic derivatives were grown in DMEM medium (Gibco, Illinois, U.S.A.) complemented with 10% heat-inactivated Fetal Bovine Serum (Biowest, France) at 37 °C under 5% CO<sub>2</sub> and high humidity. HT1080 cells medium was further complemented with MEM NEAA (Gibco, Illinois, U.S.A.).

Stable DPH2KD HeLa cells were obtained by lentiviral transduction of a shRNA targeting DPH2 (Horizon Discovery, Cat # VGH5518-200,302,258, U.K.) and selected with 4 µg/mL puromycin (Gibco, Illinois, U.S.A.). A stable GFP-PEST HT1080 clone was obtained by selecting cells with 0,5 mg/mL geneticin (Gibco, Illinois, U.S.A.) after transfection with a GFP-PEST encoding plasmid (Addgene, Cat # 26,821, Massachusetts, U.S.A.).

Transient transfections were performed using Lipofectamine 2000 (Invitrogen, Massachusetts, U.S.A.) according to the manufacturer's instructions.

**Plasmid constructs.** Plasmids used in this study are summarized in Table S1.

To construct the plasmid encoding DTA-HA, the sequence for DTA (obtained from Addgene, Cat # 42,521, Massachusetts, U.S.A.) was fused to the HA-tag sequence using the Infusion cloning strategy (Takara Bio Europe, France) with XbaI/SpeI cloning sites into a pC4Rhe backbone (ARIAD Pharmaceuticals, Massachusetts, U.S.A.). The DTA-HA construct was then subcloned into a pCDNA3.1 backbone (Invitrogen, Massachusetts, U.S.A.) using NheI/BamHI cloning sites.

To construct the plasmid encoding Palm-DTA-HA, the SNAP25 palmitoylation sequence<sup>20</sup> was inserted at the N-terminus of DTA-HA using Infusion cloning (Takara Bio Europe, France).

**Cell viability assay.** Cells were incubated for 2 h in Alamar Blue HS (Invitrogen, Massachusetts, U.S.A.) and the fluorescence signal was measured according to the manufacturer's instructions using the iD3 SpectraMax microplate reader (Molecular Devices, California, USA). For cell growth curves, cells were incubated with Alamar Blue HS at the indicated timepoints.

**qRT-PCR.** Total RNA was extracted from cells using the Nucleospin RNA kit (Macherey Nagel, France) according to the manufacturer's instructions. Equal amounts of total RNA were reverse transcribed using the iScript cDNA synthesis kit and subjected to qPCR using the iTaq SYBR green kit (Bio-Rad, France), all following the manufacturer's instructions. The following primers were used: *PGK*: Forward 5'-AGCTGCTGGGTCTGT CATCCT-3'; Reverse 5'-TGGCTCGGCTTTAACCTTGT-3'; *DPH2*: Forward 5'-CGTGCTTCGTCAACGTTTCTG-3'; Reverse 5'-TGGGTCTGGGCCTCAAA-3'. qPCR was performed in a CFX96 system (Bio-Rad, France) at 95 °C for 10 min, followed by 40 cycles at 95 °C for 15 s, 60 °C for 30 s, and 72 °C for 30 s. DPH2 gene expression was normalized to the PGK housekeeping gene according to the 2- $\Delta\Delta C_t$  formula.

**Protein synthesis assay.** Parental or DPH2KD HeLa cells were seeded in 24 well plates before being co-transfected with plasmids encoding NLuc-Hsp70 and plasmids encoding either mock, or DTA-HA, or Palm-DTA-HA. 6 h after transfection, cells were detached and split in triplicate wells of a 96 well plate. 24 h later, cells were washed with DPBS and NanoLuc activity was measured in each well using the Nano-Glo Live Cell Assay System (Promega, Wisconsin, USA) following the manufacturer's instructions using the iD3 SpectraMax microplate reader (Molecular Devices, California, USA). The percentage of protein synthesis was calculated relative to the mock-transfected cells (mock set at 100%) for each cell type tested.

**EV preparation.** EV donor cells were transfected with the indicated plasmids for 16 h before being incubated in serum-free DMEM for 20 h. Conditioned medium was harvested and submitted to a 2000 × g centrifugation for 20 min at 4 °C to remove cell debris, and then to a 100,000 × g ultracentrifugation for 1 h 30 at 4 °C (45Ti rotor and Optima XE-90 ultracentrifuge, Beckman Coulter, California, USA) to pellet EVs. The EV pellet was washed with DPBS and centrifuged 1 h 30 at 100,000 × g 4 °C (MLA 50 rotor and Optima MAX-XP ultracentrifuge, Beckman Coulter, California, USA). The washed pellet was resuspended in DPBS and EVs were either stored at -20 °C (if destined to western blot or particle metrics analysis) or immediately applied on acceptor cells.

**EV uptake assay.** EVs were obtained from parent or DPH2KD HeLa cells transfected with a plasmid encoding NLuc-Hsp70. Acceptor parent HeLa cells were seeded in 96 well plates the day before EV incubation. The same protein amount of EVs for each condition is incubated with acceptor cells for 24 h. After incubation, acceptor cells are washed twice in DPBS and NanoLuc activity was measured in each well using the Nano-Glo Live Cell Assay System (Promega, Wisconsin, USA) following the manufacturer's instructions using the iD3

SpectraMax microplate reader (Molecular Devices, California, USA). EV uptake is shown as percent of input material. Statistical significance is obtained through an unpaired t-test.

**Western blot.** Cells to be analyzed were scraped on ice in DPBS and pelleted at  $1000\times g$  for 5 min at 4 °C. Cell pellets were resuspended in PBX lysis buffer (DPBS, Triton-X-100 1%, EDTA-free protease/phosphatase inhibitor cocktail (Roche, Switzerland)) and incubated on ice for 10 min with intermittent vortexing. Samples were then submitted to a  $15,000\times g$  centrifugation for 10 min at 4 °C to pellet nuclei and unbroken cells. Supernatants (cell lysates, CL) were collected. Protein concentration of cell lysate and EVs were obtained using the Micro BCA Protein Assay kit (Thermo Scientific, Illinois, USA). Samples were mixed with Laemmli buffer (Bio-Rad, France) containing 10%  $\beta$ -mercaptoethanol, except for CD63, and CD9 detection (no  $\beta$ -mercaptoethanol) and loaded on 4–15% polyacrylamide gels (Bio-Rad, France). After electrophoresis, proteins were transferred on PVDF membranes using the Trans-Blot Turbo system (Bio-Rad, France). Membranes were incubated with DPBS containing 0.05% Tween20 and 5% non-fat milk (blocking buffer) for 30 min at room temperature, then with a 1/1000 dilution of primary antibody ( $\alpha$ -Actin (Cat # MAB1501, Millipore, Germany),  $\alpha$ -Calnexin (Cat # ab133615, Abcam, U.K.),  $\alpha$ -CD63 (Cat # 556,019, BD Bioscience, New Jersey, U.S.A.),  $\alpha$ -CD9 (Cat # cbl162, Millipore, Germany),  $\alpha$ -Hsp70 (Cat # ADI-SPA-810-D, Enzo LifeScience, New York, U.S.A.),  $\alpha$ -HA (Cat # 3724, Cell Signaling, Massachusetts, U.S.A.),  $\alpha$ -mCherry (Cat # 5993, BioVision, California, U.S.A.)) in blocking buffer overnight at 4 °C. Membranes were then washed and finally incubated with a 1/5000 dilution of HRP-coupled secondary antibody ( $\alpha$ -mouse or  $\alpha$ -rabbit, Cat # 115-035-003, Jackson ImmunoResearch, U.K.) in DPBS containing 0.05% Tween20 for 1 h at room temperature. The HRP signal on membranes was developed using the Clarity Western ECL substrate (Bio-Rad, France) and imaged using the ImageQuant LAS 4000 (GE Healthcare Life Sciences, France).

**Cytosol/membrane fractionation.** Cells to be analyzed were scraped on ice in DPBS and pelleted at  $1000\times g$  for 5 min at 4 °C. Cell pellets were resuspended in 5 volumes of a hypotonic lysis buffer (10 mM Tris-HCl pH 8, 0.5 mM MgCl<sub>2</sub>, and EDTA-free protease/phosphatase inhibitor cocktail (Roche, Switzerland)) and incubated on ice for 10 min before being homogenized with 10 up-and-down passages through a 26 g needle. Tonicity was restored by the addition of 0.25 volume of the hypotonic buffer containing 0.6 M NaCl. Nuclei and unbroken cells were pelleted at  $500\times g$  for 5 min at 4 °C. EDTA was added to the supernatant to a final concentration of 0.05 M before subjecting the samples to ultracentrifugation at  $100,000\times g$  for 30 min at 4 °C (MLA 80 rotor and Optima MAX-XP ultracentrifuge, Beckman Coulter, California, USA). The resulting supernatant constituted the cytosolic fraction. The pellet was resuspended in PBX and centrifuged at  $10,000\times g$  for 15 min at 4 °C to pellet insoluble material. The supernatant constituted the membrane fraction.

**Particle metrics.** Nanoparticle Tracking Analysis was performed using the ZetaView<sup>®</sup> QUATT (Particle Metrix, Meerbusch, Germany) and its corresponding software (ZetaView 8.02.28). For the size measurements, the 448 nm laser in scatter mode was used. The instrument settings were 25 °C, sensitivity of 80, shutter of 100 at a frame rate of 30 frames per second. 1 mL of sample, diluted in DPBS, was loaded into the cell, and the instrument measured each sample at 11 different positions throughout the cell (1 cycle per position). Image evaluation was done on particles with a minimum brightness of 30, a minimum area of 10 and a maximum area of 1000. Tracelength was set at 15. After automated analysis of all positions and removal of any outlier positions, the size distribution of the particles was obtained.

**FACS analysis.** After treatments, cells were detached from cell culture plates with 0.05% Trypsin-EDTA and washed once in DPBS through centrifugation at  $1000\times g$  for 5 min at 4 °C. Cells were finally resuspended in DPBS and kept on ice (less than one hour) until analyzed on an Attune NxT flow cytometer (Thermo Scientific, Illinois, USA). Each sample was incubated with 10  $\mu$ g/mL DAPI (Merck Millipore, Massachusetts, U.S.A.) right before analysis. The gating strategy is depicted in Fig. S1C. Data was analyzed using the FlowJo software (BD Bioscience, New Jersey, U.S.A.).

**Microscopy.** Live cells were imaged with a CellInsight—CX7-LZR (ThermoFisher, Illinois, USA), with a 20X objective. Image analysis was performed using the ImageJ software (NIH, Maryland, U.S.A.).

**Statistical analysis.** Unpaired, two-tailed t-test were performed using the Prism software (GraphPad, San Diego, California U.S.A.) on biological replicates. \*:  $p < 0.1$ ; \*\*:  $p < 0.01$ ; \*\*\*:  $p < 0.001$ ; \*\*\*\*:  $p < 0.0001$ ; n.s.: not statistically significant.

#### Data availability

The authors declare that the data supporting the findings of this study are available within the Supplementary information files. Further requests should be addressed to the corresponding author.

Received: 12 August 2022; Accepted: 17 January 2023

Published online: 19 January 2023

#### References

1. Mathieu, M., Martin-Jaular, L., Lavieu, G. & Théry, C. Specificities of secretion and uptake of exosomes and other extracellular vesicles for cell-to-cell communication. *Nat. Cell Biol.* **21**, 9–17 (2019).

2. Yáñez-Mó, M. *et al.* Biological properties of extracellular vesicles and their physiological functions. *J. Extracell. vesicles* **4**, 27066 (2015).
3. Bonsergent, E. & Lavieu, G. Content release of extracellular vesicles in a cell-free extract. *FEBS Lett.* **1873–3468**, 13472. <https://doi.org/10.1002/1873-3468.13472> (2019).
4. Bonsergent, E. *et al.* Quantitative characterization of extracellular vesicle uptake and content delivery within mammalian cells. *Nat. Commun.* **12**, 1864 (2021).
5. Sahr, T. *et al.* Translocated *Legionella pneumophila* small RNAs mimic eukaryotic microRNAs targeting the host immune response. *Nat. Commun.* **13**(1), 1–18 (2022).
6. Evers, M. J. *et al.* Functional siRNA delivery by extracellular vesicle-liposome hybrid nanoparticles. *Adv. Healthcare Mater.* **11**(5), 2101202 (2022).
7. O'Brien, K., Breyne, K., Ughetto, S., Laurent, L. C. & Breakefield, X. O. RNA delivery by extracellular vesicles in mammalian cells and its applications. *Nat. Rev. Mol. Cell Biol.* **21**, 585–606 (2020).
8. Iglewski, B. H. & Rittenberg, M. B. Selective toxicity of diphtheria toxin for malignant cells. *Proc. Natl. Acad. Sci. USA.* **71**, 2707–2710 (1974).
9. Sharma, P. C. *et al.* Recent advances in microbial toxin-related strategies to combat cancer. *Semin. Cancer Biol.* <https://doi.org/10.1016/j.semcancer.2021.07.007> (2021).
10. Sharma, N. C. *et al.* Diphtheria. *Nat. Rev. Dis. Prim.* **5**, (2019).
11. Van Ness, B. G., Howard, J. B. & Bodley, J. W. ADP-ribosylation of elongation factor 2 by diphtheria toxin. Isolation and properties of the novel ribosyl-amino acid and its hydrolysis products. *J. Biol. Chem.* **255**, 10717–10720 (1980).
12. Picco, G., Petti, C., Trusolino, L., Bertotti, A. & Medico, E. A diphtheria toxin resistance marker for in vitro and in vivo selection of stably transduced human cells. *Sci. Rep.* **5**, (2015).
13. Killian, T. *et al.* Disruption of diphthamide synthesis genes and resulting toxin resistance as a robust technology for quantifying and optimizing CRISPR/Cas9-mediated gene editing. *Sci. Rep.* **7**, (2017).
14. Yamaizumi, M., Mekada, E., Uchida, T. & Okada, Y. One molecule of diphtheria toxin fragment A introduced into a cell can kill the cell. *Cell* **15**, 245–250 (1978).
15. Mastrobattista, E., Crommelin, D. J., Wilschut, J. & Storm, G. Targeted liposomes for delivery of protein-based drugs into the cytoplasm of tumor cells. *J. Liposome Res.* **12**, 57–65 (2002).
16. Lange, M. J., Lyddon, T. D. & Johnson, M. C. Diphtheria Toxin A-Resistant Cell Lines Enable Robust Production and Evaluation of DTA-Encoding Lentiviruses. *Sci. Rep.* **9**, (2019).
17. Hoshino, A. *et al.* Extracellular vesicle and particle biomarkers define multiple human cancers. *Cell* **182**, 1044–1061.e18 (2020).
18. Shen, B., Fang, Y., Wu, N. & Gould, S. J. Biogenesis of the posterior pole is mediated by the exosome/microvesicle protein-sorting pathway. *J. Biol. Chem.* **286**, 44162–44176 (2011).
19. Lai, C. P. *et al.* Visualization and tracking of tumour extracellular vesicle delivery and RNA translation using multiplexed reporters. *Nat. Commun.* **6**, (2015).
20. Greaves, J., Gorleku, O. A., Salaun, C. & Chamberlain, L. H. Palmitoylation of the SNAP25 protein family: specificity and regulation by DHHC palmitoyl transferases. *J. Biol. Chem.* **285**, 24629–24638 (2010).
21. Greaves, J., Salaun, C., Fukata, Y., Fukata, M. & Chamberlain, L. H. Palmitoylation and membrane interactions of the neuroprotective chaperone cysteine-string protein. *J. Biol. Chem.* **283**, 25014–25026 (2008).
22. Li, X. *et al.* Generation of destabilized green fluorescent protein as a transcription reporter. *J. Biol. Chem.* **273**, 34970–34975 (1998).
23. Zhang, X. *et al.* Programmable extracellular vesicles for macromolecule delivery and genome modifications. *Dev. Cell* **55**, 784–801.e9 (2020).
24. Corish, P. & Tyler-Smith, C. Attenuation of green fluorescent protein half-life in mammalian cells. *Protein Eng.* **12**, 1035–1040 (1999).
25. Choi, H. *et al.* Targeted Delivery of Exosomes Armed with Anti-Cancer Therapeutics. *Membranes (Basel)*. **12**, (2022).
26. DePolo, N. J. *et al.* VSV-G pseudotyped lentiviral vector particles produced in human cells are inactivated by human serum. *Mol. Ther.* **2**, 218–222 (2000).
27. Shafiee, F., Aucoin, M. G. & Jahanian-Najafabadi, A. Targeted Diphtheria Toxin-Based Therapy: A Review Article. *Front. Microbiol.* **10**, (2019).
28. Keller, M. D. *et al.* Decoy exosomes provide protection against bacterial toxins. *Nature* **579**, 260–264 (2020).
29. Abrami, L. *et al.* Hijacking multivesicular bodies enables long-term and exosome-mediated long-distance action of anthrax toxin. *Cell Rep.* **5**, 986–996 (2013).

## Acknowledgements

GL thanks INSERM U932/Institut Curie (and its members C.Théry and S. Amigorena), where the project was initiated. This work is supported by INSERM, the French National Research Agency (ANR-Excellidisc, -BIOEV, -EVfusion) and Chaire d'Excellence Idex Université Paris Cité. We thank the IVeTh platform (<https://iveth.u-paris.fr>). We thank H. Salmon for initial technical support for imaging with CellInsight—CX7-LZR.

## Author contributions

E.P generate material, J.D. and GL conceptualised, performed experiment and wrote the MS. All authors edited the MS.

## Competing interests

The authors declare no competing interests.

## Additional information

**Supplementary Information** The online version contains supplementary material available at <https://doi.org/10.1038/s41598-023-28306-8>.

**Correspondence** and requests for materials should be addressed to J.D. or G.L.

**Reprints and permissions information** is available at [www.nature.com/reprints](http://www.nature.com/reprints).

**Publisher's note** Springer Nature remains neutral with regard to jurisdictional claims in published maps and institutional affiliations.



**Open Access** This article is licensed under a Creative Commons Attribution 4.0 International License, which permits use, sharing, adaptation, distribution and reproduction in any medium or format, as long as you give appropriate credit to the original author(s) and the source, provide a link to the Creative Commons licence, and indicate if changes were made. The images or other third party material in this article are included in the article's Creative Commons licence, unless indicated otherwise in a credit line to the material. If material is not included in the article's Creative Commons licence and your intended use is not permitted by statutory regulation or exceeds the permitted use, you will need to obtain permission directly from the copyright holder. To view a copy of this licence, visit <http://creativecommons.org/licenses/by/4.0/>.

© The Author(s) 2023

# CURRICULUM VITAE

## Ester Piovesana

**Born:** 29th of May 1991, Lugano, Switzerland

**Private Address:** Riva Antonio Caccia 6, 6900 Lugano, Switzerland

**Mobile:** + 41 78 759 45 21 or + 39 333 766 79 69

**Email:** [ester\\_piovesana@yahoo.it](mailto:ester_piovesana@yahoo.it) or [ester.piovesana@eoc.ch](mailto:ester.piovesana@eoc.ch)

**Professional address:** Laboratory for Aging Disorders, Ente Ospedaliero Cantonale (EOC), Bios+ Via Francesco Chiesa 5, Switzerland

**OrcID:** 0000-0002-4983-7819

## Education:

- **Since September 2020:** Doctor of Philosophy (PhD) in Biomedical Sciences – Università della Svizzera Italiana (USI), Lugano Switzerland – PhD thesis defense expected in June 2023

PhD Thesis: Tau Accumulation in Degradative Organelles is Associated to Lysosomal Stress

Project Supervisor: Prof. Dr. Paolo Paganetti

External Expert: Prof. Dr. Carmine Settembre

Internal Expert : Prof. Dr. Lucio Barile

- **September 2015- December 2017:** International Master Degree in Neuroscience, University of Trieste, Trieste Italy

Master Thesis: The role of Nogo-A Signaling in Neurite Outgrowth Inhibition

Internal Relator: Prof. Dr. Enrico Tongiorgi

External Relator: Prof. Dr. Martin Schwab

- **September 2011- March 2015:** Bachelor of Science in Medical and Pharmaceutical Biotechnology, University Vita Salute San Raffaele, Milano Italy

Bachelor Thesis: Neuronal Fundamentals of Episodic Memory

Relator: Prof. Dr. Riccardo Fesce

- **September 2006- June 2010:** Diploma of Swiss Federal High School with Specialty in Languages, Arts and Philosophy, Liceo Diocesano, Lugano Switzerland

## Professional experiences:

- **September 2018- August 2020:** PhD in Extracellular Vesicles, Immune Responses and Cancer, Instiut Curie, Paris, France – Laboratory head by Prof. Dr. Clotilde Théry

- **January 2018- June 2018:** Laboratory Technician at Brain Research Institute, Zürich, Switzerland – Laboratory head by Prof. Dr. Martin Schwab
- **March 2017- November 2017:** Internship at Brain research Institute, Zürich, Switzerland- Laboratory head by Prof. Dr. Martin Schwab
- **2016:** Clinical Research Volunteer at the International School of Advanced Studies (SISSA), Trieste, Italy
- **April 2015- July 2015:** Laboratory Assistant at University San Raffaele, Milano Italy- Laboratory head by Prof. Dr. Giovanni Piccoli

### Supervision of students:

**July 2022:** Master Student Elisa Palladino – Applied cognitive Neuroscience, University of Milan, Milano, Italy

**September 2020- July 2021:** Master Student Giorgia Senesi, Master Degree in experimental and applied Biology, University of Pavia, Pavia Italy

### Scientific awards:

**August 2018:** Marie Skłodowska-Curie PhD Fellowship - European H2020-MSCA-ITN, Paris, France

### Certificates:

**March 2015:** Felasa LTK Module 1: Introductory Course in Animal Science, Zürich, Switzerland

### Founds raising activity:

**March 2023:** Main Organizer of the Art Exhibition: Art & Science, Visions on cellular Morphogenesis, Lugano, Switzerland

### Personal skills:

Italian: Mother Tongue

English: C1

French: C1

German: B1

### Published manuscripts:

1. Carrion MDP, Marsicano S, Daniele F, Marte A, Pischedda F, Di Cairano **E**, **Piovesana** E, von Zweydt F, Kremmer E, Gloeckner CJ, Onofri F, Perego C, Piccoli G. The LRRK2 G2385R variant is a partial loss-of-function mutation that affects synaptic vesicle trafficking through altered protein

- interactions. *Sci Rep.* 2017 Jul 14;7(1):5377. doi: 10.1038/s41598-017-05760-9. PMID: 28710481; PMCID: PMC5511190.
2. Kaiser J, Maibach M, **Piovesana E**, Salpeter I, Escher N, Ormen Y, Schwab ME. TGFβ1 Induces Axonal Outgrowth via ALK5/PKA/SMURF1-Mediated Degradation of RhoA and Stabilization of PAR6. *eNeuro.* 2020 Sep 29;7(5):ENEURO.0104-20.2020. doi: 10.1523/ENEURO.0104-20.2020. PMID: 32887692; PMCID: PMC7540929.
  3. Coccozza F, Névo N, **Piovesana E**, Lahaye X, Buchrieser J, Schwartz O, Manel N, Tkach M, Théry C, Martin-Jaular L. Extracellular vesicles containing ACE2 efficiently prevent infection by SARS-CoV-2 Spike protein-containing virus. *J Extracell Vesicles.* 2020 Dec;10(2):e12050. doi: 10.1002/jev2.12050. Epub 2020 Dec 28. PMID: 33391636; PMCID: PMC7769856.
  4. Pedrioli G, **Piovesana E**, Vacchi E, Balbi C. Extracellular Vesicles as Promising Carriers in Drug Delivery: Considerations from a Cell Biologist's Perspective. *Biology (Basel).* 2021 Apr 27;10(5):376. doi: 10.3390/biology10050376. PMID: 33925620; PMCID: PMC8145252.
  5. Pedrioli G, Barberis M, Magrin C, Morone D, **Piovesana E**, Senesi G, Sola M, Papin S, Paganetti P. Tau Seeds in Extracellular Vesicles Induce Tau Accumulation in Degradative Organelles of Cells. *DNA Cell Biol.* 2021 Sep;40(9):1185-1199. doi: 10.1089/dna.2021.0485. Epub 2021 Aug 10. PMID: 34379990.
  6. Dancourt J, **Piovesana E**, Lavieu G. Efficient cell death mediated by bioengineered killer extracellular vesicles. *Sci Rep.* 2023 Jan 19;13(1):1086. doi: 10.1038/s41598-023-28306-8. PMID: 36658184; PMCID: PMC9852484.
  7. M, Rendon-Angel A, Rojo Martinez V, Sgrignani J, Magrin C, **Piovesana E**, Cavalli A, Paganetti P, Papin S. Tau protein binds to the P53 E3 ubiquitin ligase MDM2. *Sci Rep.* 2023 Jun 23;13(1):10208. doi: 10.1038/s41598-023-37046-8. PMID: 37353565; PMCID: PMC10290082.

### In submission manuscript:

1. **E Piovesana**, C Magrin, M Cicaldo, M Sola, M Bellotto, M Molinari, S Papin, P Paganetti, Tau Accumulation in Degradative Organelles is Associated to Lysosomal Stress.

### In revision manuscript:

1. L Loconte, D Arguedas, A Chipont, Rojbin El, L Guyonnet, C Guerin, **E Piovesana**, J L Vázquez-Ibar, A Joliot, C Théry, L Martín-Jaular, Detection of tumor-derived extracellular vesicles interactions with immune cells is dependent on EV-labelling methods, doi: <https://doi.org/10.1101/2023.01.04.522609>
2. C Magrin, M Sola, **E Piovesana**, M Bolis, A Rinaldi, S Papin, P Paganetti, Tau Protein modulates an epigenetic mechanism of cellular senescence, DOI: <https://doi.org/10.1101/2023.06.05.543662>

## AKNOWLEDGMENTS

Ringrazio i miei genitori Giovanna, Domenico, i miei quattro fratelli, mio zio Luca e Maria Grazia.

Un ringraziamento speciale va a mio marito Matteo. Senza il suo sostegno e la sua fiducia non sarei riuscita a concludere questo importante percorso, percorso che spesso non è stato lineare e mi ha messo a dura prova, ma che alla fine mi ha anche consentito di evolvere e diventare la persona che sono oggi. Grazie per la pazienza e aver capito che conseguire questa formazione professionale per me era molto importante.

Grazie anche alla mia piccola Gilda che nei momenti di sconforto si è fatta sentire con dei piccoli calcetti in segno di forza e presenza.

Ringrazio anche Gabriella, Marco e Zia Marisa per far parte della mia nuova famiglia, per accudirmi sempre e per avermi cucinato spesso dei piatti salva vita.

Ringrazio le mie colleghe che mi hanno accompagnato in questo percorso in particolare Martina e Cluadia, ringrazio anche gli altri colleghi dell'EOC e del cardiocentro.

Ringrazio le mie amiche e amici, particolarmente Von, Vale, Mary, Lau, Caro, Greta, Marta e Maddi.